Wear fatigue in nickel superalloys.

Watkins, Shaun Gareth

Swansea University
Prifysgol Abertawe

Wear Fatigue in Nickel Superalloys

Shaun Gareth Watkins

Submitted to Swansea University in fulfilment
of the requirements for the Degree of Doctor of Engineering

2015

Acknowledgements

First and foremost, I would like to thank my academic supervisor, Dr Mark Whittaker, for his unrivalled support and continuous guidance throughout the four years of my research. This was a very challenging research topic and without his help, it would not have been possible. His friendly and approachable personality made this research a joy to be involved in. I would also like to express gratitude to my industrial supervisor, Dr John Pursell, based at Rolls-Royce Plc, for his technical guidance and expertise. In particular, I am grateful for his lateral thinking, which largely helped with the design of the fretting fatigue rig in this research.

A massive influence on my research must be accredited to Mr. Edward Saunders, Principal Failure Investigator, Rolls-Royce, Bristol. He took me under his proverbial wing, integrated me into the Rolls-Royce failure investigation team and taught me many valuable skills that will remain with me throughout my career. I am also indebted to Rolls-Royce for the opportunity they have afforded me on my EngD programme, especially the Critical Parts Lifing and Failure Investigation departments, Bristol, for their technical assistance and hospitality during my four year placement.

I would like to pay special thanks to Dr Kalin Dragnevski of Oxford University for his time and expertise in helping me produce excellent data for this research.

A massive thanks to my friend and my personal mentor, Dr Khandaker Mezanur Rahman of Imperial College London, for always being there and providing invaluable advice.

Finally, I owe my greatest debt to my family and partner for their continuous support and love along the way.

Dedication

To my mother, Donna Ann Watkins 1960-2014

Abstract

To date, work to assess the progression of wear and the effects of wear damage on low cycle fatigue has tended to be focused on specific components and their operating conditions. Although effective in the short term to solve today's problems, these efforts often deliver insufficient understanding of the overall design space limits to have much influence of future component design.

Therefore, the following research attempts to understand how wear damage progresses and how it impacts on fatigue performance in order to develop more accurate lifing models to predict the behaviour and life of real engine components.

In order to do this, a survey of the internal Rolls-Royce database and public literature on wear damage on components from ex-service and current service engines was performed. Information relating to the wear scar morphologies in the reports was extracted as well as physically measuring and analysing wear damage on worn components within the Rolls-Royce failure investigation department. The wear damage was then replicated onto Udimet720Li laboratory fatigue specimens by a means of altering the pad pressure and pad sliding distance to produce a range of wear damage in order to carry out fatigue testing. Fatigue testing of the damaged specimens allowed fatigue knockdown factors to be calculated to determine the impact of wear on the fatigue life.

A fretting fatigue rig was also designed and built for this research to focus on in-situ fretting fatigue at high temperatures of 600°C.

Declarations and Statements

I, Shaun Gareth Watkins, certify that this work contains no material which has been accepted for the award of any other degree or diploma in my name, in any university or other tertiary institution and, to the best of my knowledge and belief, contains no material previously published or written by another person, except where due reference has been made in the text. In addition, I certify that no part of this work will, in the future, be used in a submission in my name, for any other degree or diploma in any university or other tertiary institution without the prior approval of the Swansea University.

I give consent to the copy of my thesis, when deposited in the University Library, being made available for loan and photocopying, subject to the provisions of the Copyright Act 1968.

I also give permission for the digital version of my thesis to be made available on the web, via the University's digital research repository, the Library Search and also through web search engines, unless permission has been granted by the University to restrict access for a period of time.

Signed.....

Date.....16/11/15.....

Contents

Abbreviations

Parameter	Description	Units
P	Normal load	N
Q	Tangential load	N
M	Moment	Nm
x,y,z	Coordinate system	M
u,v,w	Displacements in x,y,z coordinate directions	M
μ	Coefficient of friction	
σ_o	Subsurface bulk stress	N/m^2
h(x)	Contact geometry profile, gap function	M
a	Contact radius	M
c	Stick zone radius	M
p(x)	Normal contact pressure	N/m^2
q(x)	Contact shear traction	N/m^2
W	Wear volume per unit displacement	mm^3/m
k	Dimensional wear coefficient	$mm^3/(Nm)$
H	Indentation hardness	N/m^2
R	Radius of contact pin	M
E*	Equivalent Young's modulus	N/m^2
p_o	Maximum Hertzian pressure	N/m^2
f(x)	Slip (or shift) function	M
t	Time	Seconds
$\dot{u}$	Time derivative of displacement (=du/dt)	m/s

1 Introduction

In the aerospace industry alone, statistics show that the majority of service failures in aircraft components occur by fatigue and it amounts to about 60% of the total failures[1]. When a material fails by fatigue, the nominal maximum stress values are less than the ultimate tensile stress limit, and may even be below the yield stress limit of the material. Hence, failure can occur unexpectedly.

In most cases, fatigue failure initiates from regions of high stress intensity that provide the perfect platform for crack initiation and propagation. Sometimes the region of high stress intensity can be due to geometric discontinuities such as material imperfections, surface roughness or sharp corners, all of which decrease the fatigue life. In the case of plain fatigue, for a defect free material, regions of stress can result from the localisation of persistent slip bands caused by the movement of dislocations when the material is subjected to a repeated cyclic stress.

Contact fatigue is a damage wear mechanism concerning oscillating contacts that are intended to be fixed and can have detrimental effects on the fatigue performance of materials. For example, fretting fatigue is a form of contact wear most commonly witnessed in bolted configurations, splines, lockplates, coverplates on disc rims and most notably, the disc/blade root interface. The relative slip between the mating contacts does not have to be sufficiently large in order to produce wear by fretting. In fact, it has been experimentally measured, that the most life limiting sliding amplitude of fretting occurs on a microscale of 50μm.

The myriad of factors involved in the contact wear problem makes modelling of contact fatigue extremely difficult with previous research suggesting that fretting fatigue involves as many as 50 variables. As a result, this has generally led to focused experiments where the geometry and load conditions of a particular application are replicated as closely as possible. Experiments can take the form of full scale rig tests to sub-element testing which only replicate a section of the engine such as the disc/blade root. Sub-element wear tests aim to simulate the problems experienced in service as accurately as possible, taking into consideration factors such as stress, geometry, sliding distances, friction coefficients,

temperature and environments. However, in order to simplify the analysis phase of the experiment, i.e. FE modelling, the variables are kept to a minimum and the geometry is also kept relatively straightforward.

Though successful in the short term, such experimental investigations to reproduce and simulate each practical situation in which evidence of fretting fatigue is observed may become less feasible as costs escalate. The ensuing redesign to mitigate fretting fatigue in each instance also becomes difficult because there is inadequate understanding of the influence of the contact fatigue parameters themselves. Thus, the development of modelling methods capable of capturing the fundamental mechanics of the contact fatigue problem is required to develop next generation life prediction schemes and to maintain the current sub-element testing methodology being employed by Rolls Royce. Thus, before this can be done, the progression of wear and its effects on the components service life needs to be understood.

2 Literature Review

2.1 Characteristics of High Temperature Materials

If it were not for the remarkable ability of a certain class of materials to maintain their properties at elevated temperatures, jet flight would not be possible. It is this class of materials that we refer to as the *high temperature materials* and in the aerospace industry; they are known as the *superalloys*. These alloys are chosen for their excellent load-bearing capabilities at temperatures in excess of 80% of their incipient melting temperatures, a fraction that is higher than for any other class of engineering alloys. Their uses are wide and varied, and currently constitute over 50% of the weight in advanced aircraft engines[2], being implemented in the hottest parts of the of jet engines for components such as disks, combustion chambers, bolts, casings, shafts, exhaust systems, cases, blades, vanes, burner cans, afterburners and thrust reversers.

Indeed, consistent with the concept thermodynamics, the limiting factor to improved thrust and fuel economy in modern aeroengines is the ability to increase the turbine inlet temperatures (TIT) and this is dependent upon on the capability of the superalloys to maintain their mechanical properties at higher combustion temperatures. To reach higher TIT in the future, there will either need to be improvements in processing and developments of current superalloys, or a new generation of superalloys will need to be introduced. Current research into new and improved superalloys is already underway, with optimistic results leaning toward cobalt alloys as the superalloys of the future.

For a material to be classed as a 'high temperature material' it must be able to withstand considerable loading at an operating temperature close to its melting point. To define a high temperature material, let the operating temperature be donated as T_{oper} and the melting point, T_m. A criterion based upon the homologous temperature τ, defined, as T_{oper}/ T_m should produce a value ≥ 0.6.

Hence, a superalloy operating at 1000°C in the vicinity of the melting temperature of nickel, 1455°C, working at a τ of (1000+273)/(1455+273)$\approx$ 0.75, is classified as a high temperature material.[3]

Another desirable characteristic of high temperature materials is to maintain a substantial resistance to mechanical degradation over extended periods of time. In this case, mechanical degradation refers to two common failure systems (i) *Fatigue*, where a component is subjected to a repeated stress cycle (ii) *Creep*, a time-dependant, inelastic and irrecoverable deformation which is problematic at high temperature due to the promotion of thermally activated processes. Furthermore, as with all structural materials, the static properties of *yield stress, ultimate tensile strength* and *fracture toughness* must all be maintained over extended periods of time. In the case of superalloys, the high temperature strength is improved by the process of solid solution strengthening. The technique works by adding atoms of one element (the alloying element) to the crystalline lattice of another element (the base metal). The alloying element diffuses into the matrix, forming a solid solution. Since the strength of a material is dependent on how easily dislocations in its crystal lattice can be propagated, when solute atoms are introduced, local stress fields are formed that interact with those of the dislocations, impeding their motion and causing an increase in the yield stress of the material. Thus, the increase in strength of the material is a result of both lattice distortion and the modulus effect. However, the most important strengthening mechanism is through the formation of secondary phase precipitates such as gamma prime and carbides through precipitation strengthening and will be discussed in Chapter 2.5.

A final desirable characteristic of high temperature materials is the ability to operate in severe corrosive and oxidising environments. Kerosene used for aeroengine fuel is relatively clean but corrosion due to impurities such as potassium salts and the ingestion of sea-water can occur during operation. It is well understood that any surface degradation reduces component life considerably since flaw free materials spend most of their life in the crack initiation stage. Therefore, introducing a stress concentration effect from surface degradation provides a perfect nucleation site for fatigue cracks to propagate from.

2.2 Superalloys for Turbine Disc and Blade Applications

The primary function of a turbine disc is to provide fixing of the turbine blades. The blades are located in the gas stream, from which mechanical energy is extracted. The extracted

energy is then transferred to the fans and compressor sections via the shaft, which runs along almost the complete length of the engine. Essentially, it is the job of the turbine to keep the compressor functioning.

The turbine discs are amongst the most critical of components in the jet engine and are thus designated critical group A parts by the aerospace industry. This is because if a disc were to fail it could have severe repercussions on the aircraft's safety, since the kinetic energy that the disc fragments possess is uncontainable by the engine casing. To put this into context, the turbine disc of a modern civil turbofan such as a Trent 800 represents 20% of its total weight and rotates at 10,500rpm. Consequently, the mechanical stresses generated in the bore region may reach 1000MPa during takeoff i.e. they may exceed the uniaxial tensile yield strength of the material. Disc failures can also result in an overspeed condition, which puts higher stresses on the drive shaft. An interesting analogy put forward by Rolls-Royce is: "The energy stored in a HP turbine disc under such conditions is very significant: equivalent, in fact, to 0.75kg of high explosive, or a saloon car traveling at over 100 mph."[2]

Hence, to ensure discs have a safe working life, risk mitigation by an appropriate lifing strategy is of huge importance. Mechanical degradation during service and its acceleration due to oxidation and/or corrosion must therefore be quantified and predicted, so that each disc is withdrawn from service after a predicted number of take off/landing cycles, known as the predicted safe cycle life (PSCL) or safe working life. There are also other methods used for lifing turbine discs such as the life-to-first-crack approach, damage tolerance lifing (also known as retirement for cause) and the probabilistic method all of which can be found in literature.

2.3 Basic Stress Loads in Turbine Blades and Discs

Since it is the turbine blades job to extract energy from the gas stream and transmit it to the compressor, they must be carefully positioned in the direct path of the high velocity, working fluid. Consequently, the operating temperatures are much higher for the turbine blades ($\approx$1550°C) than the turbine disc rims ($\approx$650°C), but the stresses experienced in the discs are much greater, and extraordinarily different. This has obviously been taken into consideration when designing the discs and blades, as the two have very different compositions, microstructures and properties that are tailored to their specific operating environments.

In the case of turbine blades, a specialised manufacturing process by investment casting, termed *directional solidification* is used to produce turbine blades that have a single crystal microstructure. The drive for industry to produce blades in this way is to eliminate grain boundaries to lessen the effects of creep deformation. Creep occurs in materials that are subjected to high temperature and stresses below the materials yield stress. Over time, plastic strain is accumulated, which causes the material to elongate in length. Creep involves a combination of dislocation and diffusion mechanisms with one particular diffusion mechanism, termed Coble creep, occurring through the grain boundaries of materials. Hence, by removing the grain boundaries, coble creep is eliminated, improving the creep behavior of the material. However, creep still remains a problem in turbine blades as other mechanisms of diffusion and dislocation creep remain. These mechanisms are eased by the use of solid solution strengthening due to the presence of solute atoms or precipitation hardening such as γ' which act to pin dislocations that cause plastic strain. The effect of creep on blades can be hazardous to the aircraft, since the large centrifugal stresses cause the blades to extend outwards. If the blades are allowed to grow long enough so that they make contact with the engine shroud, multiple blade loss can occur with secondary damage to other critical rotating parts.

The hot gases inflict a complex set of stresses on the blades, not just thermally but also because of the high pressure and velocity of the gas stream. The most obvious deformation is the action of the blade bending backwards as a response to the pressure incident upon the front face of the blade. This results in bending stresses on the blade in both the axial and tangential direction and therefore induces further stresses in the blade root. However, due to the action of CF forces, the amplitude of the deflection is reduced slightly since the blades naturally try to straighten outwards from the root. It has been shown that the gas bending stresses are inversely proportional to the number of blades and the blade section modulus is directly proportional to the blade height and specific work output. Even so, the number of blades cannot be increased beyond blade fixing constraints and furthermore, reducing the height of the blades but maintaining the annulus area implies an increase in annulus mean diameter and increase in CF stresses. The second main deformation is that of a twisting motion, generated by the torsional moment about the non-symmetrical compressor blade. The effect of this torsion is limited in the high-pressure compressor but becomes much more significant in the larger low pressure compressors and fans.

Blades also experience vibration but in practice, amplitude tends to decrease as frequency increases, so the higher frequencies are considered to be of secondary importance. It is the scale of the local perturbation in the gas stream that drives the blade vibration. These perturbations are larger at higher engine speeds, so attention should be focused on the higher end of the Campbell diagram. Stresses in components are also higher at speed ($\sigma \alpha RPM^2$) and it is at these higher stresses that vibratory modes are most effective. Hence, it is usual to consider engine speeds larger than 70-80%. Vibration results in engine ordered excitations, which is a subset of high cycle fatigue (HCF). There are three main sources of excitation (1) fixed wake excitation which occurs due to vanes causing stationary flow disturbances (2) rotating stall cell excitation (3) self excitation or flutter. An example of an engine ordered excitation is caused by a stator up-wind of the rotor. As air flows past the stator, a pressure wake is set up behind it, and the rotor will experience a pressure disturbance every time it passes a stator blade up-wind. Any engine feature, which disrupts the clean airflow e.g. intermediate casing struts, can generate these disturbances and assuming sub-sonic airflow, the pressure differentials can travel both up-stream and down-stream. There are also non-engine ordered excitations caused by intake flow distortions such as crosswinds or bifurcated (s- shaped) intakes, which alter the pressures differentials within the engine. Like LCF, engine ordered excitations add up to produce destructive vibrations, and it is primarily for this reason why vibration engineers design against this phenomenon by making sure the excitation frequency never matches the natural frequency of the blades.

In the case of turbine discs, "creep resistance is also important, but traditionally it has been given less emphasis due to lower operating temperatures and because a stress relaxation capability around notches and features of stress concentration is desirable"[2]. The high rotational speeds and temperatures within the HP turbines pose a significant life-limiting factor on the rotors, due to the effects of fatigue and creep. Primarily, stresses originate from three main sources (i) Centrifugal loading of the disc material itself (ii) Centrifugal loading from external features such as blades, lockplates, spacers and coverplates (iii) Temperature gradients between bore and rim. There are also end loads from pressures on disc faces and nip loads due to rims and spacers being clamped together. Working in the disc's rotating frame of reference, the centrifugal loading acts to pull the disc material outwards generating radial stresses that can lead to radial expansion. Since, centrifugal loading is given by $m\omega^2 r$, where m is the mass, ω is the angular velocity and r is the radius, it suggests that CF loading

is highest for large radii, high rotational speeds and heavy components. The stresses experienced in the disc are not evenly distributed. For example, the radial stresses are obviously zero at the bore (radius is zero), increases to a maximum at the diaphragm and reaches a finite value at the rim. The maximum radial stresses occur at the middle of the disc profile but due to the large circumferential cross sectional area in this region, it permits the thickness to be kept relatively thin. The radial expansion (strain) caused by the centrifugal forces act to further increase the CF loading since the radius is increasing. This also causes further problems, since there must be a safe tip clearance between the blade tips and the casing structure.

To limit the effect of CF stresses, discs are designed with a complex geometry whilst achieving optimum strength at minimum weight. For HP turbine discs, which rotate with a high angular momentum, they are designed to have more mass at the bore region and less mass in the diaphragm and rim region, which reduces the $m\omega^2r$ effect. This is also why high strength to weight ratio materials, such as nickel superalloys, are vital in the aerospace industry.

Fatigue has a major effect on the life of a component. Statistics show that majority of service failures in aircraft components occur by fatigue and it amounts to about 60% of the total failures[4]. When a material fails by fatigue, the nominal maximum stress values are less than the ultimate tensile stress limit, and may be below the yield stress limit of the material. Fatigue may be classed into two domains, Low cycle fatigue (LCF) and High cycle fatigue (HCF). LCF is associated with relatively high loads that produce not only elastic strains but also some plastic strain during each cycle. In this case, fatigue lives are relatively short and occur at less than 10^4 to 10^5 cycles. For lower stress levels, wherein deformations are totally elastic, longer lives result. This is called high-cycle fatigue and is associated with fatigue lives higher than 10^4 to 10^5 cycles.

A number of factors influence the fatigue life of a component in service, (i) complex stress cycles, (ii) engineering design, (iii) manufacturing and inspection, (iv) service conditions and environment and (v) material of construction. Analysis shows that premature fatigue crack initiation in the components can be attributed to defects of various types introduced mostly inadvertently in various stages of component design, manufacture, maintenance, inspection, operation etc. Ultimate care is taken when machining jet engine components to ensure that no impurities or surface discontinuities are introduced into the component before entry into

service. A major source of stress intensification occurs when two materials come into contact with each other and cause wear, which in tribological terms, is referred to as fretting fatigue.

Other stresses associated with rotating components are hoop stresses and axial stresses. Hoop stresses act circumferentially around the disc and are found to be a maximum at the bore and decreases steadily with increasing radius. This is also another reason why more mass is shifted to the bore region compared to the rest of the disc and allows the large hoop stresses to be distributed over a larger area.

Axial stresses occur at the wider sections of the disc due to the interaction of the turbine blades with the gas stream and are a product of the expansion in the radial and hoop directions with contributions from unbalanced discs. However, since axial stresses are small, and contribute very little to the overall stress of the disc, the combination of the CF stress, hoop stress and axial stress is actually considered biaxial, as the axial stress contribution has a modest effect on the total stress. The effect of biaxiality is strongest when the constituent forces are equal, and although this is not likely to occur in a disc, there is a section near the diaphragm where the radial and hoop stresses are of equivalent magnitude. In fact, having a biaxial stress field basically enables the disc to withstand larger individual forces than the material would usually permit if the stress field were uniaxial. This can be demonstrated by employing the Von-Mises yield criterion, which is based upon the differences between the three primary stresses, and essentially states that if all three primary stresses have the same value the material will never fail.

Stresses in turbine discs are also modified by temperature gradients. One such modification causes the radial stress to be zero at the bore and rim but peak in the diaphragm. This acts to lower the tolerance the diaphragm has for mechanically induced radial stresses, meaning mass would need to be added to the design in order to compensate for this deficiency. Furthermore, temperature gradients act to modify the radial and hoop stresses from the CF forces and induce a tensile hoop stress at the bore, which drops to a compressive value at the rim. Although the rim only experiences relatively small hoop stresses, the presence of a stress concentration (Kt) feature can magnify the stresses quite significantly. The compressive stress at the rim can have a helpful effect, since it can improve the life of stress concentration features in the rim region of the disc by closing up flaws and cracks.

Other problems that turbine discs have to contend with is during the take-off/landing and acceleration stages as it is these stages that undergo thermo-mechanical fatigue (TMF). This occurs due to the overlay of a cyclical mechanical loading with cyclic thermal loading as a result of different heating and cooling rates during these regimes. It is also at these stages where the discs life deteriorates substantially and is also the most common time of failure. When the engine is operating at a steady speed i.e. cruise, the temperature gradient will start to soak out, increasing the average disc temperature but decreasing the temperature difference between the bore and the rim.

Stress concentration features such as boltholes, air holes and disc slots act to increase the stresses in the disc. Furthermore, any feature that has a sharp corner or irregular microstructure also acts to magnify the nominal stress in that region. An object is strongest when force is evenly distributed over its area, so a reduction in area, e.g. caused by a crack, results in a localised increase in stress i.e. the force lines become more intensified. A material can fail, via a propagating crack, when a concentrated stress exceeds the material's theoretical cohesive strength. Disc/blade root slots are an important feature since they are responsible for fixing the turbine blades to the discs, but are also sources of stress concentration. The stresses in this region are complex and large due to the shear forces, bending stresses and large crushing stresses that result from the interaction of the blade with the root of the disc. Modern disc slots are of two types; firtree slots and dovetail slots. The firtree slots have up to four teeth in to which the blade root is slotted, whilst the dovetail has just one large tooth. There are approximately five hotspot locations in dovetail root fixings alone and failure of all but one is containable by the engine. Most failures could at the worst release a turbine blade or blade and root together, but is containable. The most serious hotspot location is at the disc rim, located at the bottom corner of the root fixing. A crack initiating at this point can potentially result in a disc burst, which as discussed earlier, is not containable by the engine casing. Another common problem with dovetail and firtree roots is the onset of fretting fatigue, which occurs due to the very small amplitudes of movement between the disc and blade teeth. This is very similar to friction but results in the onset of micro fissures and small cracks that can grow with further stress cycles and potentially cause blade release or disc burst. The topic of fretting fatigue is the basis of this research and will be discussed in more detail in the following chapters.

2.4 Processing and Microstructure of Turbine Disc Nickel Superalloys

The microstructure of jet engine components differ from each other depending on the conditions they operate under and the properties they require. For example, as discussed earlier, turbine blades experience creep, so a single crystal microstructure helps to alleviate this by removing the grain boundaries that are partly responsible for this effect. Turbine discs on the other hand have a polycrystalline microstructure that is similar to most crystalline solids. That is, they consist of many small crystals or grains at random crystallographic orientations to each other. The polycrystalline structure is formed during the solidification process whereby the small grains grow by the successive addition of atoms from the surrounding liquid. The grain size is dependent on the speed at which the melt solidifies (or crystallises). Due to the atomic mismatch within the region where the grains meet, a grain boundary is formed, which is the basis of polycrystalline materials. The fact that each grain is at a different orientation to the next, implies that polycrystalline materials have isotropic properties i.e. the properties are equal in all directions. A single crystal turbine blade is referred to as highly anisotropic because its properties are engineered to perform better in one direction i.e. the uniaxial direction. This is because the centrifugal forces during turbine spinning are radial as discussed in the 'basic stress loads section', Chapter 2.3. However, discs require strength in all directions due to the effects of radial stress, hoop stress, centrifugal stresses and a combination of HCF and LCF. Hence a polycrystalline material displays the best properties for this purpose.

The size of the grains, or average grain diameter, in a polycrystalline metal influences the mechanical properties. During plastic deformation, slip or dislocation motion must take place across this common grain boundary. The grain boundary acts as a barrier to dislocation motion for two reasons:

- Since the two grains are of different orientations, a dislocation passing into an adjacent grain will have to change its direction of motion. This becomes more difficult as the crystallographic misorientation increases.
- The atomic disorder within a grain boundary region will result in a discontinuity of slip planes from one grain into the other.

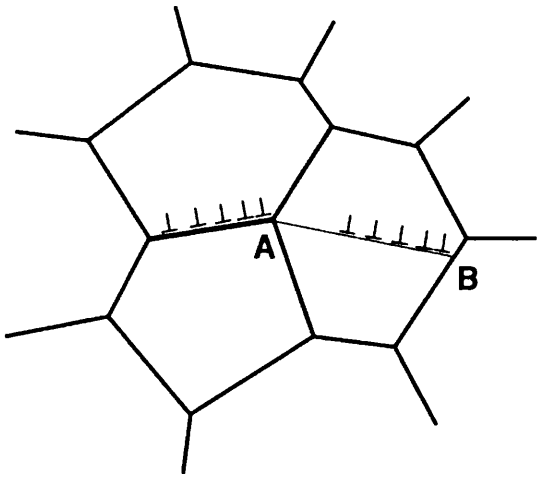

Figure 2.4.1. The motion of a dislocation as it encounters a grain boundary acts as a barrier to continued slip. Slip planes are discontinuous and change directions across the boundary[4].

It is well understood that a fine grained material is harder and stronger than one that is coarse grained, since the former has a greater total grain boundary area to impede dislocation motion. Furthermore, grain size reduction improves not only strength, but also the toughness of many alloys. For many materials, the yield strength σ, varies with grain size according to

$$\sigma_y = \sigma_o + k_y d^{-1/2} \qquad (2.4.1)$$

This expression is termed the Hall-Petch equation, where d is the average grain diameter, and σ_o and k_y are constants for a particular material. However, this expression is not applicable to both very large (coarse) grain and extremely fine grain polycrystalline materials. The grain size is dependent on many factors but primarily depends on the rate of solidification and the processing route.

The discs for the gas turbine engine are processed by the machining of superalloy forgings, using two distinct approaches. The first uses conventional ingot metallurgy, which involves the thermal-mechanical working of material produced by vacuum induction melting, electro-slag remelting and vacuum arc remelting. Billets produced in this way are referred to as *Cast and Wrought* product. A second route involves *powder metallurgy*. The choice of route depends on the chemistry of the particular superalloy[5]. Udimet 720Li, a modern nickel superalloy used for turbine discs is produced using ingot metallurgy, because the levels of strengthening elements Al, Ti and Nb are relatively low, so that the additional cost associated with powder processing cannot be justified[6].

Heavily alloyed grades such as Rene 95 and RR1000 cannot be processed using ingot metallurgy, since the levels of segregation arising during melt processing and the significant flow stress at temperature cause cracking during thermal-mechanical working[5]. For this reason, powder processing is preferred. For powder processing, vacuum induction melting (VIM) is used as in ingot metallurgy, followed by remelting and inert gas atomisation to produce a powder. After sieving the powder to improve cleanliness, the powder is consolidated by sealing it into a can, which is then degassed and sealed and hot isostatic pressing and/or extrusion follows. In essence, the number of inclusions in a product produced by powder processing will be far lower than if it was produced by ingot metallurgy. However, this accompanied by higher costs and a more complex processing route.

2.5 Composition of Nickel based Superalloys

The superalloys are amongst the most complex, intricate and laudable of materials engineered by man. The number of alloying elements that make up these exciting materials is often greater than ten with each element adding its own unique properties to the alloy. The general pattern for superalloys is that most contain significant amounts of chromium, cobalt, aluminium and titanium with small amounts of boron, zirconium and carbon often included. Other such elements that are used in some superalloys but not all include rhenium, tungsten, tantalum and hafnium from the 5d block of transition metals and ruthenium, molybdenum, niobium and zirconium from the 4d block. Hence, most of the alloying elements are taken from the d block of transition metals[7] and the behavior of each alloying element and its influence on the phase stability depends heavily on its position within the periodic table[2].

However, it does raise the question as to why nickel-based alloys have emerged as the materials of choice for high-temperature applications. Firstly, although the aerospace industry is a lucrative, budget is always important so it is advantageous that nickel is relatively cheap, since it is the fifth most abundant element on earth. For example, the platinum group metals belong to the transition metal series and have a high density and display the same structure as nickel, but they are also very expensive, thus nickel is favoured. Nickel displays the face centered cubic (FCC) crystal structure and is therefore both tough and ductile due to the multiple slip systems in FCC structures and the cohesive energy arising from the bonding imparted by the outer d electrons. Nickel is stable in the FCC form from room temperature to its melting point[2], which implies that no phase transformations will occur to cause

expansions, and contractions, which might complicate its use for high-temperature components. Conversely, the body centered cubic (BCC) metals such as Cr are prone to brittleness and undergo a ductile to brittle transition at certain temperature which means the toughness drops significantly with decreasing temperature. Another reason why nickel is ideal for its use in superalloys is its low rates of thermally activated processes. When considering the correlation between activation energies for self-diffusion and creep in pure metals, it suggests that low rates of thermally activated creep require low rates of diffusion. Thus, since diffusion rates in FCC metals are low, microstructural stability is imparted at higher temperatures[8].

The fundamental solutes in nickel based superalloys are aluminium and/or titanium, usually having a total concentration less than 10 atomic percent. This generates a two-phase equilibrium microstructure, consisting of gamma (γ) and gamma-prime (γ'). It is the γ' which is largely responsible for the elevated-temperature strength of the material and its excellent resistance to creep deformation. The fraction of γ' depends on the chemical composition and temperature, as illustrated in the following ternary phase diagrams.

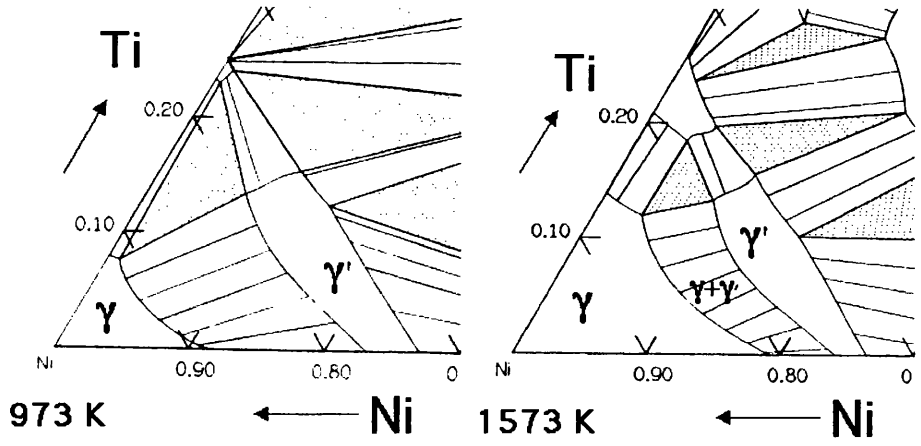

Figure 2.5.1. Ternary Phase Diagrams illustrating the amount of γ' with varying chemical composition and temperature[9].

The Ni-Al-Ti ternary phase diagram in Figure 2.5.1 shows that for a given chemical composition, the fraction of γ' decreases as the temperature is increased. This phenomenon is used in order to dissolve the γ' at a sufficiently high temperature (*a solution treatment*) followed by ageing at a lower temperature in order to generate a uniform and fine dispersion of strengthening precipitates[7].The microstructure of a nickel superalloy consists of different phases drawn from the following [10],

Gamma phase, denoted γ

This is the main constituent of the superalloy as a result of the FCC structure of nickel. In nearly all cases, it forms a continuous, matrix phase in which the other phases reside. It contains significant concentrations of elements such as cobalt, chromium, molybdenum, ruthenium and rhenium, where these are present, since these prefer to reside in this phase.

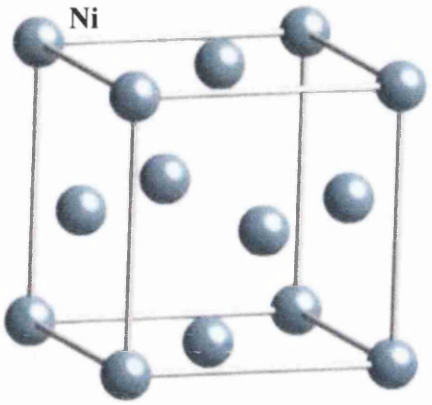

Figure 2.5.2. **FCC Crystal Structure of γ** [7]. All corners occupied by Ni atoms.

The gamma prime precipitate, denoted γ'

It has a cubic-P (primitive cubic) lattice in which the nickel atoms are at the face-centers and the aluminium or titanium atoms at the cube corners. This atomic arrangement has the chemical formula Ni_3Al, Ni_3Ti or $Ni_3(Al,Ti)$. However, as can be seen from the $(\gamma+\gamma')/\gamma'$ phase boundary on the ternary sections of the Ni, Al, Ti phase diagram, the phase is not strictly stoichiometric. There may exist an excess of vacancies on one of the sub-lattices which leads to deviations from stoichiometry. On the other hand, some of the nickel atoms might occupy the Al sites and vice-versa. In addition to aluminium and titanium, niobium, hafnium and tantalum partition preferentially into γ'.

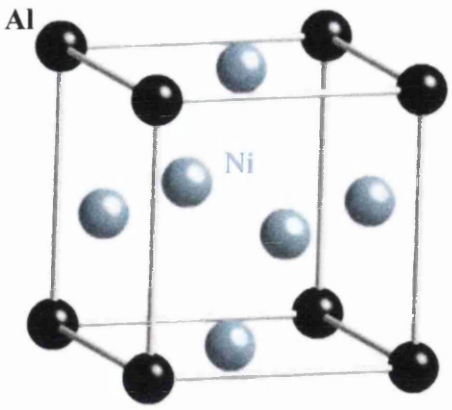

Figure 2.5.3. Ni3Al primitive cubic lattice of γ' [7]. Al atoms occupying the corners of the cube and the Ni atoms positioned at the cube faces of the lattice.

It can be seen that both the γ and γ' phases have a cubic lattice with similar lattice parameters, since its cell edges are exactly parallel to corresponding edges of the γ phase. As a result the γ' precipitates form a cube-cube orientation relationship with the γ, involuntarily. Furthermore, because their lattice parameters are similar, the γ' is coherent with the γ when the precipitate size is small. Dislocations in the γ nevertheless find it difficult to penetrate γ', partly because the γ' is an atomically ordered phase. It is this preferential ordering that interferes with dislocation motion and hence strengthens the alloy.

Another very important advantage concerning the two phases is a small misfit between the γ and γ' lattices, which is important for two reasons (i) When combined with the cube-cube orientation relationship, it ensures a low γ/γ' interfacial energy. The ordinary mechanism of precipitate coarsening is driven entirely by the minimisation of total interfacial energy. A coherent or semi-coherent interface therefore makes the microstructure stable, a property which is useful for elevated temperature applications. (ii) The magnitude and sign of the misfit also influences the development of microstructure under the influence of a stress at elevated temperatures. The misfit is said to be positive when the γ' has a larger lattice parameter than γ. The misfit can be controlled by altering the chemical composition, particularly the aluminium to titanium ratio. A negative misfit stimulates the formation of rafts of γ', essentially layers of the phase in a direction normal to the applied stress. This can help reduce the creep rate if the mechanism involves the climb of dislocations across the precipitate rafts[7].

The transmission electron micrographs shown in Figure 2.5.4 illustrates the large fraction of γ', typically in excess of 0.6, in turbine blades designed for aeroengines, where the metal experiences temperatures in excess of 1000°C. Only a small fraction (0.2) of γ' is needed when the alloy is designed for service at relatively low temperatures (650°C) as experienced in turbine discs.

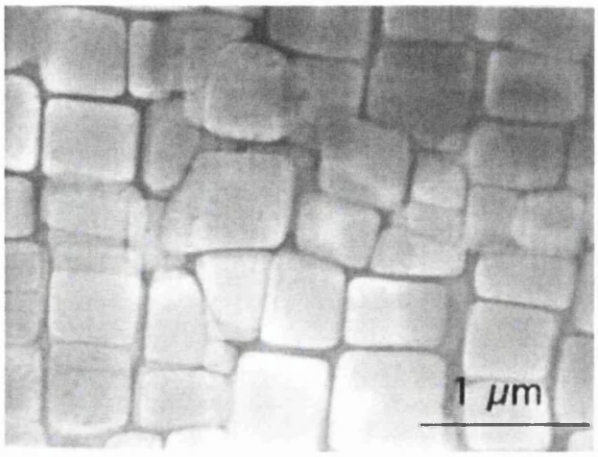

Figure 2.5.4. Transmission electron micrograph showing a large fraction of cuboidal γ' particles in a γ matrix. Ni-9.7Al-1.7Ti-17.1Cr-6.3Co-2.3W at%[11].

Carbides and borides also play a vital role in the superalloys performance. Carbon, often present at concentrations up to 0.2 wt%, combines with reactive elements such as titanium, tantalum and hafnium to form MC carbides. During processing or service, these can decompose to other species such as $M_{23}C_6$ and M_6C, which prefer to reside on the γ-grain boundaries, and which are rich in chromium, molybdenum and tungsten. Boron can combine with elements such as chromium or molybdenum to form borides, which reside on the γ-grain boundaries and prevent grain boundary sliding.

The following table provides the chemical compositions of some typical turbine disc alloys.

Alloy	Cr	Co	Mo	W	Nb	Al	Ti	Ta	Fe	Hf	C	B	Zr	Ni
Astraloy	11.5	15	2.3	5.9	1.7	3.8	3.9	0.75	-	-	0.03	0.02	0.05	Bal
Inconel 706	16	-	-	-	2.9	0.2	1.8	-	40	-	0.03	-	0.03	Bal
Inconel 718	19	-	3	-	5.1	0.5	0.9	-	18.5	-	0.04	-	0.03	Bal
Rene 95	14	8	3.5	3.5	3.5	3.5	2.5	-	-	-	0.15	0.01	0.05	Bal
Rene 104	13.1	18.2	3.8	3.8	1.4	3.5	3.5	2.7	-	-	0.03	0.03	0.05	Bal
RR1000	15	18.5	5	5	1.1	3	3.6	2	-	0.5	0.027	0.015	0.06	Bal
Udimet 500	18	18.5	4	4	-	2.9	2.9	-	-	-	0.08	0.006	0.05	Bal
Udimet 520	19	12	6	6	-	2	3	-	-	-	0.05	0.005	-	Bal
Udimet 700	15	17	5	5	-	4	3.5	-	-	-	0.06	0.03	-	Bal
Udimet 710	18	15	3	3	-	2.5	5	-	-	-	0.07	0.02	-	Bal
Udimet 720	17.9	14.7	3	3	-	2.5	5	-	-	-	0.035	0.033	0.03	Bal
Udimet 720Li	16	15	3	3	-	2.5	5	-	-	-	0.025	0.018	0.05	Bal
Waspaloy	19.5	13.5	4.3	4.3	-	1.3	3	-	-	-	0.08	0.06	-	Bal

Table 2.5.1. The chemical composition of some common turbine disc alloys in wt% [12]

The nickel base superalloy, Waspaloy, was introduced in 1967, and is still used today regardless of its limitations of strength and maximum temperature of use.

Various elements are identified as having particular effects on the chemistry/mechanical property relationships of nickel based superalloys. With particular reference to Udimet 720Li, the elements and their benefits are outlined as follows.

Cobalt (15 - 18.5 wt % range). The presence of 15 wt % cobalt generates a minimum Stacking Fault Energy (SFE) which promotes planar deformation and potentially improved fatigue crack propagation resistance. It has no significant effect on the tensile or creep strength of the alloys.

Chromium levels have been raised to improve fatigue crack propagation resistance without excessive formation of TCP phases. Chromium is also critical for oxidation resistance due to the formation of self healing Cr_2O_3.

Molybdenum has a beneficial effect on tensile strength and ductility at high temperatures, but levels have been controlled to balance the high chromium with respect to TCP phase formation.

Tantalum increases tensile strength, but segregates to form very stable tantalum carbide (MC carbide). The tantalum concentration has been controlled to allow the MC carbide to breakdown and promote the formation of grain boundary carbides.

Titanium, along with aluminium, controls the weight fraction gamma prime, and has the greatest effect on the gamma prime solvus. The titanium content has been increased to balance the reduced tantalum levels in order to maintain tensile strength, whilst also controlling the gamma prime weight fraction and TCP phase formation.

Aluminium has been balanced with respect to titanium in order to control the gamma prime weight fraction. The aluminium concentration has also been limited in order to reduce the propensity for TCP phase formation.

Boron has been reduced to levels which are beneficial to creep, fatigue crack propagation resistance and tensile strength.

Carbon has been maintained at levels to promote hot ductility and high temperature creep resistance.

Zirconium has been increased to 0.06 wt %, as it has a beneficial effect on stress rupture and creep resistance.

Hafnium has been included at 0.75 wt %. The addition of hafnium improves all properties.

Rhenium has a strong beneficial effect on creep resistance.

2.6 Strength Vs Temperature for Nickel Based Superalloys

It is well understood that the strength of most metals decreases with increasing temperature. This is largely due to thermal activation processes, which makes it easier for dislocations to overcome obstacles. However, nickel based superalloys containing γ' are particularly resistant to temperature. Ordinary slip in both γ and γ' occurs on the $\{111\}$ $<110>$. If slip was confined to these planes at all temperatures then the strength would decrease as the temperature is raised. However, there is a tendency for dislocations in γ' to cross-slip on to the $\{100\}$ planes where they have a lower anti-phase domain boundary energy[13]. This is because the energy decreases with temperature. Situations can arise where the extended dislocation is then partly on the close-packed plane and partly on the cube plane. When this occurs, the dislocation becomes locked and increases strength of the superalloy further. The strength only starts to

drop when the temperature goes beyond 600°C, which is when thermal activation processes become active enough to allow dislocations to overcome obstacles.

Hence, it is the presence of γ' which is responsible for the high strength of nickel based superalloys at high temperature.

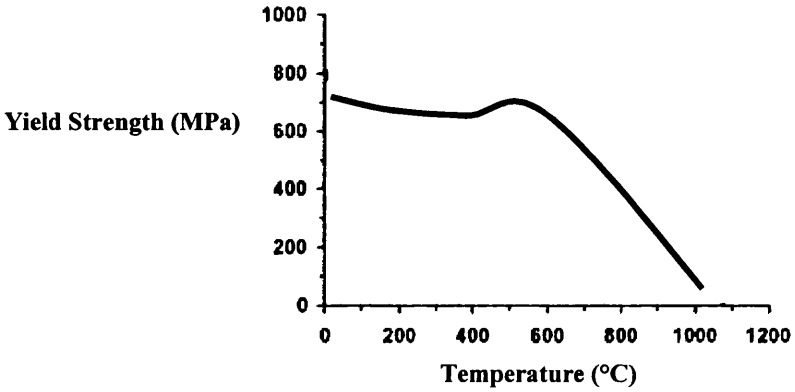

Figure 2.6.1. A theoretical prediction of the yield strength of a particular superalloy containing approximately 20% of γ' against temperature. Notice how the strength is at first insensitive to temperature but starts to drop at around 600°C.

When greater strength is required at lower temperatures (*e.g.* turbine discs), alloys can be strengthened using another phase known as gamma double prime, donated γ''. This phase occurs in Nickel-Iron superalloys, when nickel and niobium combine in the presence of iron to form a body centered tetragonal (BCT) such as Ni_3Nb. This phase, like γ', is coherent with the gamma matrix and imparts large mismatch strains. The strengthening occurs by both a coherency hardening and order hardening mechanism. This provides high strength at low to medium temperature but is unstable at temperatures above 650°C. The γ' phase is shown in Figure 2.6.2, below.

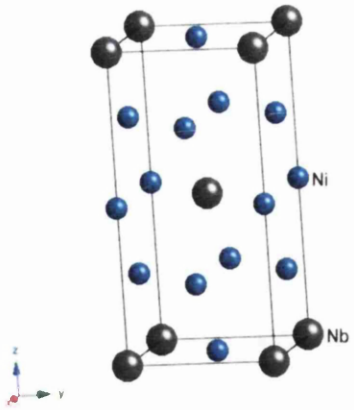

Figure 2.6.2. **Crystal structure of gamma double prime, γ"**

2.7 Manipulating the Composition and Microstructure of Turbine Disc Alloys

An added complexity in turbine discs, which does not apply to single-crystal superalloys, is the existence of grain boundaries, which must be carefully engineered. Hence, a strong appreciation of the relationship between alloy chemistry and microstructure is important if the best possible combination of properties is to be achieved.

According to Roger C. Reed, author of *The Superalloys: Fundamentals and Applications*[14], three guidelines should be adhered to achieve optimum properties in superalloys.

Guideline 1

"To impart strength and fatigue resistance, the fraction of the γ' phase should be optimised by appropriate choice of the γ'-forming elements (Al,Ti and Ta) – placing it in the range 40%-50% - and heat treatments chosen to promote a uniform distribution of γ' particles."

The yield stresses of the turbine disc alloys correlate very strongly with the proportion of strengthening phases γ' and γ'', hence the concentration of elements that promote these phases must be chosen carefully.

Guideline 2

"The grain size should be chosen for the desired combination of yield strength, resistance to fatigue crack initiation (both of which scale inversely with grain size), creep strength and

resistance to fatigue crack growth (which scale directly with it). A size in the range 30μm to 50μm is commonly chosen."

Guideline 3

"When added in small quantities, grain boundary elements such as boron and carbon are beneficial, particularly to the creep and low-cycle fatigue resistances."

2.8 Nickel Superalloy - Udimet 720Li

Udimet 720 was developed in 1986 with enhanced strength, but was found to be unstable (with respect to the formation of deleterious Topologically Close Packed (TCP) phases) and was superseded in 1990 by powder processed Udimet 720Li (low interstitial), an alloy with reduced chromium, carbon and boron. Improvements in cast and wrought (CW) processing techniques led to the introduction of CW Udimet 720Li in 1994[15]. Cast and wrought Udimet 720Li exhibits equivalent properties to those of its powder variant. However, although Udimet 720Li has adequate strength, its resistance to fatigue crack propagation is somewhat lower than Waspaloy, and its maximum operating temperature is limited to approximately 650° C.

More recently, Udimet 720 has been recognized as having outstanding strength and fatigue resistance when used in a fine grain form for turbine disk applications. From a mechanical property standpoint the alloy retains the high strength characteristics of alloys such as P/M alloy Rene 95, but has superior crack growth characteristics. Overall, Udimet 720 has the best combination of mechanical properties in its class of high strength cast/wrought disk alloys and is used in a variety of applications in small- to medium-sized gas turbine engines.

As mentioned previously, there is an alternative process route which is based on Powder Metallurgy (P/M). The key advantages of this process is that it is possible to manufacture parts with a geometry and size close to a near net shape resulting in a reduction in post machining costs. Moreover, the P/M route allows the production of a very homogeneous material, resulting in better defect detection ability by ultrasonic inspection. Nevertheless, this process suffers from other drawbacks such as the possible pollution by ceramic inclusions issued from the powder atomisation which may act as fatigue crack initiation sites, and the formation of precipitates at the Prior Particle Boundaries (PPB). Because of the

presence of small precipitates at the PPB which pin the grain boundaries, one can hardly coarsen the grains by a supersolvus heat treatment and the P/MU720 LI grain size is roughly limited to the average size of the powder particles[16]. The morphology of the gamma prime phase is controlled by way in which it is processed. This can be seen in the images below whereby the cast and wrought route yields a different geometry of gamma prime to the powder metallurgy process. As mentioned previously, the gamma prime phase is what gives these superalloys their exceptional high temperature mechanical properties.

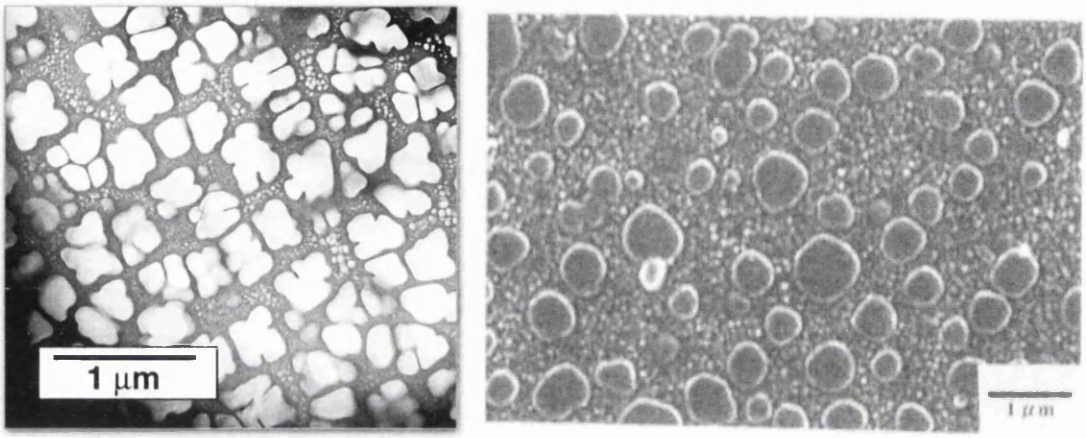

Figure 2.6.3[6]. Gamma prime morphology; Left - Cast and wrought process. Right - Powder metallurgy process.

Because of the fine grained microstructure, the behaviour of P/M U720 is usually not suitable for high temperature applications (>650°C) when good creep and crack propagation resistance are required. The PPBs have also a detrimental effect on the workability of as-HIPed material, and initial attempts to use conventional forging routes were unsuccessful[17]. Therefore, high-cost extrusion processes were developed to ensure the minimum forging ratios imposed for critical applications.

2.9 Introduction to Wear Damage

Tribology (from the Greek word meaning rubbing or attrition) is "The science and technology of interacting surfaces in relative motion, and embraces the studies of friction, wear and lubrication." *I.M. Hutchings, Tribology, 1992, Academic Press*

In the USA, the estimated direct and consequential annual loss to industries due to wear is approximately 1-2% of GDP. (Heinz, 1987). Research into wear is therefore a priority in

order to produce engineered surfaces or palliatives against wear, which extend the working life of materials, thus saving large sums of money and leading to conservation of material, energy and the environment. Methodologies to minimise wear include systematic approaches to diagnose the wear and to prescribe appropriate solutions. Laboratory tests are widely used to simulate the wear behaviour of components in service so that engineers can better understand the factors that affect it.

The word 'wear' is a very broad term for materials that degrade with time but can in fact be broken down into many subcategories. Materials don't have to be in contact in order to wear and can be as simple as being subjected to repeated stress cycles, such as fatigue. Other forms of wear which do involve materials in contact can be difficult to distinguish from each other because of their wear scar similarities although the mechanisms that drive them may not be the same. For example, there are over 50 variables that affect the fretting wear of materials in contact, which makes it very difficult to understand.

Subsurface Fatigue - Subsurface fatigue is a form of wear that occurs when a component is subjected to long-term repeated stress cycles. This causes microcracks in the subsurface of the metal, which then propagate to the surface, resulting in a piece of surface metal being removed. This type of wear does not depend on surface-surface contact.

Surface-initiated Fatigue- This type of wear damage involves components in contact and relative movement of their respective surfaces. It usually begins with a loss of the surface lubricant film. The high points of the bare metal surface, known as asperities, are removed by shearing, which initially appear as a matted or frosted surface. Once removed, the asperities can become oxidised, especially at high temperatures and become much harder than the parent metal. As a consequence, asperities can result in greater wear if they become trapped between the two surfaces.

Microcracks will eventually form on the surfaces and migrate down into the metal, interacting with other microcracks, resulting in fracture.

Temperature can have a considerable effect on the extent of wear damage to metallic components. During reciprocating sliding, under conditions where frictional heating has little impact on surface temperatures, there is generally a transition from severe wear to mild wear after a time of sliding that decreases with increase in ambient temperature. At low

temperatures, from 20-200°C, the layers generally consist of loosely-compacted particles. At higher temperatures, there is an increase in the rates of generation and retention of particles while compaction, sintering and oxidation of the particles in the layers are facilitated, leading to development of hard, very protective oxide 'glaze' surfaces. Oxide glazes are beneficial to components in contact as the friction coefficient in significantly reduced as a result. It has been proposed that an oxide film thickness of 20Å is critical in reducing the tendency of steel surfaces to scuff[18]

2.10 Friction

Contact wear is largely governed by a surface resistive force known as friction. Therefore, to gain a better understanding of wear, the concept of friction must first be understood along with the factors that affect it.

Friction is defined as the resistance to motion when one body is slid over another. Put simply, friction is high if the two materials in contact are rough and low when the materials in contact are smooth.

Universal agreement as to what causes friction does not exist, but is thought to be due to a number of mechanisms that act together contributing in different proportions under different conditions.

The '**Bowden and Tabor Theory**' suggests friction arises from two sources,

a) An adhesive force developed at the real contact areas (asperities)

b) A deformation force needed to plough the asperities of the harder surface through the softer one

The contribution of the adhesive molecular attractions was not taken into consideration until recent times. It was believed that friction was solely caused by surface roughness, but it has been established beyond doubt that the contribution of adhesive forces between two sliding surfaces is a major contributor towards the friction effect. The peripheral molecules of the two surfaces in contact are attracted towards each other, and form adhesive bonds. These bonds need to be snapped for the two surfaces to slide over each other.

Surface roughness is another leading factor resulting in frictional forces that oppose easy motion. Most solid bodies do not have precisely uniform surfaces. Even visibly symmetrical geometries are not regular, and have protrusions as well as cavities. When two surfaces slide over each other, it is extremely likely that the respective protrusions and cavities would interlock amongst themselves, leading to a force that restricts the sliding motion. This was believed to be the sole cause behind friction for many years, but is now regarded as a minor effect as compared to the above mentioned adhesive bond effect.

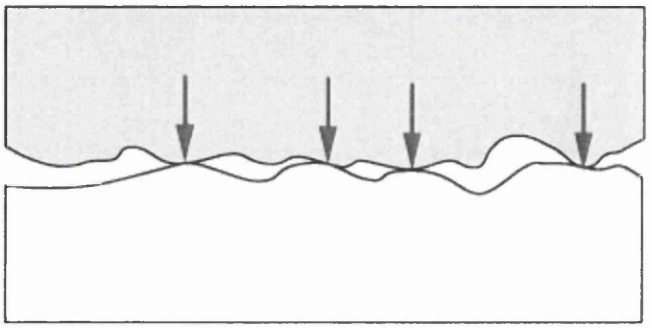

Figure 2.10.1. Actual surface contact. In reality, no surface is 'smooth'

Essentially, the deformation effect is a logical extension of the roughness factor. Soft solid surfaces are prone to getting deformed and compressed upon impact from another relatively hard solid body. In such a case, the harder and more rigid body would sink a little in the depressions caused by the contact. This sinking inhibits the sliding motion of the solid bodies over each other, and has to be overcome for the bodies to continue moving.

Friction can be represented in the equation below:

$$\textit{Frictional Force } (F) = \textit{Coefficient of Friction } (\mu) \times \textit{Normal Force } (P) \qquad (2.9.1)$$

From the equation above, it can be seen that the frictional force depends on the coefficient of friction of each material and the normal load that holds the materials in contact with each other. Every material has a unique coefficient of friction associated with it but also depends on other factors.

In some cases, friction can be useful, as in car breaking systems where high friction between the breaking pads and discs is imperative. However, as the body of this research suggests, it can also be problematic, as in engine components, where are high values of friction leads to wear damage.

2.10.1 Friction Coefficients

The friction coefficient between two surfaces depends on a number of factors:

- The materials involved (and hence the degree of mutual solubility)
- The surface roughness
- The presence of surface films (lubricating oil, grease, oxide films, contaminants)
- The temperature
- The surrounding environment (corrosion)
- Nature of the contact (conforming, non-conforming)
- Which material is static and which is dynamic
- Velocity of sliding

Therefore, it is clear that the friction coefficient is not a unique material property but depends on the conditions.

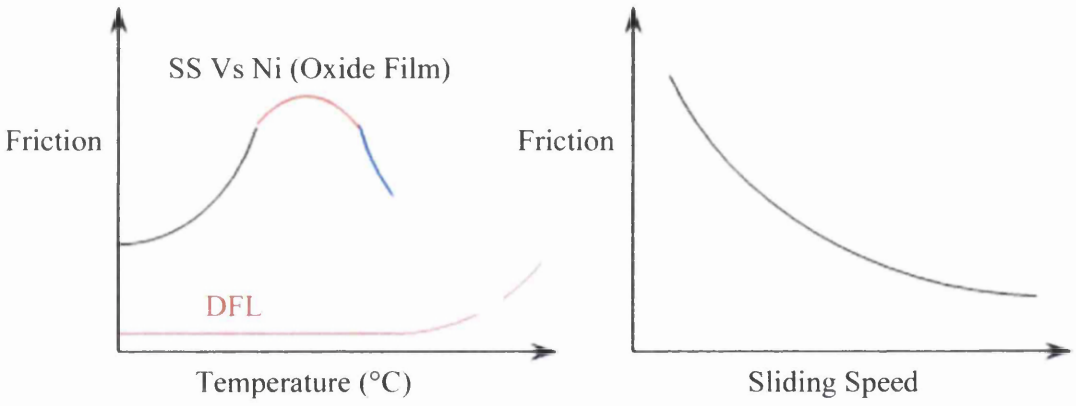

Figure 2.10.1.1 Change in friction with temperature and sliding speed.

2.11 Contact Wear Damage

When two materials are placed in contact with one another and there are small amplitudes of sliding between them, there will be some form of wear damage taking place at their surfaces. The difference between heavy wear and light wear is dependent on the contact load or the friction at the interface, as shown in the following diagram.

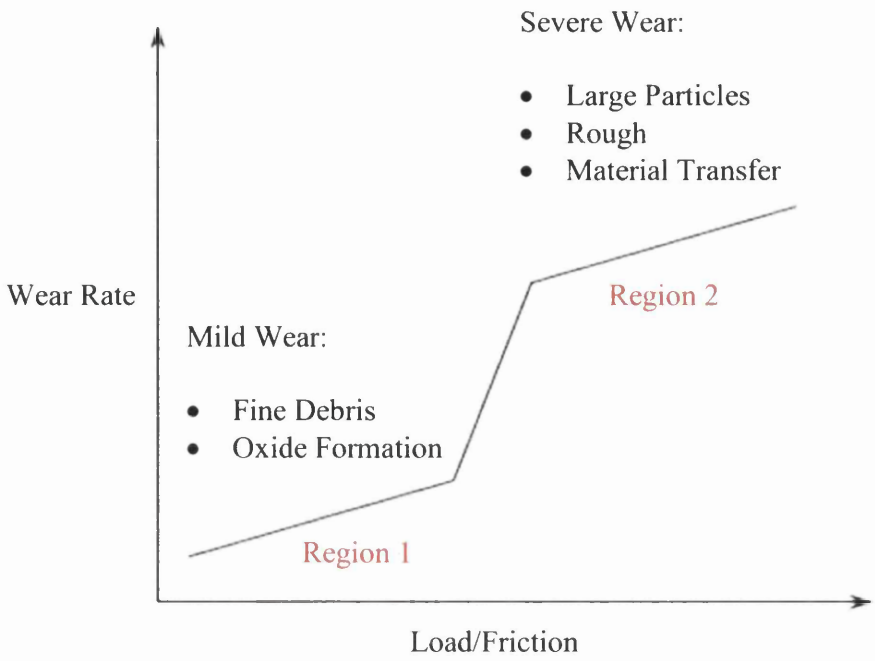

Figure 2.10.1. Ideally, low friction results in low wear but this is specific to one material couple under very specific conditions. Graph courtesy of Rolls-Royce Plc.

Wear is broken down into two subcategories, termed adhesive wear and abrasive wear.

2.11.1 Abrasive Wear

Abrasive wear usually results from particle contamination and roughened surfaces that cause cutting and damage to a mating surface that is in relative motion to the first. Abrasive wear is estimated to be the most common form of wear in lubricated machinery.

Abrasive wear usually proceeds in two ways and is outlined schematically in Figure 2.11.1.1

Three-body abrasion occurs when a relatively hard contaminant (particle of dirt or wear debris) of roughly the same thickness as the lubricant layer becomes trapped between the two metal surfaces, which are in relative motion to each other. When the particle size is greater than the fluid film thickness, scratching, scoring and ploughing can occur. This creates parallel furrows in the direction of motion, like rough sanding. Mild abrasion by fine particles may cause polishing with a satiny, matte or lapped-in appearance. At high temperatures, wear debris can be oxidised and sintered, becoming much harder than the parent material and increasing the wear rate further.

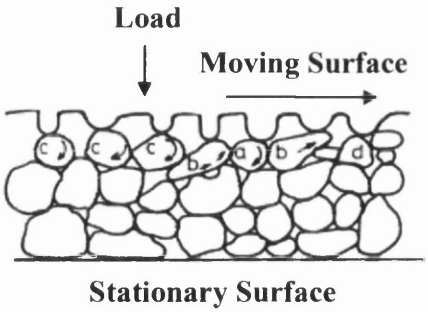

Figure 2.11.1.1. Schematic illustration of the four possible mechanisms for relative motion and escape of debris particles during sliding: (a) rotation, (b) skidding, (c) rolling, (d) entrapment.[19]

Two-body abrasion occurs when metal asperities (surface roughness, peaks) on one surface cut directly into a second metal surface. In this case, contaminant particle are not directly involved. The contact occurs in the boundary lubrication regime due to inadequate lubrication or excessive surface roughness which could have been caused by some other form of wear.

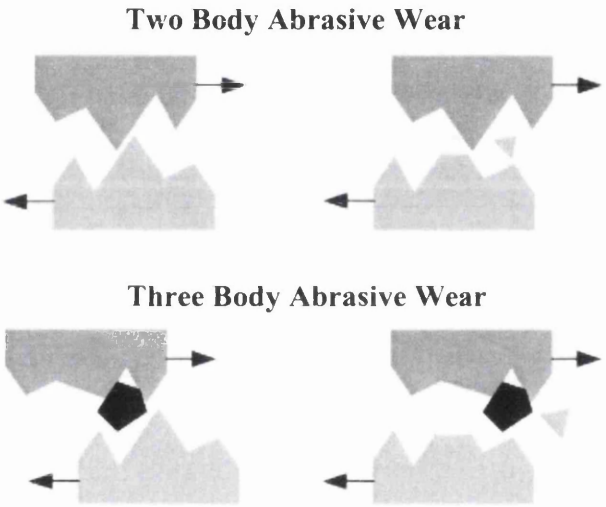

Figure 2.11.1.2. Abrasive wear occurs in sliding contacts usually due to contamination of particles[20].

2.11.2 Adhesive Wear

Adhesive wear is the transfer of material from one contacting surface to another. It occurs when high loads, temperatures or pressures cause the asperities on two contacting metal surfaces, in relative motion, to spot-weld together then immediately tear apart, shearing the metal in small, discrete areas. Although abrasive wear is more common, adhesive wear is arguably the most life limiting.

Adhesive Wear

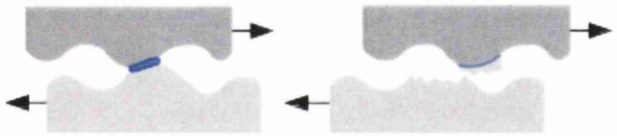

Figure 2.11.2.3. Adhesive wear is a result of micro-junctions due to welding of opposing asperities. Large tangential forces can cause the asperities to shear and break off, becoming entrapped within the surfaces.

Typical examples of adhesive wear include fretting, scuffing and galling and these will be discussed in more detail.

2.12 Fretting Fatigue

Whenever two contacting materials are subjected to a cyclically applied bulk load, the resulting highly localised edge-of-bedding (EoB) contact stresses can lead to a condition called contact fatigue[21]. If the two contacting surfaces have small amplitudes of motion relative to each other, the process is referred to as fretting fatigue. The sharp stress gradients and multi-axial stress state at the contact location can prematurely nucleate cracks resulting in a reduction of overall fatigue life. If the material is subjected to a cyclically applied bulk load, the cracks formed by fretting can grow inwards normal to the free surface, exist in elastic stress fields, hence, resulting in crack propagation and eventual bulk brittle fracture.

It is well understood that the initiation and propagation of fretting cracks are largely determined by the severe stress gradients that are generated from the effective shape of contact, co-efficient of friction and the applied bulk loads[22]. A typical contact problem is shown in Figure 2.12.1, which illustrates the frictional contact between two spheres, first solved by Mindlin[23]. This is an example of *incomplete* contact where the contact area is proportional to the applied load (i.e. spherical, cylindrical, and so called 'flat with rounded edges' contact geometries).

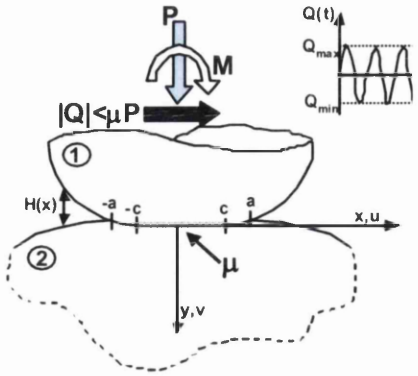

Figure 2.12.1. Schematic of a Mindlin (Spherical) incomplete contact with friction. (Where μ is the coefficient of friction, Q is the tangential force, P is the normal load and M is the centrifugal force.

Blade and disc interactions are particularly difficult to understand due to the complex load histories, complicated geometries, and extreme environments in which they operate. Figure 2.12.2, highlights in red the regions of high stress in a typical blade/disc root.

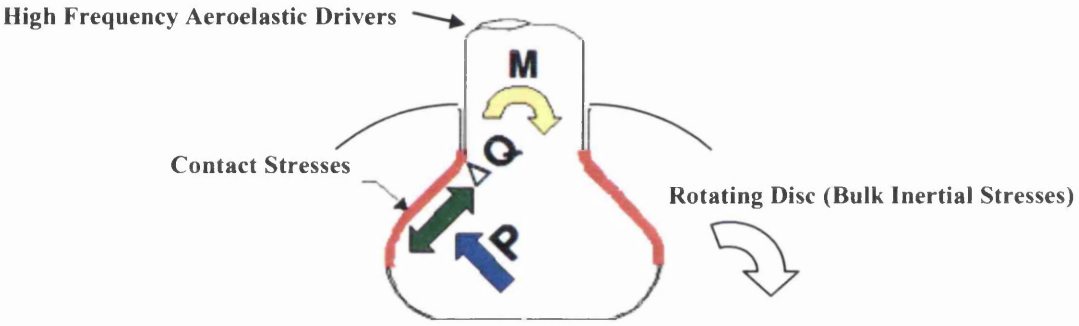

Figure 2.12.2. Schematic of critical locations in a dovetail attachment highlighting each contacting lobe (shown in red).

Fretting between two materials in contact occurs on a range of sliding distances but is considered most detrimental during the partial slip regime, which occurs on a sliding scale of approximately 50μm. For this reason in particular, most components that operate in contact with other materials will usually have their surfaces hardened by processes such as shot-peening or have their surfaces coated with anti-fretting coatings. An added problem in the fretting process is when the eroded material oxidises in air and becomes harder than the parent material. The oxidised debris can get trapped between the two materials in contact and abrade the surface further, increasing the rate of wear.

A synergistic competition between crack formation, corrosion, and wear at the contact interface leads to complex patterns of movement and an evolution of friction that is very difficult to predict. In some rig and engine hardware, these stress gradients have led to surface fissures, near surface micro-cracks, and NDE detected cracks near the EoB[24]. If the stress in the bulk material is sufficiently large, these micro-cracks, nucleated under the influence of the near surface contact stresses, have the potential to propagate by fatigue.

Unlike other forms of wear, the incidence of fretting problems in machinery has not declined over the past decades[25]. Fretting fatigue damage of components has been observed on countless occasions, some even leading to component failure. The biggest cause for concern among engineers is when fretting fatigue occurs in critical group A parts such as turbine and compressor discs that are rotating at thousands of revolutions per minute and contain huge amounts of kinetic energy. As discussed earlier, failure of such components would seriously hazard an aircraft, which is why so much care is taken to produce accurate lifing calculations to ensure that failure never occurs.

2.13 Mechanisms and Fretting Regimes

Whenever there is contact between two materials, coupled with an applied bulk cyclic loading there is an issue with *Contact Fatigue* associated with edge-of-bedding (EoB) contact stresses. Contact fatigue introduces stress raisers to a system and causes the greatest fatigue strength reduction factor (SRF) due to the large multi-axial stresses and sharp stress gradients at the EoB, which drives crack nucleation.

Since, this phenomenon reduces the fatigue life, it is imperative to understand the concept and the broad scope of situations in which it can arise.

2.13.1 Microscopic Movements Between Two Contacts Under Applied Loads

It is well understood that when two solids are pressed together and subjected to a tangential force of increasing magnitude, there is a certain value of tangential force at which macroscopic sliding occurs. Although true, it is less widely realised that micro-movements could occur below this limiting value of tangential force under an applied force. It has been revealed that these micro-movements are a fundamental feature of Hertzian contact subjected

to a tangential force[26]. There are two types of models, which attempt to explain the behavior of such contacts: The 'elastic' model and the 'elasto-plastic' model.

2.13.2 Elastic Model for Fretting Contacts

Under stationary Hertzian contact, the normal stress '**p**' rises smoothly from zero at the contact edges to a maximum at the centre of the contact as shown in Figure 4.4.2.1(a). If the coefficient of friction '**μ**' remains constant across the contact surface, the frictional stress '**μp**' resulting from the normal stress '**p**', also rises smoothly from zero at the edge of contact to a maximum at the centre of contact, as shown in Figure 4.4.2.1(b). When there is no relative movement between any two points on the contacting surfaces there is no fretting damage and the contact is said to be in the stick regime i.e. there is normal traction at the contact interface.

If an external tangential force **Q<μP** is applied to the contact, the resulting tangential stress rises from some arbitrary value at the centre of the contact to an infinite value at the edges as shown in. (b). The distribution of tang[27]ential stress 'q' across a circular contact can be described by Equation 2.12.2.1, where $\mathbf{q_x}$ is the shear stress along the 'x' axis, **a** is the radius of the contact area (m) and **Q** is the superimposed tangential force (N)[28].

$$q_x = \frac{Q}{2\pi a(a^2 - x^2)^{0.5}} \qquad (2.13.2.1)$$

This is illustrated in the diagram below.

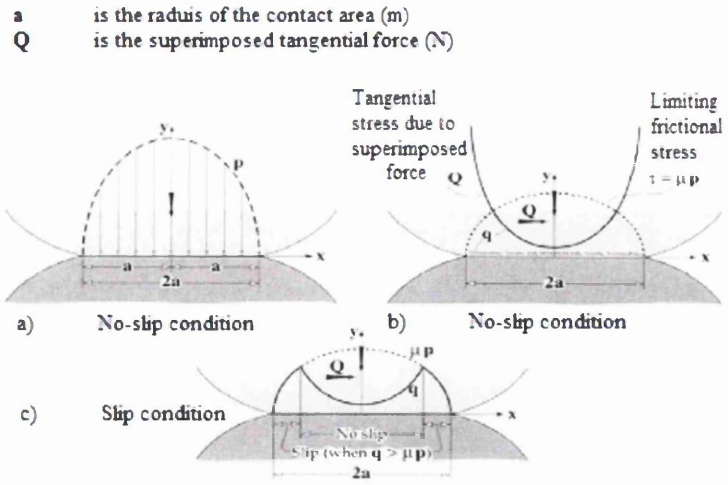

Figure 2.13.2.1 Normal and tangential stress fields for Hertzian contact with and without slip[29].

In the stick regime, the value of tangential stress was determined to be no greater than the sum of the local contact stress and the coefficient of friction. Hence, assuming the normal load, P, is kept constant and the tangential force, Q, is slowly increased from zero, then microslip is seen to occur immediately at the edges of the contact area and spreads inwards until '**Q**' approaches '**μP**'.

When the global tangential load Q, is less than required to produce relative movement over the whole of the contact area **Q<μP**, partial slip fretting fatigue occurs. Partial slip is characterised by a central non-slip region flanked by a ring of small relative movement, termed the slip zone. In general, the relative slip amplitudes associated with this condition of partial slip fretting fatigue are in the order of 1-50μm[16] although this is dependent on the material combination involved. The small relative movement, results in low levels of wear and subsequent oxidation of debris, which serve to increase the wear process as the debris are harder than the parent material.

Mindlin proposed a model for the ratio of the radius of the central non-slipped region to the radius of the contact area, shown in Equation 2.12.2.2, where:

a' is the radius of the central non-slipped region (m)

a is the contact radius (m)

Q is the superimposed tangential force (N)

μ is the coefficient of static friction

P is the normal load acting on the contact (N)

$$\frac{a'}{a} = \left(\frac{1-Q}{\mu P}\right)^{1/3} \qquad (2.12.2.2)$$

This theoretical relationship is in good agreement with experiments conducted with a steel ball oscillating on a glass surface [30] shown in the following schematic.

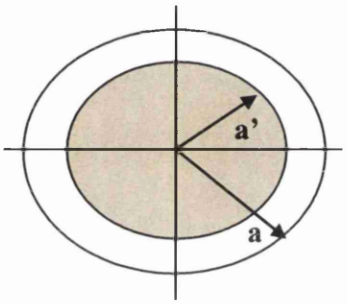

Figure 2.13.2.2 Schematic representation of the partial slip fretting regime. The central non-slip zone is denoted a' and the outer slip region, a-a'.

The large stress gradients produced at the edge-of-bedding can result in premature crack nucleation. In partial slip, the initiation of these cracks occurs at the stick-slip interface. If the tangential load, Q is increased further, the ring of partial slip grows towards the centre and the peak shear stress max, $\mathbf{q}_{x,\,also}$ increases. As a result, the fatigue strength reduction factor (SRF) also increases and the fatigue life is thus reduced. It is logical to suggest then, that the greatest reduction in fatigue life occurs at the transition between partial and gross slip ($Q \geq \mu P$) fretting regimes because it is at this point where the max $\mathbf{q}_x$ is at its highest value.

If 'Q' is increased beyond 'μP' the contact will begin to slide and gross slip can occur. In general, the relative slip amplitudes associated with this condition of gross slip fretting fatigue are in the order of 50-200μm. In this regime, the sliding distance is large enough to slide over the whole contact surface and the wear rate increases at a greater rate due to the entrapment of debris. Although the subsurface material sees large peak stresses at the EoB, the increased wear rate effectively removes premature crack initiations as debris that would

otherwise have propagated as bulk fatigue cracks[16]. This effect accounts for the increase in fatigue life observed as the relative sliding distance increases away from the partial slip fretting fatigue regime.

The appearance of the gross slip regime is a complete slip zone with no central non-slipped region. A real life comparison of the partial slip and gross slip fretting regimes is shown in Figure 2.13.2.3.

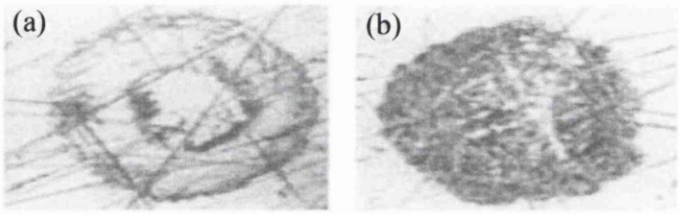

Figure 2.13.2.3. Comparison of (a) partial slip and (b) gross slip fretting regimes as a result of increasing the sliding distance between contacts (adapted from[31]).

If the global tangential load is greater than required to produce full sliding across the whole contact ($Q>>\mu P$), reciprocating sliding occurs. At this point, Q is no longer directly related to the relative slip between the two bodies. It differs from gross sliding, since the relative movement is large enough that every point of the wear surface comes out of contact during some point of the cycle, so that effectively, no debris are entrapped. Wear rates remain high but are constant with increasing slip amplitude.

To determine what fretting regime will occur with respect to its slip amplitude, refer to Figure 2.12.2.4, which shows a simplistic relationship between wear coefficients and slip amplitude with its corresponding fretting regime and fatigue life.

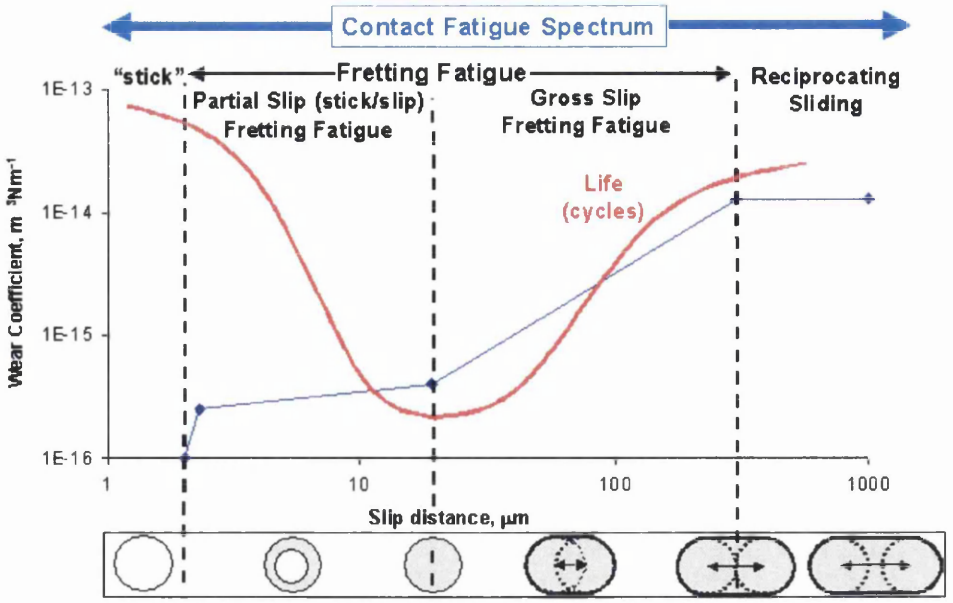

Figure 2.13.2.4 Fretting regimes corresponding to the value of slip amplitude[13].

For the notice of the reader, fretting fatigue is a highly debatable topic and it is important to realise that some academic work has defined fretting fatigue as only occurring in the partial slip (or stick/slip) regime and not after gross slip across the contact occurs. For this reason, the definitions used above are adopted by Rolls-Royce and may differ to those defined in other literature. The boundary between these regimes is material-specific, and should therefore be obtained experimentally for each material combination. Each regime will have a unique impact on the fatigue life, and so it becomes paramount to not only understand where the boundaries lie for the materials, but to also know where on this graph the component in question operates. From experimental investigations to date, there is strong evidence to suggest that a location close to the transition region between partial slip and gross slip fretting fatigue results in the most pronounced reduction in fatigue life as illustrated in

Figure 2.13.2.4 by the minimum on the red curve and is approximately 50µm.

2.13.3 Elasto-Plastic Model for Fretting Contacts

The 'elasto-plastic' model offers a more realistic explanation. It assumes that the asperities in the central non-slip zone deform elastically, surrounded by a zone in which the asperities have undergone slight plastic yielding, but have not undergone fracture. The plastic zone is then flanked by a slip zone, where the asperities have been subjected to fracture, as in the

case of the elastic model. Hence, the 'elasto-plastic' describes a constant gradient to final fracture, unlike the 'elastic-model', where the stress gradient is sharp at the interface between the stick and slip zone. The elasto-plastic wear morphology is evident in Figure 2.13.2.3, shown previously.

2.14 Initiation and Propagation of Fretting Fatigue Cracks

Fretting fatigue affects the initiation and propagation of cracks. In essence, the propagation of cracks is no different from plain fatigue, although there are some differences such as non-proportional loading, multiaxial stress states, variable R-ratio and high stress gradients. Therefore there has been much interest in recent years in the initiation of fretting cracks with question being raised such as is there an initiation threshold? What role does surface damage play? Is there a special fretting effect or is it just a sharp stress concentration? Finally can we predict initiation life?

The fatigue process can be roughly divided into three stages: cyclic hardening/softening, crack initiation, and crack propagation leading to final fracture. In flaw-free materials a significant fraction of the total lifetime is spent before the first detectable microcracks appear. At low amplitudes the initiation stage can occupy even the majority of the lifetime. At high amplitudes the initiation is usually accomplished within a small fraction of the fatigue life. Furthermore, the fatigue limit can be reduced by up to about 40% if fretting damage occurs in the contact area, since fretting damage accelerates the initiation of cracks.

Another fraction of the lifetime is needed for the propagation of the microstructurally small cracks to reach the size of the physically small cracks (i.e., cracks of the size about 0.1±1 mm). Propagation of physically small cracks and macrocracks (i.e., cracks of the size of the order of millimetres and more) can be quantitatively described by means of fracture mechanics. On the other hand, there is no generally accepted quantitative description of the initiation process and there is no widely applicable description of the propagation of the microstructurally small cracks. Thus, any numerical analysis of the initiation of microcracks and following propagation of microstructurally small cracks must be preceded by deeper understanding of physical mechanisms.

Direct observations of surfaces have shown that there are three types of initiation sites: (i) Initiation at fatigue slip bands (ii) Initiation at grain boundaries and (iii) Initiation at surface inclusions.

When fretting occurs the surface of the material becomes deformed, which causes the dislocations to shuffle around and slide over one another along slip planes in order to accommodate the induced plastic strain. When this occurs, the dislocation density builds up and becomes intensified in this area, shifting material and forming structures known as persistent slip bands (PSB). PSBs are areas that rise above (extrusion) or fall below (intrusion) the surface of the component. This leaves tiny steps in the surface that serve as stress raisers where fatigue cracks initiate from. A crack at the edge of a PSB taken with a scanning electron microscope is shown in the following image:

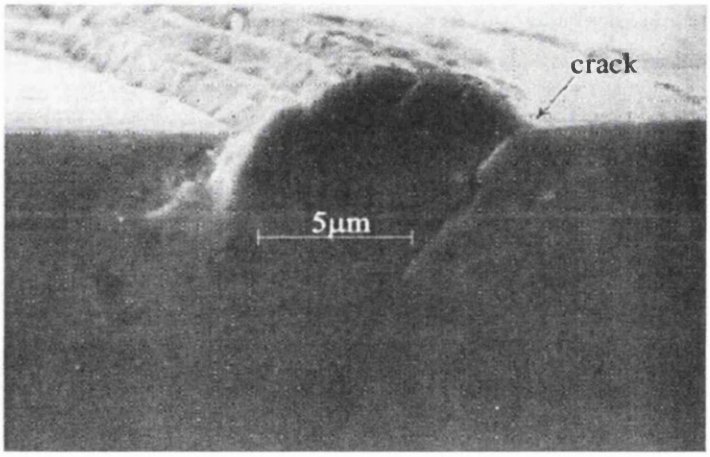

Figure 2.13.1. A crack at the edge of a PSB. (Suresh 1991) [32]

Once a crack is formed, the life of the material is shortened dramatically. The stress intensity is large and a plastic zone develops at the tip of the crack. As the applied load increases, the plastic zone increases in size until the crack grows and the material behind the crack tip unloads. The crack will eventually be large enough to cause catastrophic failure of the material.

2.15 Application to Engine Hardware

It is important to consider fretting fatigue during normal engine running. Up to now, only the effect of contact force and sliding distance on fretting fatigue has been discussed. In actual

engine hardware, the operating environment, mission history, evolution of friction and bulk stresses arising from three-dimensional geometry and rotating inertial stresses, result in a complex evolution of stick and slip at the contact interface. Consequently, this history-dependant stick/slip interface behaviour affects the resulting near surface stress and life of contacting components.

2.15.1 Effect of Environment and Temperature

The effect of environment and temperature can be both beneficial and detrimental to the fretting process in engine hardware. In a reduced atmosphere, wear debris have limited oxygen with which to oxidise in. For some metals, this can be favourable, if the oxide debris acts as an abrasive between the contact surfaces. For others, however, oxidation is essential to creating an oxide film that protects the surface from further wear. For example, Ni alloys form a Ni-oxide 'glaze' layer above 250°C, which becomes relatively self-healing, and therefore more stable, above 400°C. In vacuum, this glaze layer cannot form, and so the base material continues to wear[33]. This research is will touch upon the impact of glaze on the fretting fatigue life of U720Li. It is hypothesised that the presence of a glaze will reduce the SRF.

2.15.2 Effect of Bulk Stress

In addition to the stresses due to contact, the engine spool-up and operational loads (as well as variation in operating temperatures) generate a significant bulk stress in the subsurface material. These bulk stresses can result in the development of relative slip at the contact interface. Figure 2.15.2.1a illustrates a condition of symmetric slip, which results from a cylindrical punch held against a flat body with a symmetrically applied bulk load.

Note that Figure 2.15.2.1b illustrates the shear traction, q(x), that results from the application of the bulk stress, σ_o according to the geometry and loading conditions of Figure 2.15.2.1a. This figure illustrates that as the subsurface material is pulled out from under the punch, slip to the left of the centre of contact ($a<0$) is sliding in one direction where as slip to the right of the centre of contact ($a>0$) is in the opposite direction. This phenomenon has been called symmetric slip. Symmetric slip manifests itself in the signs (or direction) of the shear traction being opposite. It is important to note that Figure 2.15.2.1 only shows a bulk stress in one body. In practice, a bulk stress exists in both contacting bodies and can also influence the

contact tractions. This shear traction behaviour must also be accounted for in the case of complicated load histories.

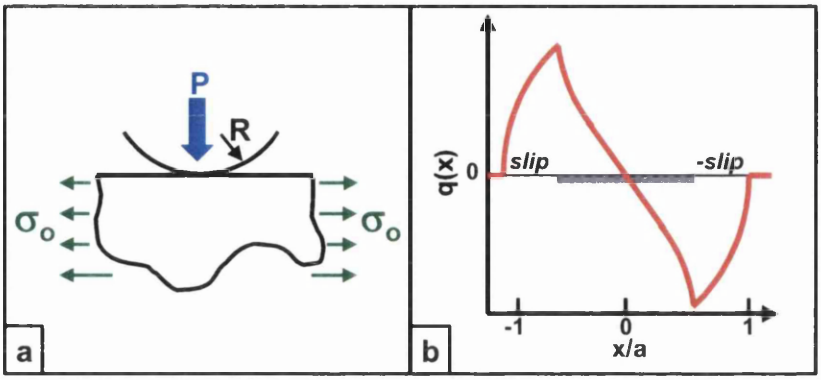

Figure 2.15.2.1. (a) Contact involving round punch on flat body subjected to a subsurface bulk stress. (b) Representative plot illustrating contact shear traction and symmetric slip that occurs due to applied bulk stress, σ_o.

2.15.3 Effect of Mission History

In aircraft engines, complex cycles lead to operation in various relative movement regimes associated with the defined contact fatigue zones. For example, engine dovetail and firtree attachments can see the full range of fretting fatigue contact at various times within the flight cycle. The duration spent in each relative movement regime (partial slip and gross slip fretting fatigue) is mission and engine dependent. Since the life is dependent on the contact fatigue regime of operation, it therefore becomes necessary to determine the regime(s) in which each engine operates and the approximate duration that the flight cycle spends in each regime.

2.16 Methods of Controlling Fretting

Fretting can be efficiently controlled through design optimisation (e.g. geometry changes) and through the applications of surface treatments such as coatings and shot peening.

2.16.1 Design Optimisation

The control of fretting by design optimisation entails geometric modifications of components aimed at mitigating excessive shear stress concentrations at the interface.

The geometry of the contacting bodies can have significant influences on the near surface stresses as illustrated in Figure 2.16.1.1. Given certain restraints, for two components in contact, reducing the radius and increasing the flat length may allow a larger area of contact over which to distribute the contact loads. However, a sharp radius can lead to excessively high EoB stresses and consequently, a reduction in life. The illustration in Figure 2.16.1.1 suggests there is an optimum geometry under given constraints that will result in the best contact fatigue performance. In general, larger edge radii are desirable. However, in the case of design optimistaion, there is a compromise between reduction of strength caused by the larger edge radii and relief from fretting[20].

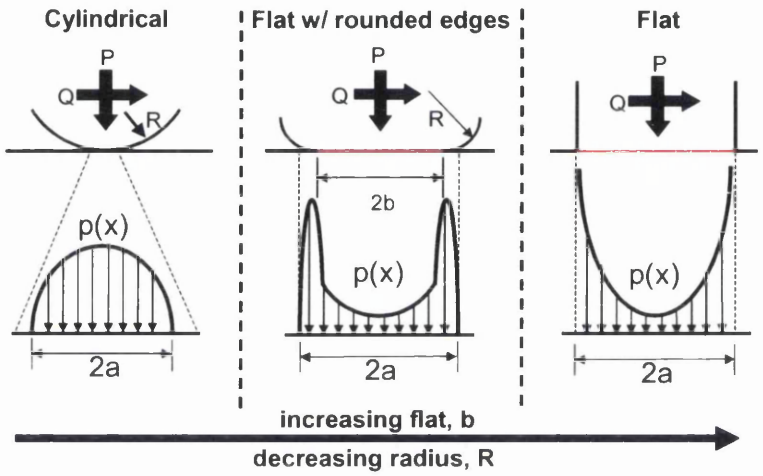

Figure 2.16.1.1. Schematic of contact normal tractions that develop when a normal load is applied to a cylindrical geometry (left), a flat with rounded edges geometry (centre), and a flat-punch, or *complete contact*, geometry (right)[13].

For the blade/disc contact problems, internal discussions have also taken place to insert cut-outs in the blade roots at the edge of bedding contact zone to relieve the overwhelming stress concentrations in this region.

2.16.2 Lubrication and Anti-Fretting Coatings

Fretting fatigue cracks tend to occur at the boundary between fretted and non-fretted regions where shear stresses are sufficiently high[20]. A reduction in fatigue strength due to fretting can be best estimated from the following equation, noting how the fatigue strength is lower for high coefficients of friction[34]:

$$S_{fr} = S_o - 2\mu p_o\left[1 - e^{(-1/k)}\right] \qquad (2.15.2.1)$$

Where:

S_{fr} is the fretting fatigue strength (MPa)

S_o is the fatigue strength in the absence of fretting (MPa)

μ is the coefficient of friction

p_o is the contact pressure (MPa)

l is the fretting amplitude (μm)

It can be seen from Equation 2.15.2.1 that by reducing the coefficient of friction between contacting surfaces, higher fatigue strengths can be gained. Application of lubrications and coatings to the surfaces is one way of achieving this.

The basic principle of lubricants and coatings is to cover the fretting surfaces with a non-metallic layer which suppresses adhesion and stops the oxidation caused by fretting of plain metal surfaces. The lubricants will separate the contact surfaces by generating a fluid film and will reduce the coefficient of friction in almost every case. The lubrication will reduce fretting wear by manipulating the fretting process, so that the sliding distance is increased above the partial slip sliding regime. The purpose of using lubrication is to keep the sliding distances in the gross slip regime or indeed the reciprocating sliding regime, which will tend to reduce the large complex stresses associated with partial slip fretting fatigue and edge of bedding effects. Fretting in turbine engine dovetail blade/disk contact surfaces is commonly reduced by using inorganic substances such Molybdenum Disulphide (MoS_2) dry film lubricant (DFL).[35]

Titanium carbides, chromium nitrides and copper nickel indium (Cu-Ni-In) anti-fretting coatings are currently the most common coatings used for aerospace components. The coatings behave as soft metallic films, keeping the substrate surfaces from coming into contact and dissipating vibrational energy by intra-coating shear mechanisms. However, in the case of Cu-Ni-In, at temperatures above about 1000°F (538°C), accelerated oxidation will

rapidly deteriorate the coatings, allowing the substrate surfaces to come into contact and fret[36].

There are a variety of methods used for applying the coatings to components. These include: thermal spray, plasma spray, CVD (chemical vapor deposition), PVD (physical vapor deposition), and IBED (ion beam enhanced deposition). The major disadvantage of anti-fretting coatings is that the component performance depends upon the integrity of the coating/lubricant system during service. Continuous rubbing at the contact surface during operation tends to remove the lubricant and wear away the coating, eventually exposing the base metal to fretting damage. Furthermore, the performance of the coating depends heavily on the process in which they are applied. For example, plasma nitriding appears to be a good treatment in elevating the fretting fatigue resistance of stainless steels. The nitriding temperature of 520°C was found to be most effective in achieving a coating with good fretting fatigue resistance. A coating produced at a lower temperature of 400°C was less effective.

2.16.3 Surface Treatments

A new approach to mitigate fretting fatigue damage has emerged through the use of surface treatment processes that impose deep compressive residual stresses. For example, shot peening is the most popular method and involves impacting a surface with shot (round metallic, glass or ceramic particles) with force sufficient to create plastic deformation. Plastic deformation induces a residual compressive stress in a peened surface, along with tensile stress in the interior. Surface compressive stresses confer resistance to fretting fatigue by creating a hetrzian stress field which acts to pin dislocations by increasing the stress required for a dislocations to slip along its plane. The tensile stresses deep in the part are not as problematic as tensile stresses on the surface because cracks are less likely to start in the interior. [37]Several methods, including shot peening, laser shock peening (LSP), and low plasticity burnishing (LPB) work in a similar way.

2.16.4 Surface Finish and Material Properties

It is important to note that 'manipulating hardness is found to be an unreliable means of improving fretting resistance[20]. For example, fretting studies of alloyed steel surfaces revealed that hardness has no direct relation to the level of fretting wear[38]. In some cases, if a

hard and soft material is fretted against each other, the harder material can be worn as well as the softer one. For example, aluminium alloy A357, is a non-ferrous alloy that is softer than 52100 bearing steel. When this alloy is fretted against a steel ball, there is an initial adhesion of aluminium alloy to the steel surface. If the fretting between these materials occurs in open air then the aluminium wear debris eventually oxidises to form aluminium oxide. Since aluminium oxide debris are harder than steel, the oxidised debris is able to abrade the steel ball.

"It is commonly known that a good surface finish accentuates damage due to fretting and to minimise the damage rough surfaces are preferred. At elevated temperatures as in the disc/blade root, the converse is true, i.e. surfaces with better surface finish suffer less damage than rough surfaces"[39]

2.17 Numerical Methods for Fretting Fatigue Life Predictions

The numerical methods used for fretting fatigue life predictions are many and varied. A large number of them are based on the blade /disc attachments where complex multiaxial stresses and friction are very difficult to predict.

Current life prediction efforts are aimed at using specimen test results directly with a simple scaling from a frictionless model. Recent work has shown that modelling with friction predicts failure locations in sub-element tests better than the frictionless model. Based on these observations, 3D friction modelling is likely to show that geometric skew effects significantly impact stresses. This necessitates the development of more robust methods capable of capturing 3D and history dependent frictional effects for the engine. In order to illustrate the plan for implementation and development of the chosen 2D/3D hybrid contact fatigue lifing tool, the following comments will assume geometry and loading representative of gas turbine engine blade attachments.

As illustrated in Figure 2.16.1, the damage due to frictional contact accumulates because of:

- Wear and high stress gradients on the contact interface / wear patch near the EoB
- Sharp gradient, multi-axial stresses due to contact and bulk stresses just below the contact surface, and in the case of engine attachments

- Stress concentrations arising from notch (or bulk) stresses influenced by the presence of frictional loading (illustrated in Figure 2.16.1c)

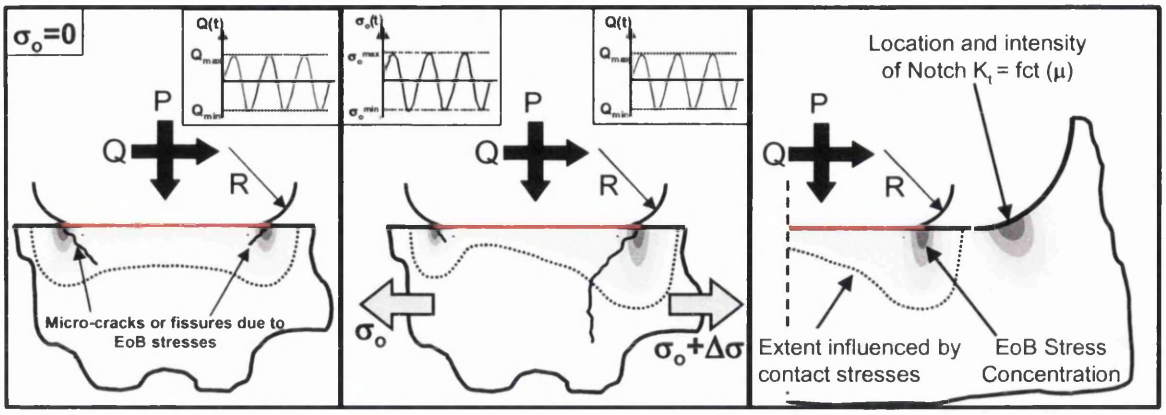

Figure 2.16.1: Illustration of damage due to contact and notch stresses for different contact fatigue configurations. (a) Contact fatigue due to pure contact loading as seen in button-on-plate tests where no bulk stress is present to propagate fissures or micro-cracks nucleated by contact stresses. (b) Contact fatigue due to combined contact and bulk stresses as seen in in-line fretting fatigue test rigs. Note that while under the influence of highly multi-axial contact stresses, cracks grow at an angle to the surface. Once the crack grows beyond the influence of the contact stresses, it grows perpendicular to the direction of applied bulk stress. (c) Contact fatigue due to interaction of EoB stress concentration and frictionally modified notch stresses as seen in engine blade/disc attachments (dovetails, firtrees) [16].

Therefore, in order to assess mechanical integrity of the blade/disc joint, both conventional fatigue outside the contact region and fretting fatigue at the EoB must be characterised. To address conventional fatigue, finite element analysis will be used to determine the stresses in the attachment notch region. The analysis will include the effects of friction which tend to shift the position and magnitude of the peak stress. The effects of creep and plasticity may also need to be accounted for in the notch analysis.

In order to address the fretting fatigue issue, the localised EoB stresses must also be determined. There are currently no well established methods for determining such stresses in a high temperature, multiaxially loaded component. It is proposed that a three level approach is adopted: (Sourced from[13])

Level 1 involves the use of a coarse 3D FE model of the full attachment in order to determine lobe load distributions. This is likely to include material non-linearity as well as frictional effects.

Level 2 is a more refined submodel of the first level model aimed at resolving frictionally modified notch stress behaviour and magnitude for a specific lobe. This may include material non-linearity.

Level 3 is likely to be a quasi-analytical approach which may require further FE submodelling to resolve the EoB stresses. This level of stress resolution is likely to require an extension of existing SIE and/or bounded asymptote methods currently employed for analysing EoB stresses for simplified contact conditions.

If the coefficient of friction is sufficiently low, it may be possible to treat the EoB stress concentration and the frictionally modified notch stress concentration separately. However, as the coefficient of friction increases, the stress concentration initially located in the notch approaches the EoB stress concentration and the two can superpose to result in a significant decrease of contact fatigue life.

2.17.1 Contact Fatigue Analysis

Despite the complexity of the contact fatigue problem, current research and experience have led to the development of several contact fatigue analysis and modelling schemes. Before a mechanics based assessment of contact fatigue life parameters can be performed, an appropriate contact stress analysis method capable of resolving the EoB stress concentrations, relative motion and sharp stress gradients must be developed. These stress analysis methods generally fall into four categories: (1) numerical analyses (finite element (FE) modelling, FE submodelling, boundary element (BE) modelling), (2) Analytical Methods (2D half-plane and 3D half-space solutions), (3) asymptotic analyses (crack analogue, bounded asymptotes), and (4) hybrid methods that combine the computational efficiency of 2D quasi-analytic methods with 3D FE modelling to capture out-of-plane effects.

The modeling department associated with solid mechanics in the university technology centre (UTC) at Oxford University is developing a bounded asymptote approach. Although there has been some promising results for lifing correlations thus far, further work is required so that this method can be implemented into lifing prediction methods.

2.17.2 Finite Element (FE) Modelling

In finite element modelling techniques[40,41] the structure of interest is separated into an assembly of solid elements (termed finite elements) each of which have a stiffness relation. When taken collectively, the applied boundary conditions can be used with equilibrium and compatibility requirements to iteratively solve for the displacements, stresses, and strains within the body. The accuracy of the solution then depends on the complexity and number of elements used to model the domain of interest. Since an infinite number of elements would be required to get the exact solution, FE is classified as an approximate method.

Even though computational power continues to advance at a rapid pace, any stress analyst employing a finite element (FE) code for contact stress solutions must be conscious of the extremely fine mesh required for resolving EoB stress peaks and stress gradients related with contact and fretting fatigue. The computational demand and convergence difficulties increase further when solving three-dimensional problems. It therefore becomes important to identify the FE mesh resolution required to capture the EoB stresses that drive the nucleation of micro-cracks and determine if the resulting model will be prohibitively large.

Rolls Royce has employed FE technology via the use of the commercially available FE code ABAQUS and a computationally efficient in-house FE code, SC03, developed specifically for static and dynamic stress analysis of gas turbine engine components. Previously, SC03 has been used for modelling contact in engine attachments. However, SC03 does not currently allow for inclusion of frictional effects and truncates the contact geometry to result in sharp corners at the EoB. As a result, SC03 cannot capture changes in contact area with applied normal load as seen in incomplete contacts. FE modelling efforts that have required frictional contact solutions have usually been employed in ABAQUS.

2.17.3 Boundary Element (BE) Modelling

Boundary element modelling[42,43] in principle serves to convert the domain equations defined throughout a body into equations defined around the periphery of the component. The advantage of this method over FE modelling is in its ability to capture the stress solution within the body from a mesh only defined on the body's surface. Hence, meshing

geometry is significantly easier. The disadvantage in this approach is that the mathematical formulation of each surface element becomes significantly more complex. Although BE is currently primarily suited for linear elastic solutions, the data to define the model and the output results are concise and concentrated at the boundary where most stress concentrations occur. As a result, the file storage requirements are modest, boundary conditions are easier to apply, and, therefore, greater compatibility with CAD generated data. FE still remains a superior candidate due to its ability to handle non-linear problems, well-established procedures and developed software (commercially and in-house), as well as its ability to produces full information throughout the defined domain.

2.17.4 FE Submodelling

To alleviate the computational expense associated with solving a frictional contact problem for an entire engine component, some stress investigations have exploited the FE method[44,45,46,47] to form a different method known as submodelling. In submodelling, a smaller, appropriately refined mesh (submodel) local to the contact can be used to get converged stresses in the area of interest by applying displacement boundary conditions interpolated from a larger global model of the contacting component. This submodel method takes advantage of the fact that stresses and displacements away from highly stressed regions converge at a faster rate. Hence, a global (coarse) model of the blade and disc competent of modelling the service engine load and boundary conditions is first constructed. The global model mesh is refined until displacement convergence occurs at the boundary of a smaller, more localised submodel defined in the identified region of stress concentration to be analysed.

The submodelling process employed for the frictional contact problem in dovetail attachments of turbomachinery has been investigated for two[36] and three[37] dimensions. Submodelling has also been used to discover the partial slip contact stress behaviour for contact between a polycrystalline nickel sphere and single crystal nickel specimen[38]. Thus, using a suitably defined coefficient of friction and sufficiently refined submodel, this technique is able to model relative slip, tractions, stress characteristics of contact problems and fretting fatigue.

2.17.5 FE Super-Elements

The use of super-elements in the contact problem has been investigated by the Nottingham University UTC and was based on the spline fretting fatigue research effort. It was found that the computational expense (length of time) required to solve the contact problem with super-elements was greater than the time required to solve the contact problem with conventional FE elements.

2.18 Analytical and Quasi-Analytical Methods

2.18.1 2D Half-Plane Methods (Singular Integral Equations)

Initially, the closed-form contact stress solutions were for a frictionless, isotropic, similar material contact of a general Hertzian configuration including plane, axisymmetric, and general second order geometries. Interestingly, for the Hertzian configuration, research shows that with the existence of friction, the shear traction associated with partial slip due to a monotonically increasing tangential load can be found as the superposition of two shear tractions: one which gives gross sliding over the whole of the contact, and another that restores stick over a central region[15]. Many of the devised half-plane solutions have been aimed at capturing the stresses arising from this partial slip solution since model sizes of equivalently fine FE solutions become computationally time consuming and prohibitive.

The problem of contact between half-spaces has been analysed by a number of researchers for specific geometries. Jager[48] presented a general solution for half-space contact modelling in the form of a set of singular integral equations (SIE) for contact of polynomial surfaces subjected to combined normal and tangential loading. Oxford developed a numerical method for analysing contact stresses arising from complex loading histories including the bulk stress effect using quadratic programming[49]. Murthy et al.[50] solved the more general problem of combined normal, tangential, and moment loading on a 2D plane strain, similar material contact between two arbitrary shapes sufficiently flat in the area of contact. The solution involved evaluating the SIEs with a computationally

efficient Fourier transform approach while accounting for bulk stress effects on tractions. Experimental results are consistent with these efficient calculations[51].

Contact of dissimilar materials was initially investigated by Spence [52] and was revisited by Nowell[53] who developed partial slip solutions for the two-dimensional case. Rajeev[54] developed a contact solution for dissimilar bodies undergoing normal, tangential, and moment loading of varying load histories. This was achieved by first observing that the Stroh formalism can be used to obtain Green's function for the surface displacements of an anisotropic half-space subjected to a line load[55]. It is important to note that when analysing anisotropic or orthotropic material contacts in which the orientation of the material principal axes are arbitrary, application of in-plane loading on half-planes could produce out-of-plane displacement. This in turn could produce relative slip and therefore a shear traction in the out-of-plane direction at the contact interface. To simplify this problem, Rajeev's solution assumes an 'anisotropic coefficient of friction' such that the friction in the out-of-plane direction was equal to zero. Without this assumption, three coupled singular integral equations would need to be solved to obtain the contact tractions.

Hills et al.[56,57,58] have provided several good reviews of known and potential solutions capable of capturing partial slip contact behaviour. Most of these solutions have been solved for the case when the contact problem can be reduced to two-dimensions (a half-space). In many cases, however, complex 3D geometry and material behaviour necessitates the development of 3D contact modelling methods to accurately capture the out-of-plane displacements and stresses associated with such problems.

2.18.2 3D Half-Space Methods

For evaluating stresses for a three-dimensional frictional contact between a sphere and half-space of similar material, closed-form equations have been generated[59,60]. Hills, Nowell, and Sackfield provide an excellent survey of the partial slip contact solutions as well as subsurface stress solutions for axisymmetric contacts of similar, isotropic materials [50]. Later, these solutions were extended to dissimilar, isotropic materials for the full-sliding, three-dimensional[61] and partial slip, axisymmetric cases[62]. These approaches provided solutions arising from a normal load and tangential load only. As the complexity

of the problem increases (e.g. geometry, different material contacts, anisotropic material behaviour, etc.), analytical solutions become sparse.

Hills, Nowell and Sackfield can be quoted saying that for analytical solutions, "...the inescapable fact is that three-dimensional problems cannot be solved without re-course to the theory of potentials[50] ". The displacements for the problem of a concentrated load on an anisotropic, 3D half-space have not been found analytically. Therefore, it is unlikely to expect the development of a complete analytical solution to the anisotropic contact problem without employing numerical methods. Pragmatically, this has required the use of numerical solution procedures like FE or BE when solving problems of complex 3D geometries that have anisotropic and/or dissimilar materials in contact.

2.19 Asymptotic Analyses

2.19.1 Crack Analogue

The crack analogue method [63,64] derives a relationship between the stress field close to the edge-of-bedding and the tip of an elastic crack. The correlation can be clearly seen by recalling the pressure distribution for a flat rigid punch (with sharp corners) resting on a half-plane as given by:

$$p(x) \Rightarrow \frac{P}{\pi\sqrt{a^2 - x^2}} \tag{2.19.1.1}$$

Taking an asymptotic expansion of the above using a coordinate r = x + a to give for the left side:

$$p(x) \Rightarrow -\sigma_{yy} \rightarrow \frac{P}{\pi\sqrt{2ar}} \tag{2.19.1.2}$$

Where $x = 0$ lies at the centre of contact, P is the normal load, $p(x)$ is the contact pressure as a function of x, and a is the contact half-width.

The only downside to this method is that it is restricted with regards to geometry.

2.19.2 Notch Analogue

Notch analogies[55] derive a correlation between the stress field close to the EoB and the root of a notch. If the most highly stressed point is at the EoB and the contact is incomplete, the normal and shear tractions go to zero leaving only the stress parallel to the surface non-zero. Hence, the stress state at the point of crack initiation is uniaxial, or close to it. This suggests that the complexity of multi-axial parameters may be unnecessary in some circumstances. Note that the notch stress gradients are not as high as in EoB contact problems. Also, if crack nucleation occurs at locations other than the EoB, multi-axial stresses will exist.

2.19.3 Bounded Asymptote

In the bounded asymptote methods[65,66,67,68], contact stresses are obtained by appropriately bounding analytical (asymptotic) solutions with the help of an appropriately refined stress solution. Bounded asymptotes do not relate so directly to crack solutions, but provide a way of correlating fretting contacts under different geometries and loadings.

As an example, consider the problem of a flat-with-rounded-edges contact. When sufficiently away from the EoB, the centre contact region of the punch looks much like a flat punch which has a solution for pressure as illustrated in the following equation.

$$p(x) \Rightarrow \frac{P}{\pi\sqrt{a^2 - x^2}} \qquad (2.18.1.1)$$

Hence, the stress behaviour in the centre of the punch should asymptote to the flat punch behaviour when the flat is large with respect to the edge radii. Alternatively, the EoB location of the contact looks like a rounded punch whose contact pressure can be determined from the Hertzian solution. Hence, the stress behaviour near the EoB should asymptote to the Hertzian solution. The overall stress behaviour at the contact interface is then bounded by the flat punch and Hertzian stress solutions. Using these principals, analytical expressions can then be used to bound the "real" stress field.

The potential advantage of this approach is that the contact stress field is fully defined by "contact stress intensity factors" and, hence, the length scale is accounted for in the solution.

This removes the necessity of volume averaging. The contact stress intensity factors come out of the asymptotic solutions. Although this method has demonstrated significant promise in modelling idealised fretting fatigue tests, the work is in very early stages. Significant further development is required before its potential can be fully assessed. Specifically, the procedure must be developed to enable contact stress calculation associated with dissimilar, anisotropic materials in frictional contact with 3D geometries.

2.20 Hybrid 2D/3D Schemes

Use of conventional FE modelling techniques require significant computational time to implement the fine meshes required for EoB stress analysis. As noted above, 2D analytical approaches for evaluation of contact stresses have proved to successfully model the contact stress behaviour in significantly less computing time than that associated with an equivalently fine FE result. However, 2D methods ignore 3D effects such as out-of-plane stresses and slip. In order to reduce the required run-time of the contact problem in FE and maintain the stress point calculation resolution required for EoB stress analysis, methods for mating coarse mesh 3D FE solutions with 2D analytical solutions allow for computationally efficient, high-resolution contact stress evaluation where 3D models fail.

Numerical / analytical hybrid methods use coarse FE models to attain the component bulk stresses, loads, and moments. Equivalent 2D contact loads are then calculated at parallel planar slices for several locations along the depth of a contacting surface. These 2D line loads can then be used to evaluate the associated contact stresses at each depth location. Many 2D analytical methods employ half-plane models to solve for near surface stresses arising from the surface tractions alone. Hence, the final hybrid solution is obtained by superposing the analytically calculated EoB stress gradient with the bulk stress behaviour obtained by the coarse FE model.

When 3D effects become significant, the chosen hybrid model must account for the resulting out-of-plane stresses and slip. As a first order approximation, the out-of-plane normal stress has been corrected by multiplying the 2D plane strain result with an appropriate correction factor and has ignored the effects of out-of-plane slip and shear. As 3D effects become increasingly more influential, however, the error associated with this approach becomes progressively larger. Future work may involve the solution a second set

of 2D slices perpendicular to the original to better capture the out-of-plane contact tractions.

2.21 Modelling the Friction Coefficient

The actual behaviour of the coefficient of friction between two contacting bodies is the result of a complex combination of load, surface geometry, surface condition, materials, and environment. Understanding the frictional behaviour generally requires an experimental reproduction of contact parameters, representing the actual condition as closely as possible. A key measurement is the average coefficient of friction and how it evolves with continued cycling. Details of how the average coefficient of friction is measured as the contact transitions from static to dynamic friction at the point of gross sliding has been documented in literature[69]. After experimentally obtaining the average coefficient of friction behaviour, literature also details how to model the local friction coefficient behaviour and how it evolves within the contact area for the case of partial slip fretting fatigue [32,70]

For contact between similar, isotropic materials, Hills and Nowell[48] and Dini and Nowell[62] showed that the slip zone coefficient, μ_s, could be determined in terms of the average coefficient of friction, μ, and the initial coefficient of friction, μ_o. A numerical method was also developed by Murthy[63] to obtain μ_s in terms of μ and μ_o for the case of dissimilar isotropic materials. In this method, μ_s is increased in an incremental manner, starting from μ_o, until the solution of the sliding contact problem yields the experimentally measured average coefficient of friction, μ. Both of these methods assume the slip zone coefficient evolves with time, but remains constant across the slip zone, and the coefficient of friction in the stick zone does not change. Initially, the coefficient of friction is assumed to be constant ($=\mu_o$) throughout the contact zone. As the slip zone coefficient, μ_s, increases, so does the stick zone size which locks in the evolved coefficient of friction value at that point. In each increment, the ends of the stick zone are determined by solving the partial slip problem, taking into account the remote tension applied and the material dissimilarity of the two contacting bodies. Keeping track of the previous increments allows for determining the distribution of the coefficient of friction within the contact zone at a current increment. It is important to note that these devised friction calculation methods do require a partial slip solution for the

contact geometry and materials being investigated because of variations in the coefficient of friction with wear.

In gross sliding, the coefficient of friction can be assumed to be constant across the whole of the contact. This value can be captured by a series of experiments. It is important to note that current models capable of capturing the evolution of friction coefficient for partial slip are primarily 2D. Hence, these models do not account for significant axial slip.

2.22 Measuring the Average Coefficient of Friction

In order to characterise the coefficient of friction in slip zones of the contact, important friction experiments are performed. Measurements of the coefficient of friction are imperative to accurate evaluation of contact stresses. The coefficient of friction evolves as two material surfaces wear or fret against one another. It should be noted that wear in partial slip fretting fatigue is occurring only within an annulus of slip whereas the wear in gross slip fretting fatigue is occurring over the whole of the contact surface. As such the magnitude of the slip zone coefficient of friction cannot be measured as the tangential force divided by the normal force, (Q/P).

It is important that a suitable set of experimental friction tests are performed to measure the behaviour and magnitude of the average coefficient of friction, μ, for different contact situations. This is because the frictional behaviour of materials is greatly dependant on a variety of factors such as surface condition, lubrication, third bodies, temperature, environment, and contacting materials. Determining values for different contact situations can be fed into a database, which can be contact modeling purposes. Previously, button-on-plate (spherical button on flat plate) tests have been performed at Rolls-Royce and in line fretting tests have been performed at Oxford University and Purdue University which measure the coefficient of friction between two specimens.

2.22.1 Button-on Plate Test for Measuring Co-Efficient of Friction

To-date, all coefficient of friction measurements (static and dynamic) at Rolls-Royce have been obtained from button-on-plate friction testing. The button-on-plate wear test determines metal removal rates and the sliding friction coefficient of the material combination tested.

The rig applies a sinusoidal reciprocating sliding motion between a spherical test button and flat test plate. Usually, the test is run at a sliding distance of 2.54mm, which is unrealistic for many real world problems. A frequency of 20 cycles per minute, normal force of 9.81N, and test duration of 2 minutes[71] are also typical parameters used in a button-on plate test but can be tailored to suit specific requirements. It must be noted that at elevated loads, the frequency must be reduced to avoid the momentum of the rig interfering with the friction results [65].

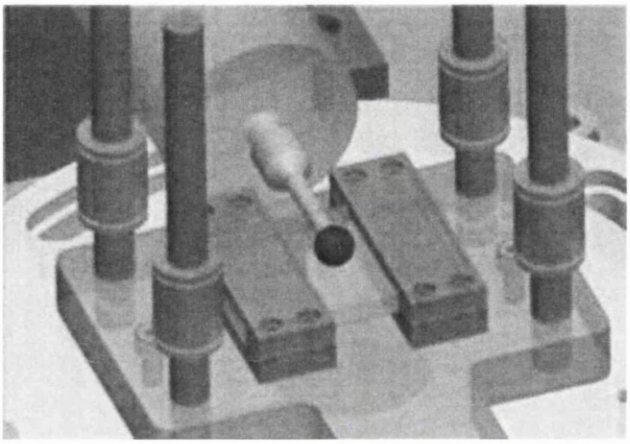

Figure 2.22.1.1. Button-on Plate Test[72]

The disadvantage of the button-on-plate friction test is that it is limited by the specimen geometry and upon initial point contact there is an extremely high contact stress at the start, but quickly reduces to much lower values following wear65. Lastly, because friction is often but not always dependant on contact stress, the resultant coefficient of friction value may be unrepresentative of the contacts found in real life machinery such as engine components.

2.22.2 In-line Rig Friction Tests

These friction tests require the use of an In-line fretting fatigue rig similar to those developed by Oxford University[48] and Purdue University. They are a superior alternative to button-on-plate tests because they allow a more accurate representation of the geometry and loading conditions experienced in service. Figure 2.22.2.1 shows a basic in line fretting test. A bulk cyclic load (Q) is applied to the specimen in the axial direction, whilst the fretting pads apply a contact force to the specimen to generate a fretting condition. The whole rig is placed in a furnace to replicate the service temperature.

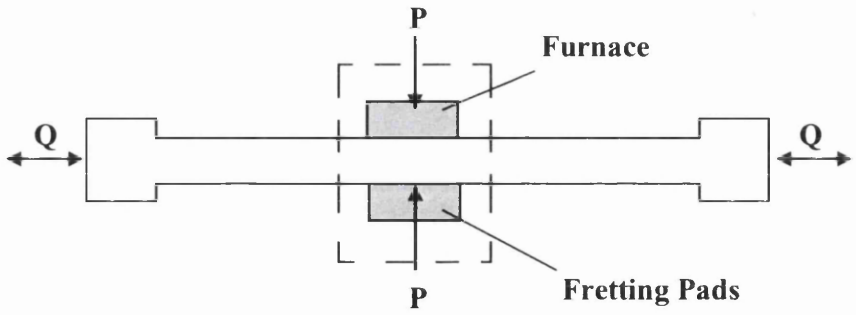

Figure 2.22.2.1. Schematic of In-Line fretting test

When the pads are made from similar isotropic materials, an approach outlined in Hills and Nowell[48] is used to determine the slip zone coefficient of friction, μ_s, in terms of the average coefficient of friction, μ and the initial coefficient of friction, μ_o[73]. Dini and Nowell[62] generalised this formulation for application to a 'flat with rounded edges' contact. These solutions work for the case of similar material contacts. However for dissimilar materials, the solution for the contact pressure and the shear traction are coupled. Therefore, it becomes difficult to deduce a closed form relation between μ_s, μ and μ_o.

To obtain μ_s in terms of μ and μ_o, experiments can be performed and numerical methods can be used. Basically, μ_s is increased incrementally, starting from μ_o, until the solution of the sliding contact problem yields the experimentally measured average coefficient of friction, μ. This process is explained in Farris et al (2003)[61] and has been performed for Ti-6Al-4V/Inco718 contact by Rajeev and Farris (2002)[74]. However, it is important to note that these methods rely on a 2D formulation of the contact problem and ignore 3D effects. Nonetheless, the methods provide a good understanding of the behavior of the coefficient of friction under engine type loading

2.23 Contact Life Assessment Methods

Since the mechanisms related to contact fatigue are not well understood, the determination of an appropriate life assessment method often is dependent on the specific contact situation (e.g. material, temperature, microstructure, geometry, etc.) being investigated as well as the contact stress analysis method being used. Hence, the main priority is to develop an adequate contact stress model to assess a range of lifing parameters / methods for their ability to model contact fatigue life of the desired contact pair. For this reason, a survey of current contact fatigue life parameters and methods will be presented but will not be assessed in lieu of the development of the contact stress analysis. It is generally accepted that contact life

assessment methods fall into two main categories: (1) stress-based methods and (2) fracture mechanics methods.

2.24 Stress-Based Methods

2.24.1 Crushing Stress

Attachment bedding design is currently addressed at Rolls-Royce by ensuring the crushing (or bearing) stress is below a specified maximum. This ignores shear, slip, and edge-of-bedding normal stress peaks. Currently, the crushing stress is usually calculated from truncated contact geometry in SC03, which does not currently allow for inclusion of frictional effects. The crushing stress is defined as the load normal to the contact surface, P, divided by the contact area, A ($\sigma_{crushing}$ = P/A). It is important to note that the contact area can change significantly if accurate EoB geometry is employed with plasticity.

2.24.2 Stress at a Point / Area / Volume

A general overview of "notch analogue" life prediction methods has been reviewed by Nowell, Dini and Hills[58]. This method derives a correlation between the stress field close to the edge-of-bedding and the root of a notch. If the most highly stressed point is at the EoB and the contact is 'incomplete', the normal and shear tractions will fall to zero leaving only stresses parallel to the surface non-zero[58]. Hence, the stress state at the point of initiation is then treated as a uniaxial stress state. This method suggests that the complexity of multi-axial parameters may not be necessary in some cases. The EoB life can then be predicted by correlating the EoB contact stress to the stress / life resulting from an appropriately shaped notch [75]. Through this analogy, fretting fatigue life can then be predicted with conventional notch fatigue data using the 'point', 'line', and 'area' methods[69]. There will be a degree of empiricism in determining the critical distance. Note that the contact stresses are highly multi-axial and undergo non-proportional loading. Hence as soon as a crack is nucleated or formed in an area other than the EoB, multi-axial stresses will exist which are not captured in the notch analogue approach to contact fatigue lifing.

2.24.3 Empirical Parameters

Early attempts at predicting contact and fretting fatigue performance used special empirical parameters formulated specifically for the contact fatigue problem. For fretting fatigue, Ruiz, Boddington, and Chen[70] formulated parameters based on products of the local slip amplitude (δ), maximum shear stress (τ), and maximum local stress parallel to the contact surface (σ). The first parameter was an energy-based parameter comprised of a product of δ and τ. The second parameter proposed, $\sigma\tau\delta$, better captured the location of crack initiation, but its physical interpretation is less clear. It is unlikely that these parameters could be regarded as material constants; however, they do provide an acceptable means of correlating across a range of experimental conditions for a given pair of contacting materials[76].

2.24.4 Multiaxial Parameters

While many theories for contact and fretting crack nucleation have been proposed, most of them fall short of quantitative prediction of the cycles to crack nucleation[77]. From the contact stress analysis, it is clear that the stress state underneath the contact is a highly complex and multiaxial one. Therefore, this stress behavior must be accounted for in any model used in quantitative prediction of nucleation life.

Szolwinski and Farris have offered[71] and validated[78] an approach for predicting fretting crack nucleation through application of a multi-axial fatigue life parameter that links the near-surface cyclic stresses and strains to the number of cycles required to nucleate a crack along a critical plane. The success of the critical plane approach in this effort motivated the investigation of several multi-axial parameters for application to different material contacts. A range of parameters including the Fatemi-Socie-Kurath[79] and Smith-Watson-Topper [80] approaches were employed to investigate fretting fatigue tests on PH 13-8 stainless steel[81] as well as Al-4Cu and Ti-6Al-4V[82]. Dang Van's mesoscopic parameter[83] has also been employed to predict fretting fatigue life of a low alloy steel (30NCD16) using conventional fatigue in the same material[84]. This required the use of an averaging dimension to account for high fretting fatigue stress gradients (size effect). A range of multi-axial parameters (including the Soci[85], Findley[86], Chu-Conle-Bonnen[87], alternating Walker equivalent stresses[88], resolved shear stress[89], Fatemi-Socie-Kurath[73], McDiarmid[63], and Smith-Watson-Topper[90] parameters) were also recently evaluated as to their ability to predict fretting fatigue in an FCC single crystal nickel alloy[63].

Stress invariant life parameters offer an approach for life calculation that is independent of the coordinate system and without the need to calculate a critical plane orientation. These parameters can be determined quickly and efficiently from the given stress field. Murthy et al.[42] have applied a modified Manson-McKnight multiaxial model, which employs a stress invariant parameter, σ_{eq} (alternating Walker equivalent stress), as defined by Doner et al.[80]. This method showed some success in predicting nucleation lives for materials such as titanium (Ti-6Al-4V)[83] and aluminium (Al 2024)[91]. Though successful for polycrystalline materials, Murthy showed that critical plane methods (i.e. Findley[92] and Chu-Conle-Bonnen[79] parameters) better modeled the crack nucleation behaviour in a FCC single crystal nickel[63].

Experiments show that higher peak stresses are required to produce failures in notch specimens as compared to smooth specimens using the same stress parameter. This is attributed to the fact that a smaller volume of material is stressed for a notch fatigue test than for a smooth bar fatigue test. As the area of stress increases, there is a greater chance of finding a material flaw. Hence, there is a greater probability of finding a flaw and failing earlier in the smooth bar specimen. As a result, both the critical plane and stress invariant multi-axial parameters require a method for accounting for the size effect (total area or volume of material being stressed). This has been accomplished by employing weakest link methodologies[63,68] as well as other stressed area or stressed volume corrections[58].

2.25 Fracture Mechanics Methods

2.25.1 Crack Analogue

The crack analogue[56, 93] is based on the assumption that the crack nucleation site is at the EoB and can be represented as a crack in mode II (shear) loading. Giannakopoulos et al. conducted a series of fretting tests on this basis. The crack life was broken down into three stages: (1) the contact interface is treated as a crack loaded in shear, (2) immediately after the crack grows into the base material it is treated as a short crack growing from the EoB position under the influence of contact stresses, and finally (3) after growing beyond the influence of the contact stresses, a conventional long crack fatigue behaviour is assumed due to the bulk stresses. In the second step, the crack will grow at an angle to the worst principal stress

(WPS) as it is strongly influenced by the contact shear loading. Eventually, the crack will grow away from the contact stress field and is treated by conventional fatigue according to the Paris Law driven by the WPS in the third stage of growth. There are two limitations to this approach, both associated primarily with stage 1 of the analysis procedure. First, it assumes that the contact surface is fully adhered and therefore ignores relative motion between the two surfaces. Second, it assumes a square root singularity for the stress field, which is not necessarily the case in contact conditions.

2.25.2 Bounded Asymptote

As mentioned previously, the bounded asymptote method[58,57,94,95] is based on the assumption that a contact stress field can be idealised to a standard form close to the EoB position so as to produce contact "stress intensity factors". These parameters can then be used analogously to stress intensity factors in linear elastic fracture mechanics (LEFM) for lifing purposes.

2.25.3 Short Crack Arrest

Short crack arrest methods[56,96,97] are an infinite lifing method that does not give a quantitative measurement of life. Kitagawa and Takahashi showed that when a crack length is less than a critical value, α_o, the short crack propagation threshold is found as a function of the crack length, α. Short cracks, $\alpha < \alpha_o$, will propagate if the applied stress range exceeds the fatigue limit ($\Delta\sigma > \Delta\sigma_{fl}$). Writing the stress intensity factor range, ΔK, in terms of the short crack stress range reveals that short cracks arrest if $\Delta K < Y\Delta\sigma_{fl}(\pi\alpha)^{1/2}$. Conventional long crack fatigue dominates once $\alpha > \alpha_o$ at which point crack arrest occurs if $\Delta K < \Delta K_o$. Further details are presented in Nowell et. al[56].

2.26 Previous Fretting Fatigue Experiments

In order to develop appropriate contact fatigue lifing methods for real jet engine components, laboratory controlled fretting fatigue experiments tests are carried out to closely simulate the fretting processes that occur during engine functioning. The tests are also used to provide further understanding of the fretting fatigue process by analysing and characterising the fracture surfaces associated with test specimens in order to provide evidence regarding the physical nature of fretting and fretting fatigue cracks.

Fretting fatigue experiments aim to simulate the fretting conditions as accurately as possible, taking into consideration, factors such as stress, geometry, sliding distances, friction coefficients, temperature and environments. As mentioned earlier, there are reported to be as many as 50 variables associated with the contact fatigue problem, but in order to simplify the analysis phase of the experiment i.e. In FE modeling, the variables are kept to a minimum and the geometry is also kept relatively straight forward.

Since the problem of fretting fatigue is hugely dominated by the disc/blade root contact problem, most tests discussed in literature are designed with this in mind. Although not all, most of the laboratory test methods can be applied to a general case of fretting fatigue and can be easily manipulated to other fretting fatigue issues. For example, reports have shown fretting to occur between disc rims and external features such as lockplates and coverplates. Furthermore, reports have shown fretting to be the cause of rig test failures, where fretting has occurred within the bolt holes of backing discs and the tests discs. In this case, a bolted configuration can be implemented into the test design.

In the following chapter, a few fretting fatigue experiments will be briefly discussed. The reader will notice that the test setup used for most of the experiments is quite. The most obvious similarity will be the use of fretting pads on a test specimen to represent the contact fatigue element of the fretting process. For this reason in particular, the tests discussed are those which have been successful and designed leaders in this field. However, for the interested reader, there are a plethora of published articles in open literature outlining a vast number of fretting fatigue experiments.

Experimental investigations of fretting fatigue have taken a number of forms over recent years. Initially it was common to use bridge type fretting pads as shown in Figure 2.25.1. Unfortunately, there are a number of difficulties with such a simple arrangement. Contact conditions at the pad feet are difficult to characterise, especially if there is bending in the bridge itself. Further, conditions at each foot will not be completely identical and it is expected that one foot will slip before the other, even under nominally symmetric conditions. This means that the slip regime during the experiment is often unknown.

A series of papers were published in the late 1960s and early 1970s by Nishioka and Hirakawa[98]. These used a quite different contact configuration of cylindrical pads clamped

against a flat specimen Figure 12.1b. This geometry has a number of advantages: pad alignment is less critical and the stresses may, in principle, be predicted by classical contact analysis[99,100]. Further, the important parameters for subsequent stress analysis (normal load, P, tangential load Q (t), and specimen remote stress r (t)) may all be readily measured and controlled. The geometry has since been adopted by a large number of other researchers, including Bramhall[101], Hills et al.[102], and Szolwinski and Farris[103]. In this type of test the normal load is normally fixed, whereas the tangential load is cycled, and applied using springs Figure 2.25.1b.

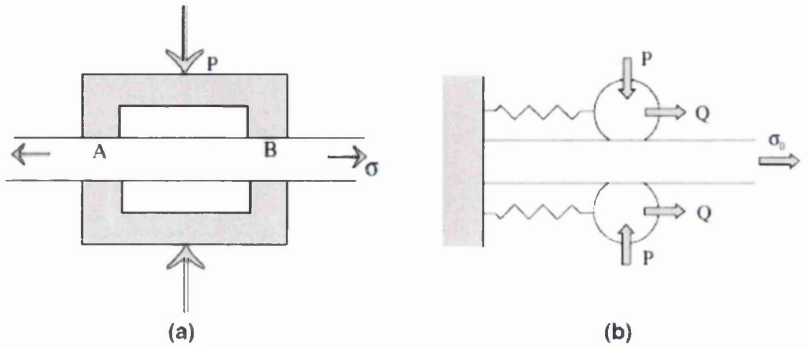

Figure 2.25.1. (a) Bridge pads (b) Cylindrical pads on flat specimen

2.26.1 H-Testing

H-Testing is used to support disc-lifing and is designed for fretting fatigue problems and EoB under static and vibratory loading and high temperature (optional).

It is specific to disc/blade root fretting fatigue and can be classified as a subset of In-line fretting fatigue testing. As can be seen in Figure 2.26.1.1, a typical turbine disc /blade firtree root is simulated using the exact same geometry. By factoring down the loads experienced in service to the scale of the laboratory rig, near equivalent loading conditions can be achieved. The effects of temperature and environment can also be tested by placing the rig an in an 'environmental box'. In the figure, Force Q is applied to simulate the centrifugal force exerted in the root when the disc is spinning.

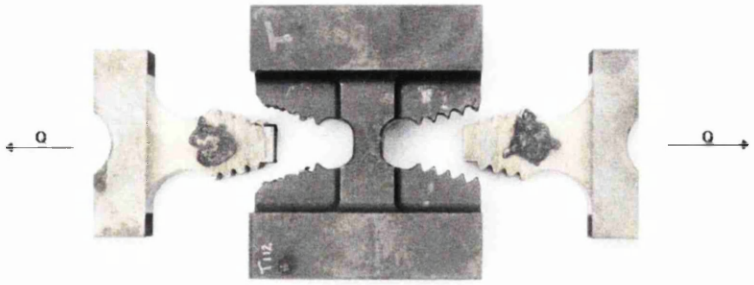

Figure 2.26.1.1. Photograph of H-Specimen simulating the disc/blade firtree root.

2.26.2 Servo-Hydraulic Fatigue Testing Machine with Fretting Chassis

The apparatus shown in Figure 2.26.2.2 was developed by Purdue University in order to conduct a fretting fatigue test that simulates the loading conditions of the disc/blade dovetail root. The experiment uses a servo-hydraulic test machine with the addition of a fretting chassis that brings two nominally flat contact pads into contact with the flat dog-bone specimen. The experimental design is based on the fact that the blade/disk contact is equivalent to a nominally flat indenter in contact with a flat surface[104]. It is worth noting that this set-up has been adaptable for a wide range of materials, indenter geometries and load conditions[14].

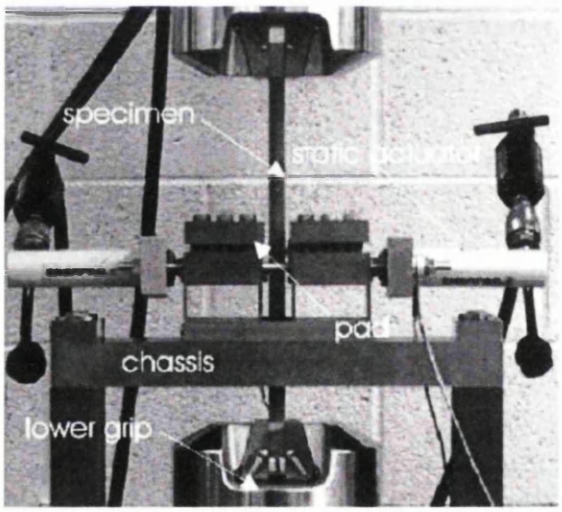

Figure 2.26.2.2. Photograph of Purdue University fretting fatigue experimental testing apparatus

The servo-hydraulic machine applies a cyclical bulk load to the dog-bone specimen whilst the static hydraulic actuators apply a compressive load through the contact pads to the dog-bone

specimen. The normal load that is transferred to the specimen by the pads also creates a shear traction that is generated due to the bulk load displacement. This tangential force is then measured by calculating the difference in the applied force and reaction force by load cells at the upper and lower load cells, respectively[95].

It is important to mention that this experiment creates the partial slip condition disseminating the familiar ring pattern, where the centre is in the stick regime and the outer flanked ring is the slip regime. As discussed previously, it is the partial slip condition that brings about the highest reduction in fatigue life. The small relative displacements induce large localised stresses at the edge of contact that can potentially initiate and propagate cracks. Due to these highly localised stresses, fretting fatigue crack nucleation sites can be accurately predicted with analytical tools on various geometries and materials[105]

2.26.3 Fretting Wear Testing Machine

The fretting fatigue testing machine below designed by Purdue University[106] and involves two stationary cylinder specimens, attached to a rotary table, and clamped both sides to a reciprocating specimen. The advantage of this machine is that the rotary table allows for different angles of contact to be made between the stationary and moving specimens. When the stationary specimens are clamped at 90° to the moving specimen, cross specimen geometry is achieved which gives a well-defined point contact without suffering any alignment problems. Furthermore, varying the angle between the fixed and the moving specimens can obtain an elliptical contact of varying aspect ratio. See Figure 2.25.3.2

Dead weights on top of the upper stationary specimen provide the normal loads of contact and because of the simple nature of the set-up, this force can be varied easily. A piezoelectric force sensor is situated inside the connection between the actuator and the moving specimen. This force sensor measures the tangential force applied by the actuator. The output of the force sensor is routed to the same data acquisition card (DAQ) driving the actuator.

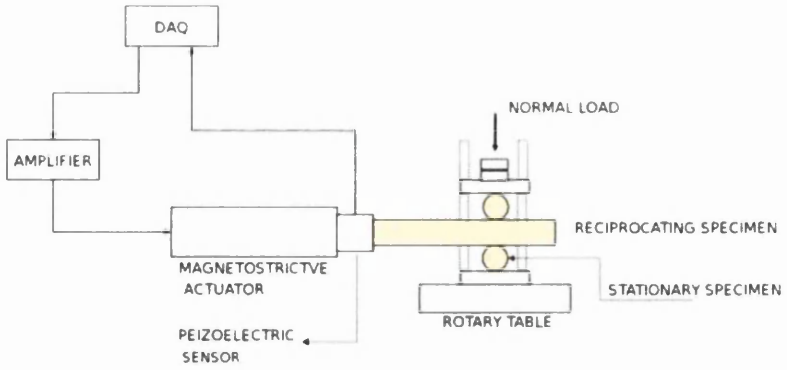

Figure 2.26.3.3 - Fretting wear testing machine as used by Purdue University, USA[97].

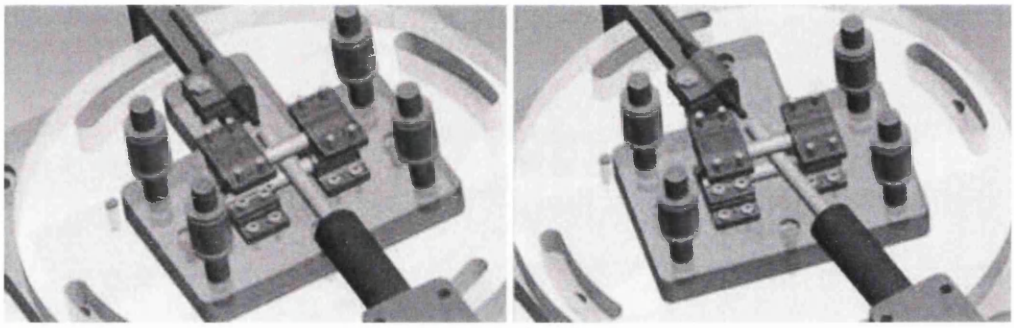

Figure 2.26.3.4 - Various contact angles between moving specimen and stationary specimens[97].

A microscope head inserted into a slot machined above the sapphire window enables easy observation of the fretting contact as it undergoes wear.

Unfortunately, the rig does not introduce a fatigue element to test fretting fatigue. However, Purdue University has confirmed that the rig may have some scope for customisation to introduce fretting fatigue if a more powerful motor is used. The motor would need to have the capability of introducing a cyclical bulk stress to the moving specimen so that the effects of fretting fatigue can be induced in the specimen.

2.26.4 Servo–Hydraulic fatigue Testing Machine with Two Actuators

The servo-hydraulic machine shown below was designed by *D.Hills et al.* [48] and has two separate actuators that introduce fretting wear and cyclic bulk stress independently to a specimen. This allows a more representative approach to fretting fatigue, as components in

service are often subjected to varying shearing stresses and bulk stresses from independent sources. The set up is shown in Figure 2.26.4.5.

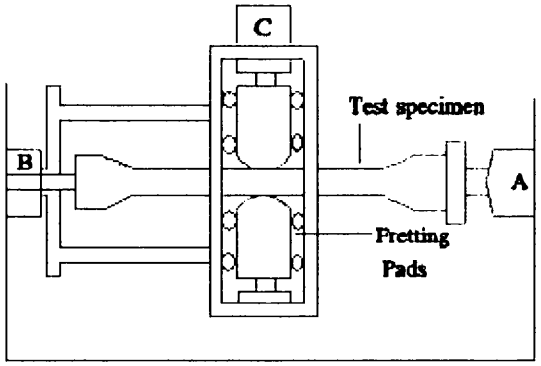

Figure 2.26.4.5 – Two actuator fretting fatigue apparatus[48]

The hydraulic actuators are mounted co-axially, one to provide the bulk tensile loading (Actuator A) and one to provide the shearing force (Actuator B) The second actuator is connected by a set of rods to a carriage supporting the fretting blocks, which are self-centering but pressed together by a third small actuator (Actuator C) which is loaded statically by a mall hand pump[48].

2.26.5 Fretting Fatigue Experiment Based on a Constant Deformation

The fretting fatigue apparatus shown in Figure 2.25.5.1 is a relatively simple design compared to the servo-hydraulic testing machine. It was developed by K.Endo and H.Goto et al[107] and uses a constant deformation type of plane bending fatigue testing. Essentially, the specimen comes into contact with a cylindrical surface of the fretting pad of the same material. The contact load is applied by dead weights, which are connected by a pulley. Hence, as the contact surfaces wear down, the dead weights maintain a constant contact load. The fretting pads (2) are fixed through a bearing (4) and are able to move along the direction of the bending deflection of the specimen (1). The relative reversed slip, which is synchronised with repeated stress occurs because of the difference in displacement of the specimen and ultimately leads to fretting[101]. The tangential force of fretting on the contact surface induces strains in the rotating shafts connected to the fretting pads. The tangential force is then measured by strain gauges that are fixed to the shaft and recorded dynamically by an electromagnetic oscillograph. The gauges work by measuring the relative slip amplitude between the specimen and the pads.

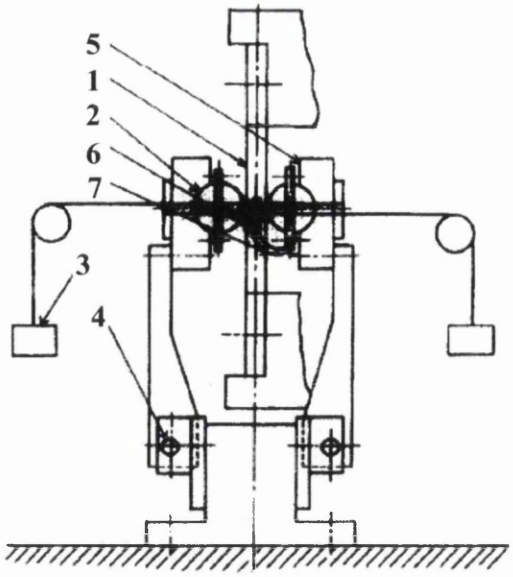

Figure 2.26.5.1. Fretting apparatus: (1) specimen (2) fretting pad (3) dead weight (4) bearing (5) block fixing fretting pads (6) thin plate (7) strain gauge[101].

The resulting fatigue crack depths were measured continuously using a precision type double bridge by the electrical resistance of the specimen, which varied due to the flow contraction at the crack portion. This is shown in Figure 2.25.5.2.

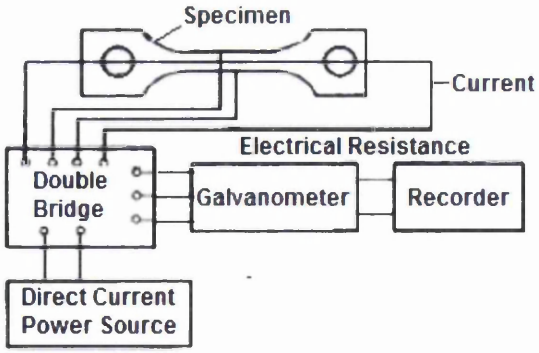

Figure 2.26.5.2. Block diagram of the crack detector

The apparatus shown in Figure 2.26.5.2 are also capable of testing environmental effects on fretting fatigue. For this type of experiment, the specimen and fretting pads are housed in an 'environmental box' which can be set to a required temperature and filled with various gases or liquids.

2.27 Bolted Configurations

In the aerospace industry, there have been many instances of fretting in and around bolted configurations that have led to fatigue fracture. In the modern aircraft industry, the main objectives of aircraft design are weight saving and reliability of aircraft. The fatigue life of key components are mainly determined by the geometrical detail design such as fastener holes, filleting, where stress concentration occurs. According to statistic, fatigue fracture of fastener holes account for 50–90% of fracture of aging plane[108]. Within Rolls-Royce, bolt hole fretting has mainly been a problematic in rig tests. For example, in one particular high pressure compressor (HPC) rig test, fretting from within a bolt hole had resulted in failure of a backing disc, compressor test disc and shaft.

There are many factors involved in the fretting of bolted configurations, such as material combination i.e. bolt and mating surfaces, and the way they interact with each other. By this, one means the coefficient of friction between the materials. Obviously, if the coefficient of friction is high, then the fretting severity will be worse. Other factors include the stresses on the bolted configuration. For example, under high centrifugal loads, the bolt hole will naturally form an elliptical shape, due to the shift of material in the axial direction. This effect narrows the bolt hole and clamps onto the bolt with a larger force, essentially increases the fretting process. Further, the bolt itself will naturally want to be 'thrown out' by the large centrifugal forces and thus causes larger forces between the hole and bolt. The clamping force or tightening torque of the bolt head also plays a vital role on the stress concentration close to the hole, the fatigue life of the configuration and also influences the crack nucleation origin. For example, as shown in Figure 2.26.1, the crack position at the bolt hole changes position with increasing tightening torque.

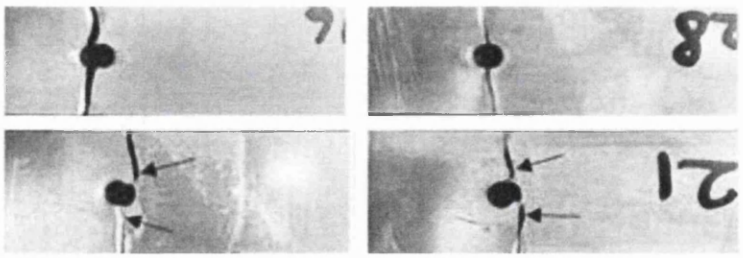

Figure 2.26.1. Typical bolt hole failures in specimens with initial clamping force of 1.15 kN (Top) and initial clamping force of 11.8 kN (bottom) and applied maximum gross axial stress of: (a) 144 and (b) 210 MPa. Note how the crack position changes with increasing initial clamping force[109].

Hence, there exists an optimum tightening torque that depends upon thread pitch, bolt diameter and the friction coefficient between the nut and bolt[110]. According to Shigley [111], to a first-order level of accuracy, it can be shown that the tightening torque is given by:

$$T = KFd \tag{2.26.1}$$

Where K is the thread coefficient and d is the bolt diameter.

The thread coefficient may vary between 0.12 and 0.20, depending on many variables, such as thread material, surface finish and coefficient of friction. From tests typically it is found that:

$$F = \frac{5T}{d} \tag{2.26.2}$$

The effect of bolt pre-loading or tightening torque is very important to the fatigue lives of bolted configurations and invites much discussions over the way in which it preloading helps to do so. One might ask whether the bolt preload - prior to joint separation - eliminates the bolt from "feeling" any of the external load, or whether it reduces the magnitude of the external load felt. To help understand the concept of a pre-load, the bolted joint spring analogy can be used which is shown in the following diagram.

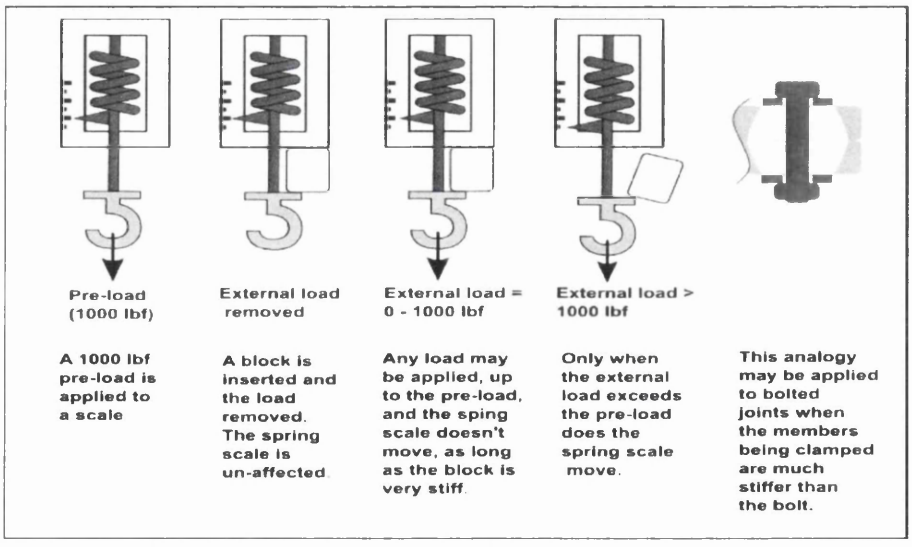

Figure 2.26.2. Bolted Joint Spring Analogy[112]

Referring to Figure 2.26.2, the modulus of the clamped material is much higher than the modulus of the bolt. In the limiting case of an infinitely stiff block, the bolt feels nothing until preload is exceeded. This is equivalent to the joint diagram where the slope of the green line (stiffness of the clamped material) is vertical. More realistically, if the clamped material has some stiffness, there is sharing of loads in proportion to the ratio of stiffness. Studying the diagram, one would agree that as long as the external load is less than 1000 lbf, the bolt will feel a load of 1000lbf. But the 'source' of that load varies. For example, if a 250lbf load is applied, the bolt will feel 1000lbf, 250lbf from the load, and 750lbf from the block. With a 900 lbf load, the bolt will feel 1000lbf, 900lbf from the load, and 100lbf from the block. With no load at all, the bolt will still feel 1000lbf, but all of it from the block.

Referring to the diagram in Figure 2.26.3, it can confirm the argument above i.e. that the bolt does indeed "feel" part of the external load, albeit with a greatly reduce magnitude which itself depends on the relative stiffness of the bolt and joint members.

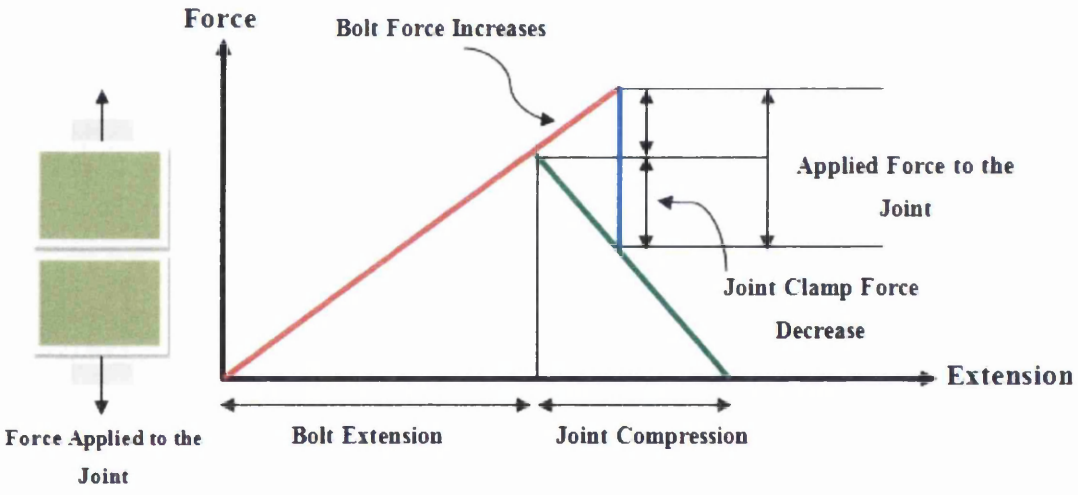

Figure 2.26.3. Forces on a bolted Joint.[113]

Many studies have shown that the details of holes will affect the fatigue life of fastener holes, such as bolt and processing quality. Ralph et al.[114] have studied the quality of holes that drilled by various aircraft production drilling procedures. Zhang and Pei[115] have investigated the surface roughness of holes drilled by different drilling processes and predicted the fatigue life.

Depending on the location, the bolted configuration is also subject to vibration. Vibrations can increase relative slip between the bolt head and mating surfaces and can also loosen the joint which further increases the fretting process. An added problem caused by bolt head loosening is a hammering effect caused by the bolt head on the mating surface of the disc. The ever present effect of corrosion can also reduce the fatigue life of bolted joints, which occurs mainly under the bolt head or from within the hole itself. It is more problematic in engines but can also occur in rig tests if an engine environment is simulated. As mentioned earlier, lubrication applied between two materials/components in contacts can increase the fatigue lives. This is also true for corrosion prevention compounds (CPC) that help to reduce the corrosion in bolted joints.

Geometry and design of the bolted configuration is probably of the most importance. For example, on one occasion, a bolt hole failure occurred due to a threaded bolt in a non-threaded hole. The threads acted to abrade the inside of the hole, causing surface roughening and therefore a source of high stress concentration, which eventually developed into a crack. Mitigation of sharp corners and rough surfaces is paramount to extending the fatigue life in bolted joints.

It is therefore possible to see the large scope of research surrounding bolted joints and the drive to find an optimum design for eliminating failure by fretting fatigue. Carrying out various experiments to simulate the bolted joint of say, a rig test, with the aim of understanding the effect tightening torque, vibration, lubrication, corrosion, geometry and material combination can have huge potential rewards for the aerospace industry.

2.27.1 Bolt Hole Experiments

The following chapters will outline some interesting experiments for investigating fretting fatigue around bolted/fastened joints. An important point of interest to note in these experiments is the inherent increase in stress concentration factors that accompany the geometry of the specimen, hole in specimen and the bolt through hole. This is shown in Figure 2.26.1.1.

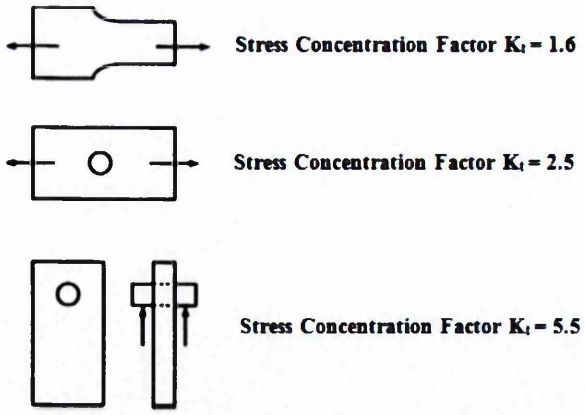

Figure 2.26.1.1 Stress concentration factors for test specimen sections

2.27.2 Reverse Double Dog Bone Test[116]

In this experiment, a series of fatigue tests were conducted to investigate the fatigue behaviour of fastener holes in reverse double bone specimens. With respect to finite element results, the fatigue life of fastener holes in reverse double bone is predicted based on critical plane approaches, including Smith–Watson–Topper (SWT) model and Wang–Brown (WB) model. After that, the predicted values are compared with that from tests. The effect of bolt clamping force on fatigue life of fastener holes is also investigated based on the two models. The reverse double dog bone specimen is shown in Figure 2.26.2.1 and involves two specimens bolted together in a servo-hydraulic fatigue testing machine, shown in Figure 2.27.2.2. The main point regarding the reverse double dogbone specimen is that the two specimens clamped together have different gauge lengths with the purpose of inducing different strains in each specimen, when a cyclic bulk stress is applied to them by the machine. The effects of different materials combination and other variables on the fatigue life of bolted joints can also be investigated.

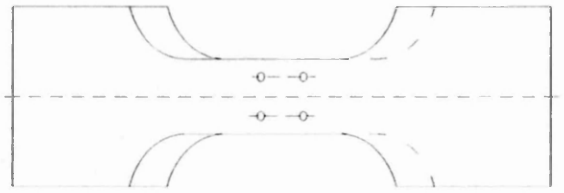

Figure 2.26.2.1. Reverse double dog bone specimen incorporating two specimens of different gauge lengths.

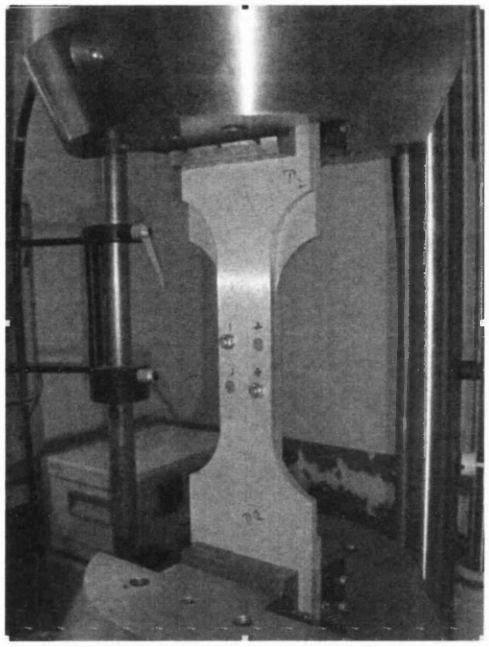

Figure 2.27.2.2 Reverse Double-Dog Bone test setup.

The experiment concluded the following:

1. The critical plane approach is capable of predicting the fatigue life of fastener hole in reverse double bone specimens.

2. For the fastener holes in reverse double bone specimens, the SWT approach achieved a better accuracy than the WB approach for high cycle fatigue (HCF) while the opposite holds for low cycle fatigue (LCF).

3. The fatigue life of fastener holes decreases with the increase of bolt clamping force as shown in Figure 2.27.2.3.

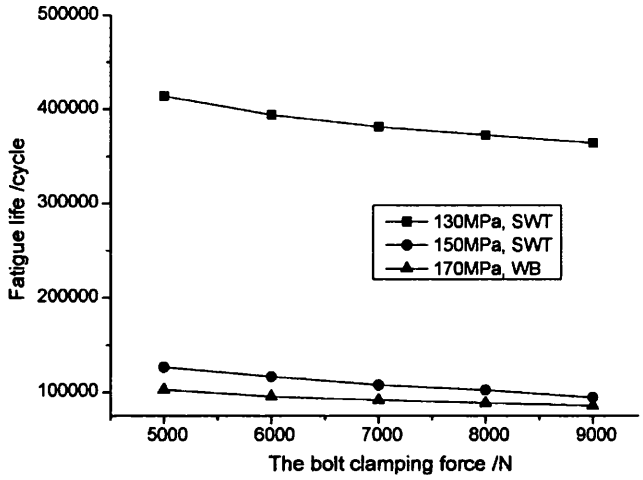

Figure 2.27.2.3. Predicted fatigue life against bolt clamping force

2.27.3 Single/Double Lap Joint Fatigue Test[117]

In this particular experiment, an investigation was carried out to investigate the effect of tightening torques on the life of bolted plates using single and double lap joints. The effect of plate thickness using an aircraft grade aluminium alloy with double lap joints was also studied. Constant amplitude fatigue tests, under load control, were carried out, with a near zero stress ratio, on plain specimens (for bench mark purposes) and on both single and double lap joint specimens, for which several torque levels were applied on the bolted joints. The objective of the fatigue tests was to demonstrate failure trends for each joint type, material thickness and torque loading, rather than the generation of comprehensive S/N curves.

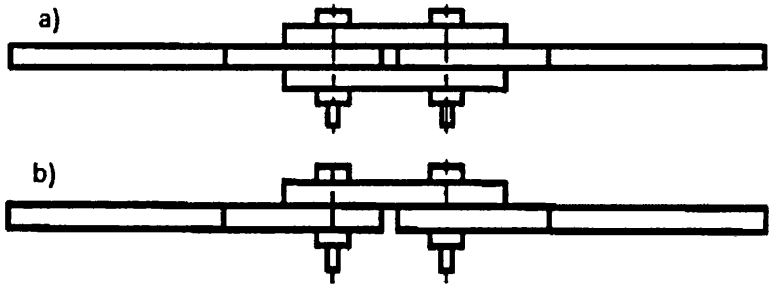

Figure 2.27.3.1. (a) Double Lap Joint (b) Single Lap Joint[108]

The tightening torque applied to the bolts results in a compression of the joint plate members, which causes friction between them, and so prevents their relative slipping. Thus, the bearing

of the bolt against the hole edges is avoided, or at least relaxed, and a high proportion of the shear load may be transmitted through the joint by friction. In this way, the load is distributed over a larger area around the hole, so that the stress concentration factor is diminished and the fatigue performance of the joint is much improved.

It was found that in all torque tightened joints, a greater fatigue life resulted, often greater than 10 times longer than zero torque tightened joints. Nonetheless, once the tightening torque is strong enough to prevent the slipping of the joint members and the bearing of the bolt against the hole edges, increasing the torque only has the benefit of spreading the load transmission over a wider area. Since the rigidity of the joint members helps extend this area, a thicker joint may benefit from a high tightening torque further than a joint between thinner members.

It follows that the experiment is beneficial for the failure types associated with joints loaded in shear as shown in Figure 2.27.3.2.

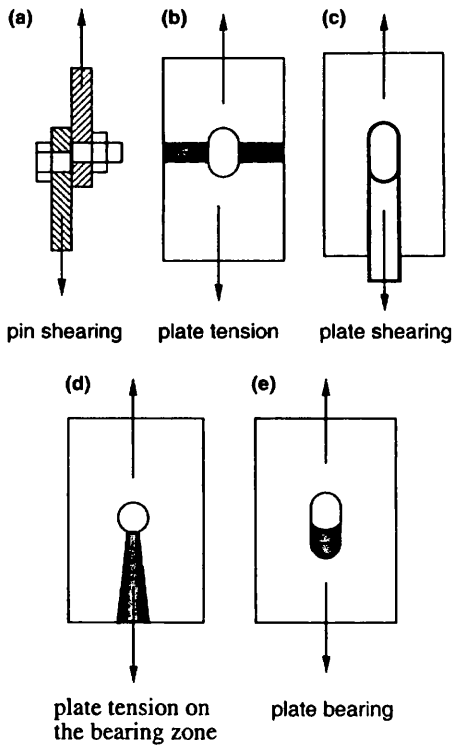

Figure 2.27.3.2. Failure modes for joints loaded in shear[108]

2.27.4 Four Point Bend Test

The setup shown involves loading a test piece in Four Point Bend and is designed to damage the bore of the bolt hole. This is achieved by offsetting the bolt hole in the test piece which encourages failure in bore of the hole. A pair of identical bolt carriers is fastened on either side of the test piece by a Waspaloy bolt (Waspaloy is the material of choice for most modern bolted configurations in the aerospace industry). The bolts are loaded in such a way that the bolt is forced down and the shank presses against the test piece.

The pressure on the bolt hole depends on (i) Position of the rollers in the lower fixture and (ii) stiffness of the bolt carrier arms.

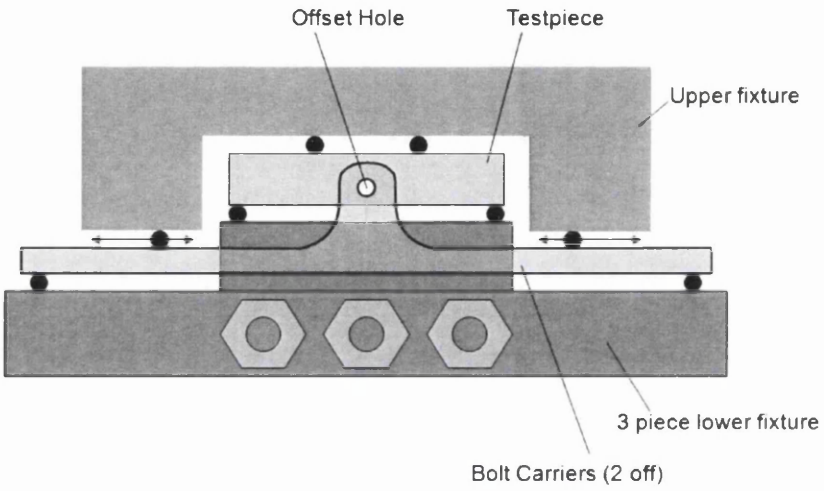

Figure 2.27.4.3. Four Point Bend Test for Bolt hole Fretting Fatigue Tests

The fatigue element of the test comes from the repeated cyclic bending and the value of stress exerted by the machine depends on what the user is testing. For a LCF test the stress would be large with small amplitude and the opposite would be true for HCF.

The 4 point bend test in Figure 2.27.4.3 has been designed with the purpose of testing bolt hole fretting. The test boasts the simplicity of geometry which is ideal for FE modeling prediction methods. The test can be utilised to study the effects of many factors on the fretting fatigue life of certain material combinations, such as bolt design, bolt tightening torque/preload, specimen thickness, lubrication, geometry, temperature and environment.

2.28 Examples of Previous Wear Damage in Rolls-Royce Jet Engine Components

There have been and will continue to be numerous cases of wear damage on engine components at Rolls-Royce. Some cases have been serious resulting in disc failure and some have resulted in blade loss which ultimately causes secondary damage to discs. Other cases have shown wear damage on these components but have been noticed during routine inspection before further serious damage is caused.

Having researched the archives of the Rolls-Royce failure investigation department, Bristol, it was immediately apparent that the most common area of wear damage was located at the disc/blade roots as a consequence of fretting fatigue. Regardless of whether the components had failed or not, the wear scars were all very similar, exhibiting the stick/slip pattern i.e. the centre of the contact is not moving but the outer edge of the contacts is. Frequently, fatigue cracks were also seen emanating from the boundary between the two regions, where the stress concentrations are at their maximum. However, there were a lot of cases of wear damage that did not resemble the typical partial slip fretting morphology. It is well known that fretting can occur over a range of sliding distances and does not always need to have the typical partial slip fretting pattern. Once the sliding distance increases above a specific value (usually quoted as 50μm but is in fact material specific), there is a transition into gross sliding and larger distances which moves the wear into reciprocating sliding. It is these sliding distances that cause confusion between tribologists and engineers alike, since the damage may or may not be fretting but could in fact be scuffing, galling or other kinds of wear with entirely different failure modes. It is important to remember that the surface roughness of wear scars is not a direct correlation to its fatigue life deficit since partial slip fretting usually has a low surface roughness but large effects on fatigue life to the propensity to form cracks readily at the edge of bedding.

Fretting fatigue in blade/disc roots requires extensive testing and modelling to capture the exact mechanisms of failure. The geometry of the blade/disc root adds to the complexity of the problem especially when trying to computationally model the problem on a microscale due to the very fine meshes involved. Testing usually relies on matching the exact geometry of a disc/blade root so that it's as realistic as possible.

Wear damage was also seen on the rim of turbine discs due to cover plates and lock plates which mate up against the rim and hold the blades in place. This can form a combination of hammering and sliding wear and as a result, makes it very difficult to replicate in a test environment. There are many other instances of wear damage in jet engine components such as splines and couplings but these components are outside the scope of this project.

Regardless of the location and the components involved, it is possible to replicate the same kind of damage in laboratory environments with relatively simple apparatus and at the operating temperatures experienced by the components.

2.29 Adour 2nd Stage Low Pressure Compressor Blade Root Cracking

This case was highlighted as a red top and involved 2 Incidences of blade/disc root failure. The blade material was Titanium 6/4 and coated with a graphite dry film lubricant (DFL) over all root and underside platform but was not shot peened. The blades had a 2000 hour overhaul life but both blades failed to meet this waypoint as one blade was found with gross cracking at 1762 hours and the other failed prematurely at 1803 hours.

The blade failure location is shown in Figure 2.28.1. Note the two regions of wear damage. The largest (dark grey) area appears to be lighter than the heavier (light grey) section which either suggests that there are two types of wear damage present or it is the same form of wear but with different severity. This is a perfect example of how wear damage definitions can be misconstrued or overlapped and is the reason why this particular case has been chosen for discussion. In this investigation, both Rolls-Royce and Turbomeca refer to the wear as fretting.

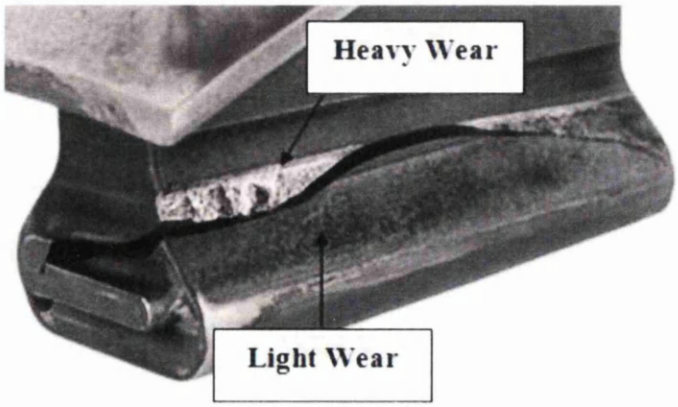

Figure 2.29.1. Cracking at the edge of bedding in a blade root

The blade found with gross cracking is shown in Figure 2.28.2. The wear damage is heavy on both pressure and suction side, though pattern from one side to the other is very different. Both sides show full contact, though variations across flank axial length in terms of heaviness. There are also appears to be pitting/ scallops formed by adhesive wear with radial directionality on the pressure side and a heavy rippled effect with axial directionality on the suction side.

It can be seen from the following images that fissures are abundant at the edge of bedding and progressing into the parent material shown by the yellow arrows. The total depth of these fissures is 150μm. With increasing load cycles, these cracks would have grown larger and caused fracture.

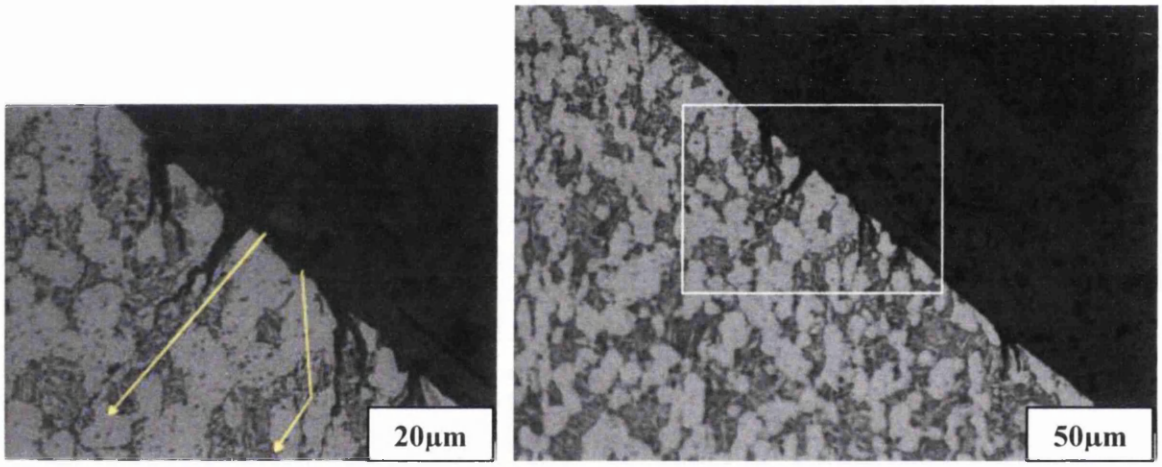

Figure 2.29.2. Micro-fissures present at the edge of bedding in the un-failed blade. Image courtesy of Turbomeca and Rolls-Royce.

Dye penetrant inspection of the other blades in the same engine also showed indication of fretting damage which further illustrates how big of a problem fretting in dovetail roots is.

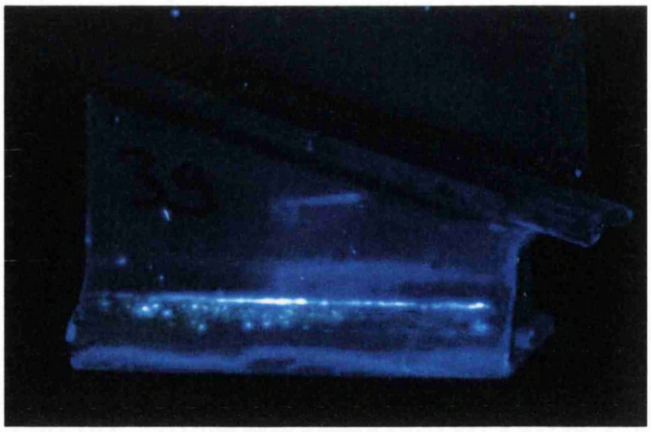

Figure 2.29.3. Dye penetrant inspection shows sign of wear damage. Shown in light blue.

Case Outcomes

The outcomes of this case were that DFL starts to erode after approximately 100-200 hours (previous case in another engine type at Rolls-Royce was certainly the case) and as a result, friction increases and the EoB stresses go up correspondingly. With a 2000 hour overhaul life, this is a long time to operate under high friction. The contact stresses and relevant slip distances in this case were considered large by Turbomeca, so raisers the question as to whether fretting fatigue was the dominant wear process. Or had the wear progressed into a more aggressive form such as scuffing or galling which would explain the removal of the DFL and the surface of the parent material. The diagram in Figure 2.28.4 illustrates how DFL starts to slowly fail with increasing contact pressure and temperature.

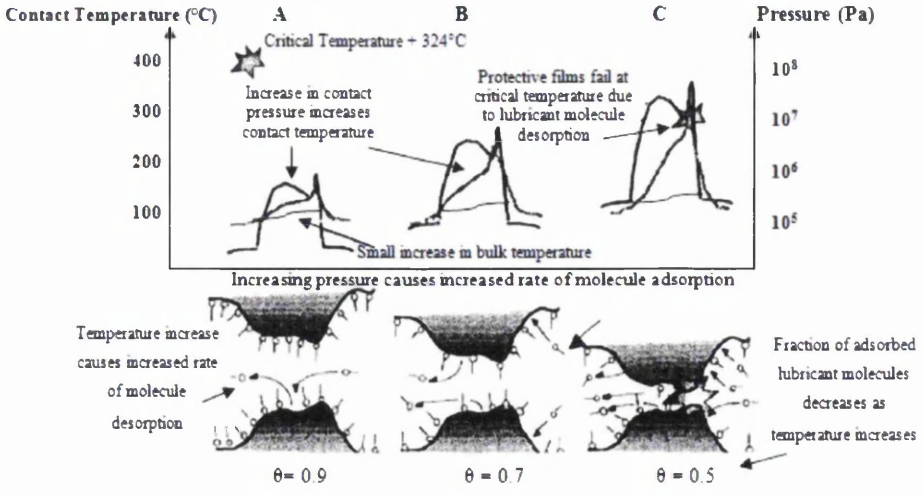

Figure 2.29.4. DFL starts to slowly fail with increasing contact pressure and temperature.

There are further examples of wear damage on blade roots from other engines, shown in Figure 2.28.5. These also show signs of heavy wear with gross material removal, spalling and pitting. In all cases of inspection, it is important to note that unless the oxide/glaze layer is removed, it is impossible to confirm whether cracks present in the bedding wear surface extend into the substrate. On this basis, it is possible that there are fretting and contact fatigue nucleated micro-cracks present below the oxide layer that go undetected.

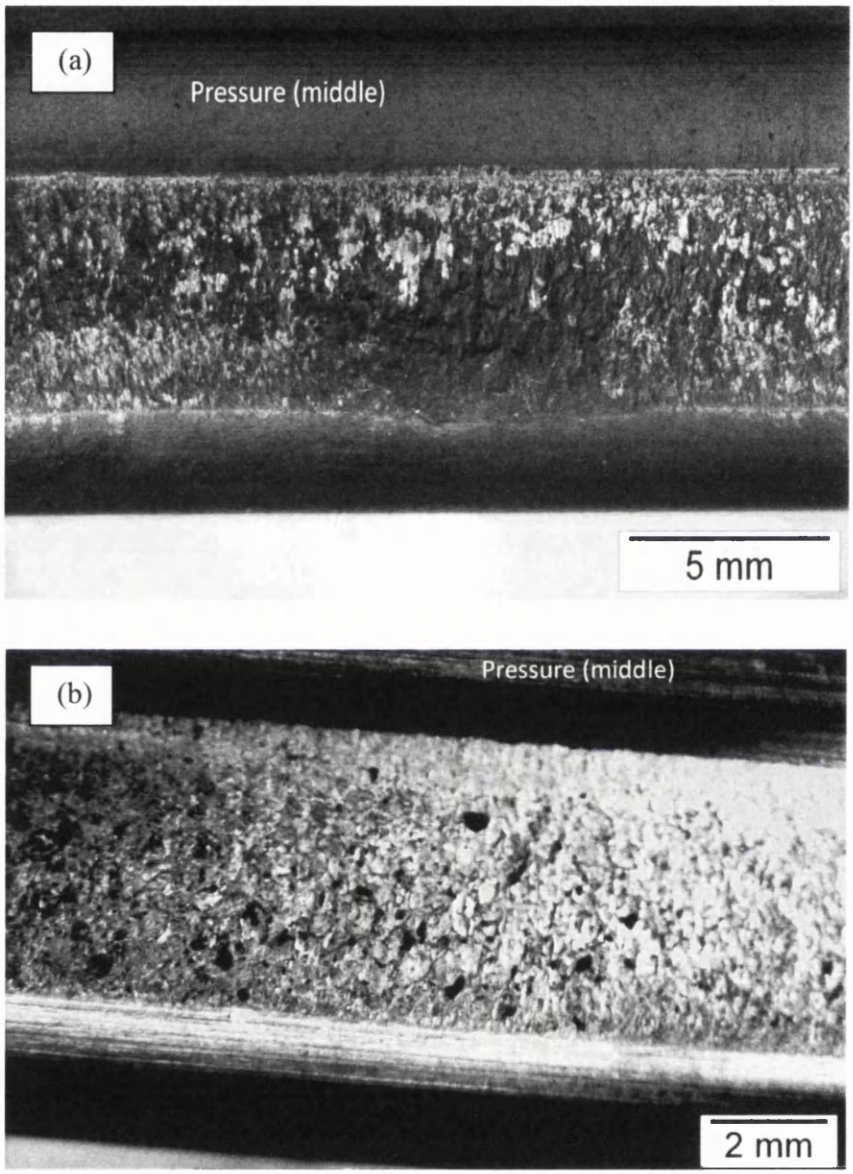

Figure 2.29.5. Both (a) and (b) shows wear damage on a turbine blade root from ex-engine. Images courtesy of Turbomeca and Rolls-Royce.

2.30 Sliding Wear of U720 Trent 500 HP Turbine Cover Plate and Disc

As a consequence of the difference in mass and therefore heat sink capacity between the Udimet 720Li Trent 500 HP turbine disc (Part No.FW21059) and cover plate (Part No.FW23346) there is relative movement between the two components because of the temperature changes experienced during the flight cycle. Examination of test engine components showed this movement leads to pronounced sliding wear of the cover plate and disc which exceeds the Engine Manual limits of 25µm (0.001") after only a few cycles.

The following images show the wear on the disc posts and the cover plates.

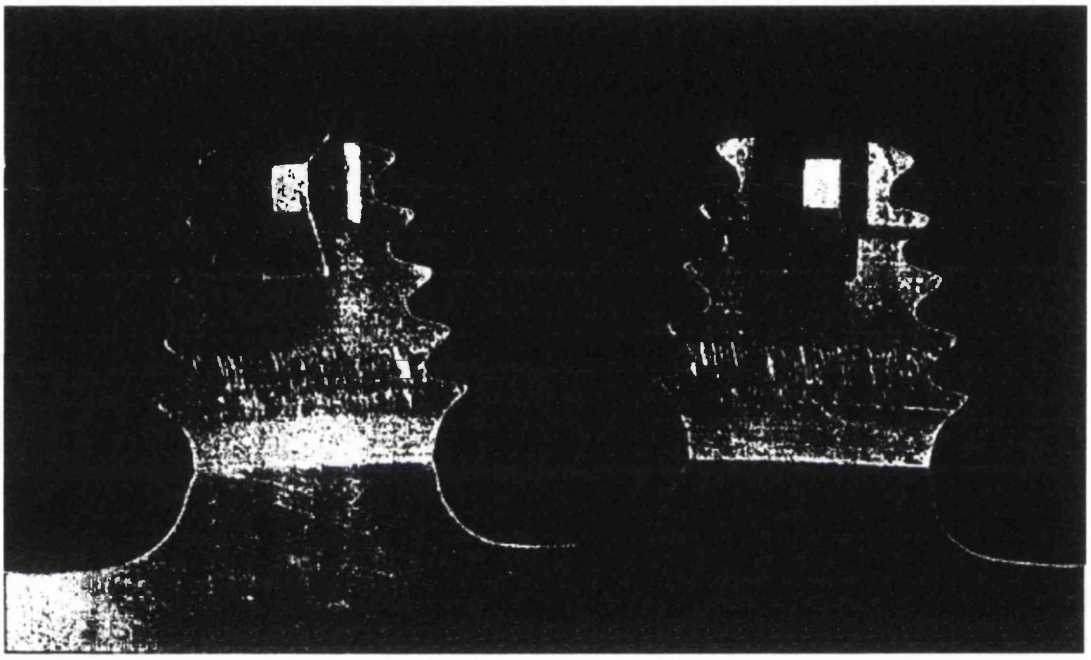

Figure 2.30.1. Disc rim wear due to cover plate sliding

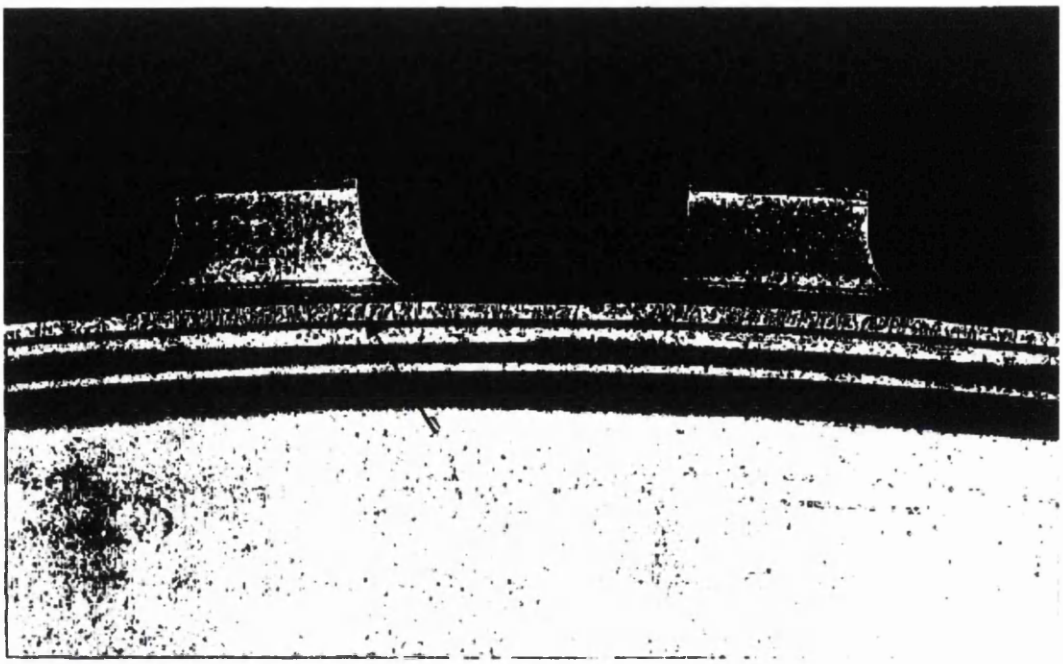

Figure 2.30.2. Cover Plate wear

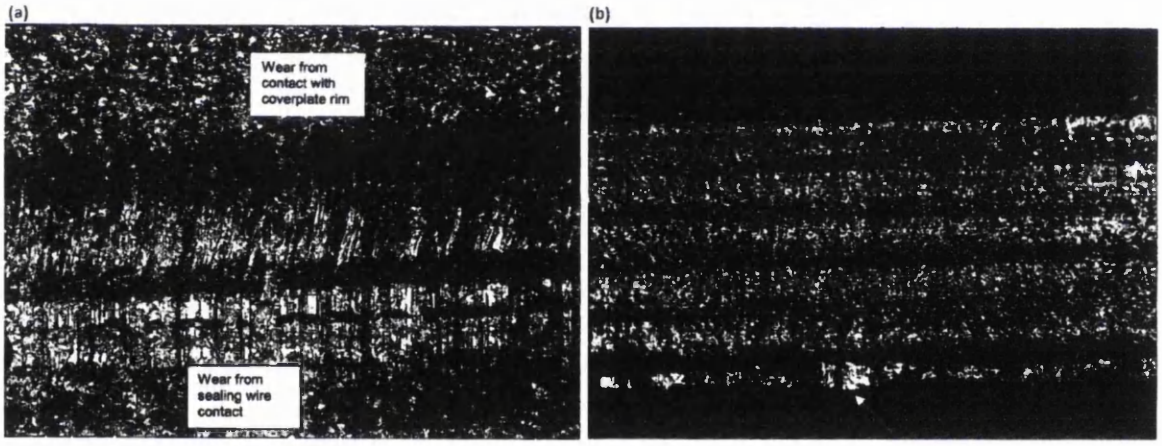

Figure 2.30.3. (a) Black putty replica of wear on disc due to cover plate sliding (b) The sealing wire between cover plate and disc causes more wear to concentrate on the bottom edge as shown by white arrow.

The wear shown above has numerous score marks running along both the x and y axis due to both the cover plate 'finger' contact and the Haynes 25 sealing wire which seals the cover plate to the disc. There have been numerous incidences involving the sealing wire in previous components and this has added to the severity of the wear problems especially since the

Haynes 25 sealing wire is harder than the U720 disc material. The resultant material removal is therefore large and unclear as to whether fretting wear caused this damage Unfortunately, since these images were taken from the Rolls-Royce archives, there was not any measurement as to how deep the wear scar was or the surface roughness characteristics but on comparing these images to other forms of wear, it would imply that this all the trademarks of a galling wear i.e. large material removal.

A modification to the interface between the two components is therefore needed which would reduce the degree of wear to acceptable limits. The modification was approached from two fronts. In the existing design the contact between the cover plate and disc is restricted to a 1 mm wide "finger" on the cover plate. Furthermore, the cover plate distorts, so that only a corner of the 1mm wide finger is in contact with the disc for part of the time. A modification to the geometry of the cover plate was sought which reduced the contact stresses.

Secondly, a suitable surface coating on the cover plate to minimise wear of the disc, without excessive wear of the coating itself, was also sought. Coating the disc was not considered a desirable option in view of the potential fatigue penalty the coating would inevitably introduce and because restricting the coating to the central region of the firtree front face avoiding the firtree roots would mean achieving good coating adherence and robustness would be very difficult

Simple button-on-plate wear tests (Test Method MM31021) were carried out to record the various wear rates of surface coatings. A ranking procedure was then used to select the best surface coating which was found to be Tribomet T104CS. Modifying the cover plate finger to a "barreled geometry to alter the contact stresses between the disc and cover plate reduced the wear measured on the disc specimen. However, this was not to a sufficient degree to suggest that the required number of flight cycles could be completed before wear exceeded engine manual limits.

2.31 Oil Pipe Failure by Residual Torsion – Lynx Helicopter

Most fatigue failures, without the presence of wear are caused by low cycle or high cycle fatigue as discussed previously whereby constant stress amplitude is acting on the component. This ultimately causes the movement of dislocations to relive the stress the component is under in that high stress vicinity, which leads to a high density of slip bands –

weakening in the material in this region. Hence failure can occur through no interaction with other components but simply by the means of the stress it is subjected to.

However, in one such case at Rolls-Royce, an oil pipe failure occurred on a Gem engine, which is a turboshaft engine developed specifically for the Westland Lynx helicopter in the 1970s. The oil pipe was made from Alloy C263 is an aluminium-titanium age hardening nickel base superalloy. The Gem engine and the location of the Number 8 bearing oil pipe is shown in Figure 2.30.1.

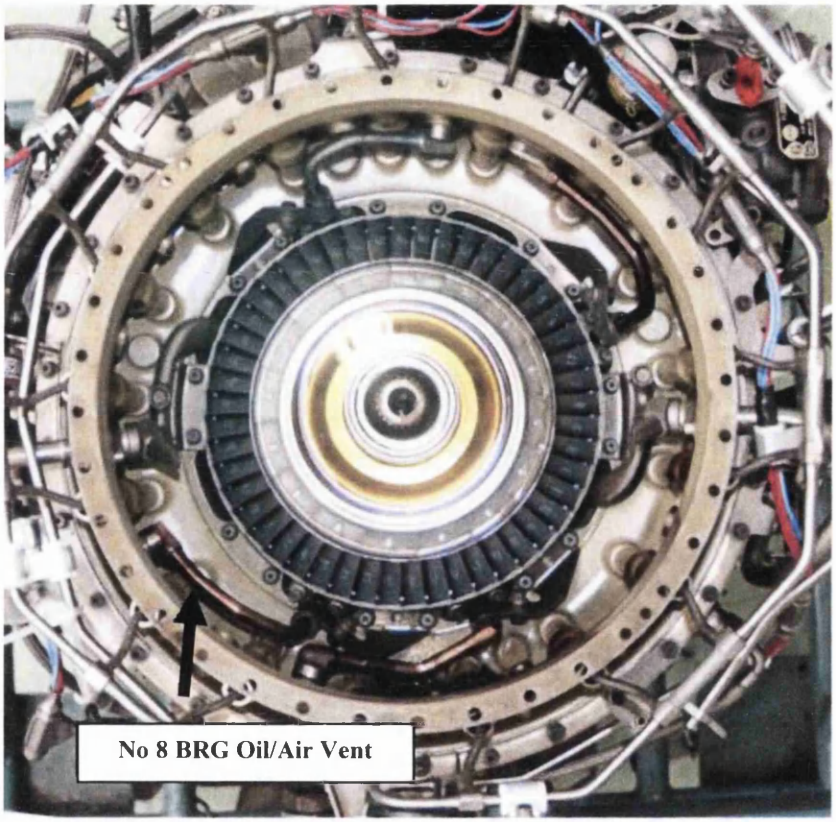

Figure 2.31.1. Gem engine from lynx helicopter and the location of the No 8 bearing oil pipe

In this case, the pipe had failed by a mixed mode of fatigue i.e. the failure started due to high cycle fatigue as a result of engine vibration and then changed to low cycle fatigue as the pipe progressed to failure. Additionally, there existed heavy 'cross-ways' rub marks across both sides of the fracture surface (obliterating about 1/3 of the visible fracture surface). This was due to both sides of the fracture moving over one another after failure. On alignment of these rub marks it can be seen that they do not sit over the same portions of the fracture surface on

comparing one side to the other i.e. they have twisted with respect to each-other. This indicates that prior to failure of fracture #2 there was torsion ('twist') in the pipe that relaxed on failure.

This discovery led to an inquiry into how the pipe was fitted and it was unanimously agreed that the pipe had been manipulated into position which caused a residual stress by torsion in the pipe.

This is not direct wear contact and does not call for a contact wear damage inquiry but it is a form of fatigue wear and does show that interference, whether by contact or not can considerably reduce the life of components. This outcome is also helpful when considering fatigue testing and the loading of specimens into the servo-hydraulic machines since much care should be taken not put torsion into the specimen when fastening into the machine.

2.32 Simulating Wear Damage

This chapter will discuss how specific types of wear damage will be replicated onto specimens for the following test programmes. The way in which replication of wear damage is performed is important so that it coincides with wear damage seen on current and ex-service engine components and also to some extent with the existing definitions of these types of wear in literature.

Simulating damage is not straightforward as it is such a complex phenomenon involving many variables. Assuming the tests are carried out in a regular laboratory environment and the material combination and their surface characteristics (surface finish and surface treatments such as DFL and shot peening) remain the same, the main variables which can be changed to achieve wear scars of different morphologies are the slip distance of the pad and specimen, contact pressure between the pad and specimen, frequency of slip and temperature.

Even with a preconception of the intended damage, it is still difficult to obtain the types of damage seen in service since there are many other factors that contribute to the contact wear within real engine components. For example, consider the blade and disc in a blade-disc joint, they are subjected to two different loads. One load is the low cyclic radial centripetal force from rotation and the other is high cycle and originates from lack of media flow as the blade

passes vanes. Hence, depending on the contact design, the combination of the two loads will give different normal and tangential contact distributions as well as bulk stresses in the contact surfaces. This is exacerbated by the thermal stresses at such high temperatures which can further alter the contact mechanics.

However, aside from the complex problem of thermal and cyclic stresses, there is also the added problem of the flight profile and mission history - which for engines such as the EJ200 or other military jet engines, not one operation is the same, and so this can give rise to unpredictable stresses and complex patterns of movements between components in contact. Components in contact that have different mass and thermal expansion values also slip differently relative to each other at higher temperatures [84] and this can lead to unpredictable contact mechanics.

The tendency of a material to wear as a result of contact is affected by the ductility of the material. Typically, hardened materials are more resistant to contact wear whereas softer materials of the same type will wear more readily. The propensity of a material to wear is also affected by the specific arrangement of the atoms, because crystals arranged in a face-centered cubic (FCC) lattice will usually allow material-transfer to a greater degree than a body-centered cubic (BCC). This is because a face-centered cubic has a greater tendency to produce dislocations in the crystal lattice to accommodate the increase in stress and therefore plastic deformation occurs more readily. Due to this, an FCC metal is more prone to wear damage such as fretting, scuffing and galling and the surface roughness is likely to be larger than that of a BCC material.

Another consideration is that if a metal has a high number of stacking faults (a difference in stacking sequence between atomic planes) it will be less likely to cross-slip at the dislocations[118]. Thus, a material's resistance to wear is usually measured by its stacking-fault energy. A material with high stacking-fault energy, such as aluminum or titanium, will be far more susceptible to wear than materials with low stacking-fault energy, like copper, bronze, or gold. Conversely, materials with a hexagonal close packed (HCP) structure, such as cobalt-based alloys, are extremely resistant to wear damage[119].

The following chapter briefly discusses three mechanisms of wear damage known as scuffing, fretting and galling and provides example images of what each wear damage scar

typically looks like in service. The images as well as wear scar measurements will be used in the ongoing test programmes so that it can be replicated in laboratory specimens.

2.32.1 Scuffing

Scuffing, like all the other contact wear mechanisms has been a research topic of vast interest for many years but the factors that account for it are poorly understood. Even defining what constitutes scuffing has not yet been fully resolved. The majority of research has focused on the macroscopic observations of failure to define the onset of scuffing. Familiar terminology includes "gross damage"[120], "solid-phase welding"[121] and "adhesive wear"[122]. On a microscopic scale "a roughening of surfaces by plastic flow whether or not there is material transfer"[123] has also been presented as an alternative definition.

Scuffing is frequently used in describing the breakdown of lubrication usually at high sliding speeds and low loads. It is generally accepted that failure occurs when the rate of film removal is greater than the rate of film formation[124]. These films could be the dry film lubricants applied during manufacture, oxide films or in the case of nickel superalloys, nickel oxide glazes. Nevertheless, the failure of these films is due to an unknown additional mechanism and some evidence suggests that film breakdown is dependent on the operating conditions, the physical and chemical nature of the lubricant, the surrounding atmosphere and the material properties of the surfaces[125].

There is strong evidence to imply that scuffing failure may be a result of thermal effects and frictional heating due to interacting asperities is a significant factor. Under operational test conditions, scuffing generally results in a drop in the electrical contact resistance in a critically worn area, indicating a breakdown in the surface film and the base metal[126].

It should be noted that if the DFL has been worn away or if the oxide layer or nickel oxide glaze does not have time to reform, then the bare metal will be exposed and full metal-to-metal contact will occur. Further sliding will result in the initiation of fatigue cracks. This may be speeded up by other factors such as wear debris (that become trapped between the contacts), stress gradients between the worn and unworn regions and if other mechanisms

come into play such as spalling and plucking which loosens the surfaces and causes it to break off.

There are numerous scuffing models that can help better understand this wear mechanism and these are outlined in W.F. Bowman and G.W. Stachowiak – '**A review of scuffing models**'[127] among others.

Examples of scuffing damage are shown in Figure 2.32.1.1 (a) and (b.) The wear damage in (a) was caused by lock plates that are designed to mate up against the disc rim and prevent the blade roots from coming out of the disc slots. However, due to engine running and vibration, there is small relative slip between the two which can cause contact wear. From the scuffing descriptions given in literature, it would lead one to believe that the wear damage in this case is scuffing since the material removal is very small, just enough to remove the surface coating. The most severe wear depth measured for (a) was recorded as 20μm (0.02mm) and the surface roughness was relatively low at 1.34μm in contrast to its standard surface roughness of 0.82μm. The damage shown in Figure 2.32.1(b) is a result of slip between bolt and washer against the surface of a high pressure BR715 turbine disc. As in the case of (a), the damage is not in a visually severe condition but the wear depth was higher than (a) and found to be 0.06μm at it most sever point. The corresponding average surface roughness values were found to be 2.43μm in contrast to its original surface roughness of 0.79μm.

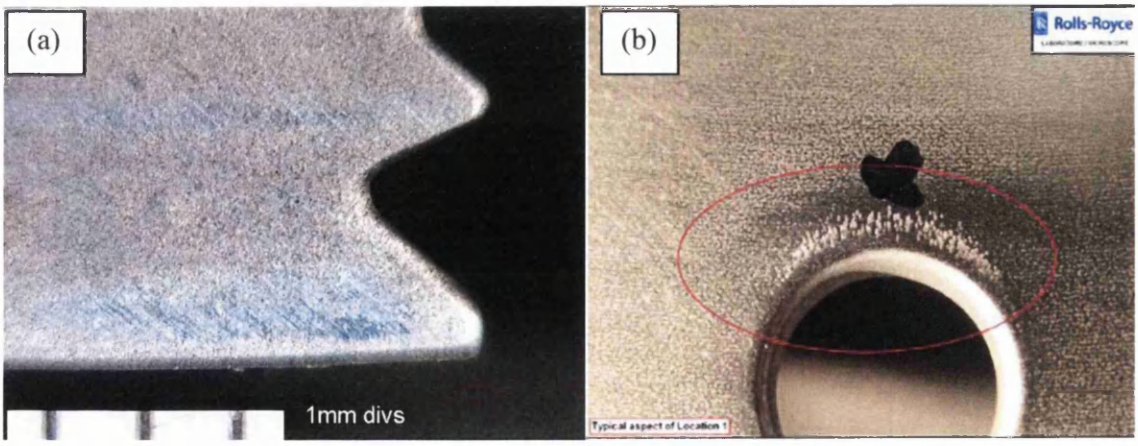

Figure 2.32.1.1. (a) Scuffing wear on a disc firtree root of the front face near the rim and (b) scuffing wear around a bolt hole due to bolt/washer contact on a BR715 HP turbine disc. In both cases the wear is mild but spread over a large area. Images courtesy of Rolls-Royce.

From the examples seen in ex-service components within Rolls-Royce, the wear scar morphology of scuffing tends to be widespread and relatively smooth. Closer inspection reveals linear wear tracks with patches of oxide layer removed.

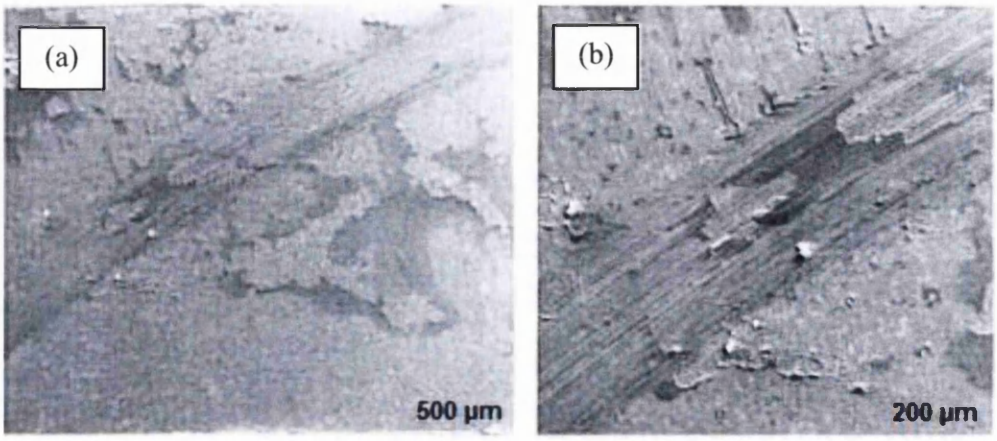

Figure 2.32.1.2. SEM images of wear tracks on a firtree root with scuffing (a) 20x (b) 50x. Image courtesy of turbomeca and Rolls-Royce.

Further general images are shown below to provide examples of scuffing in automotive engine components.

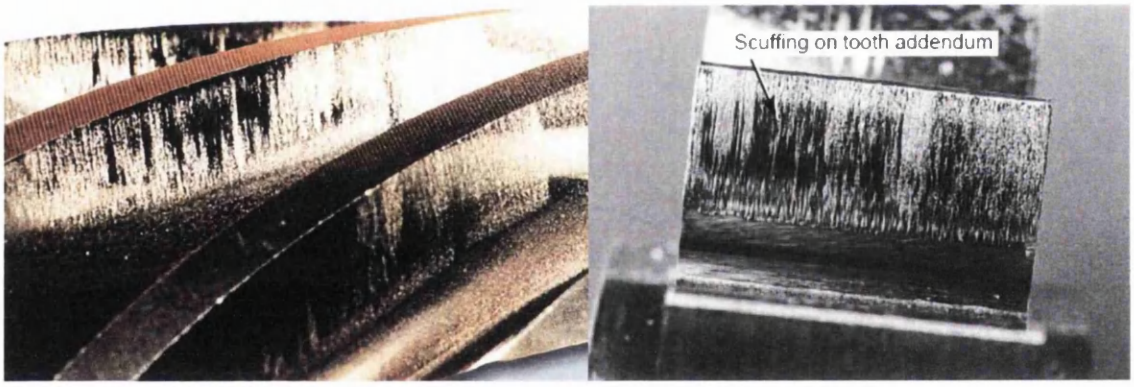

Figure 2.32.1.3[128]. Scuffing on gear teeth. Note how the wear is widespread, light and just enough to remove part of the surface coating.

Damage evolution is directly related to the contact sliding condition. Hence when simulating scuffing damage onto laboratory specimens it is important that the contact force is relatively low and the sliding distance is large as not to create large material removal. Furthermore, since high frequency is generally associated with scuffing wear this should be taken into consideration during the test. Since replicating wear damage is purely empirical, it is

accepted that the key to achieving the most realistic wear scar morphologies is through a trial and error basis. Hence, it is important to recall on previous components that have undergone scuffing and compare them with laboratory worn specimens until they are as similar as possible before carrying out tests.

2.32.2 Fretting

Whereas sliding wear usually results from two solid surfaces moving over one another with relatively large sliding distances, fretting often arises between surfaces which are intended to be fixed and as a result, the sliding distances are very small. The small amplitude of movements are generally created as a result of vibration or because of the complex stress systems in that particular area of the engine e.g. disc/blade root.

Even though fretting occurs within a small sliding scale, its effect can be more damaging than larger sliding distances. Partial slip fretting occurs in the sliding scale range 1-100μm and research has shown that the greatest life reduction occurs when the sliding amplitude is approximately 50μm but this is material specific. The point at which the partial slip regime moves into gross slip fretting is not clear and again depends on the material involved, the mechanical properties of the two contacting materials, and the environmental conditions. The transition to sliding wear has been reported at amplitudes as large as 300μm, and as small as 50μm. However, once the gross slip regime is achieved, material removal increases and interestingly the fatigue life increases since cracks that are formed can be removed during the wearing process. In general, although fretting wear could be regarded as reciprocating sliding wear with very small displacements, there are enough differences in both wear rates and mechanisms to warrant the use of a separate, distinct terms.

Since the sliding amplitude at which fretting becomes sliding is material specific, it makes fretting more difficult to understand. To distinguish between the two, one must consider the dimensionless wear coefficient, K. It should be noted that under fretting conditions, K is dependent on displacement but under sliding conditions, it is not.

The volume worn per unit sliding distance, Q, can be estimated using the Archard Wear Equation[114].

$$Q = \frac{KWL}{H} \qquad (2.32.2.1)$$

This equation relates wear to the macroscopic quantities W, the normal applied load, L, the sliding distance, H, the indentation hardness of the softer material, and K, the Dimensionless Wear Coefficient. The value K is of particular importance as it provides a valuable means of comparing the severity of wear in different systems.

For engineering applications, the value W/H is often replaced with the symbol k, which is the Dimensional Wear Coefficient and represents the volume of material removed by wear per unit sliding distance per unit normal.

$$\textit{Dimensional Wear Coefficient}, k = \frac{\textit{Wear Volume}}{\textit{Normal Load x Total Sliding Distance}} \qquad (2.32.2.2)$$

k the dimensional wear coefficient can replace W/H.

At very small amplitudes, the wear rate is negligible due to the contact zone 'sticking'. As the amplitude is increased, microslip will arise at the outer edges of the contact zone. As a result, a mixed stick and slip, or 'partial slip', situation is reached. During this 'partial slip' phase, the proportion of microslip increases and k rises slowly. Once the area of microslip covers the whole of the contact area, 'gross slip' is achieved and k begins to increase more rapidly. k continues to rise until eventually leveling off at a constant value expected for the sliding regime.

Although fretting tends to produce less wear volume than sliding, it is this regime that causes the most problems. Fretting wear can firstly lead to loosening of components that are intended to be fixed, resulting in a further increase in the relative movement and/or vibration, and a consequently accelerated rate of further wear. Since the debris formed by fretting are predominantly oxide, which in most metals occupies a larger volume than its originating material, fretting wear can also lead to seizure of parts that are designed to slide or rotate with a small clearance. Whether fretting leads to increased clearance, or to seizure, depends on the ease with which the wear debris can escape from the contact region. Fatigue cracks can also initiate at fretting sites leading to fretting fatigue.

Typical images of fretting are of the partial slip kind. However, since fretting encompasses the gross slip and reciprocating sliding regimes, it is important to show these kinds also. As already mentioned, fretting generally results from components in contact that have more freedom of movement that the design limits intended. This can result from engine vibration which is very difficult to control. The following images shows a typical example of fretting wear on an ex Rolls-Royce firtree root.

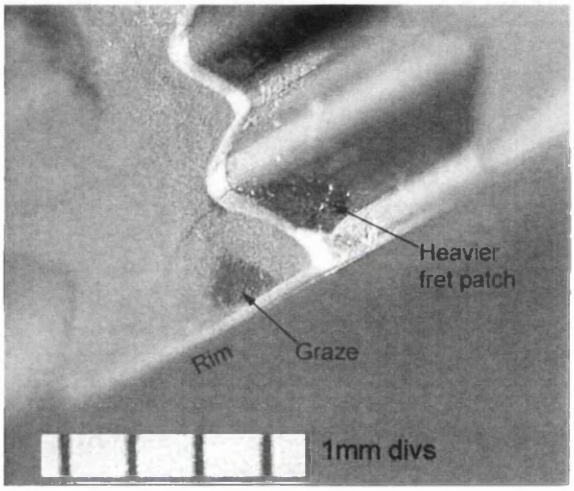

Figure 2.32.2.1. Fretting wear damage resulting in a crack running through the front face of a disc post. The average surface roughness of the fret patch was recorded as 5.26μm.

The following set of images was taken from an internal Rolls-Royce report which was written to detail the outcome of a Trent 1000 HPC4 rig test. The diagram below shows the layout of the rig test MRA47610.

Spacer

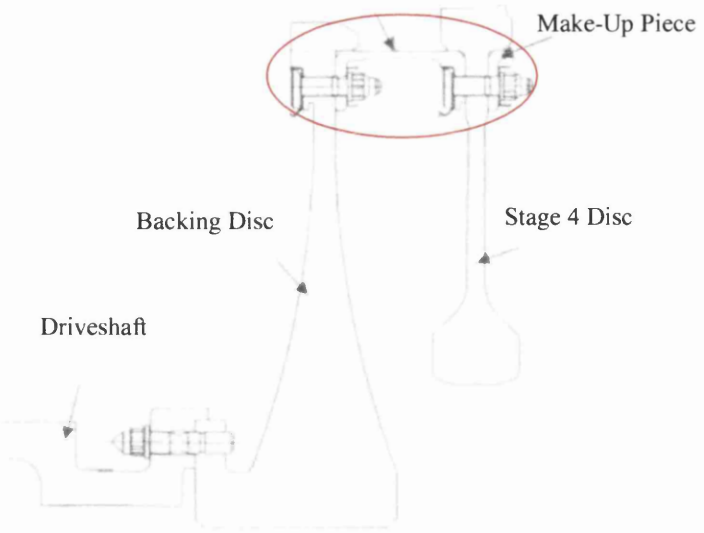

Figure 2.32.2.2. Trent 1000 HPC4 Spin Test No.MRA47610 layout. Red circle indicates region of fretting wear damage.

The wear damage on the rig test components, shown in Figure 2.31.2.2 has been described as fretting wear by Rolls-Royce failure investigation team, Derby. The damage itself occurred around the bolt holes where the spacer plate is attached to the RR1000 HPC4 disc. It is not known how much displacement takes place at this location (circled in red in Figure 2.32.2.2) but there is certainly considerable damage as a result of the centrifugal force during spinning. During the test, the bolts "fidgeted" in the holes resulting in wear of the washers and mating surfaces as well as contact wear between the bolt shaft and holes. As a result, six of the bolts in the spin test failed. One bolt that did not fail is shown in Figure 2.32.2.3d.

The damage around the HPC4 bolt holes was found to be ≈0.1mm deep on average with a large surface roughness of 5.97μm. The wear scar morphology was not uniform and exhibited sharp asperity features, more typical of severe galling wear. On the other hand, the fretting wear shown on the bolts had a much smaller wear depth of only 0.05mm and a relatively low surface roughness of 1.22μm. The Waspaloy washers also had lower values of surface roughness compared to the RR1000 disc at 4.35μm.

Close up inspection of the spacer in Figure 2.31.2.4 shows unpredictable patterns of movement whereby the wear marks are orientated in different directions. This suggests that the sliding displacements altered during the course of the rig test.

It is important to realise that once the damage exceeds the partial slip regime, the wear scar resembles that of full sliding to a high degree of likeness and it makes characterisation difficult, due to the irregular wear scar morphology.

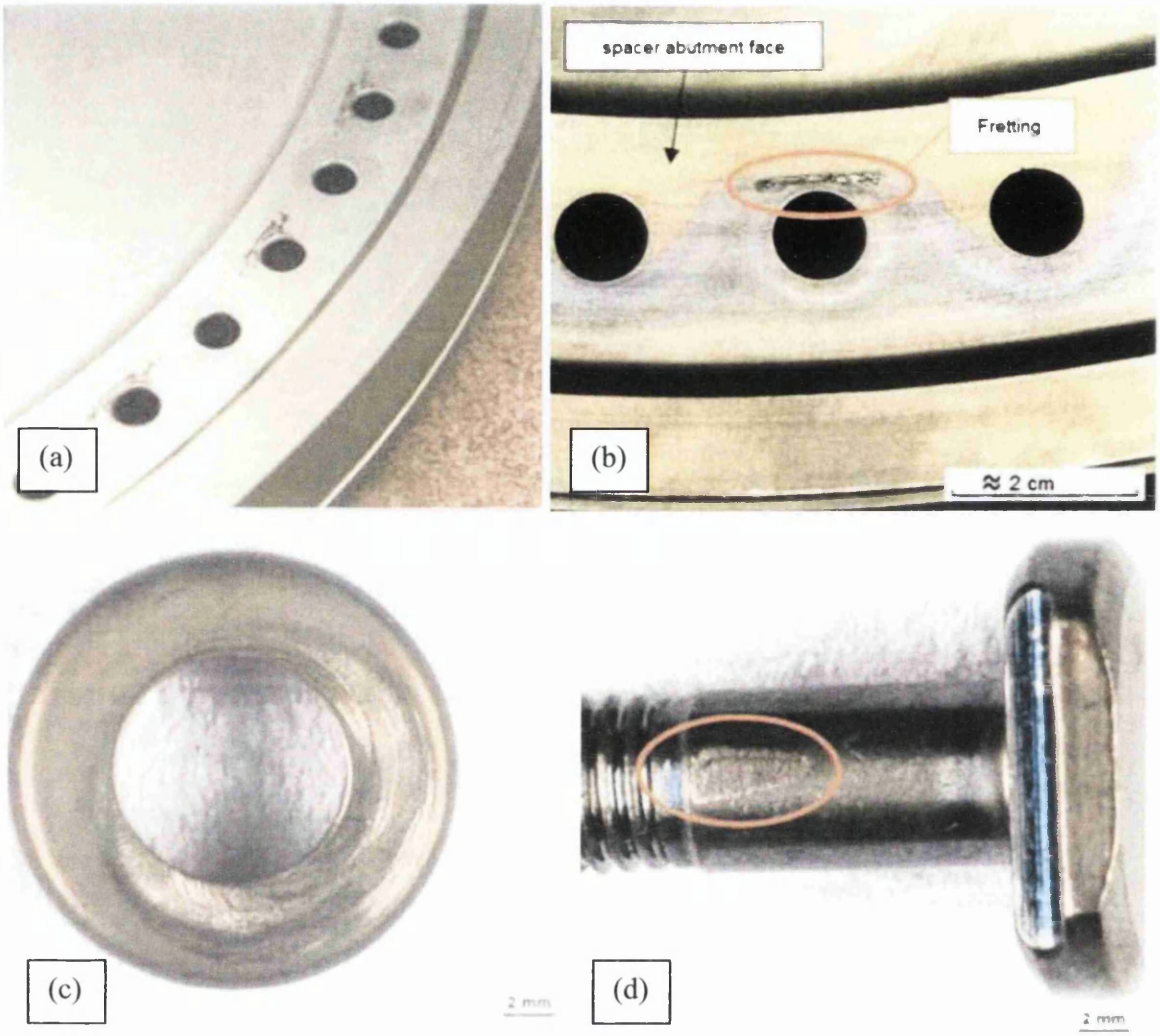

Figure 2.32.2.3. Components with stated fretting damage after a HPC4 rig test. (a) and (b) HPC4 RR1000 (c) Waspaloy washer (d) Waspaloy bolt with fretting wear. It is difficult to determine whether the damage is in fact fretting once the gross slip regime is entered.

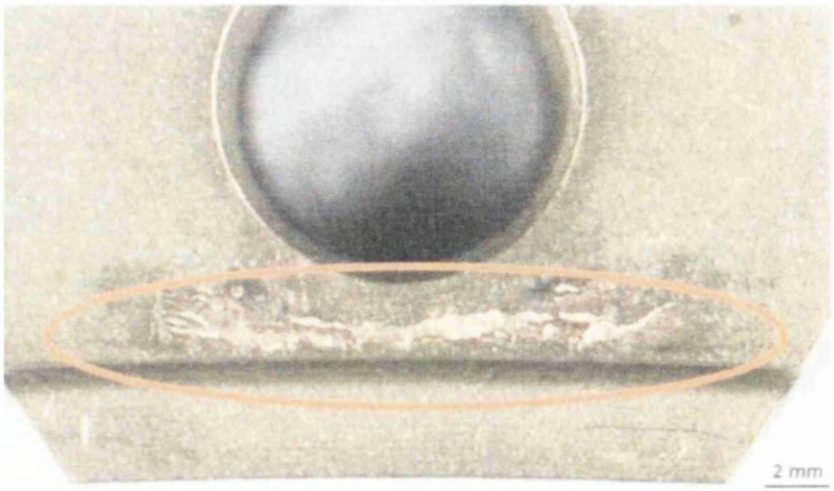

Figure 2.32.2.4. Close up view of fretting around the disc abutment face of a spacer. Image courtesy of Rolls-Royce.

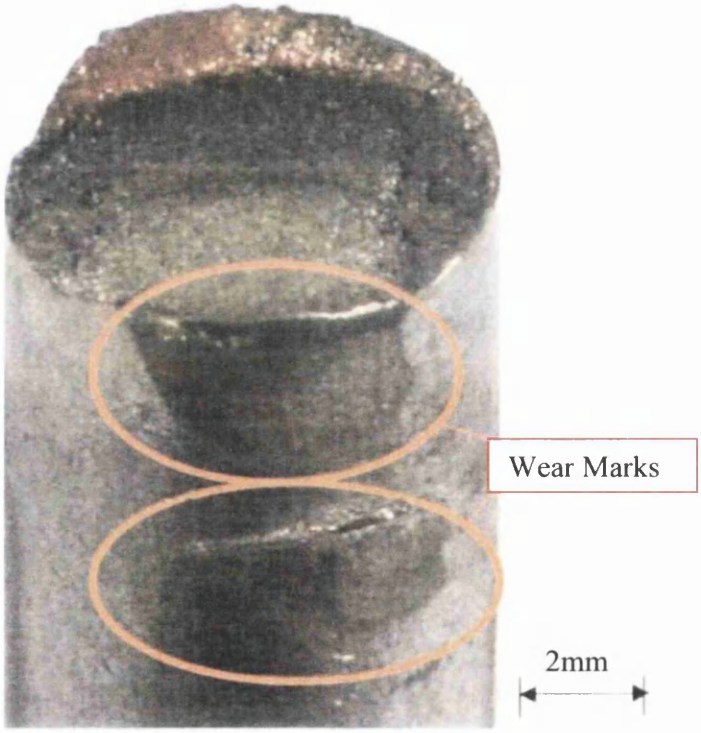

Figure 2.32.2.5. Failure of a Waspaloy bolt as a result of fretting fatigue. Image Courtesy of Rolls-Royce.

In order to simulate fretting damage in all its regimes, large contact stresses will be adopted in the range of 150-250MPa and the sliding distances will be chosen in the range of 0.05-1mm to simulate the partial slip, gross slip and reciprocating sliding regime. The rate of

material removal should be small resulting in a wear depth of no larger than 0.5mm deep. However, this will be difficult to control once the wear test begins.

Since there is more emphasis on the contact load and sliding distance in fretting, the frequency of sliding will kept at a standard frequency of 2.5Hz used for most fretting wear tests at Oxford University.

2.32.3 Galling

Galling is a more severe form of scuffing due to local welding and is associated with gross surface damage. The word often refers to damage resulting from unlubricated sliding at low speeds and high loads, characterised by severely roughened surfaces and transfer or displacement of large fragments of material. Galling may occur in nominally lubricated systems when the lubricant film breaks down and can be followed by seizure of the surfaces and consequent gross failure of the sliding surface. Certain metals will generally be more prone to galling, due to the atomic structure of their crystals. Since aluminum is relatively soft, it will gall easily, whereas harder materials such the nickel base alloys are slightly more resistant to galling. The harder the material, the more resistant it is to wear and this is true for all other forms of wear damage also.

Examples are shown in the following images and it can be seen that their surface morphology is highly irregular and roughened and its corresponding surface roughness values are much higher than that of fretting and scuffing.

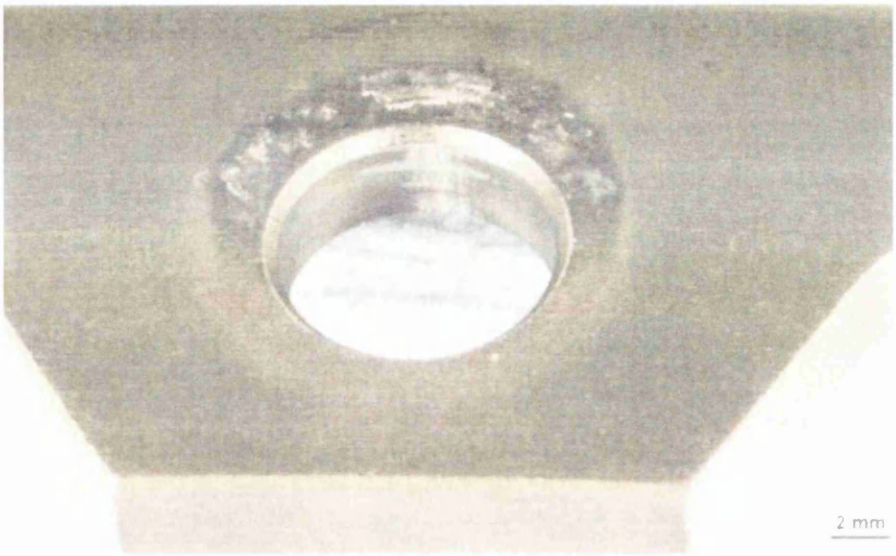

Figure 2.32.3.1 Galling wear around a spacer bolthole. Worst case was 0.8mm depth into material. Image Courtesy of Rolls-Royce

The image above shows a heavy galling patch around a spacer bolthole. The damage illustrates a characteristic uneven surface. There does not appear to be a repeatable pattern of continuous lines or stripes and the entire contact zone is patchy with exposed bare metal, some of which is raised or dropped below the surface. This is a highly severe form of adhesive bonding between the metal surfaces. The largest depth of wear was measured at 0.6mm which is relatively large when compared to fretting and scuffing. The surface roughness was recorded at a staggering 7.34μm which illustrates the severity of galling wear.

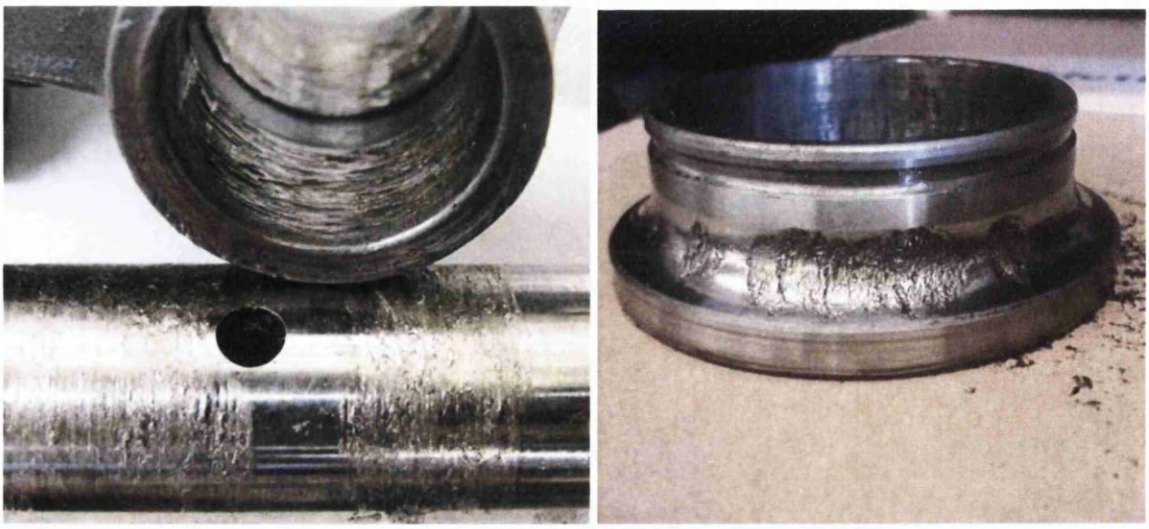

Figure 2.32.3.2. Examples of severe galling wear. Images taken from a private forum.

The images shown in Figure 2.32.3.2 illustrate highly severe galling wear. It can be seen in both images that large quantities of material removal have taken place. When simulating galling damage onto specimens, it is important that a highly roughened surface is produced with large surface roughness values to coincide with the examples shown above. The mechanisms that drive galling wear are very different to fretting and failure results from the overwhelming loss of material which increases the stresses in that region[129].

2.33 Literature Review Summary

This literature review has given a comprehensive overview into an array of topics that lays a solid foundation for further research into the complex subject of contact fatigue of metals and in particular, some of the contact problems in nickel superalloys in turbomachinery. With this knowledge and awareness of the problems seen in jet engine components during real operation, it allows one to concentrate on a particular area (or sub assembly) that will benefit the industry and hopefully prevent or lower the number of failures in the future.

Referring to other institutions and building on the work they have carried out, new tests can be developed to gain a more specific understanding of variables which have not yet been tested or little understanding exists. Until now, there has been little work on fretting fatigue at high temperature and therefore the vision of this research is to focus on this specifically.

3 Experimental Methods

The material chosen for the programme of work in this project was Udimet 720Li, a popular material of choice for turbine engine discs within jet engines as well as land based turbines, where operating environments require excellent thermal and corrosion properties as well as good creep and fatigue properties.

The material was supplied by Rolls-Royce and all the specimens were manufactured from the same disc forging which ensured consistent material properties from one specimen to the next. It was also stipulated that all specimens were cut out of the disc forging with the same orientation i.e. uniaxially from the bore to the rim.

The table below provides the properties and composition of Udimet 7201Li.

Material	Young's Modulus (GPa)	Poisson's ratio	Yield Stress (0.2 % offset), (MPa)	Chemical Composition (%)
Udimet720LI	219	0.33	881	Cr(15.5-16.5), Co(14.0-15.5), Al (2.3-2.8), C(0.01-0.02) B(0.01-0.02), Mo (2.8-3.3), W(1.0-1.5), Zr(0.03-0.05) Ti (4.8-5.3), Ni (Balance)

Table 3.1. Typical elastic properties and composition for U720Li.

Fatigue Specimens were made to the dimensions shown in Figure 3.2 with very fine tolerances and polished to remove any surface imperfections that would otherwise weaken the material.

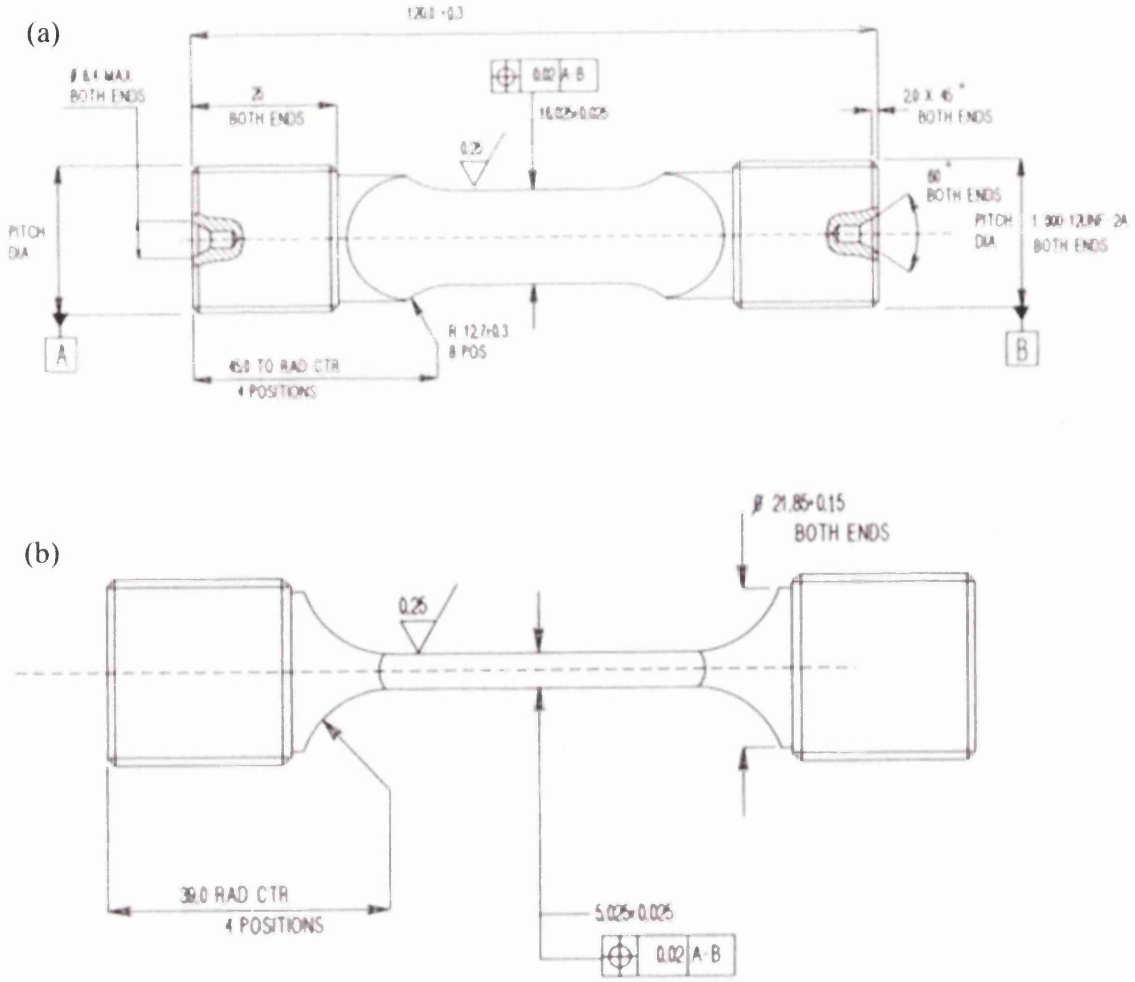

Figure 3.2. (a) A front view technical drawing of a fatigue specimen of U720Li used throughout this entire project (b) A side view technical drawing of a fatigue specimen of U720Li used throughout this entire project

3.1 Tensile Testing

In order to choose the appropriate stress amplitude for baseline fatigue testing, the ultimate tensile strength (U.T.S) of U720Li was first established. Discovering the UTS value ensures that the stress value chosen for baseline fatigue testing is not above the UTS value which would otherwise give zero fatigue cycles and would therefore be a waste of a specimen.

It has been shown that the yield stress and ultimate tensile strength of U720Li remains relatively unaffected by temperature until about 600°C, typical of superalloys strengthened

by fine and coherent intermetallic Ni3Al-based precipitates[130]. As a result, the tensile tests had to be carried out at the same temperature that that the fatigue test would be undertaken at, which is 600°C. This is a typical operating temperature for the bore of turbine discs during service.

Three tensile tests using U720Li specimens shown previously were carried out on a 100kN servo-hydraulic machine at a temperature of 600°C. The U720Li specimens were loaded into the machine and enclosed within a 100mm diameter split furnace and further insulted using Kao wool to prevent heat loss. The furnace was allowed to heat up until the temperature stabilised at 600°C ±3°C but every effort was made to ensure that the temperature was as close to 600°C as possible. Once the temperature had stabilised, the specimen was allowed to 'soak' for one hour before the test was started. Soaking allows the specimen to reach equilibrium so that even the core of the material is approximately 600°C, relieving any thermal gradients from the surface to the core.

Tests were conducted with a constant strain rate of $10^{-4}s^{-1}$ until tensile failure of the sample. The Phoenix software assigned to the machine produced a stress strain curve for the test specimen allowing the relevant data to be extracted with the most important properties being yield stress and UTS.

3.2 Baseline Testing

The cyclic stress level of the first set of tests is a large percentage of the UTS (≈80%), which produces failure in a relatively small number of cycles. Ensuing tests are run at lower cyclic stress values until a level is found at which a reliable S-N curve can be created.

Baseline fatigue tests were carried out on a 100kN servo-hydraulic machine at a temperature of 600°C. The procedure of preparing a specimen for testing is identical to that of the tensile test section above in that the specimen was allowed to 'soak' for one hour prior to starting the fatigue test as this minimises thermal gradients form the specimen surface to its core.

The thermocouples used for measuring the temperatures within the furnace were 'N' type.

Five specimens were initially tested with an R ratio of -1 to provide tests with only bulk elastic deformation and a trapezoidal waveform of 1-1-1-1. A further two series of baseline

tests were also carried out to achieve greater accuracy. The stresses that were chosen for each test series are shown in the tables below.

Baseline Test 1	
Specimen Number	Stress Amplitude (MPa)
1	800
2	750
3	725
4	700
5	650
Baseline Test 2	
Specimen Number	Stress Amplitude (MPa)
1	800
2	750
3	710
4	690
5	650
Baseline Test 3	
Specimen Number	Stress Amplitude (MPa)
1	800
2	750
3	725
4	650

Table 3.2.1. Stress Amplitudes for baseline testing

The number of cycles to failure was recorded for each stress amplitude and plotted on a Stress Vs Number of cycles (S-N) graph in order to produce an S-N curve. This was repeated a further two times so that three S-N curves were produced. These curves would be used for future reference when choosing stress values for ongoing wear damage testing and to compare life reduction factors between baseline and damaged specimens.

3.3 Wear Testing at Oxford University - The Dartec Rig

The first series of wear testing was part conducted at the University of Oxford using the Dartec servo-hydraulic wear testing machine. The main aim of the programme was to subject ten specimens to a range of pre-determined, reciprocating sliding wear damage at room temperature thus producing artificial damage. After each specimen had been subjected to

damage, they were fatigue tested at 600°C in order to determine the overall effect on its fatigue life when compared to baseline tests. Ideally, it would have been more realistic to impart wear damage and fatigue at the same time as in the case of real life components. Part of this project will attempt to deal with this particular problem.

The Dartec servo-hydraulic tensile testing machine consists of a hydraulic ram, a 125kN load cell, a cast iron chamber mounted on the machine base, hydraulic pistons, two fretting pads, a specimen and a LVDT (linear voltage displacement transducer) used for accurate displacement measurement.

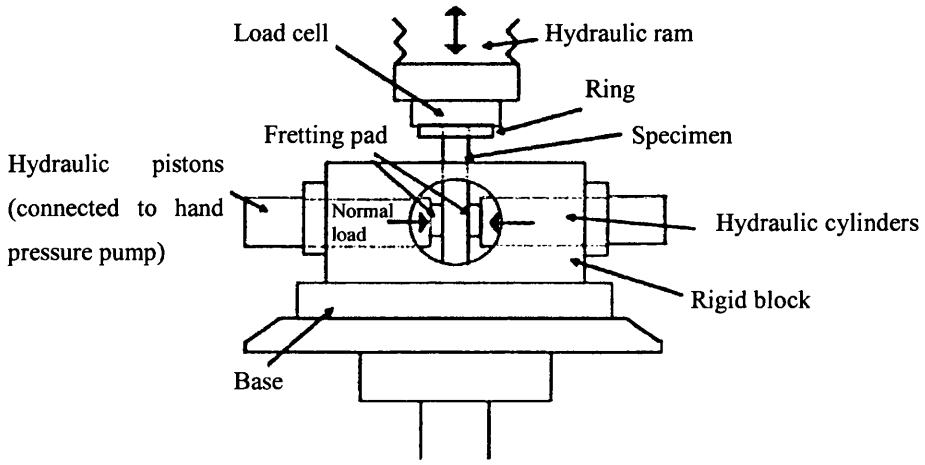

Figure 3.3.1. Schematic of the fretting wear rig.

Figure 3.3.2. Photograph of the fretting wear rig mounted on the servo-hydraulic

A pair of U720Li fretting pads with a flat-and-rounded geometry was used for the tests and was machined back to their original geometry after every test. Furthermore, the contact surface of the pads was polished with emery paper down to 1000 mesh after each machining.

Since the Dartec machine had only previously been used for performing wear tests on one type of specimen shape - in order to use fatigue specimens from this project, a custom specimen holder had to be designed and made. The specimen was connected to the cross-head of the testing machine by means of a specially designed threaded grip and this is shown in Figure 3.3.3.

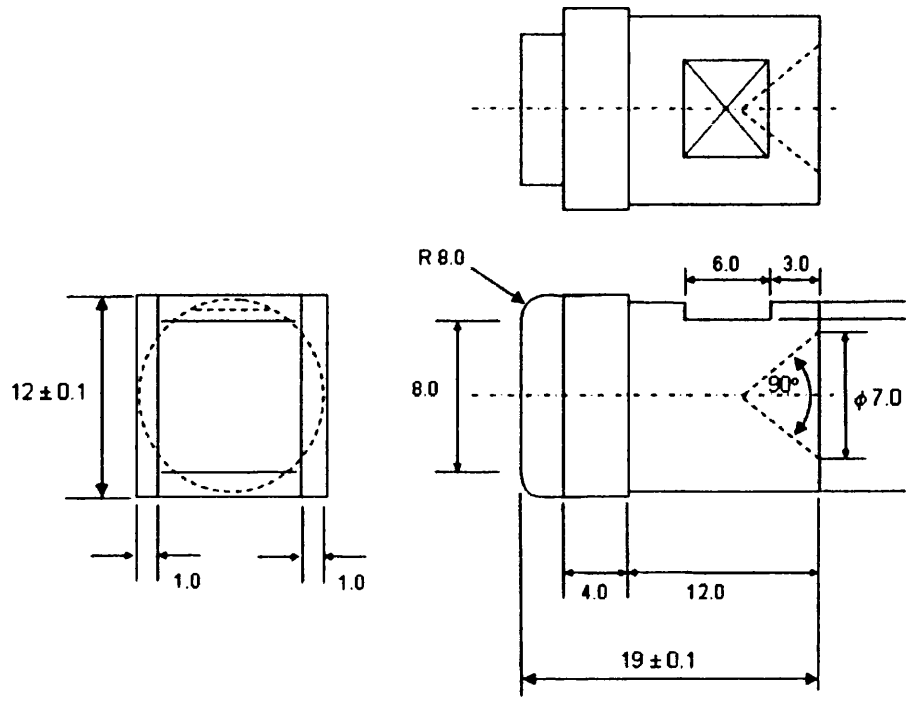

Figure 3.3.3. Schematic representation of a fretting wear pad

Vertical motion of the specimen between the pads induced slip between the contacting surfaces, provided that the prescribed cross-head displacement range was sufficient to exceed the displacement taken up in the specimen and rig elastic compliance. The fretting pads were pushed against the specimen through a pair of hydraulic cylinders capable of moving horizontally, perpendicular to the specimen axis.

During the test the normal force applied to each pad was maintained constant and equal. The load cell measures the total shear force applied to both contacts. The force in each contact is assumed to be half of this. The coefficient of friction was then readily computed as the ratio of the shear force to the normal force produced by the hydraulic cylinders on each pad, during the sliding phase of each cycle.

Test Number	Pad Pressure (Mpa)	Displacement (mm)	Frequency (Hz)	Number of Cycles
1	150	0.05	2.5	20,000
2	50	2	2.5	20,000
3	250	0.5	2.5	20,000
4	200	0.05	2.5	20,000
5	150	0.8	2.5	20,000
6	150	2	2.5	20,000
7	50	0.1	2.5	20,000
8	100	0.05	2.5	20,000
9	100	1	2.5	20,000
10	25	1.5	2.5	20,000

Table 3.3.1. Test matrix for 10 specimens with different pad pressures and displacement

The variables within the matrix parameters are the pad pressure and pad sliding displacement and these were chosen carefully to give a spread of wear damage similar to what had been seen in service on engine discs and other jet engine components.

The test was stopped when the cycle (peak to peak) count reached 20,000 cycles. The frequency was chosen to be 2.5Hz which is a typical value chosen for wear tests of this kind.

3.3.1 Digital Profilometry - Surface Roughness Measurements

Digital 3D profilometry was carried out on an Alicona IF-Profiler and was used to measure the surface finish of each sample in high resolution. Surface roughness is measured based on the extraction of a linear profile known as average surface roughness, R_a and the root mean square roughness, R_q and is completed according to ISO 4287/88.

The surface roughness measurements were carried out on the tested specimens in an attempt to provide further information, both quantitative and qualitative, about the damage obtained from the test. Surface roughness measurements were first taken of a plain specimen with zero damage as a baseline measurement. Measurements were then taken of the damaged specimens at different locations within the wear scar as it was anticipated that the surface roughness would not be uniform over the whole area. Hence, measurements were taken at the centre and the surrounding area.

3.3.2 Fatigue Testing of Damaged Specimens

The worn specimens were then fatigue tested at Swansea University to determine the effects of wear on the specimens fatigue life when compared to baseline tests conducted on U720Li earlier in the project.

The value of stress amplitude was chosen for this particular set of fatigue tests was selected from the baseline data that corresponded to a fatigue life of 20,000 cycles as this was the number of cycles that the wear tests were performed at in Oxford University using the Dartec wear test machine. Therefore, this test assumes that for each fatigue stress cycle, there is one wear cycle from peak to peak occurring at the same time.

The tests were performed at 600°C with an R ratio equal to -1 and a trapezoidal waveform (1-1-1-1) which is the preferred waveform for Rolls-Royce when carrying out fatigue testing. R ratios of -1 simulate the compression and tension experienced in components in jet engines more realistically. The same procedure was the same for these tests as the baseline tests discussed earlier.

3.4 Fretting Fatigue Testing

To focus on fretting fatigue, a fretting fatigue testing apparatus was designed in order to develop a series of in-situ tests that involves fretting at high temperature. The fretting test uses a pair of clamping plates which hold replaceable fretting pads against the surface of fatigue test specimens. The clamping plates are clamped together with high tensile bolts at either end. The bolt tension is balanced by the compressive force in the fretting pads, which transmit normal forces. The compressive force encourages fretting of the pads against the specimen surface during deformation (caused by the Poisson effect when the specimen cross sectional area decreases during tensile loading).

A schematic of the test arrangement is shown in Figure 3.4.1 and illustrates how the fretting pads are held in contact with the specimen by use of clamping plates. Figure 3.4.2 shows an image of the actual arrangement used during the tests. The plates were manufactured using CNC milling at Rolls-Royce Plc, Bristol.

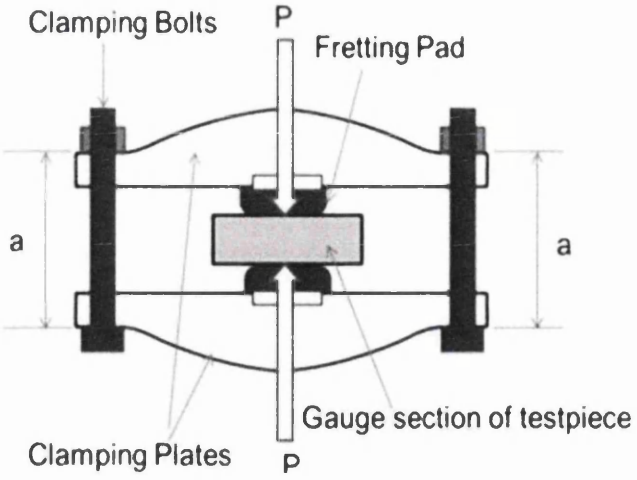

Figure 3.4.1. Birdseye view drawing of clamping plates and fretting pads

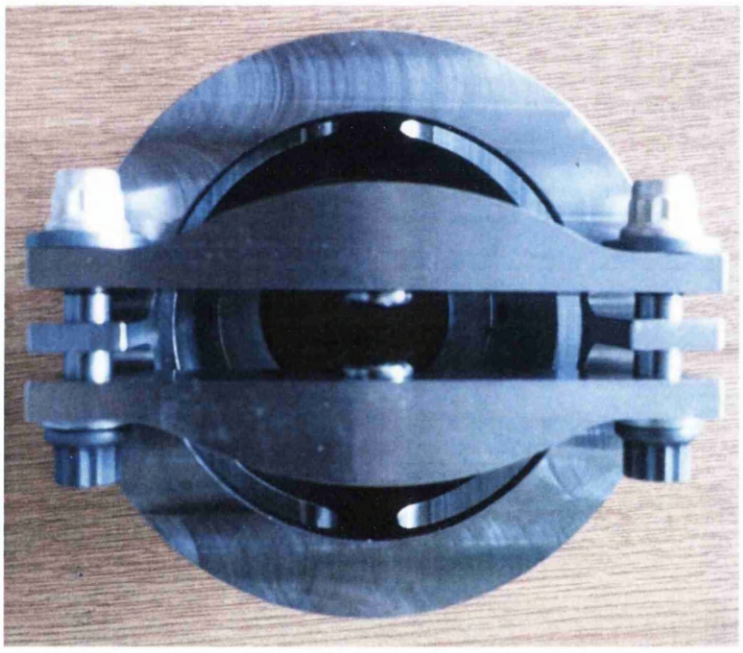

Figure 3.4.2. Bottom view of the clamping plates showing the fretting pads and plates

The following images show CAD drawings (drawn in AutoDesk Inventor) of the clamping plates for the initial part of room temperature testing and a technical drawing outlining the dimensions of the clamping plates.

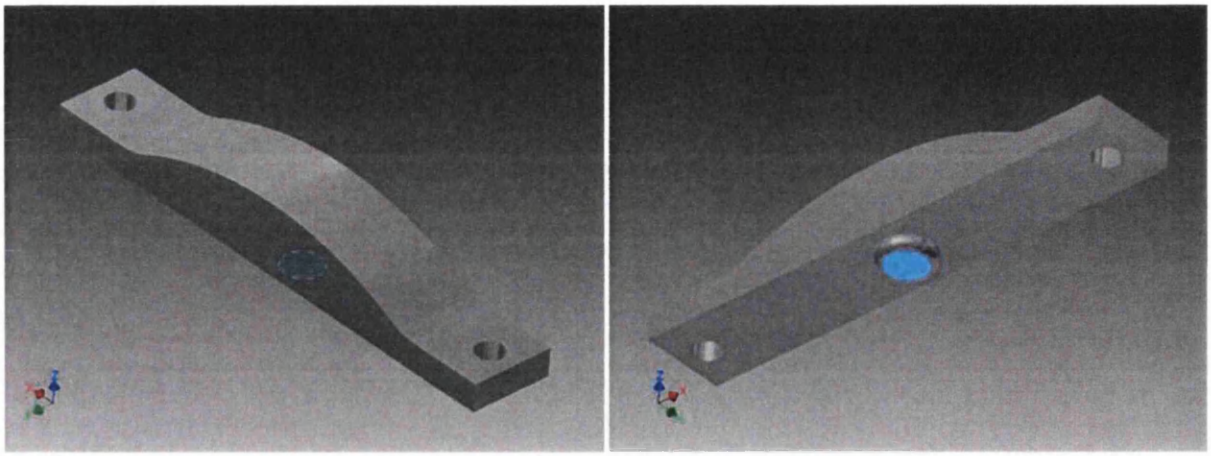

Figure 3.4.3 CAD drawing of clamping Plates created in AutoDesk Inventor.

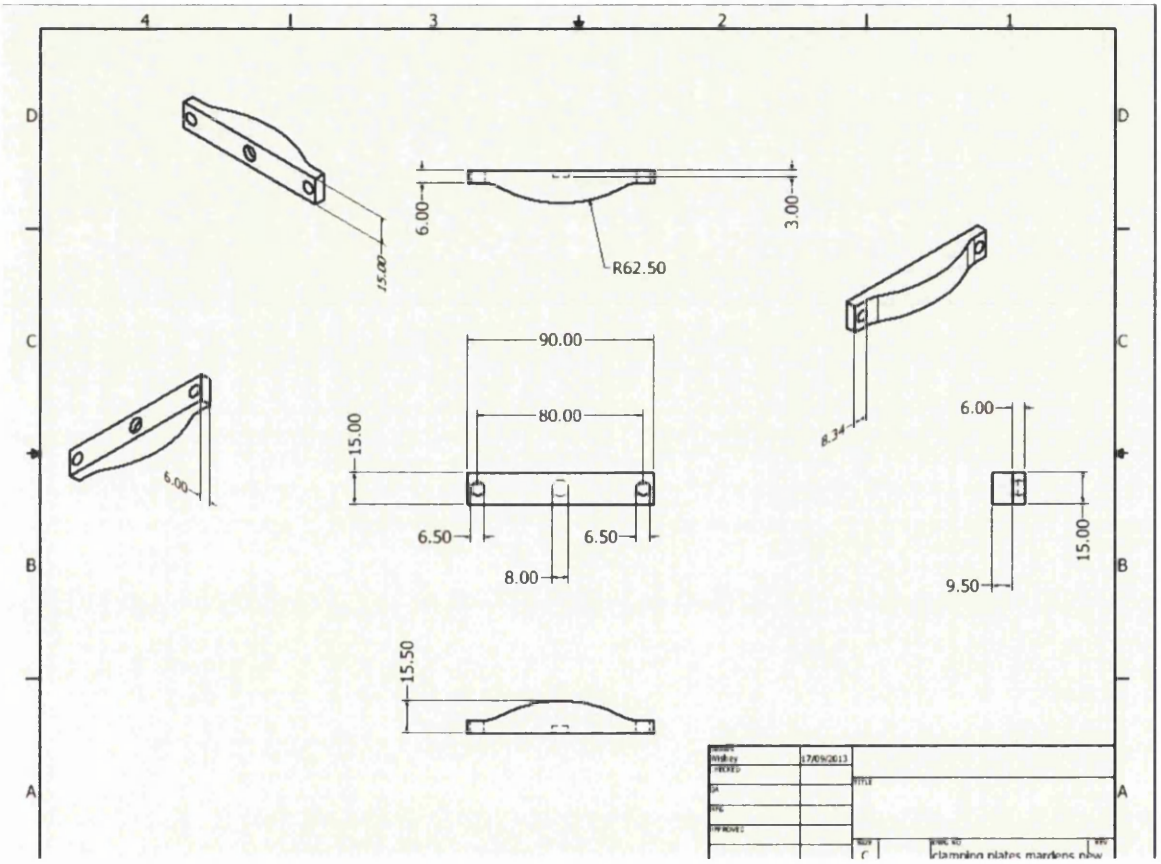

Figure 3.4.4. Technical drawing of clamping plates.

During the testing programme, it became apparent that the clamping plates shown above in Figure 3.4.3 were not going to last the testing programme. This was due to the permanent deformation of the plates as a result of yielding during room temperature testing. The problem would only be exacerbated during the high temperature testing section where the

plates would be exposed to 600°C. As a result, new clamping plates were redesigned and are shownin Figure 3.4.5. Note how the plates are a simple rectangular shape rather curved which negates high concentrations of stress in the fillet radii regions of the previous plates.

The redesigned clamping plates remained at 90mm in length and so did the distance between the bolthole centres and height of the plates which is 80mm and 15mm alike. The only difference is that the thickness of the plates has increased to 16 mm to cope with the high demands of stress. The new clamping plates were manufactured at Swansea University workshop using stainless steel 316.

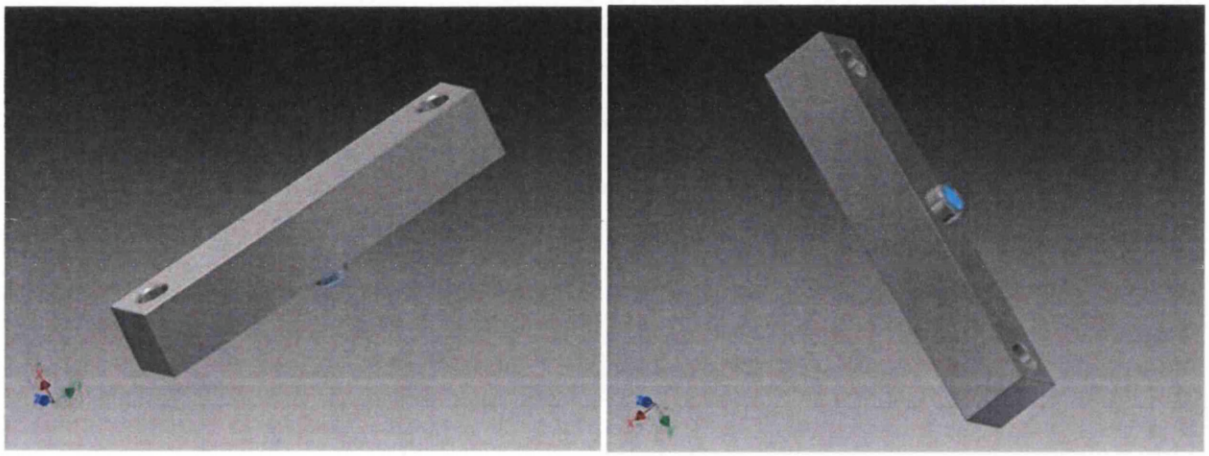

Figure 3.4.5. CAD Drawings of re-designed clamping plates.

In order to hold and locate the clamping plates over the specimen a rig was designed and fabricated. The rig was designed to allow fretting of the pads and specimen in the positive and negative y-direction but not in the x-direction.

The fretting cup has been designed to fit directly onto the servo-hydraulic pull rod. This makes it a relatively cheap and easy to use piece of kit for generating reliable results in a short space of time. The most suitable and cost effective material for fabricating the cup was stainless steel 316. This material offers relatively high temperature capabilities and adequate strength for this particular programme of testing.

Machining of the fretting cup was relatively straight forward using the turning method by use of a lathe at the Swansea University.

A 3D rendered model is shown below.

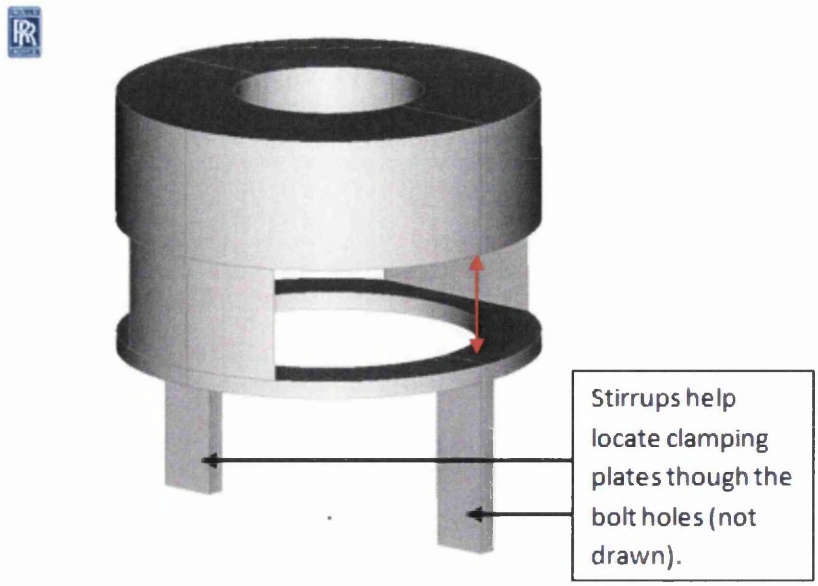

Figure 3.4.6. 3D rendered model of fretting fatigue rig. The red arrow between the cut outs illustrates how the unit will move during the test.

The cut outs in the side of the fretting cup were designed in order to encourage compliance in the unit and encourage natural movement, since the unit was not intended transmit all the force through the pads but only enough to encourage partial slip.

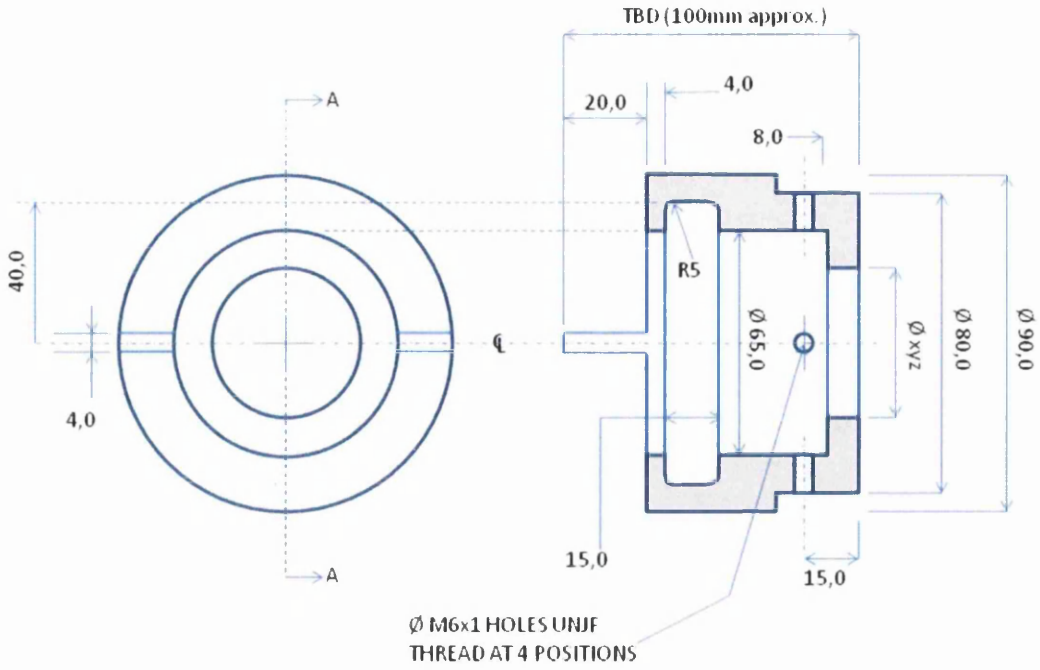

Figure 3.4.7. Technical drawing of fretting cup showing the dimensions.

The fretting rig setup complete with clamping plates is shown below.

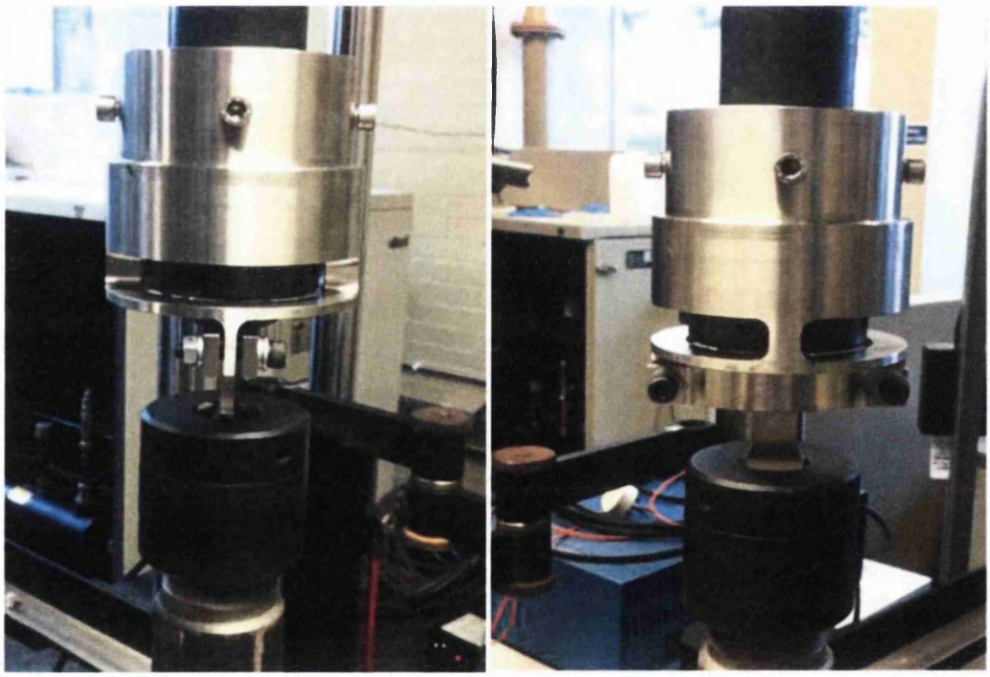

Figure 3.4.8. Images of fretting fatigue rig and clamping plates as it would look during a fretting fatigue test. The left image is a side view and the right image is a front view of the cup.

3.5 Measuring the Fretting Pad Pressure

A method of measuring the pad pressure acting on the specimen is now explained. Ideally, it would be beneficial to have a value of the pressure during the entire test so that pad pressure can be closely monitored to determine whether the pressure drops off at during the wear process at high temperature. However, a search for force/pressure sensors within the project budget were fruitless and most other sensors would not operate at temperatures in excess of 200°C and some 400°C. Furthermore, because of the large pressures through the pad (up to 355MPa) there were no pressure sensors on the market capable of withstanding these pressures.

3.5.1 Torque Wrench

To establish the initial pad pressure prior to encasing the setup within the furnace, a Clarke ¼" drive digital torque wrench was used to supply tension to the bolts. The wrench was calibrated to BS EN ISO6789 and was capable of supplying torque of up to 30Nm which is ample enough for the requirements of this project.

The bolts were tightened up equally on either side by slowly and incrementally turning the wrench on each bolt until they both reached the required torque value in Nm which is displayed digitally. Furthermore, the distance between the plates being bolted together from the outside surfaces and inside surfaces (shown in Figure 3.5.1.1) was also measured with a set of vernier calipers. This ensured that the mating surface of the fretting pad was in full contact with the specimen on both sides and it was necessary in order to perform finite element analysis which will be discussed in the next section.

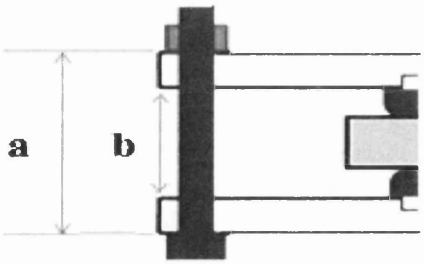

Figure 3.5.1.1. Schematic of the clamping plates set-up highlighting how the distance between the plates was measured between a and b on both ends of the plate before and after bolt torque up.

3.5.2 Finite Element Analysis

The clamping plates have a characteristic stiffness which enables the compressive force to be estimated from the separation of the bolt head and the nut ('a' in Figure 3.5.1.1).

An FE model was created in Autodesk Inventor from a geometric model as shown in the images in Figure 3.5.2.1. Using this information, finite element analysis was performed to calculate a rough estimate of the pressure through the pads.

The FE model assumes that the clamping plates are made from stainless steel 316 which is the material of choice for the clamping plates. This has an elastic modulus of **193 GPa.** The model was loaded by applying a normal restraint on the fretting pad and then displacing the upper rim of the bolt holes according to the real measurements taken in the laboratory.

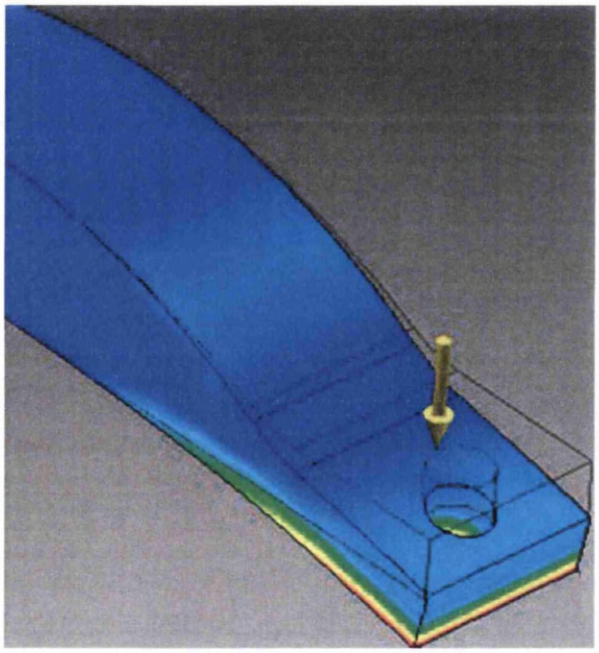

Figure 3.5.2.1. A section of a finite element model illustrating the stresses in the original clamping plates when a displacement is applied to upper rim of the bolt section.

3.5.3 Bolts

Initially, Waspaloy aerospace grade bolts and nuts were used because of their high temperature capabilities and superior creep and tensile properties. The part number for the bolts was AS22520 and has a double hex head which is typical of aerospace grades.

Waspaloy is a nickel base, age hardenable superalloy with excellent high temperature strength and good corrosion resistance, notably to oxidation, at service temperatures up to 1200°F (650°C) for critical rotating applications, and up to 1600°F (870°C) for other, less demanding applications.

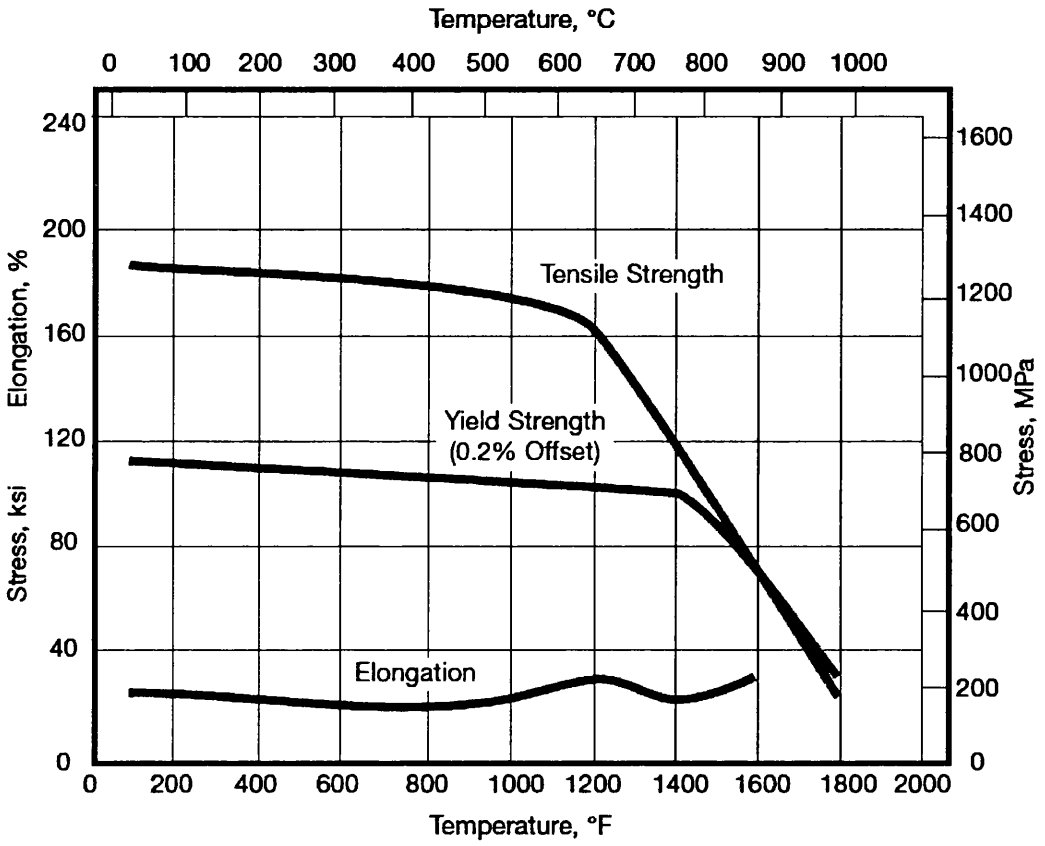

Figure 3.5.3.1[131]. Graphs gives the properties of Waspaloy in a graphical format.

Since the design of the plates was changed and made thicker, the Waspaloy bolts were too short. It was decided that 12.9 high tensile steel cap screws (M10) would be used instead. The cap screws were cheaper, more accessible and had sufficient materials and mechanical properties for use in the ongoing tests.

Technical Data	
Material	Class 12.9 Zinc Plated Steel
Standard	DIN 912
Thread Diameter	10mm
Thread Pitch	1.5mm
Socket Size	8mm
Head Height	10mm
Head Diameter	16mm

Table 3.5.3.1. Cap screw materials and dimensions

The manufacturer's website, www.bossards.com claims that continuous operating at elevated temperatures may result in significant stress relaxation. The results of their own tests for 12.9 (M10) caps are shown in the table below. The screws are exposed to the temperatures shown for 100 hours and the yield stress is measured.

For this reason, the cap screws were replaced after each test.

Property class	Temperature				
	+ 20 °C	+ 100 °C	+ 200 °C	+ 250 °C	+ 300 °C
	Lower yield stress, R_{eL} or stress at 0,2% non-proportional elongation [N/mm²]				
12.9	1100	1020	925	875	825

Figure 3.5.3.2[132]. Temperature and yield strength tests performed by Bossards showing how temperature exposure results in loss of yield strength.

4 Results and Discussion

In order to better understand the effect of wear damage on components, an extensive internal damage survey was carried out on past and current engine discs with known wear damage. The information was collected from the internal technical reports or by physically taking measurements and images from the actual components. The information gained from the wear scars allowed correlations to be drawn between the different types of damage as well as the subtle differences between them.

Diagnosing a specific type of wear damage on a component is difficult as there are no detailed guidelines in place. Although opinions will almost certainly differ from each institution to the next, it would be helpful (for Rolls-Royce at least) to have an agreed definition in place for common wear damage such as scuffing, galling and fretting and have rigid damage metrics in place which define them.

An extensive review of literature has proven fruitless in achieving clear definitions of various forms of wear. The vague way in which wear is defined without clear damage metrics has led to a 'research enquiry' which attempts to understand in more depth the differences between certain types of wear. For example, one person's idea of scuffing may be fretting to another, but the mechanisms that drive them are significantly different and so it is vitally important to have a more clear understanding of these differences.

Furthermore, it would be useful for component lifing specialists to have a database in place of how *specific* forms of wear with *specific* dimensions affect the fatigue life of materials. This may allow fatigue life knockdown factors to be easily applied to components in order to calculate safe working lives. At the very least, more accurate fatigue lives may be achievable, rather than being too conservative or too bold due to improper diagnosis.

A programme of wear testing involving specimens with a range of wear damage may prove useful to engineering specialists. The information gained can be used to construct deformation maps or a datum which contains information on the wear scar characteristics such as depth, wear scar area and volume, surface roughness, debris size, optical and SEM images, temperature, contact loads, sliding frequency and fatigue life. It is envisaged that future worn components can be compared to information outlined on the database for correct damage identification and clear-cut fatigue life predictions. Once enough information has

been gathered, it is envisaged that the boundaries between different forms of wear can be more easily defined. Nevertheless, for a more in depth understanding, a large range of wear tests with different test parameters would be required to take this research and develop it further. The results gained from this research will not only be fed back into the lifing methodology but may contribute towards improving and developing engineered surfaces and lubrications, which are widely known to reduce wear damage.

4.1 Research Results

The following chapter will discuss the work involved in attempting to better understand engine component wear damage by a combination of wear tests and fractograhic examination. The results will be analysed to determine the effect of various wear damage on the lives of components and to come up with clearer definitions of various forms of wear.

4.2 Baseline Testing of U720Li

4.2.1 Stress-Life (S-N) Curves

In order to generate a set of S-N curves for U720Li at 600°C, a programme of baseline fatigue testing using constant amplitude-loading was carried out. These curves would allow information to be gathered on the correct stress amplitudes to use for further wear damage testing.

In reality, in-service components that are subjected to cyclic loads will not always have entirely constant stress amplitudes. However, in general, unless other factors are involved such as vibration, the amplitudes tend to remain constant enough so that one can assume that a laboratory fatigue test carried out at constant amplitude will replicate the components in service stress amplitude accurately. If the stress amplitude was not constant, it would be difficult to determine what constitutes a cycle and this would make the fatigue life calculations somewhat more complex[133].

A set of three S-N curves is shown in the fatigue data below.

Baseline Fatigue Data for U720Li at 600°C

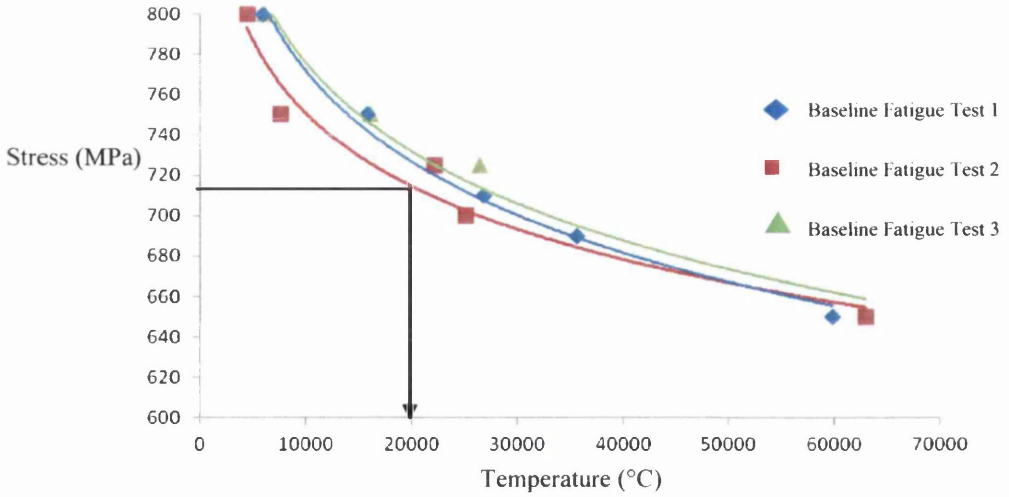

Figure 4.2.1.1. Baseline S-N data for U720 at 600°C, R-1, trapezoidal waveform (1-1-1-1).

Initially, only one programme of baseline testing was carried out and the stress amplitude required to produce 20,000 cycles was extracted from this curve, which was found to be 715MPa. This stress value was chosen for all ongoing wear damage tests thereafter. A further two programmes of baseline testing was carried out at a later date in order to create error bars and to account for data scatter.

4.2.2 Examination of Failed Baseline Specimens

The failed fatigue specimens were each studied under a scanning electron microscope to rule out any abnormality in the fracture surface and microstructure and to confirm that a combination of fatigue and possibly creep were the main modes of failure.

In the absence of surface damage, fatigue fracture is complicated, involving the process of initiation and propagation. The stresses are alternating (or cyclic) and in this case, well below the flow stress of U720Li. As discussed previously, dislocations play a major role in the fatigue crack initiation phase (also known as stage I fatigue). In this stage, dislocations accumulate near surface stress concentrations and form structures called persistent slip bands (PSB) after a large number of loading cycles. PSBs are areas that rise above (extrusion) or fall below (intrusion) the surface of the component due to movement of material along slip planes. This leaves tiny steps in the surface that serve as stress risers where tiny cracks can initiate. These tiny cracks (called microcracks) nucleate along planes of high shear stress which is often 45° to the loading direction.

During the fatigue process, it is the initiation that is the longest lasting phase with the actual propagation occurring over a relatively short time span in comparison. It can be seen from the SEM images that follow, fatigue cracks tend to initiate at free surfaces, although sub-surface initiation can occur.

The process of initiation is accelerated by the presence of damage, defects, scratches, corrosion, pits and wear damage – all of which act to cut initiation time significantly.

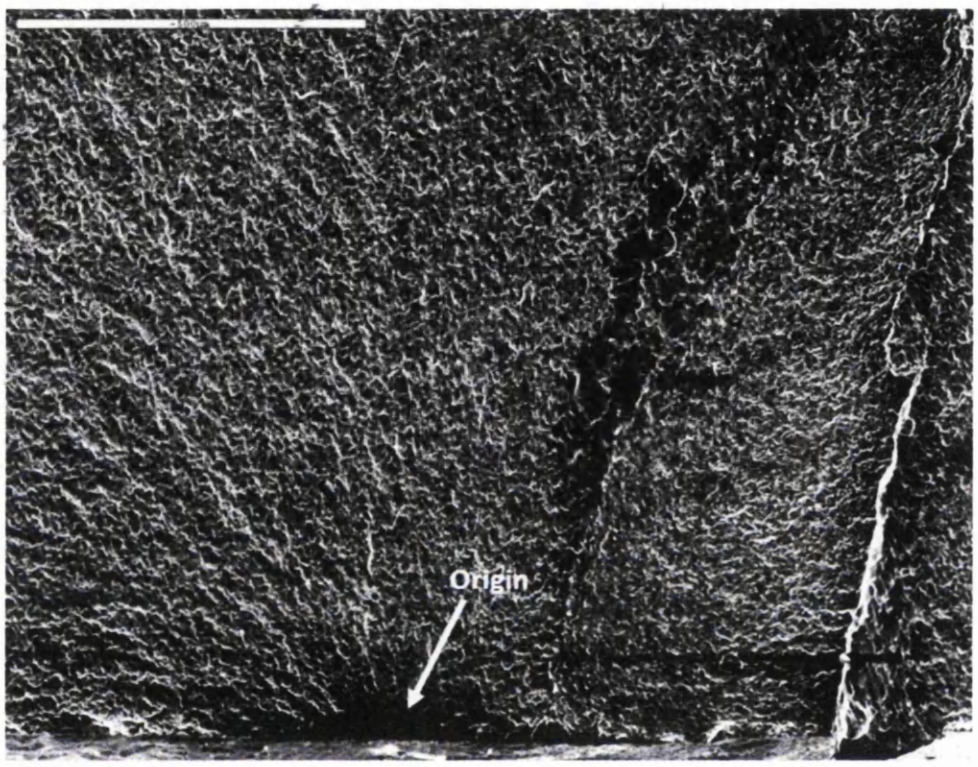

Figure 4.2.2.2. An arrow shows a fatigue initiation site at the surface of a U720Li fatigue test specimen at 800 MPa and 600°C.

The intrusion/cracks now propagates at an angle of approximately 45° to the tensile stress and surface and is described as stage 1 propagation. The 45° cracks are identified as the shallow depth (narrow) initiation zone on fracture surfaces after failure. It should be noted that some high-strength nickel and cobalt-based alloys have exceptionally large areas consisting of 45° type cracking.

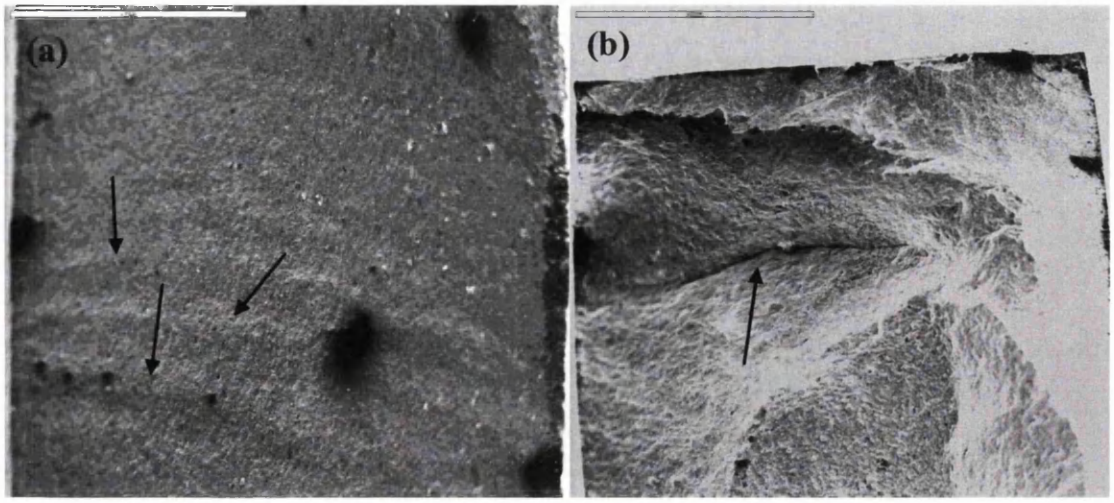

Figure 4.2.2.3. (a) Beach marks typical of fatigue and (b) secondary crack in the fracture surface of U720Li fatigue specimen.

After the initiation phase in stage 1, which involves propagation at 45° to the tensile stress direction, stage 2 growth takes over with advancement perpendicular to the tensile stress. This occurs when the plastic zone at the crack tip exceeds the microstructural unit (e.g. grain, phase etc). Propagation continues to advance with each loading cycle, generally leaving striations on the surface. However, it must be noted that a ratio of 1:1 striation to load cycle does not necessarily hold true. Striations in the U720Li baseline sample at 700MPa are shown in the following image.

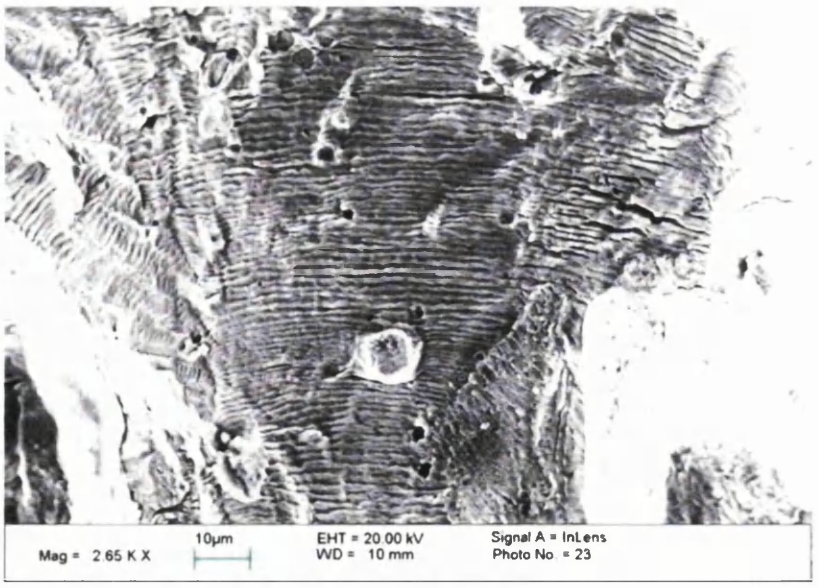

Figure 4.2.2.4. Striations in U720Li specimen after fatigue.

Crack propagation in stage 2 leaves certain characteristics. Macroscopically, these appear as beach marks (or bands) that occur at the crack front – perpendicular to the direction of growth. Each applied load cycle results in intensive plastic deformation that locally occurs around the crack tip. This is known as the plastic zone and can be kidney shaped in form. For polycrystalline microstructures such as U720Li, the crack front may be subdivided locally onto a number of separate planes, resulting in numerous parallel crack paths that form steps (or 'cliff edges' where they join together).

The following image in Figure 4.2.2.5 shows the fracture surface of an U720Li specimen after a fatigue test at 700MPa and 600°C taken using a 3D surface imaging machine. The arrow points to the site of initiation at the surface of the material and advances perpendicular to the tensile loading. The initial plastic deformation of stage II fatigue can be seen where the arrow is pointing too and is a typical kidney shape with a circular front radiating from the origin. Ductile propagation then takes over and is this stage is relatively fast in comparison to stage 2. In the case of the following 3D image shown in Figure 4.2.2.5, ductile overload occurs leaving a roughened dull surface with an irregular surface morphology.

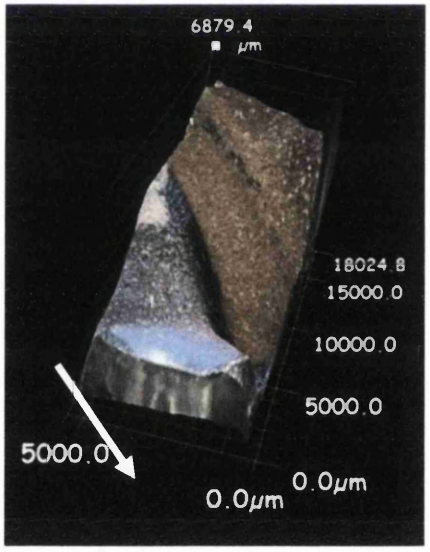

Figure 4.2.2.5. A 3D image of fracture surface of a failed U720Li fatigue specimen that underwent baseline fatigue testing at 750MPa and 600°C. The white arrow shows the kidney shaped plastic zone.

At higher magnification, proof of ductile overload fracture can be shown by the fibrous like morphology, shown below in Figure 4.2.2.6.

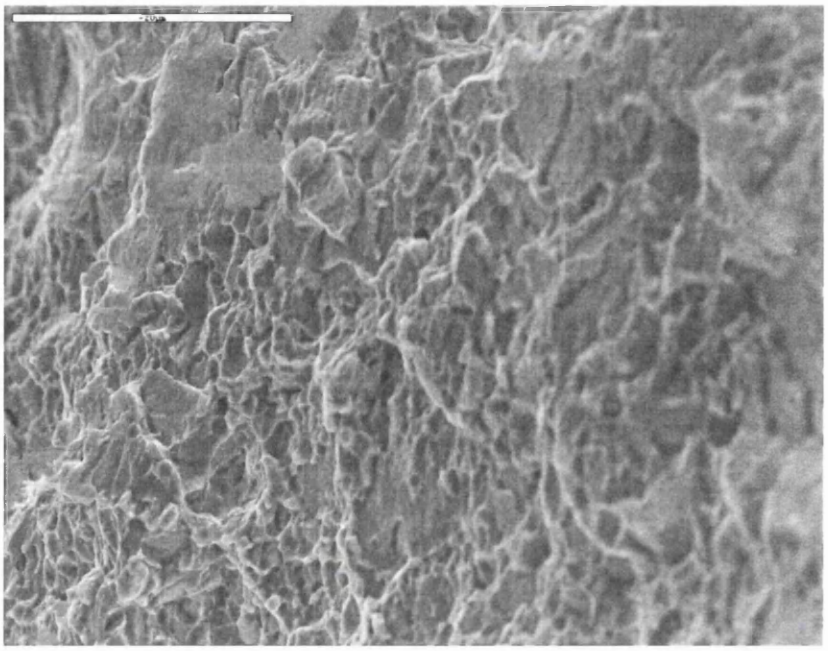

Figure 4.2.2.6. High magnification of ductile fracture in a U720Li specimen that underwent baseline fatigue testing at 750MPa and 600°C.

Since high temperature is an integral part of the fatigue testing in this project, creep must also be considered since turbine engine discs are also susceptible to creep at some point of their working life. In this case, it was important to discover if creep played a part in the failure of the specimens during baseline testing. Generally, the presence of creep can be evident in the fracture surface at high magnification and in particular, micro-voids and void coalescence can be seen. However, after inspection of the fracture surfaces, is was concluded that no creep had occurred.

4.3 Wear Testing on U720Li – University of Oxford/ Swansea University

This chapter will discuss a programme of wear testing part carried out at the University Of Oxford. The tests were performed at room temperature as previously described in the 'experimental methods' section and the material chosen for these tests was U720Li i.e. U720Li fretting pad in contact with a U720Li specimen. However, since the tests were performed at room temperature, the growth of a nickel oxide glaze depends entirely on the flash temperatures generated through sliding.

After being subjected to pre-determined wear damage, the specimens were fatigue tested at 600°C, a temperature at which nickel oxide glaze grows readily. However, it is highly probable that the development of a nickel oxide glaze is negligible on the fatigue life of the specimens since it was formed after the introduction of wear.

Although, it is desirable to produce wear damage in-situ with high temperature and a cyclic bulk stress to coincide with realistic service failures, it is also advantageous to be able to inspect the wear scars after each wear test prior to fatigue testing so that comparisons and contrasts can be drawn between the specimens.

4.3.1 Introducing Damage onto Specimens Using Dartec Wear Test Machine

Having seen examples of previous wear damage in current and ex-service engine components and being able to identify and differentiate between them should allow better simulation of the damage onto wear specimens for testing. With this in mind, the following test matrix was chosen for the programme of testing.

Test Number	Pad Pressure (Mpa)	Displacement (mm)	Frequency (Hz)	Number of Cycles
1	150	0.05	2.5	20,000
2	50	2	2.5	20,000
3	250	0.5	2.5	20,000
4	200	0.05	2.5	20,000
5	150	0.8	2.5	20,000
6	150	2	2.5	20,000
7	50	0.1	2.5	20,000
8	100	0.05	2.5	20,000
9	100	1	2.5	20,000
10	25	1.5	2.5	20,000

Table 4.3.1.1. Wear test matrix

The variables within the matrix parameters are the pad pressure and pad sliding displacement and these were chosen carefully to produce a spread of wear damage similar to what had been witnessed on service components. It was agreed that the frequency of sliding should remain as 2.5 Hz for all tests as this is the standard frequency used in most sliding contact tests at

Oxford University. The temperature of the test could not be altered or controlled as the Dartec machine does not have these capabilities at present.

The range of parameters were chosen so that the known forms of wear such as scuffing fretting and galling (the main area of focus) would be simulated. The wear test matrix has been incorporated into the following graph to illustrate the spread of wear and its intended simulation, represented by the colored rings.

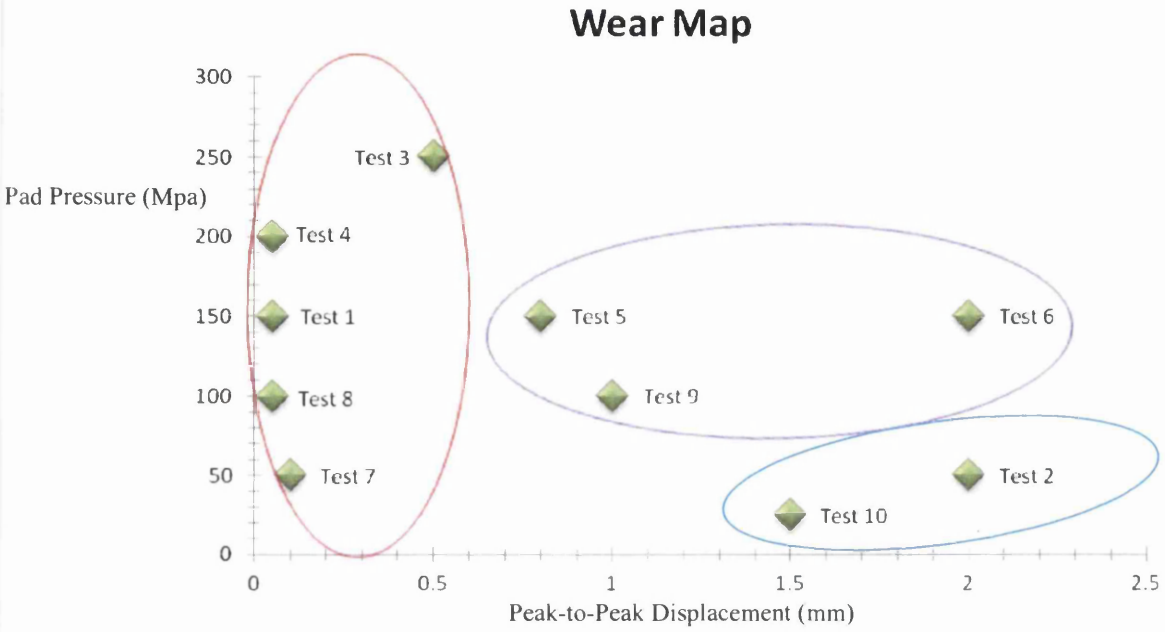

Figure 4.3.1.1. A map outlining the wear matrix parameters chosen for the wear test experiment. Points within each circle are attempting to simulate a type of wear damage. Fretting = red, Galling = purple, Scuffing = blue

Scuffing is considered to have a low wear rate. According to Hutchings[114] 'Scuffing wear occurs when the contact force between two materials is relatively low when compared to fretting and galling and the sliding distance is large'. For these tests, the loads for scuffing have been chosen in the range of 25-50MPa with large sliding distances of up to 2mm. Fretting occurs with large contact loads and small sliding displacements (10-100μm). Hence, to simulate fretting damage, contact loads in the range of 50MPa-250MPa and sliding amplitudes of 100μm and smaller were used. Since galling is a severe form of wear, large sliding distances and large contact forces were chosen to produce substantial quantities of material removal with unpredictable surface morphology as seen in service.

The tests were performed as described in the experimental section. After the tests were completed each specimen was photographed using a standard SLR camera and then the wear

scars of each specimen were photographed more closely using an Alicona 3D surface imaging machine to determine the surface roughness and inspect the surface profile. The images are shown in Figure 4.4.1.2.

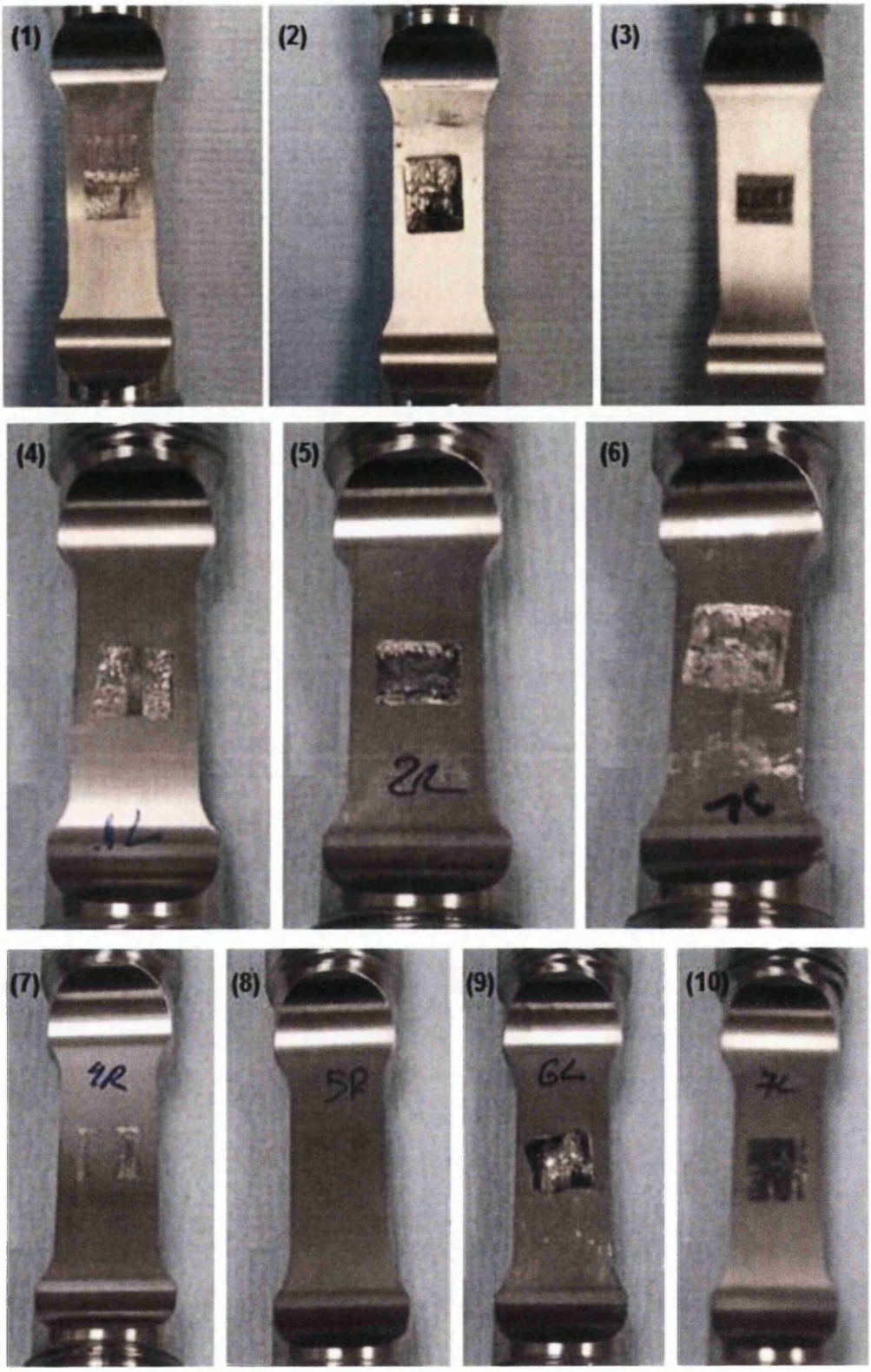

Figure 4.3.1.2. Wear specimens 1-10.

It can be seen from the images above how the severity of wear differs from one specimen to the next by simply changing the contact force and sliding amplitude. Test 5, 6 and 9 in particular show very serious signs of material removal. These specimens in particular were not subjected to the largest contact loads of the group, but were subjected to relatively large slip distances in order to replicate galling. This immediately suggests that for the greatest wear volume removal to occur, provided that the contact load between two surfaces is large enough, the slip distance is responsible for the greatest rate of material removal. This can be proved by comparing specimens that have had the same contact pressure applied to them but different sliding distances such as specimens 1, 5 and 6 where there is a definite increase in wear volume and severity as the slip distance is increased. This holds true for specimens 2 and 7 also where one can see an increase in material removal with an increase in pad sliding distance.

Test specimens 1,3,4,7 and 8 attempt to simulate fretting wear but more specifically, partial slip fretting. Referring to the images, it is evident that the stick/slip pattern is visible on specimens 4, 7 and 8 due to the unworn elastically deformed centre which is essentially 'stuck' and the plastically deformed circumference which is 'slipping'. This pattern is fundamental to fretting in disc/blade roots. Test 1 and 3 appear to have a mixed mode of contact wear since the partial slip pattern is observed as well as full sliding across the whole wear scar. This is characterised by wear tracks running linearly across their surfaces.

Finally, for specimens 2 and 10, scuffing wear was envisaged due to the relatively low contact loads (smaller than for galling wear specimens 5, 6 and 9) and large sliding distances chosen. However, it was surprising that specimens 2 and 10 showed large material removal. As discussed previously, scuffing is generally characterised by light surface damage removing only the top layer of a materials surface such as the DFL or the oxides that have formed naturally. Since the pad pressures chosen for specimens 2 and 10 are relatively small compared to the pad pressure on the other specimens, this also reinforces the theory that slip distance is the more dominant factor in the wear process.

Close up optical images using an Alicona digital profilometer of specimens 1-10 taken at the centre of the wear scars (including an undamaged specimen for reference) is shown in Figure 4.3.1.3.

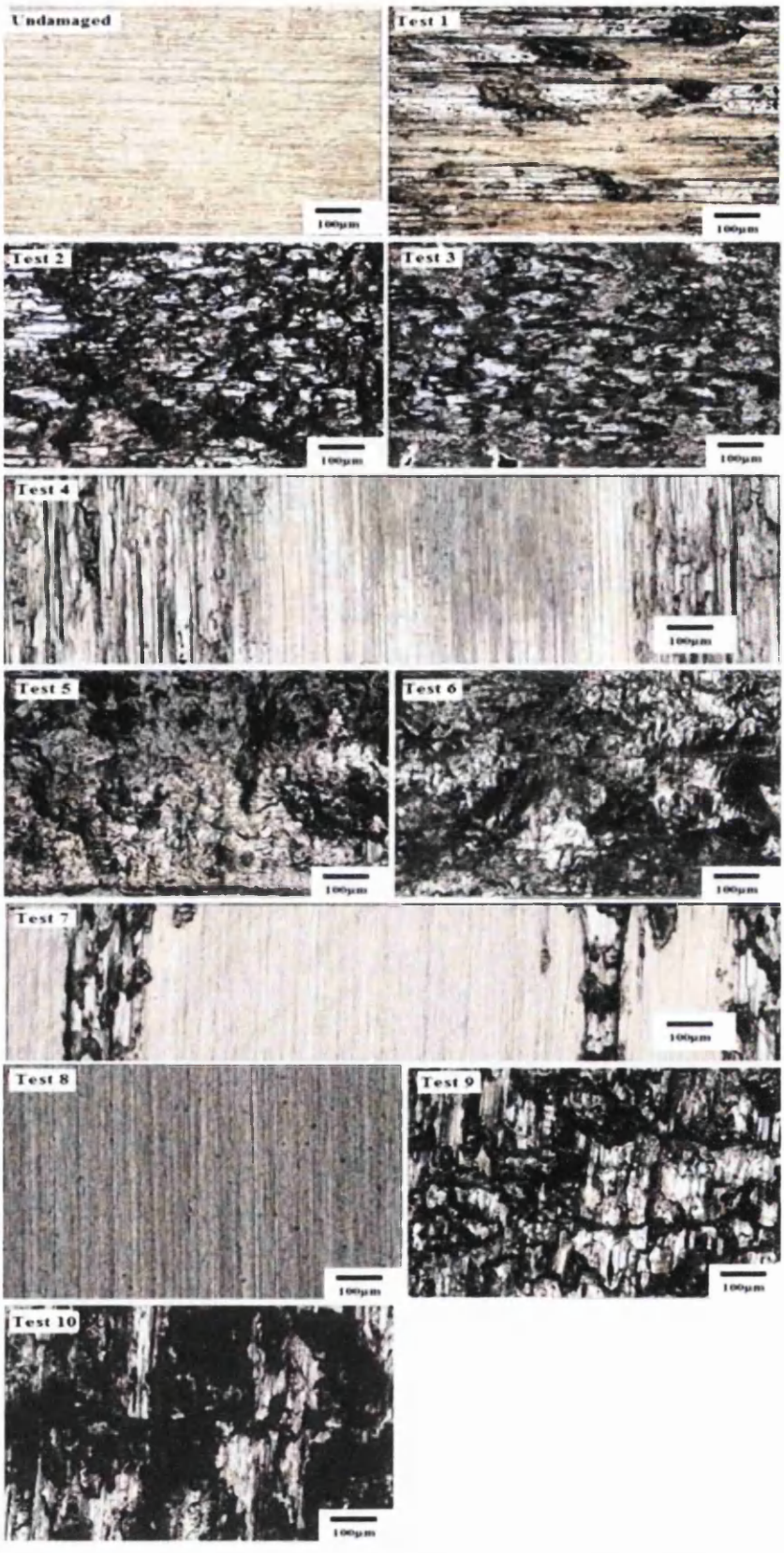

Figure 4.3.1.3. Optical images of the damaged surfaces of specimens 1-10.

The specimens were expected to have different surface roughness values for different regions of the damaged area. Above all, since specimens 1,3,4,7 and 8 attempt to replicate partial slip fretting wear, a considerable difference in roughness from the centre of its wear scar to its outside is expected. This proved to be the case when the Alicona measurements were carried out. This is demonstrated in the figure below for specimen 1.

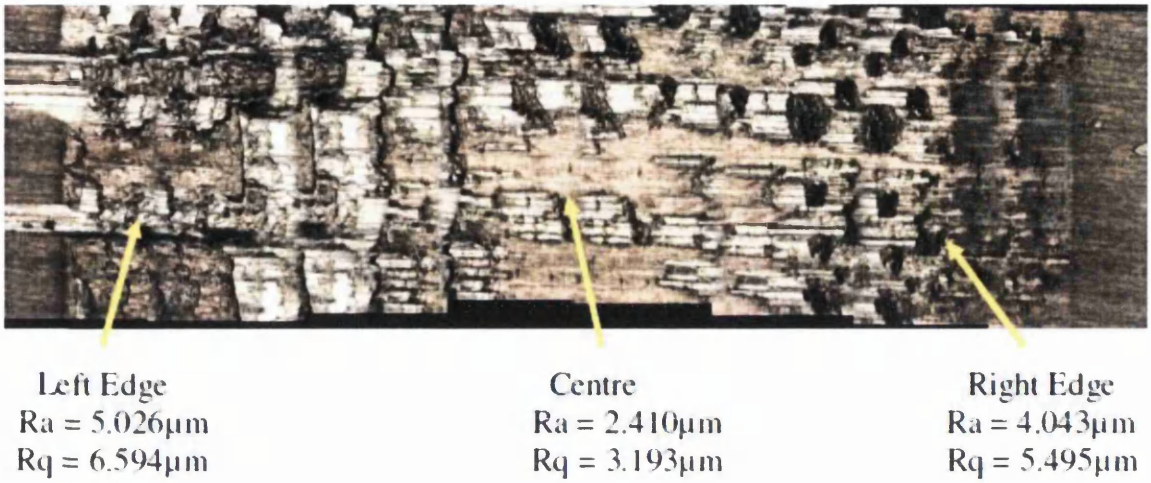

Figure 4.3.1.4. Detailed individual area measurements from the tested surface of specimen 1.

It can be seen in Figure 4.3.1.4 above that neither gross nor reciprocating sliding has occurred for specimen 1 and as a result, the centre of the wear scar has a relatively low average surface roughness compared to its left and right edge. Furthermore, there are regions of the centre that have not experienced slip which has confirmed the presence of unworn parent material (gold colour), which indicates that this specimen was in partial slip fretting regime.

Specimen Number	**Left Edge**		**Centre**		**Right Edge**	
	Ra (µm)	Rq(µm)	Ra (µm)	Rq(µm)	Ra (µm)	Rq(µm)
1	5.026	6.594	**2.410**	**3.193**	4.043	5.495
3	2.98	4.46	**1.222**	**1.558**	3.01	4.54
4	3.69	5.16	**1.92**	**2.46**	3.76	4.97
7	4.71	4.91	**2.14**	**3.06**	3.49	4.93
8	2.15	3.64	**1.98**	**2.42**	2.01	3.32

Table 4.3.1.2. Specimens with anticipated fretting wear. Values in bold (centre) are the used values for further analysis.

Since the surface roughness does vary across the wear scar, an average value of the roughness is used and is given for all of the specimens in the table below along with a root mean square roughness value.

Test Number/Position	Ra (μm)	Rq(μm)
Undamaged	0.7	0.89
Test 1	2.41	3.193
Test 2	4.882	6.382
Test 3	1.222	1.558
Test 4	1.92	2.46
Test 5	3.57	4.61
Test 6	5.18	7.27
Test 7	2.14	3.06
Test 8	1.98	2.42
Test 9	3.49	4.04
Test 10	5.27	6.14

Table 4.3.1.3. Specimen and corresponding average surface roughness (Ra) and root mean square surface roughness (Rq).

Measured values of displacement do not represent the actual relative slip displacement at the interface because of compliance of the bodies between the displacement measurement location and contact interface. Hence, measured values of displacement amplitude are in reality reference values that depend on test method, geometries, and contact configurations etc. Wear scars and hysteresis loops are the best indicators of the slip condition. The morphology of the wear scar aids in determining the coefficient of friction to use in the analysis. In reality, the coefficient of friction often varies along the interface.

Hence, the results are presented in graphical formats for each test. There are two plots:

i) A plot of the evolution of the Tangential Force Ratio (Q/P) versus number of cycles [max (*Bar Load*)–min (*Bar Load*)] / [4 × *Pad Normal Load*];

ii) A plot of three example load cycles – in most cases, choosing an early cycle where the surface was "*fresh*", one from the middle and one from the end of each individual experiment.

Note that if the contact is sliding, the Tangential Force Ratio may be interpreted as equal to the coefficient of friction. In partial slip, the coefficient of friction must be greater than the tangential force ratio. However, it should be noted that in some experiments, the tangential force, Q shows a sharp peak at the end of the sliding stroke, probably caused by wear scar interaction. This raises the maximum force above that caused during the main part of the sliding stroke. Hence, in this case the Tangential Force Ratio is probably an overestimate of the coefficient of friction.

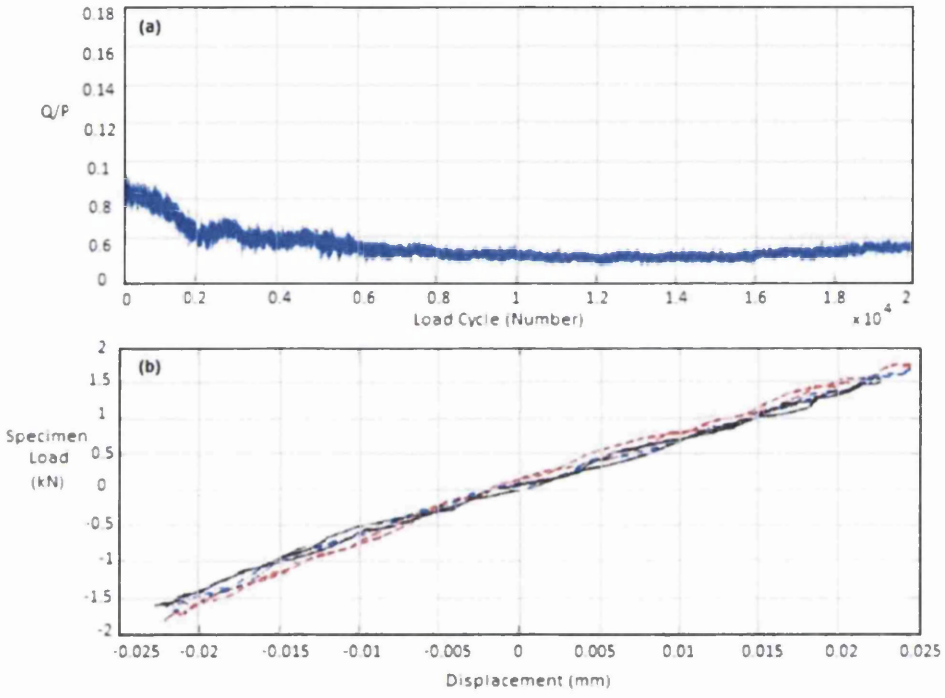

Figure 4.3.1.5. Test 1 – Tangential Force Ratio (Q/P) vs. number of cycles for Test 1 *(a)* & (b) example load cycles obtained during Test 1 from 3 different periods of the experiment (red – beginning, blue – middle & black – end)

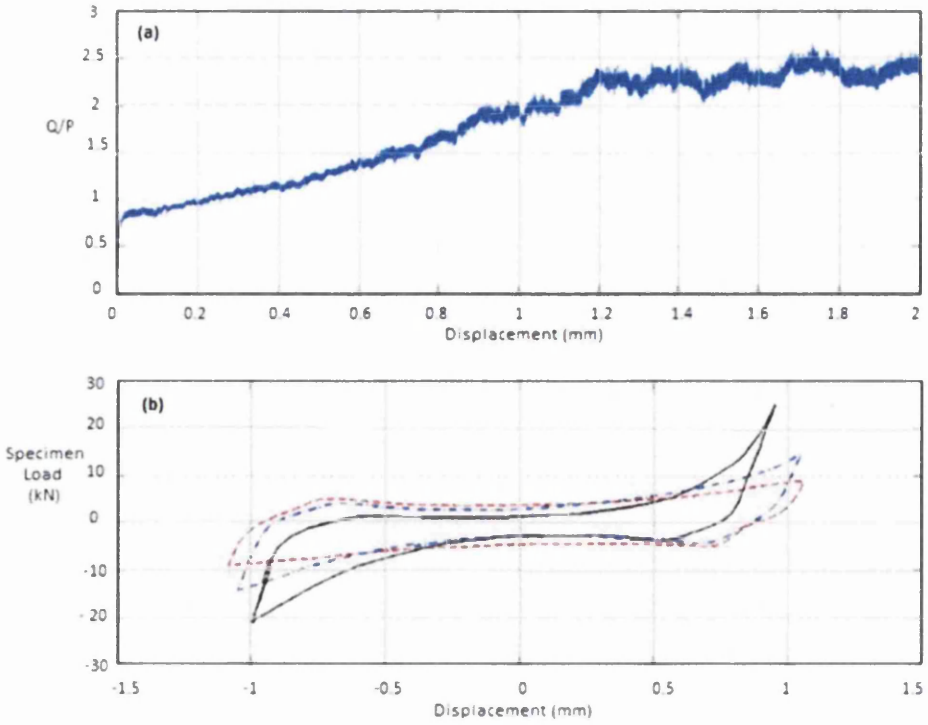

Figure 4.3.1.6. Tangential Force Ratio (Q/P) vs. number of cycles for Test 2 *(a)* & (b) example load cycles obtained during Test 2 from 3 different periods of the experiment (red – beginning, blue – middle & black – end).

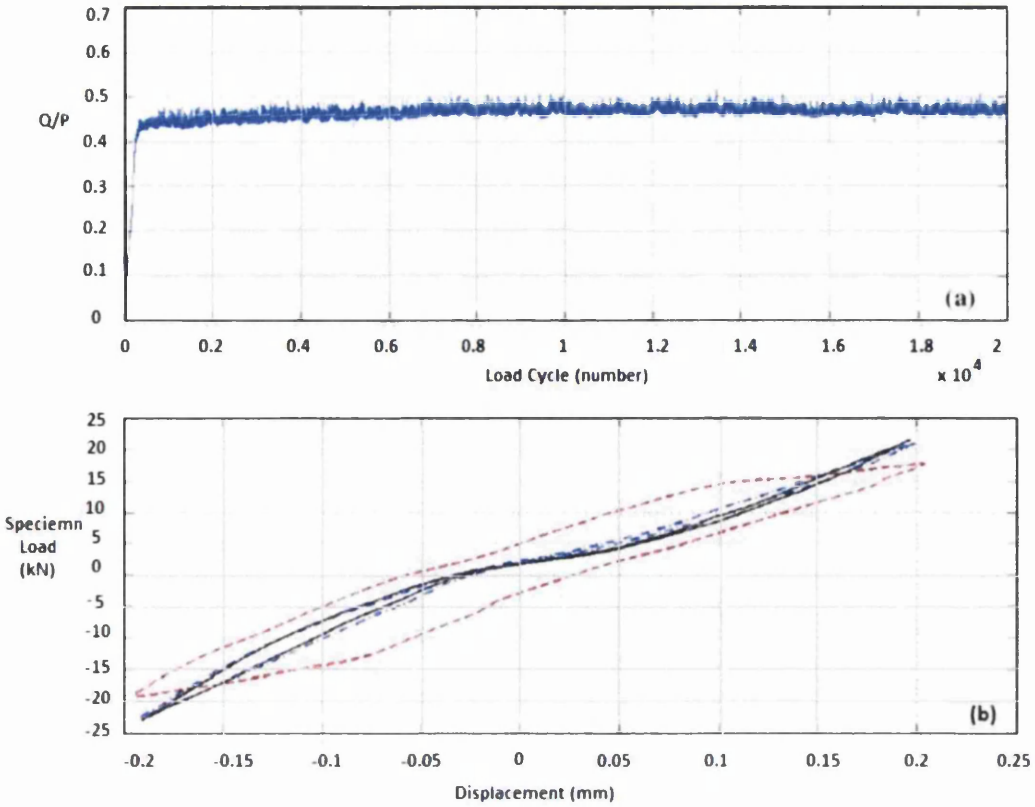

Figure 4.3.1.7. Tangential Force Ratio (Q/P) vs. number of cycles for Test 3 *(a)* & (b) example load cycles obtained during Test 3 from 3 different periods of the experiment (red – beginning, blue – middle & black – end).

As discussed previously, a heterogeneous film of oxide can occur naturally on all metallic surfaces (usually only a few angstroms thick) as well as natural impurities or environment dependent contaminant layers[48]. The small-amplitude oscillation and corresponding relative motion between the surfaces wears away the contaminant and oxide layer and can lead to adhesion and plastic deformation of the substrate metal[134]. This results in what has been termed micro-welding of the contacting surfaces[135]. Experimental observations in air at room temperature indicate that the coefficient of friction values are typically low during these first few cycles, suggesting the existence of a surface oxide and contaminant layer[136].

Damage morphology and its evolution are directly related to the contact sliding conditions. For minute sliding amplitudes ($\leq 100\mu m$) the tangential force presents a quasi proportional evolution displacement which leads to a closed partial slip hysteresis loop characterising the partial slip fretting condition and the resulting central stick domain surrounded by a sliding domain wear pattern. Such a condition favors the appearance of cracks. For larger sliding displacements, the tangential force eventually reaches a constant value leading to full sliding over the whole contact area. The hysteresis loop displays a quadratic shape defined as the gross slip condition or full reciprocating sliding regime. This condition favours the wear induced by the debris formation.

It can be seen from the hysteresis loops that test 1 was probably in partial slip for much of the test, since the area occupied by the hysteresis loop is very small. The tangential force starts off relatively high but then drops off as the cycle's progress. In this case, the initial friction is high due to the adhesion of asperities of the two contacts that weld together due to the large contact forces. Further sliding shears the asperities which break off and become wear debris and the friction drops slightly. The debris can either be pushed out or can become trapped between the contacts and cause an increase in wear.

For Test 2, the area occupied by the hysteresis loops is large which suggests it is in full sliding and exhibits the wear scar interaction effects discussed above. The coefficient of friction starts off low (0.6) but increases gradually to its highest point of 2.7. The wear observed in this case involved a high degree of material removal, typical of full sliding wear, such as galling and scuffing. If engine components are seen with damage of this kind, one can

assume that the slip distances are relatively large with full sliding across the contacts and moderate to large contact forces.

Test 3 appears to have been in sliding initially, but transitioned to partial slip as the coefficient of friction increased slightly. This is known as mixed slip and the boundaries between these regimes are controlled by the other fretting parameters including surface finishes, environment, and compliance of the test system. Albeit an increase, note how the tangential force remained relatively constant for the duration of the experiment which reinforces the premise **that the contacts were in partial slip ('bedding in') with little sliding** amplitude i.e. not enough to overcome the coefficient of friction, $Q<\mu P$.

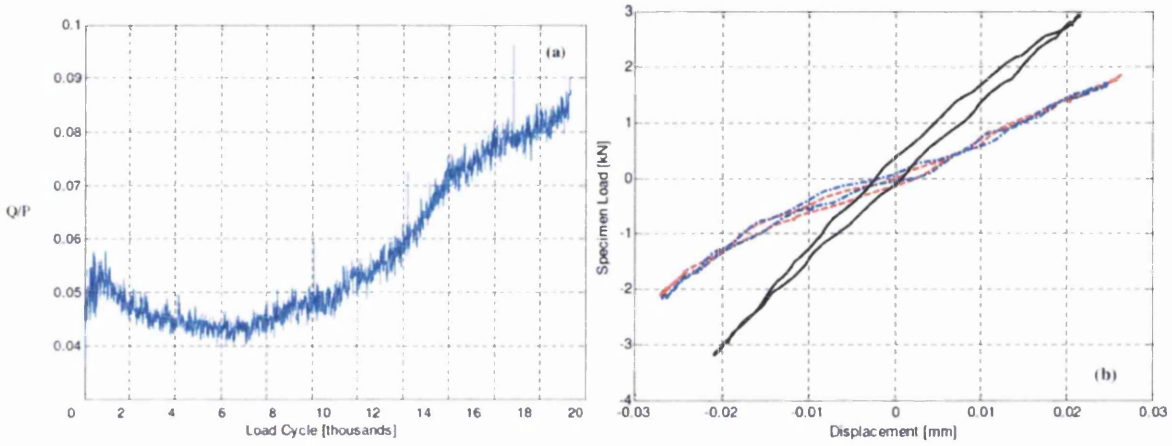

Figure 4.3.1.8. Tangential Force Ratio (Q/P) vs. number of cycles for Test 4 ***(a)*** & **(b)** example load cycles obtained during Test 4 from 3 different periods of the experiment (**red** – beginning, **blue** – middle & **black** – end).

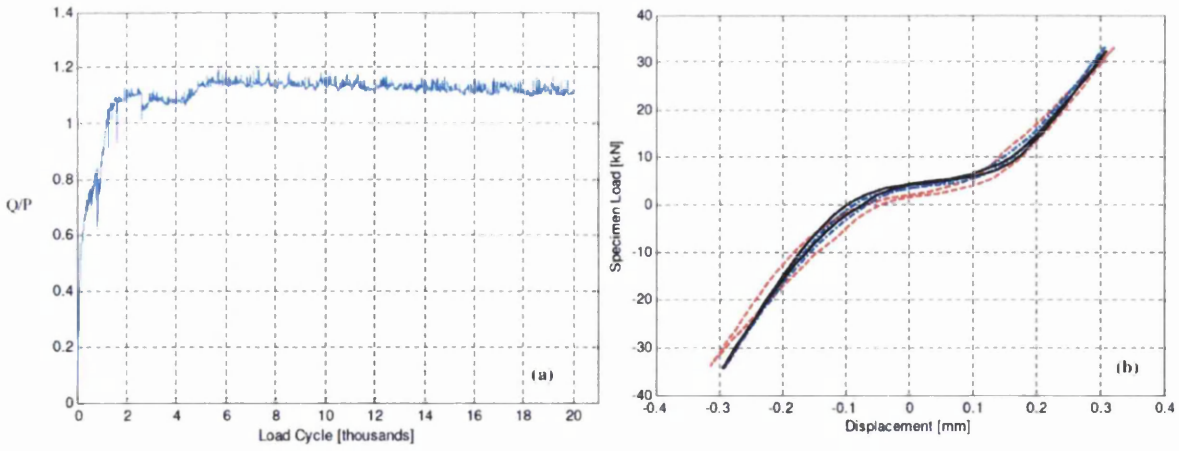

Figure 4.3.1.9. Tangential Force Ratio (Q/P) vs. number of cycles for Test 5 **(*a*)** & **(b)** example load cycles obtained during Test 5 from 3 different periods of the experiment (**red** – beginning, **blue** – middle & **black** – end).

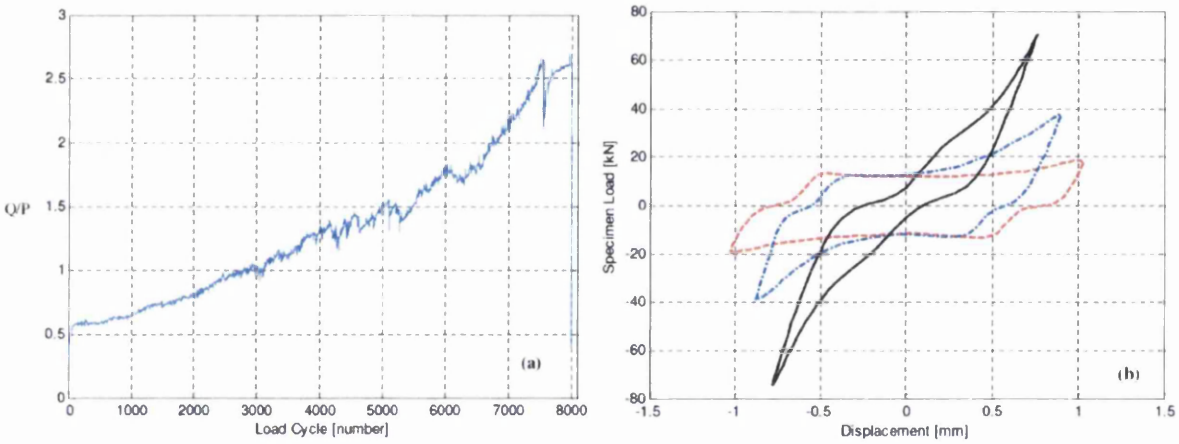

Figure 4.3.1.10. Tangential Force Ratio (Q/P) vs. number of cycles for Test 6 **(*a*)** & **(b)** example load cycles obtained during Test 6 from 3 different periods of the experiment (**red** – beginning, **blue** – middle & **black** – end).

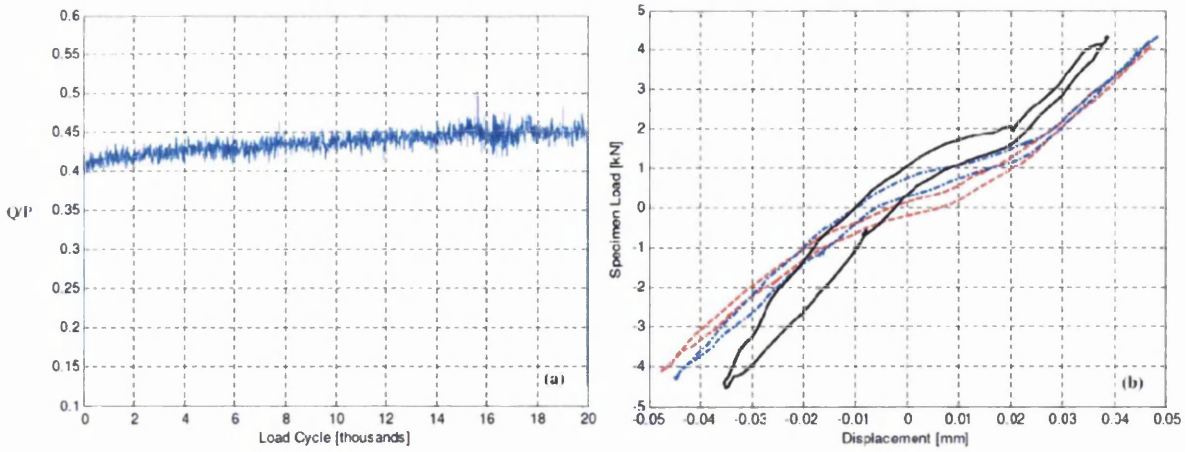

Figure 4.3.1.11. Tangential Force Ratio (Q/P) vs. number of cycles for Test 7 (*a*) & (b) example load cycles obtained during Test 7 from 3 different periods of the experiment (red – beginning, blue – middle & black – end).

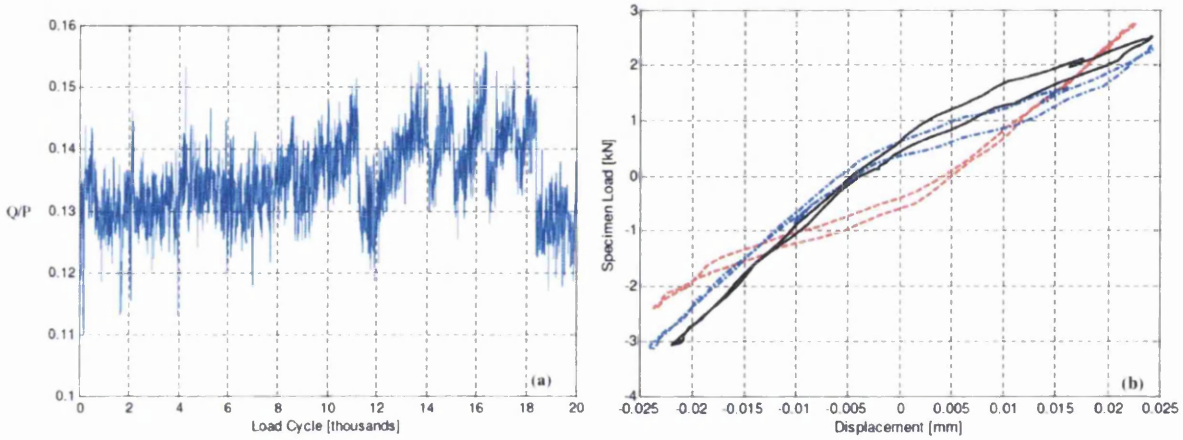

Figure 4.3.1.12. Tangential Force Ratio (Q/P) vs. number of cycles for Test 8 (*a*) & (b) example load cycles obtained during Test 8 from 3 different periods of the experiment (red – beginning, blue – middle & black – end).

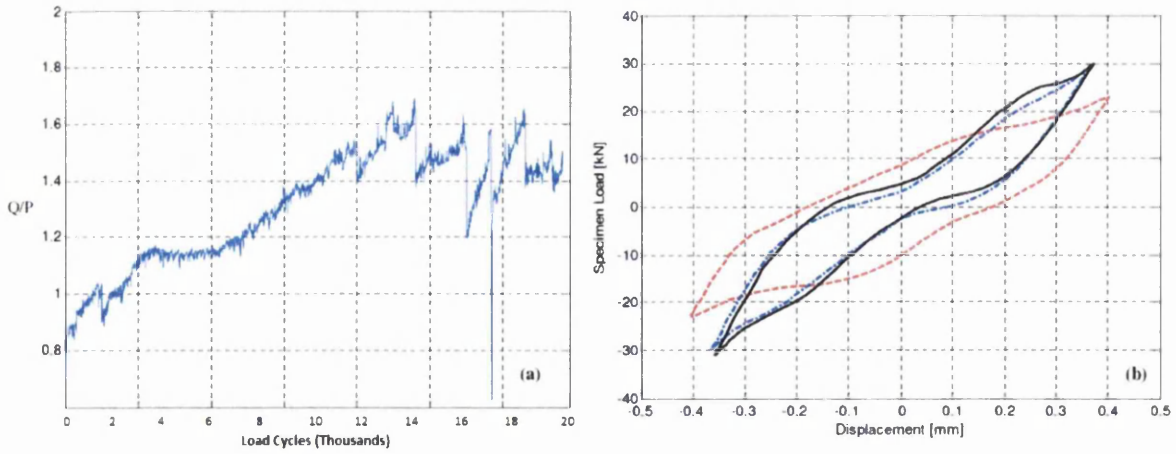

Figure 4.3.1.13. Tangential Force Ratio (Q/P) vs. number of cycles for Test 9 (*a*) & (b) example load cycles obtained during Test 9 from 3 different periods of the experiment (red – beginning, blue – middle & black – end).

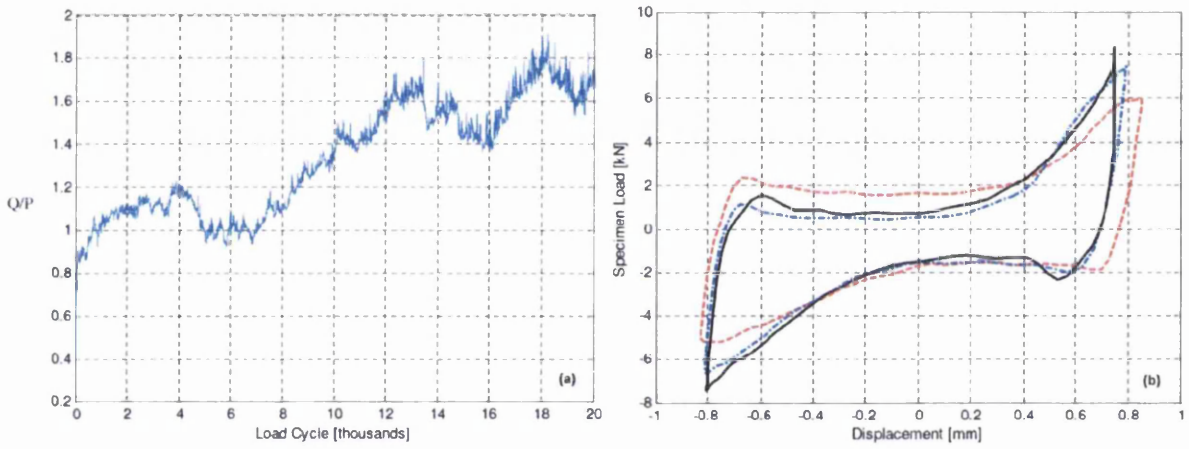

Figure 4.3.1.14. Tangential Force Ratio (Q/P) vs. number of cycles for Test 10 (*a*) & (b) example load cycles obtained during Test 10 from 3 different periods of the experiment (red – beginning, blue – middle & black – end).

It can be seen from the hysteresis loops above that test 4, 5, 7 and 8 were probably in partial slip for much of the time. Although, for test 4, the coefficient of friction started to increase towards the end stage of the test and full sliding started to take over giving a mixed slip fretting regime.

Tests 6, 9 and 10 were in full sliding and this was evident from the large area occupied by the hysteresis loops and the increasing tangential ratio from the onset of the test to the end. The

graphs suggest that material removal is large and is backed up by the surface images in Figure 4.3.1.2 and Figure 4.3.1.3.

The final wear scar produced for Test 8 appears very light in comparison to all the other tests. Referring to the optical images, it is quite difficult to differentiate test 8 from an undamaged U720Li surface. The tangential force readings for Test 8 appear to fluctuate aggressively through the whole test. This may be due to the formation of an oxide glaze created from the flash temperatures during contact slip as discussed earlier. Alternatively, it may also be due to the creation and removal of wear debris. The wear debris would certainly increase friction but the friction would drop off as soon as they are removed. The hysteresis loops also show an intermittent display of partial slip and sliding wear from start to finish, never seeming to settle. Towards the end of the test the wear transitioned to partial slip as the coefficient of friction increased.

Test 9 had to be stopped after 8000 cycles, as the specimen holding fixture and the pad holders failed under the excessive loads that the system exhibited during the test (≈80kN). From the table above, it can be seen that Test 9 was by no means subjected to the biggest contact forces but the slip distance was relatively large, reinforcing the idea that sliding distance accounts for the most material removal and wear damage.

It is important to realise that although the wear tests are being performed in the absence of a bulk cyclic stress; contact stresses, especially fretting, can still initiate cracks. However, these stresses are likely to be confined to the surface and have a steep gradient. Therefore, as the crack propagates under contact fatigue, it may arrest after it grows beyond the influence of the contact. Once a cyclic substrate or bulk stress is present the contact nucleated crack can propagate if the subsurface stresses are sufficiently large. This is illustrated in the following figure.

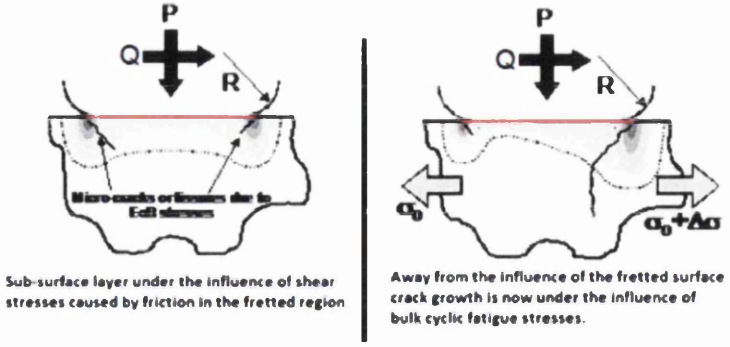

Figure 4.3.1.15. Microcracks under the influence of contact and bulk cyclic stress.

4.3.2 Fatigue Testing of Wear Specimens

The ten worn specimens were fatigue tested to the procedure outlined in the experimental methods. The stress amplitude chosen for all the worn specimens was 715 MPa as this was the approximate stress amplitude that yielded a fatigue life of 20,000 cycles for an undamaged U720Li specimen at 600°C and is therefore used as a reference.

The fatigue life as a consequence of surface roughness is shown in Figure 4.4.2.1 for each of the 10 worn specimens.

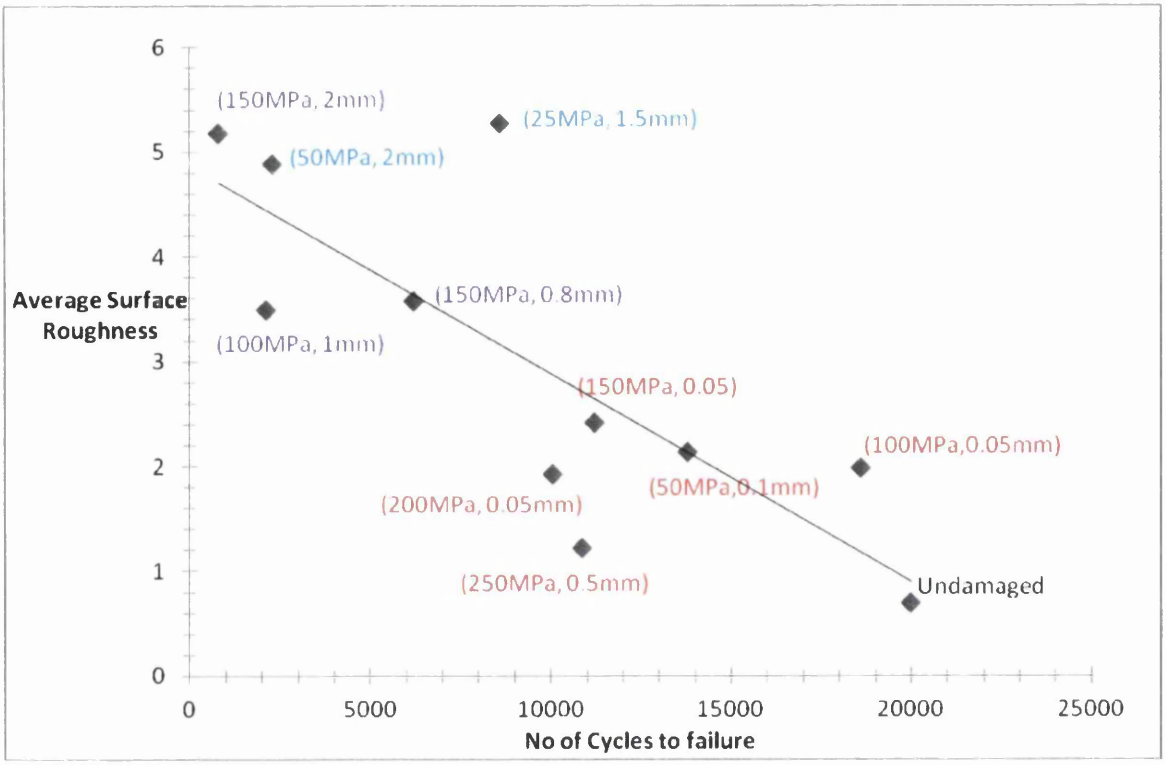

Figure 4.3.2.1. Average surface roughness of wear scar Vs the number of cycles to failure at 600°C, R-1, Trapezoidal (1-1-1-1). Fretting = red, Galling = purple, Scuffing = blue

Figure 4.3.2.1 illustrates how difficult it is to predict the fatigue life in response to surface roughness. This is because albeit fretting wear, it would be obvious to assume that in general, materials that have a large surface roughness values would have a low fatigue life due to the presence of multiple nucleation sites. However, the results in the graph do not show this entirely. The graph does go some way to suggest that for a larger value of surface roughness, the number of cycles to failure is smaller in most cases but it does not hold true for all. Average surface roughness values only give an average value of asperity height of the whole wear scar. However, although this will account for regions of larger surface roughness or extremities, which are of course the largest stress concentrations, it will go unnoticed, unless the whole wear surface is inspected in more detail. Hence, although a wear scar may have a relatively low surface roughness value, it may contain regions of severely high stress raisers which can limit fatigue life considerably.

Although the technique used to supply the wear damage to each specimen is controlled by the machine and ultimately, its software, repeat experiments would be beneficial to account for any anomalies or differences in the wear scars or corresponding fatigue life.

The graph in Figure 4.3.2.2 shows the fatigue life reduction with respect to root mean square surface roughness, Rq, which is a statistical measure of the magnitude of a varying quantity of asperity heights. It is especially useful when variants are positive and negative. This differs to the average surface roughness which only gives an average of the asperity heights.

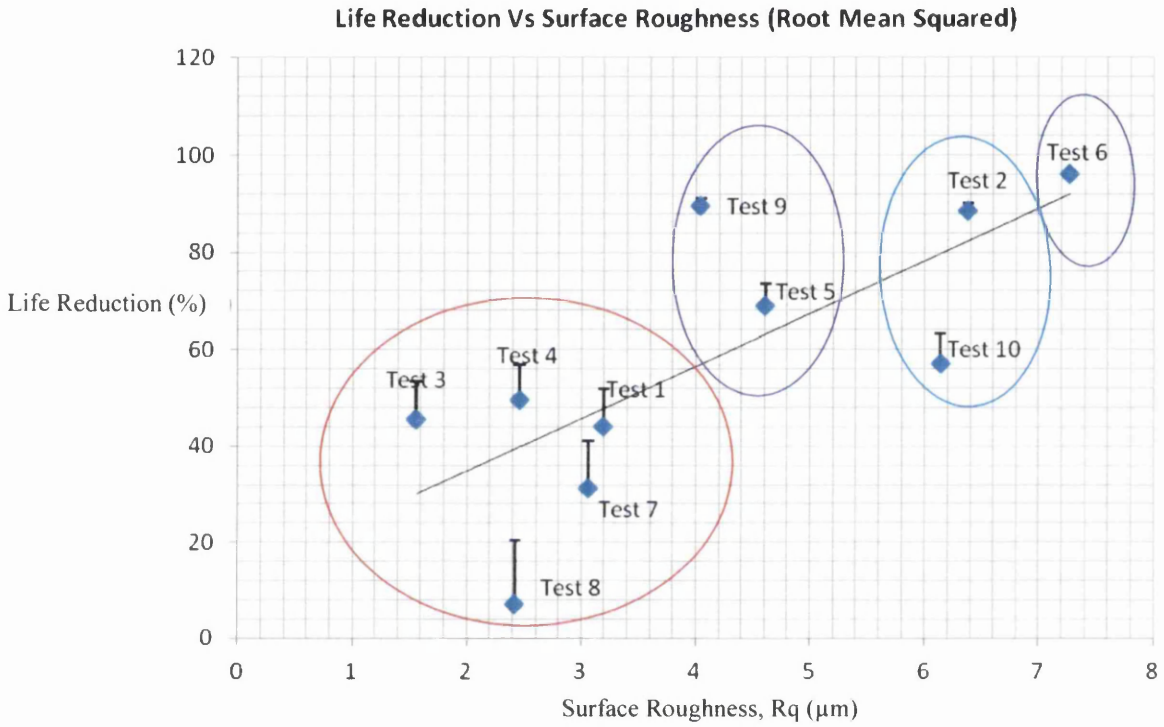

Figure 4.3.2.2. Fatigue life reduction of damaged specimens as a consequence of their surface roughness when tested at 715MPa at 600°C. Fretting = red, Galling = purple, Scuffing = blue

The graph above shows a positive trend for how the life of a specimen decreases with increasing surface roughness. Error bars were also calculated to take into account the other baseline fatigue tests that were performed with the same parameters. Essentially, the fatigue life reduction could actually be larger for all specimens.

Although, it has been discussed that fretting wear, especially partial slip fretting is highly life limiting to components, when compared to highly severe forms of wear such as galling, where there is a considerable material removal, it cannot be compared in the same context and must be looked at in a different way. Fretting relies on the large and complex stress

concentrations at the edge of bedding to form and propagate cracks so it is very difficult to look at every aspect of the fretting process. Therefore, for components that are intended to be fixed together but have very minute oscillation, fretting is a significant problem that can go unnoticed.

Focusing only on the fretting wear specimens (Test 1,3,4,7 and 8) and referring to Figure 4.3.2.2 and Table 4.3.2.1. for convenience, one can observe a tendency for a high contact load and small slip amplitude to produce a higher fatigue life reduction. For example, Test 4 gives the largest life reduction of the group. This particular specimen was subjected to slip amplitude of 50μm (typical of partial slip fretting) and a large contact pad pressure of 250MPa. Its surface roughness is low at 1.92μm which is one of the lowest in the group. However, regardless of the severity of the wear scar and only concentrating on its fatigue life reduction value, it suggests that there is a criterion for partial slip fretting conditions in which contact load and slip distance combine to form the most life limiting state and Test 4 may have reached this threshold. As discussed previously, this criterion is material specific and the results in this work only apply to U720Li. Although, repeat tests need to be carried out to increase trust in this experiment, it is encouraging that this data echoes previous work that partial slip fretting results in large life reduction factors due to the large shear stresses at the stick/slip interface.

Test 8 has the lowest life reduction of all the specimens tested. Its slip distance is typical of partial slip fretting but the contact loads chosen were relatively small in comparison to the loads used for the other perceived fretting wear specimens (test 1, 3 and 4), except Test 7 which was half its value at 50MPa. The wear scar morphology of Test 8 appears to be relatively smooth in comparison to all other specimens - but there are definitely characteristics of partial slip fretting which is why it is found to be in the same vicinity as Tests 1, 3, 4 and 7.

Further up the surface roughness scale (>4μm), whereby the sliding amplitude and contact forces are relatively large, the fatigue life reduction also increases. The surface topography of the specimens (shown in Figure 4.3.1.3) in this region shows a rough, uneven surface with no regular pattern. There are numerous sites for crack nucleation to take place and the reduction in specimen volume as result of excessive material removal in the wear zone increases the

tensile stress in this region. As a result, the fatigue life of these specimens is drastically less than that of the specimens with fretting wear.

It can be seen from the graph above that specimen 6 has the largest surface roughness and greatest fatigue life reduction. Due to the large sliding distances and relatively large contact forces chosen, it was anticipated that galling wear would occur with large quantities of material removal. It is very interesting that relatively small changes in either the sliding distance or contact pressure can account for highly noticeable changes in wear scar morphology and fatigue life.

Specimen Test Number	Ra (µm)	Rq (µm)	Pad Pressure (MPa)	Slip Amplitude (mm)
Undamaged	0.7	0.89	n/a	n/a
Test 1	2.41	3.193	150	0.05
Test 2	4.882	6.382	50	2
Test 3	1.222	1.558	250	0.5
Test 4	1.92	2.46	200	0.05
Test 5	3.57	4.61	150	0.8
Test 6	5.18	7.27	150	2
Test 7	2.14	3.06	50	0.1
Test 8	1.98	2.42	100	0.05
Test 9	3.49	4.04	100	1
Test 10	5.27	6.14	25	1.5

Table 4.3.2.1. Fretting = red, Galling = purple, Scuffing = blue

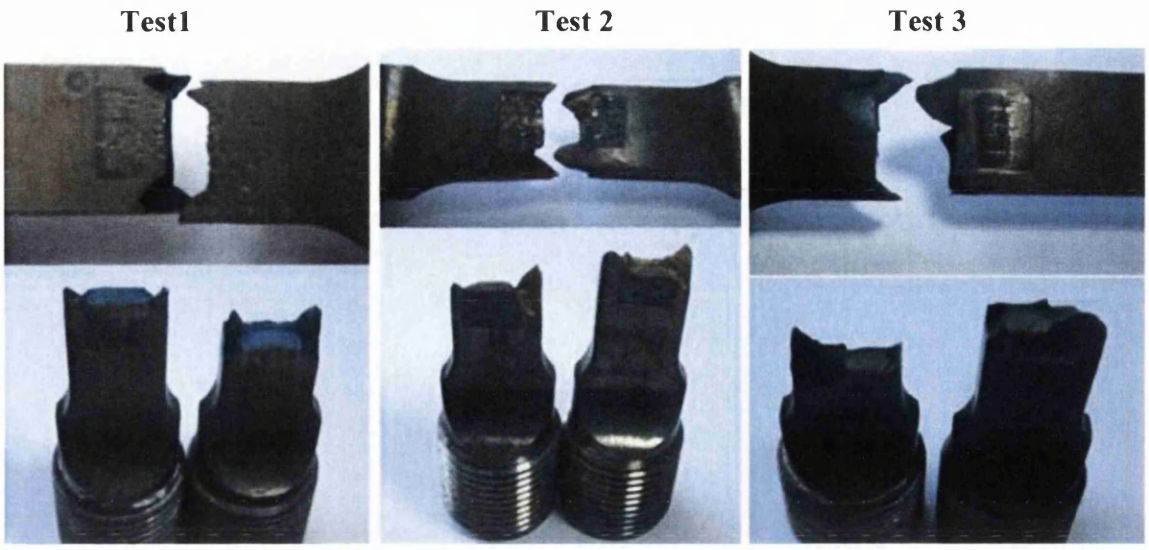

Figure 4.3.2.3. Failed fatigue specimens 1-3 with known wear damage.

It can be seen from the images in Figure 4.3.2.3 that for Test 1, crack nucleation has nucleated at the interface between the stick/slip region where the stress concentrations are large and complex and there is change in surface morphology (and surface roughness) from the central zone to the plastically deformed slip zone. The following image shows a 3D topography of Test 1 displaying the edge of bedding where the stress and failure originated from (shown by red arrow).

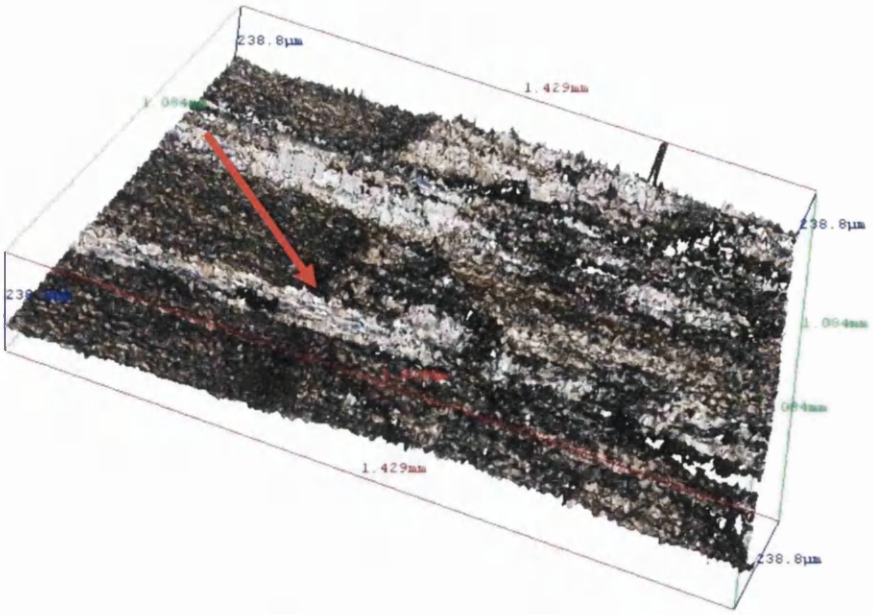

Figure 4.3.2.4. Left edge of Test 1 showing the edge of bedding and where the failure originated during fatigue testing. In real life components that exhibit fretting fatigue, the edge of bedding is generally the region where failure occurs.

Test 3 recorded the lowest Ra and Rq of all the specimens. However, due to the large slip distances (i.e. > 100µm) chosen, partial slip fretting was not envisaged for Test 3. Rather, reciprocating sliding fretting was expected with full contact across each contacting surface. However, referring back to Figure 4.3.1.7 of tangential Force Ratio (Q/P) vs. number of cycles, it can be seen from the hysteresis loops that initially there was gross sliding but then transitioned into partial slip towards the middle and end of the test. Furthermore, surface inspection showed this was not that the wear scar exhibited a **plastically deformed 'slip'** region (outside) **adjacent to an elastically deformed 'stick' region** (centre), which results in elevated shear stresses at or near the material surface. Given this, the stress concentrations between these two regions were not sufficient enough to initiate failure.

Thus, under bulk cyclic loading, the fatigue merely served to locate a feature with the highest stress concentration, which was at the corner of the wear scar i.e. the edge of bedding. This sudden sharp change in stress concentration and surface roughness between the wear scar and the undamaged part of the specimen increases the Kt factor and provides a perfect platform for crack initiation and propagation. This is shown in Figure 4.3.2.5.

Figure 4.3.2.5. Test 3 Crack nucleation site. Black arrows show the increased surface roughness surrounding a central zone with low surface roughness. Red arrow shows crack initiation point. Note the central black region is heavily oxidised.

The results in this programme of testing have proven that specific kinds of wear damage can be replicated onto test specimens by changing the pad contact pressure and the sliding distance of the pad. By adopting a small sliding distance of around 100μm or less, the partial slip fretting regime has been achieved and damage has occurred either from the edge of bedding or at the boundary between the stick/slip regions which coincides with theory in literature[60]. Larger sliding distances have resulted in larger material removal, unpredictable surface morphologies and a significant reduction in fatigue life. In addition to the multiple stress concentration features on the wear scar surface, the reduction in fatigue life can be attributed to the lack of bulk material in the gangue section of the specimen. The axial cyclic stresses and are therefore magnified in this region.

It has been demonstrated through this work that fretting wear should be considered on an entirely separate basis since the mechanisms that drive it are very different to that of sliding wear such as scuffing and galling. The minute sliding distances involved in fretting and the

complex stresses that accompany it make it very difficult to analyse and replicate in the most realistic way. For this reason, customised tests need to be employed which have greater control over the parameters involved.

From the results gained in this programme, it can be seen that the average surface roughness values of fretting with sliding distances of 100μm or less are no larger than 2.41μm. This is in contrast to the other specimens with anticipated scuffing and galling wear which had significantly higher values of surface roughness. For example, specimens with relatively low contact pressures and large sliding amplitudes were intended to simulate scuffing wear, and the surface roughness values for these were in the higher range of the ten specimens tested i.e. 4.882μm-5.27μm. Specimens with larger values of sliding amplitude and relatively large contact pressures were intended to simulate galling wear, a more severe form of scuffing and surprisingly, these were found to have a mid range surface roughness with values in the range of 3.49μm-5.18μm. This suggests that the surface roughness values and the resulting wear scar in response to changing the sliding distance and pad contact pressure is not straightforward. However, these tests have shown that a combination of a large sliding distance and low pad pressure results in a greater rate of material removal compared to a combination of large contact pressure and smaller sliding distance which results in less material removal. However, if the wear mechanism is fretting, then the rate of material removal is not the most important factor, since it is the complex mechanisms that drive fretting that is the most life limiting and these occur synergistically on a microscale.

4.4 Fretting Fatigue Testing

To focus on fretting fatigue, a fretting fatigue testing apparatus was designed in order to develop a series of in-situ tests that involves fretting at high temperature.

In order to fully understand the effects of fretting, the tests must be carried out in as realistic conditions as possible. Therefore, unlike the previous test whereby wear was introduced onto the specimens before fatigue testing, in this case, fretting fatigue will be tested in-situ and at 600°C. The rig is shown in the experimental section in Chapter 3.4.

As explained in the experimental section, the fretting test uses a pair of clamping plates which hold replaceable fretting pads against the surface of fatigue test specimens. The clamping plates are clamped together with high tensile bolts at either end. The bolt tension is

balanced by the compressive force in the fretting pads, which transmit normal forces. The compressive force encourages fretting of the pads against the specimen surface caused by the extension of the specimen in response to axial cyclic stresses during fatigue.

Due to the large contact pressures between the pad and specimen and high operating temperatures of the test, it was not possible to locate suitable pressure/force sensors to measure the pressure between the pads and specimen before or during the test. Therefore, the pressure of the pads on the specimens could not be controlled as in the test performed at the University of Oxford using the Dartec machine. In this case, the bolt tension may be estimated from the torque tightening requirement but this is not a direct measurement and does not take into account factors such as loss of energy during friction. The torque supplied to each bolt was recorded using a torque wrench and the separation distance was also recorded between the clamping plates before and after torque up. The clamping plates have a characteristic stiffness which enables the compressive force to be estimated from the separation of the bolt head and the nut. The computation of the resultant pad pressure will be discussed in due course.

Mock testing was carried out at room temperature using stainless steel fretting pads on U720 fatigue specimens to determine the performance of the rig and its effectiveness for achieving fretting fatigue. The ultimate goal was to produce fretting damage within the partial slip regime having the characteristic ring pattern. Achieving this would be totally empirical, since the rig was being used for the first time.

The following table provides the torque values supplied to each of the two bolts for four separate tests.

Test Number	Torque per Bolt (Nm)	Resultant Pad Pressure (MPa)
1	3	70
2	6	160
3	9	250
4	12	355

Table 4.5.1. Torque per bolt (Nm)

The results are shown in the following graph.

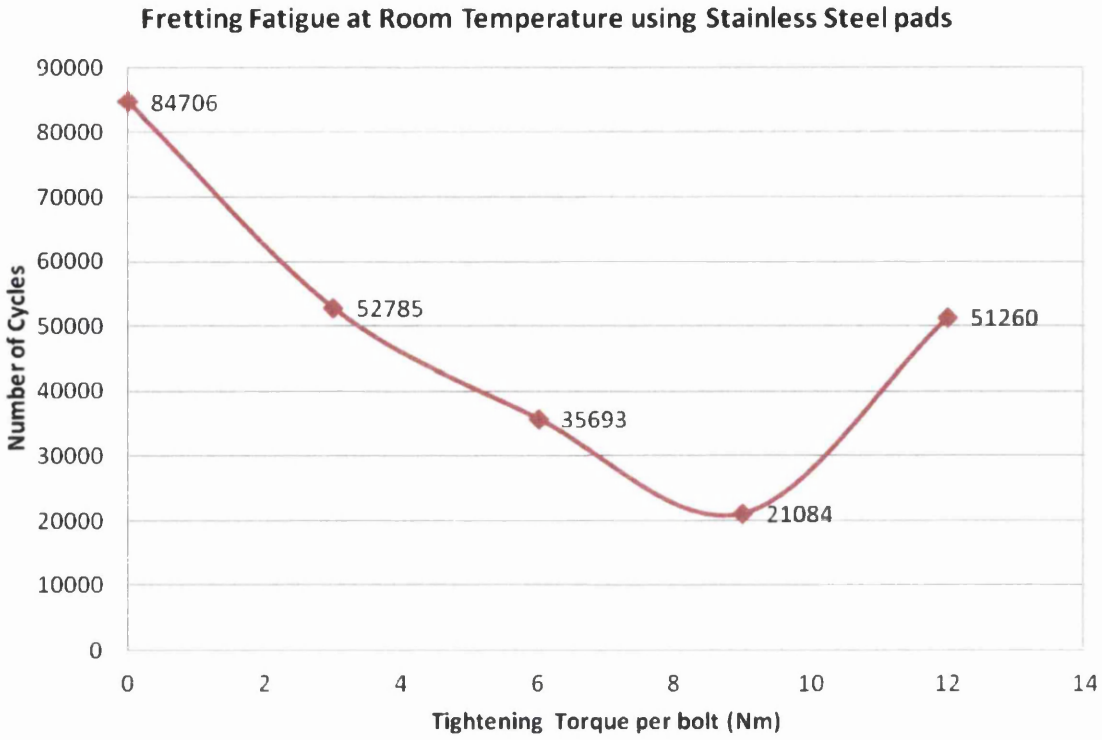

Figure 4.5.1. A graph showing the number of cycles to failure in response to tightening torque when U720 is in contact with stainless steel pads. (Cyclic stress amplitude = 715MPa).

From the results in Figure 4.5.1, it is possible to calculate the loss in fatigue life as a result of the fretting fatigue in comparison to plain fatigue.

The fretting fatigue reduction factor can be calculated as follows.

$$Fretting\ Fatigue\ Reduction\ Factor = \frac{Fretting\ Fatigue\ Life\ Cycles}{Plain\ Fatigue\ Life\ Cycles} = \frac{Fretting\ Fatigue\ Life\ Cycles}{84706}$$

(Equation 4.5.1)

Test Number	Fretting Fatigue Life (cycles)	Fretting Fatigue Reduction Factor	Life Lost (%)
1	52785	0.6232	37.68
2	35693	0.4214	57.86
3	21084	0.2489	75.11
4	51260	0.6052	39.48

Table 4.5.2. Values of fretting fatigue life reduction factors and corresponding life lost.

The fretting fatigue wear scars in response to change in pad pressure are shown below. For all specimens, the failure started at the edge of bedding which is where most of the wear damage is located and where the surface roughness values are highest. The images show a typical partial slip fretting response and this is easy to see as there is little oxide covering the surface except for the circumference of the wear scar where the large temperatures as a result of sliding have created an oxide scale.

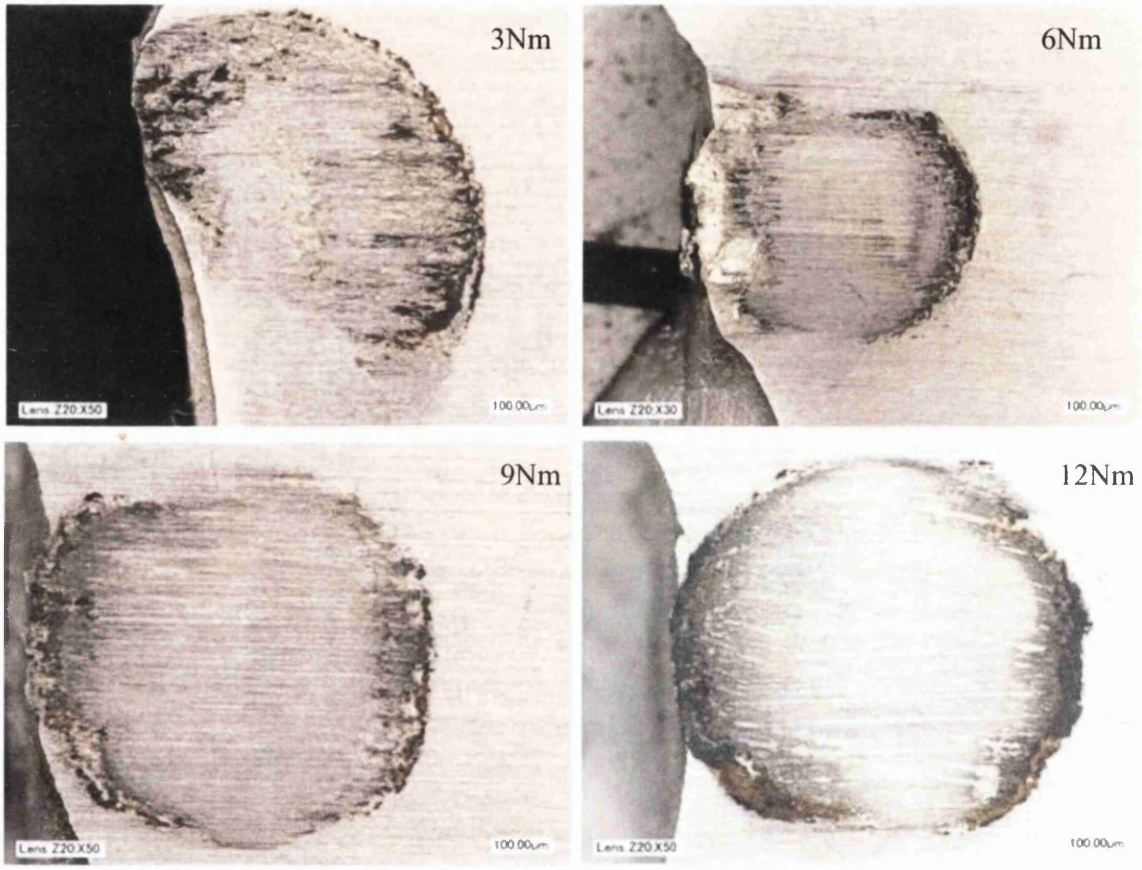

Figure 4.5.2. Wear Scars as a result of fretting fatigue.

The surface roughness values for each wear scar are shown in the following table. Note that for Test 3, the surface roughness values for the outside edge of the wear scar are larger on average than the other specimens and this resulted in the largest fatigue life reduction.

Specimen Number	Left Edge		Centre		Right Edge	
	Ra (μm)	Rq (μm)	Ra (μm)	Rq (μm)	Ra (μm)	Rq (μm)
1	3.06	4.76	**1.62**	**1.91**	2.86	3.67
2	3.12	3.95	**1.54**	**1.86**	3.01	3.13
3	4.01	4.34	**1.13**	**1.66**	3.45	3.76
4	2.23	2.54	**1.11**	**1.54**	2.01	2.32

Table 4.5.3. Pad pressures, torque per bolt and surface roughness of 4 fretting fatigue specimens.

	Fretting Pad Ra (μm)	
Test Number	Centre	Outside
1	1.24	1.69
2	1.21	1.54
3	1.16	1.78
4	1.19	1.46

Table 4.5.4. Surface roughness values for fretting pad.

The graph in Figure 4.5.1 reveals an interesting relationship between tightening torque (pad pressure) and the number of cycles to failure. It can be seen that the number of fatigue cycles deceases as the tightening torque increases from 3Nm to 9Nm but then starts to increase with increasing tightening torque from 9Nm to 12Nm. This can be explained by the Hertzian contact force and relative slip which results from varying the pad pressures.

In essence, if the pad pressure is low as in the case of a 3Nm tightening torque, ample slip between the pad and specimen will occur and may be considered outside of the partial slip fretting regime. Inspection of the wear scar surface shows wear across most of the contact which further reinforces the theory that the slip amplitude was large and probably in the gross lip fretting regime. As a result, microcracks (which normally form prematurely under the partial slip fretting condition) may be removed by the constant wearing process[137] and the life of the specimen is therefore extended. However, the gross slip fretting process in this case will increase the roughness of the surface due to asperity shearing and the formation of debris which will become trapped and increase abrasive wear. This is reflected in the surface roughness value shown in the table above but most of the roughened surface is located on the outside of the wear scar, which is where final failure initiated, shown in Figure 4.5.3 and Figure 4.5.4. The origin in Figure 4.5.3 resembles that of a chip and therefore suggests that

another wear mechanism such as spalling has occurred as a result of the large sharp stress gradients in that region.

Figure 4.5.3. Crack Initiation point for test 1 with 3Nm tightening torque and a corresponding pad pressure of 70Mpa.

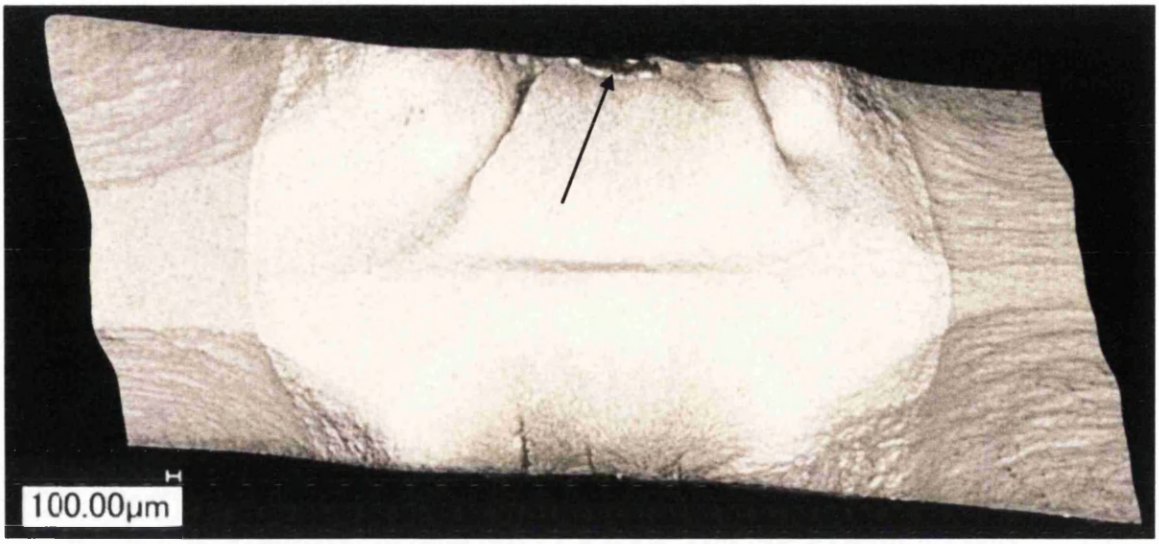

Figure 4.5.4. 3D Birdseye view of fracture surface and fatigue origin shown by black arrow.

At 6Nm tightening torque, the fatigue life reduction is larger with a slightly higher surface roughness, mostly concentrating around the outside of the scar as in the other cases. The failure origin again occurs at this location.

At a tightening torque of 9Nm, we see the lowest fatigue life of all specimens which suggests that the slip distance and pad contact pressure have combined to produce partial slip fretting in its most detrimental state. Visual examination of the wear scars and fracture surface reveal the trademark pattern.

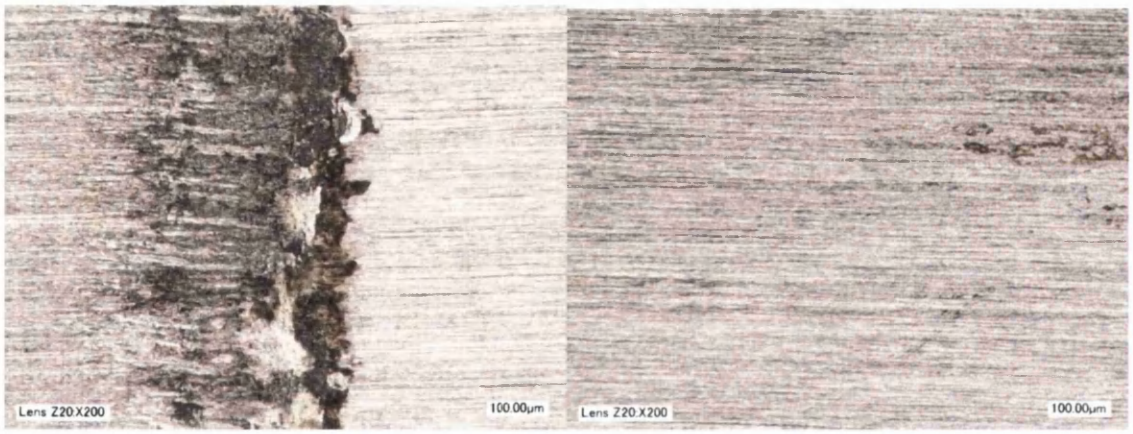

Figure 4.5.5. Test 3 with 9Nm tightening torque and pad pressure of 250MPa. Left – Edge of Bedding partial slip fretting and Right - Wear scar centre.

One of the many life limiting features of partial slip fretting fatigue is that microcracks which form at the edge of bedding due to the large stress concentrations and limited slip are not removed by wear, producing multiple origin sites. These small microcracks or fissures can go undetected during routine inspection and under the influence of further stress cycles, the cracks can grow, leading to premature ductile failure. Unfortunately, it was not possible to observe the formation and growth of cracks in this experiment but it would be advantageous to quantify the time it takes for initiation and propagation of cracks during fretting at these conditions.

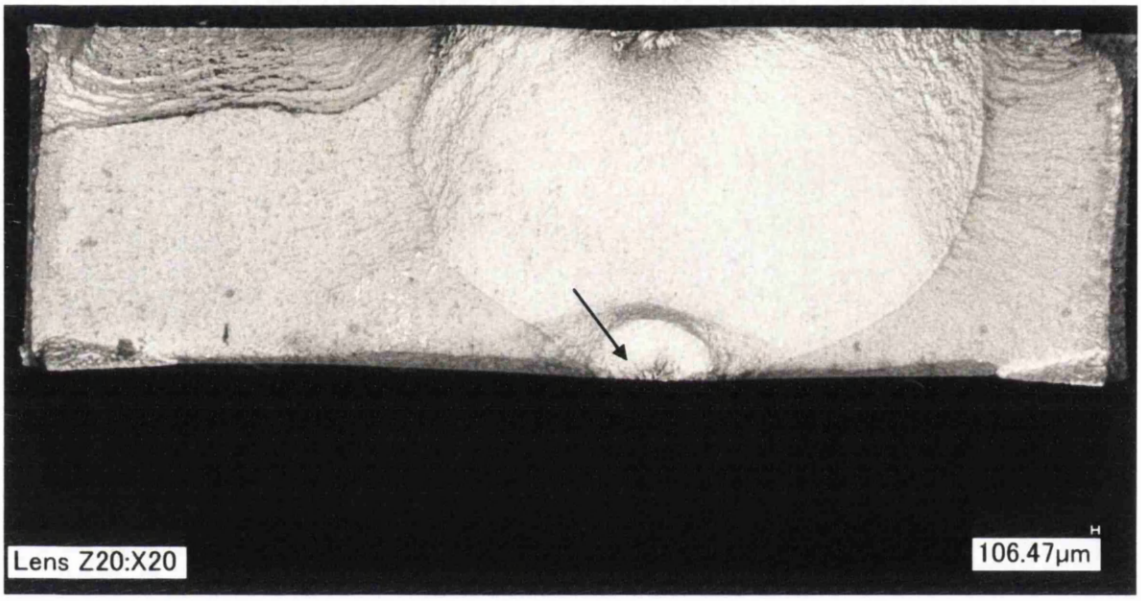

Figure 4.5.6. 3D Birdseye view of ductile fracture surface and fatigue origin for Test 3. (Shown by black arrow).

The explanation for the increase in life after 9Nm may be due to restricted slip between the contacts, suggesting the contacts were approaching the 'stick position' and therefore most of the wear surface was only elastically deformed during the test. In this case, mircocrack formation will be limited and the fretting fatigue life reduction factor will be lower. This is reflected in the surface roughness values of the fretting fatigue specimen with a tightening torque of 12Nm which has the lowest value for all four specimens. This value as well as inspecting the optical micrographs indicates that little movement across the contact surface took place, except for the outside of the wear scar which does account for some relative slip. The crack initiation site was again found to be in the outside region consistent with all the

other specimens. The initiation site for Test specimen 4 is shown below in Figure 4.5.7 and occurs at the edge of bedding.

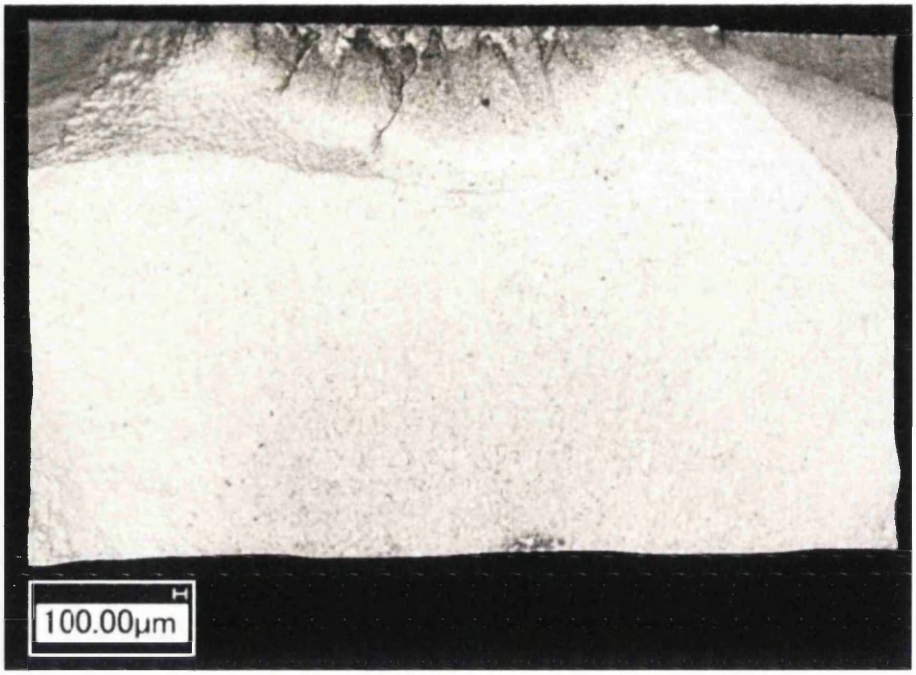

Figure 4.5.7. Fretting fatigue origin for Test 4.

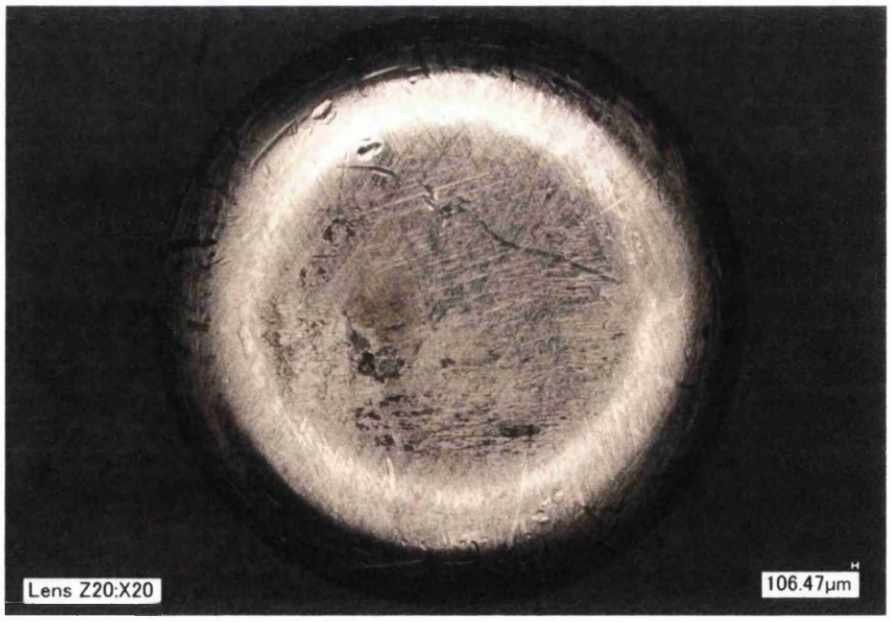

Figure 4.5.8. Stainless Steel fretting pads after a test which supplied 3Nm torque per bolt.

The image of the surface of the stainless steel 316 fretting pad shown above was taken after test 3 which was at a pad pressure of 250MPa and a tightening torque of 9Nm per bolt. It can

be seen from the image that the outside region of the pad is highly worn (shiny appearance) compared to the lesser worn centre which is dull in color and slightly oxidised. This suggests slip occurred mostly at the edges and agrees with the theory that this test simulated partial slip fretting fatigue. A surface roughness reading also showed that the centre was considerably lower than the outside edge at 1.16 and 1.78 respectively.

Stainless Steel 316 is softer than U720Li and as a result, the wear rate between the steel fretting pad and U720Li is expected to be lower, compared to a harder material combination such as U720Li against U720Li, Waspaloy or Inco718. On account of stainless steel 316 being softer than U720Li, steel will suffer a larger volume of material removal and there may be transfer of its debris onto the U720Li specimen, known as smearing. Further analysis using EDX can confirm this. Furthermore, although these tests were carried out at room temperature, at higher temperatures, oxidation can lead to the hardening of debris which can increase abrasion and reduce fatigue lives. The following table below illustrates the difference in hardness of the two materials.

Material	Hardness (Hv30)
Stainless Steel 316	140
U720Li	458

Table 4.5.5. Hardness values for stainless steel 316 and U729Li.[138]

4.5 Fretting Fatigue Testing at High Temperature Using U720Li Fretting Pads

Since good results were achieved at room temperature, the experiments were repeated at higher temperatures of 600°C. However, the steel fretting pads were exchanged for U720Li and the clamping plates were also redesigned to better cope with the higher temperatures and accompanied thermal stresses. The change in design can be seen in the experimental methods section, 3.4 but the design change essentially involves removing the radii from the plates and increasing the volume of material. The material remained as stainless steel 316.

In this series of tests, as a result of the high temperatures involved, the formation of an oxide glaze is a certainty which can reduce the rate of wear dramatically. Fretting wear tests performed by M.M Hamdy on the nickel base alloy, Inconel at 540°C saw a decrease in fatigue life by only 15%[117] due to the presence of an a nickel oxide glaze.

Five Udimet720Li specimens were tested with different values of pad pressure at 600°C to determine its effect on fatigue life when compared to baseline specimens.

Test Number	Pad Pressure	Torque per Bolt
1	70	4
2	160	6
3	250	9
4	355	12
5	390	15

Table 4.5.1. Pad pressures subjected to U720Li at 600°C.

The results are shown in the graph below.

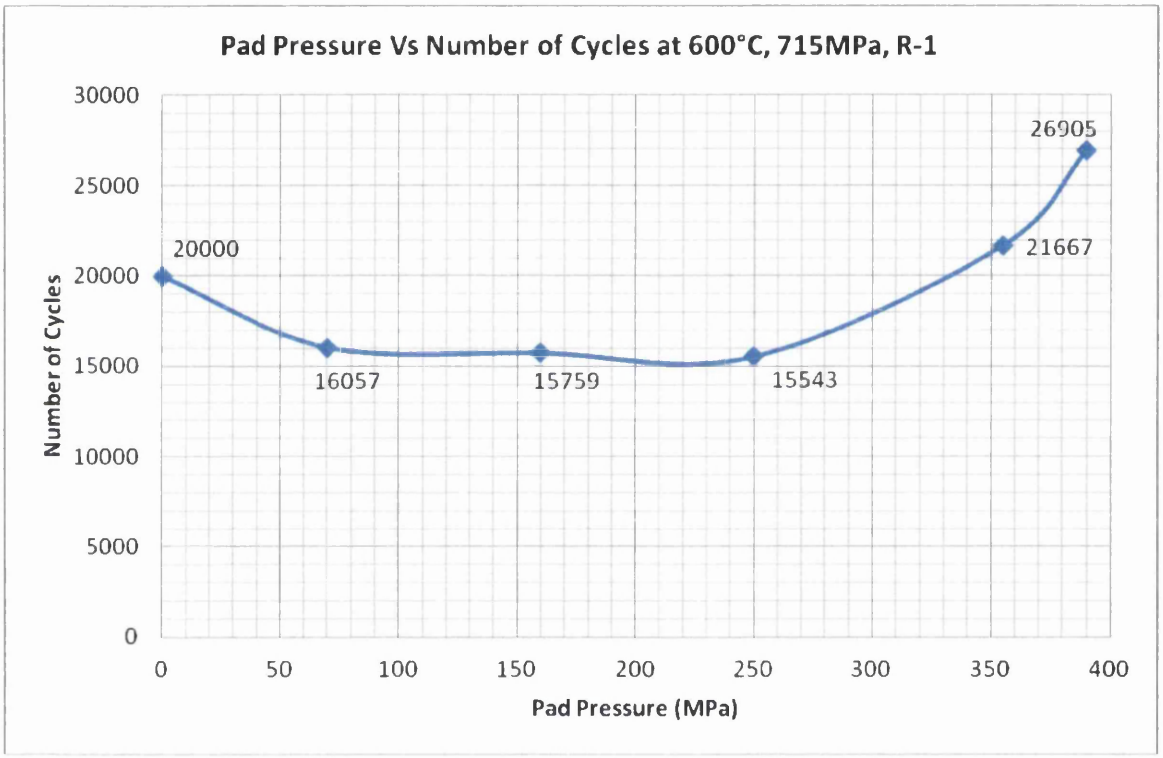

Figure 4.5.1. A graph of pad pressure Vs number of cycles to failure at 600°C for U720Li.

Test Number	Fretting Fatigue Life (cycles)	Fretting Fatigue Reduction Factor	Life Lost (%)
1	16057	0.803	19.7
2	15759	0.788	21.2
3	15543	0.777	22.3
4	21667	1.083	+8.3 gained
5	26905	1.345	+34.5 gained

Table 4.5.2. Fretting fatigue life reduction factors at 600°C for U720Li fretting fatigue specimens.

The graph in Figure 4.5.1 shows a similar relationship to the fretting fatigue tests carried out at room temperature with steel fretting pads previously. It can be seen that the fatigue life decreases with increasing pad pressure up to a certain value, which in this case is approximately 250MPa and then starts to increase with increasing pad pressure.

To explain this phenomenon, the dimensional wear coefficient, k, must be taken into account. This is because there exists a boundary between sliding wear and fretting but it depends on many factors and it is not a palpable one. Under fretting conditions, k is dependent on displacement but under sliding conditions (>100μm) it is not. Wear rates under a sliding regime are significantly greater compared to fretting. This is due to a greater amount of relative movement, creating more asperity fractures, and hence more debris. Figure 2.13.2.4 in Chapter 2.13.2 illustrates this theory well and will be used to help provide an explanation of the results in Figure 4.5.1.

At a pad pressure of 70MPa, the force through the pads is relatively small and allows for greater slip. The image of the wear scar, shown in Figure 4.5.2(a), confirms this and reveals that full sliding contact has occurred across most of the surface. Recalling the regime requirements for fretting and full sliding wear, it can be asserted that the slip distance as a result of a pad pressure of 70MPa, is too large to produce partial slip fretting. The tangential force is considerable enough to overcome the frictional force between the contacts i.e. $Q>\mu P$. Referring to the red curve in Figure 2.13.2.4, this would place the wear damage to the right hand side of the minimum of the red curve. Thus, the wear can be considered gross slip fretting fatigue since slip (or wear tracks) is evident occurs across the majority of the contact area. In this regime, any cracks formed can be removed as a result of material removal and the fatigue life is higher as a result.

At 160MPa the rate of slip decreases due to the increased contact force and the microcracks that form are not always removed. The slip distance is small enough so that the contact wear damage moves into the partial slip fretting regime. Hence, a lower fretting fatigue life is accomplished.

An increase in contact force to approximately 220MPa shows the lowest life for all the data points. This suggests that the partial slip fretting regime has reached its most severe point where the stress concentrations are at their highest and most life limiting. Referring to Figure 2.13.2.4, this would be shown as the minimum on the red curve. SEM inspection of the specimen with 250MPa pad pressure revealed fissures on its plastically deformed wear surface and also within the bulk material close to the fretting wear. Their approximate locations are shown Figure 4.5.2(b).

At 250MPa the fretting fatigue life starts to increase due to the increase in contact force which restricts relative slip between the contacts. As a result, there is very little wear and fewer formations of microcracks and this can be shown by the red curve in Figure 2.13.2.4. It is also observed that the life of two specimens is greater than the baseline fatigue life (20,000 cycles) at the same test conditions. A 34.5% and 8.3% gain in fatigue life is observed. It is well understood that specimens that are the same material, dimensions and surface finish will generally have different fatigue lives and this can be due to a number of reasons including the presence of microstructural anomalies that cannot always be detected. For this reason, error bars are often included to show the spread of data. However, in this case, even the error bars cannot account for the increase in fatigue lives.

One theory for the increase in fatigue lives due to the large contact pressures is the compressive residual stress zones created at and around the fretting pad contact zone. Compressive residual stresses are widely used to enhance fatigue life in engine components, especially in the aerospace industry. It can be thought of in much the same way as shot peening or surface rolling whereby a compressive layer produces a local plastic deformation and helps to suppress the movement of dislocations and effectively slow down the process of microcracking. The majority of researchers agree that the presence of compressive residual stresses has a beneficial influence on the fatigue life of rolling contacts[139,140,141].

The wear scars of specimens with pad pressures of 70MPa, 250MPa, 390MPa are shown below. Note how the wear specimens have oxidised under high temperature and have become a dark grey/brown colour.

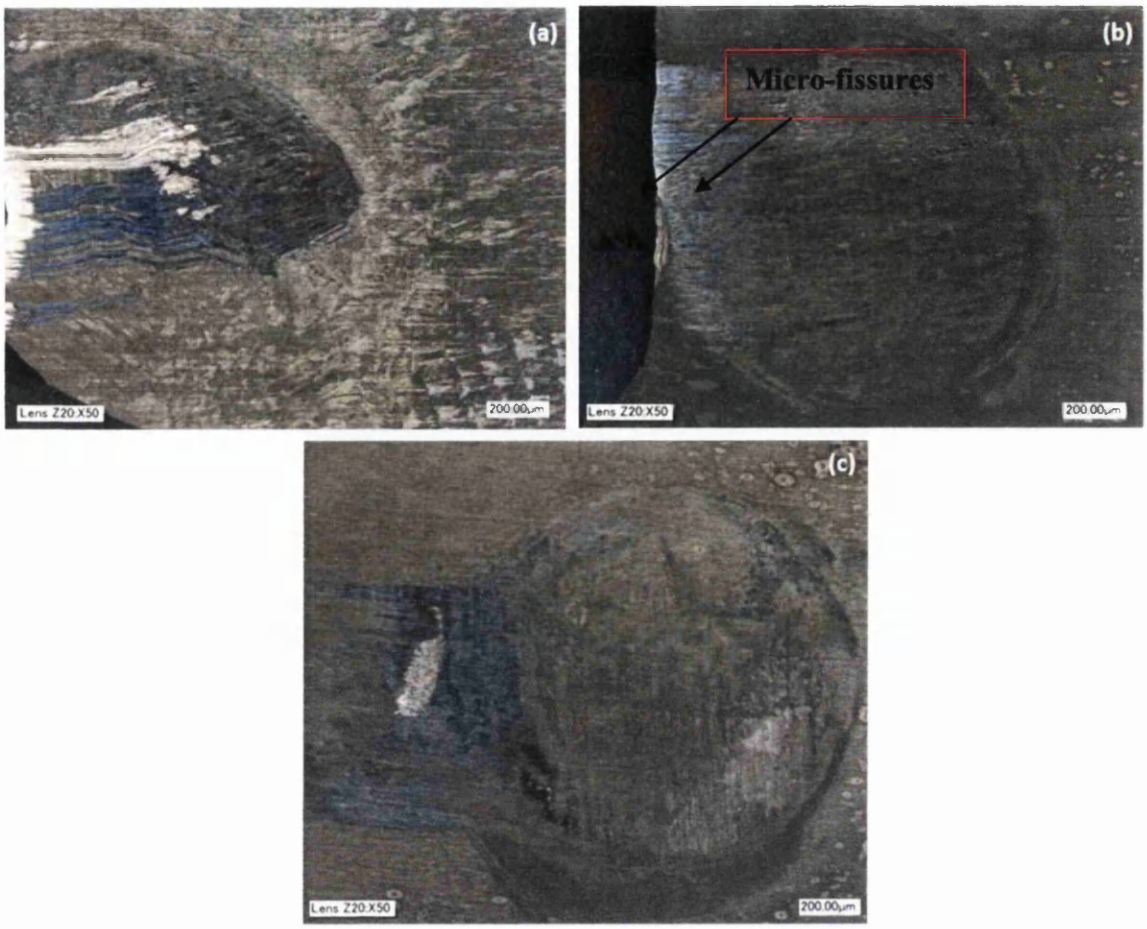

Figure 4.5.2. (a) 70MPa (b) 250MPa (c) 390MPa

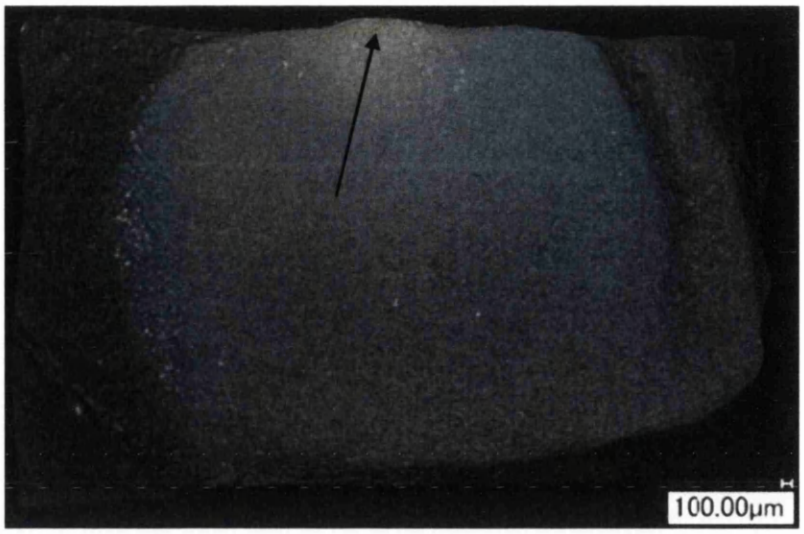

Fracture surface of (a) showing crack origin due to sliding wear (Black arrow).

Fracture surface of (b) showing failure initiation point for at edge of specimen (Black arrow).

Fracture surface of (c) showing the failure initiation point on the side edge, away from fretting damage (Black arrow).

Figure 4.5.3.

With the exception of the specimen subjected to 70MPa, the images shown in Figure 4.5.2 and Figure 4.5.3 above reveal how the failure origins have initiated away from the fretted

areas. This indicates that the fretting wear has not had a direct effect on the failure location of the specimens and has instead located a feature with a higher concentration of stress away from the wear scar e.g. surface defect at the specimen's edge. However, the change in surface roughness from the centre of the wear scar to the fretted region should be more than adequate to form large stress concentrations, so it is surprising that failure did not occur in this region. The change in surface morphology is shown below in Figure 4.5.4. This is especially true for Test 3, since a change in surface roughness such as this would be adequate enough to initiate failure in service components.

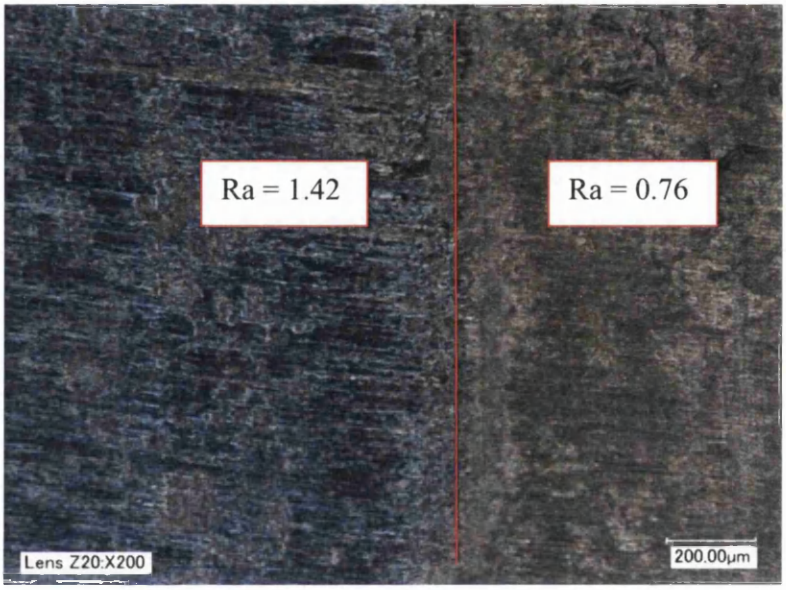

Figure 4.5.4. Change in surface condition for Test 3. The red line indicates the change in surface condition.

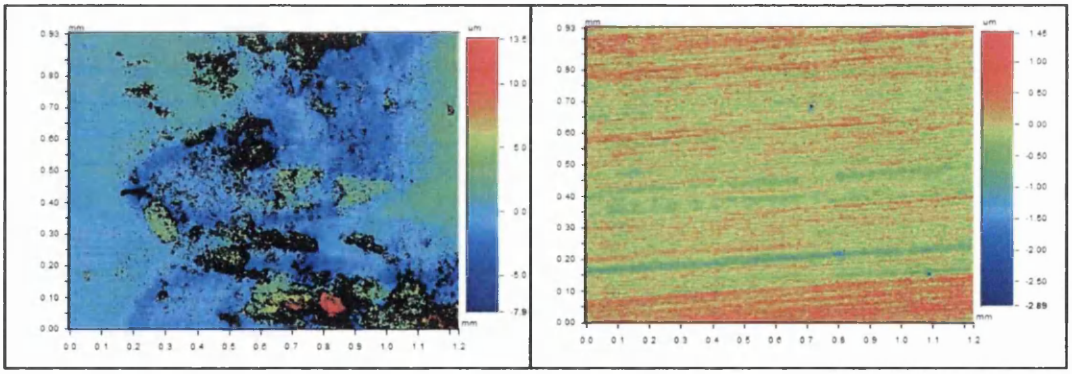

Figure 4.5.5. Average surface roughness images for (b) showing the fretted region and the relatively unworn region.

The following table provides the pad pressure and surface roughness values for all five tested specimens.

Test Number	Pad Pressure	Torque per Bolt	Ra (μm)	Rq (μm)
1	70	4	1.26	1.77
2	160	6	1.13	1.66
3	250	9	1.02	1.48
4	355	12	0.92	1.33
5	390	15	0.86	1.31

Table 4.5.3. Pad pressure and surface roughness values.

Although the initiation site is not in the direct vicinity of the wear damage, the wear can still have an effect on the fatigue life. The true concern in contact fatigue is not the generation of surface damage or wear due to relative motion between the surfaces. Rather, it is the premature nucleation of micro-cracks or fissures which could extend beyond the bedding surface and subsequently propagate by fatigue into the body of a disc or blade under the influence of bulk stresses. Indeed, it is possible to initiate cracking, with very little surface damage, if the stress levels are high enough.

Fractographic examination of all the specimens revealed that the EoB cracks displayed a multi-nucleated and stepped behaviour. This is characteristic of fatigue initiation under high stresses. Furthermore, higher magnification assessment of the fracture surfaces near the crack origin of Test 3 revealed a series of fissures aligned in the same plane as the main fracture surface. These observations are also consistent with surface fissure and micro-cracking damage observed in fretting fatigue tests presented in literature[142]. Although failure initiation did not occur at these sites, it suggests that they can still be created as a result of the large contact stresses due to fretting fatigue.

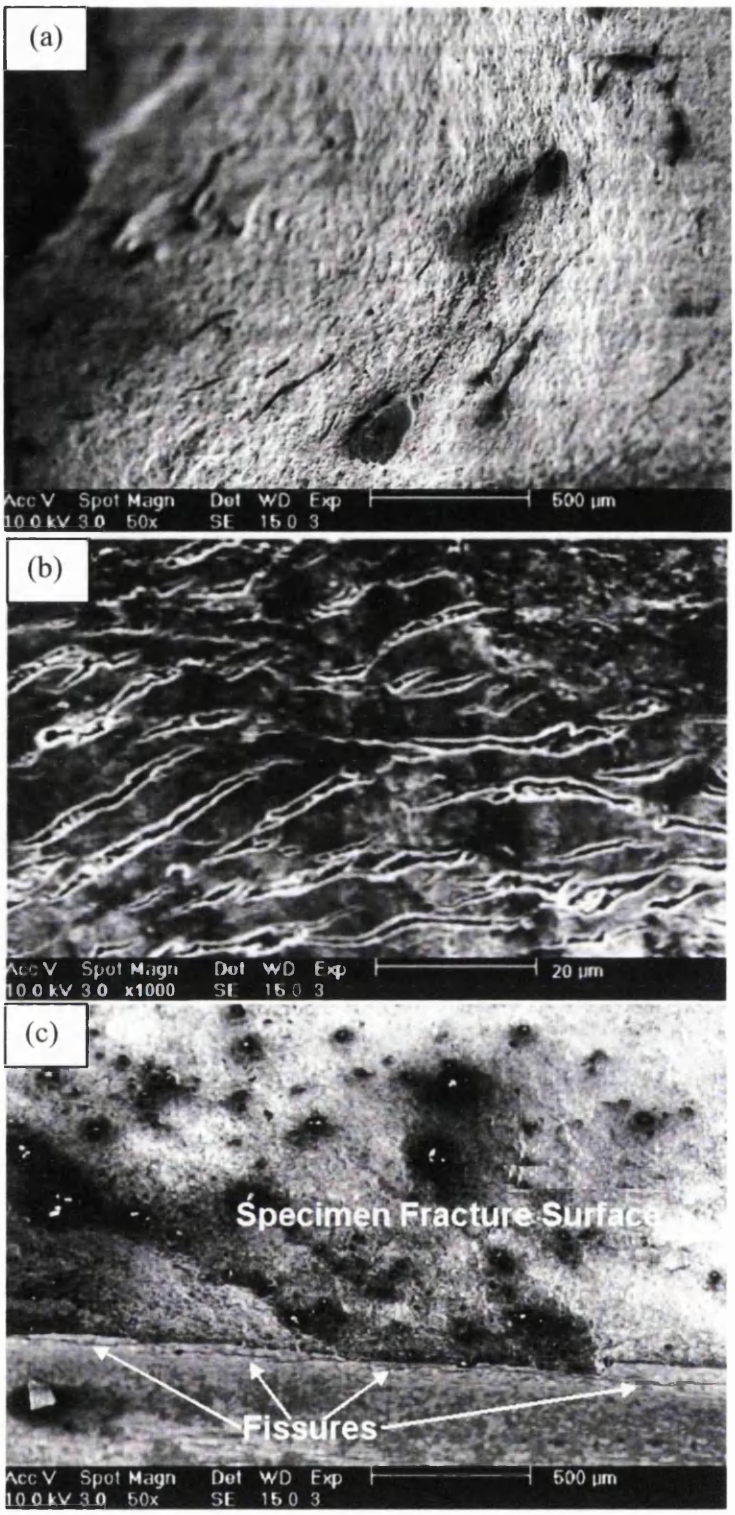

Figure 4.5.6. SEM image of (a) micro- fissures in the bulk material (b) microfissures observed in the oxide glaze layer on the fretted surface for the U720Li specimen with a contact pressure of 70Mpa (c) micro-fissures near fretting damage on Test 3.

Many of the fissures, or micro-cracks, observed in the oxide/glaze layer of the contact surface never propagate into the base material. Although the observation of fissures on the contact surface is consistent with contact and fretting fatigue[143], fissures in the oxide/glaze layer of the specimen wear surface are not conclusive evidence of contact fatigue crack nucleation.

It is important to note that even though the images above show crack formation on the wear scar immediately at the edge of bedding, unless the oxide/glaze layer is removed, it is impossible to confirm whether cracks present in the bedding wear surface extend into the substrate. On this basis, it is possible that there are fretting and contact fatigue nucleated micro-cracks present below the oxide layer that go undetected. Either way, if microcracks are created and lie dormant under the glaze layer, it is difficult to determine if they account for failure in locations that do not initiate there.

4.6 Apparent Lack of Fretting Wear and the Effect of Nickel Oxide Glaze

The apparent difference in wear damage compared to the room temperature tests is highly likely a result of the high operating temperature. Temperature can affect the fretting wear in two ways.

- Corrosion and oxidation rates usually increase with temperature
- Mechanical properties usually change with temperature – this includes the fretting rig components

The temperature effects on fretting are best described in terms of surface oxidation kinetics. It is well known that at high temperature, nickel oxide glazes can form readily and can have a considerable effect on the degree of fretting and the fretting fatigue life. The coefficient of friction of nickel oxide glaze varies but is approximately 0.2 for nickel base superalloys such as U720LI. The oxide film not only reduces friction but prevents metal-to-metal contact from occurring and this is the main reason for the lack of wear damage. The oxide films produced vary in thickness and morphology and are formed at different temperatures for specific materials.

In this case, the materials are the same. They will form an oxide glaze at the same rate and they will also have the same hardness. Referring to the Button-on-Plate Tests in 4.7.1, it will be shown that U720 performs very well having a relatively low wear rate. Hence, the rate of

wear will be relatively low for U720LI on U720Li and the fretting fatigue life is also expected to be higher. This is seen in the images above where there is considerably less fretting compared to the stainless steel 316 on U720Li in the room temperature tests.

4.7 Wear Performance of U720Li

Since U720Li is used extensively in this research it is important to understand how it responds to material interaction and its resultant wear damage in terms of material removal. Furthermore, since U720Li is a nickel base superalloy, it is well known that at high temperature, nickel oxide glazes can form preferentially, which can be highly beneficial to its wear response. The formation of the nickel oxide glaze and its benefits will be discussed in the following chapters.

4.7.1 Button-on-Plate Tests

Previous tests at Rolls-Royce using standard button-on-plate wear tests have been carried out to compare the wear performance of various disc alloys against CMSX4. The alloys of interest are as follows: CMSX4, Udimet 720Li, Waspaloy and RR1000.

The results of these tests are shown below and suggest that of all the disc alloys, Udimet 720 has the lowest rate of wear[144].

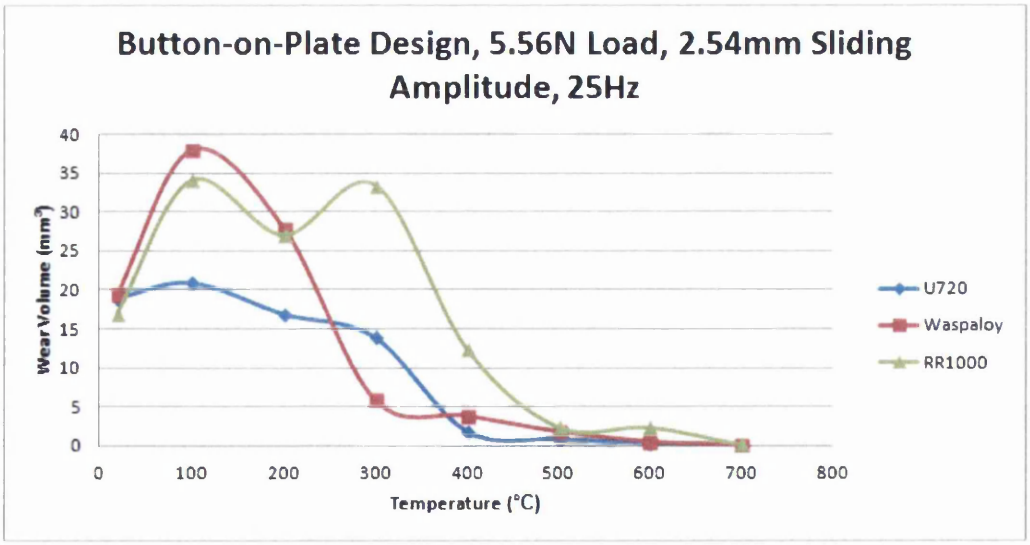

Figure 4.7.1.1. Comparison of Disc Alloys in Terms of Sliding Wear against CMSX4[135].

It can be seen in Figure 4.7.1.1 that for all of the materials, the volume of material removal is greatly reduced at higher temperatures. This can be explained due to the formation of a nickel oxide glaze which forms preferentially at high temperatures. The oxide glaze formation is very important as it greatly reduces the rate of wear between two materials in contact acting as a natural lubricant.

4.7.2 Formation of Nickel Oxide Glazes

Flash temperatures of several hundred degrees can be generated in contact sliding alone. Even at room temperature and only small sliding velocities, the temperature can be increased enough to produce significant increases in surface oxidation. In fact, it has been shown that oxide thicknesses that would organically take a year to grow under normal conditions can develop in hours or even minutes during sliding wear[145].

The 'Oxide glaze' that Nickel alloys such as U720Li form makes them particularly interesting as they can form a relatively stable oxide layer at elevated temperatures. Below 250°C, an oxide layer is formed from the compacted wear debris. This initially protects the surface from further damage, but as soon as it is broken down by further sliding and a subsequent increase in wear rate is seen. Above 250°C, the compacted oxide layer is sintered (oxide particles combine under the influence of load and heat), which gives rise to the smooth glaze layer developing on top of the compacted oxide regions. Although this glaze is more stable than the compacted oxide layer alone, it is not until 400°C that it reaches its full potential[114]. Above this temperature, the glaze becomes self-healing, which inhibits any subsequent break down. The temperatures used in the high temperature fretting experiments are well above this temperature; hence nickel oxide glaze formation is an important factor in the wear process.

Without the formation of a nickel oxide glaze, the working life of components such as the disc and blades would be much lower and in the case of the high temperature fretting test programme above, the wear damage would have been greater.

In the wear process, upon initial sliding any naturally occurring oxide film, or any due to pre-oxidation, is quickly removed from the surface, exposing virgin alloy to the atmosphere. However, transient oxidation forms immediately on the exposed alloy, forming oxides of mixed metal origin, depending on the particular alloying constituents. The amount of wear

and alloy deformation that follows is dependent upon the high temperature strength of the alloy.

During the wear process, most of this transient oxide is removed from the load-bearing areas, due its moderately low shear strength but it is rapidly reformed due to the high, localised temperature. Eventually, the buildup of oxides is sufficient to form a layer of compacted oxide particles, and the debris particles are broken down to a critical size allowing them to become embedded into the wear tracks. At this point, the rate of wear decreases and there is a 'severe to mild transition'.

The smooth glaze generated above 250°C is not always present as a continuous layer across the whole surface, but often as discrete islands that appear on top of the compacted oxide layer. Its effectiveness, however, in decreasing friction and shear stresses, will increase with increased surface coverage. The islands of glaze are usually visible as smooth dark regions with a bluish tint to the eye, which stand proud of the surrounding area. Their elevation above the rest of the surface suggests that these glazed regions are the main load bearing areas of the contact zone. This is also enforced by the many small abrasion grooves that appear parallel to the direction of sliding on the glaze surface, but not on the remaining scar area. Grooves on even the smallest of islands, gives an indication of the high level of adhesion that the glaze has to the underlying oxide layer. This is shown below in Figure 4.7.2.2.

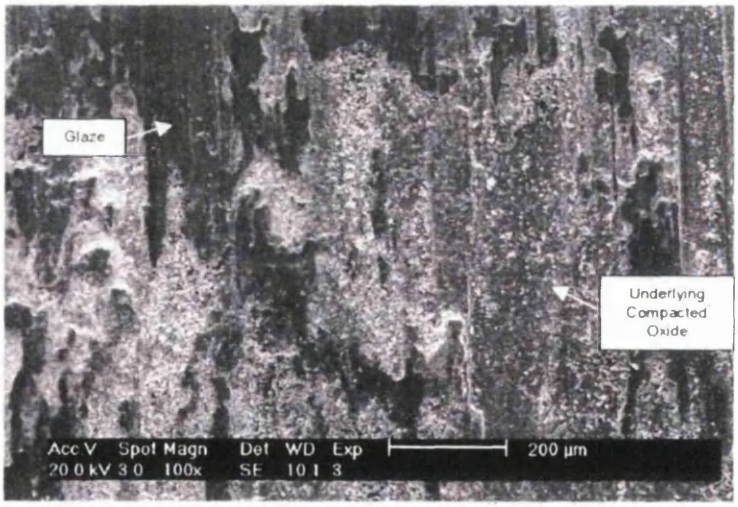

Figure 4.7.2.2. Glazed Regions on a Standard Udimet 720 Wear Scar (Testing Carried out at 400°C)

4.7.3 Effect of Oxide Glaze on Friction and Fatigue

It has already been previously stated that the presence of an oxide glaze leads to a dramatic decrease in friction. Simple friction tests show that on average, bare Ni alloys have a coefficient of friction of about 0.7. A compacted oxide particle layer formed at room temperature decreases this value to about 0.6. A nickel oxide glaze however, decreases the coefficient of friction even further to around 0.2[146], a dramatic reduction.

Despite some differences in test results, it can be said that a glaze layer decreases friction, which reduces shear stresses at the surface. As a result, the fatigue deficit upon subsequent fretting will be reduced. Testing carried out on Inconel 718[147] (Table 4.7.2.1) has shown that at 20°C and 280°C, the fatigue strength is reduced by 56% and 63% respectively, due to the action of fretting. At 540°C, the presence of a glaze reduces this impact on fatigue such that the fatigue strength is reduced by only 15%.

Temperature (°C)	Normal Fatigue (cycles)	Fretting Fatigue (Cycles)	SRF
20	275	120	2.29
280	325	120	1.71
540	325	275	1.29

Table 4.7.2.1. Fatigue strength of Inconel 718 in MPa tested at 10^7 and a mean strength reduction factors (SRF). Tested at a mean stress of 550MPa.

It is evident from this research that the presence of a glaze not only reduces friction and wear, but also prevents the surface damage that can lead to the initiation of fretting fatigue cracks. For the glaze to be effective, however, it must firstly a) form rapidly with the onset of fretting (especially as the initiation of cracks is known to occur in the first few thousand cycles), b) be stable and resistant to subsequent delamination, and c) if it does breakdown, be self-healing. All these factors depend on the conditions to which a system is subjected and will be discussed in the following section.

4.7.4 Factors Affecting Glaze Formation

4.7.4.1 Temperature

Oxidational wear theory explains how the rate of wear should increase with an increase in temperature due to an increased rate of oxidation. However, when talking about nickel alloys, this does not hold true due to the formation of an oxide glaze which helps to protect the surface from further wear. It is still highly debatable as to why this formation occurs but J Lang et al[116] explains that this may be due to the increase in particulate attraction that an increase in temperature provides. The development of protective layers is closely related to the adhesion between wear debris particles, and not purely on the rate of oxidation. Any rise in temperature will increase the attraction between these particles, and aid glaze formation. The same author plotted the graph below, which shows how the rate of wear volume changes considerably at approximately 250°C. Temperatures higher than 400°C also show a decrease in material volume removal.

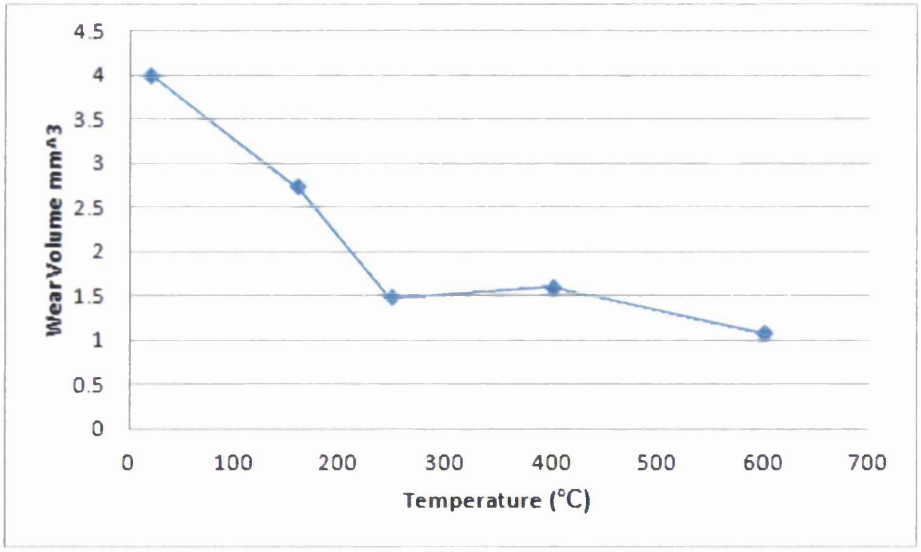

Figure 4.7.4.3.1 Effect of Temperature on the Wear Rate of Nimonic 80A.

4.7.4.2 Normal Applied Load

Jiang et al[116] reported that the size of wear debris particles increases with increased normal load (due to cracks propagating deeper into the surface). As a result, wear particles find it more difficult to become embedded into the wear tracks, and so the formation of protective layers is hindered. The severe to mild wear transition is delayed or, if the load reaches a critical value, can become altogether impossible. This critical value of load is not quoted. However, similar testing has been carried out internally up to a contact pressure of around 600MPa. At these conditions, percentage glaze average continued to increase with increased load, suggesting that the 'critical value' of load had not yet been reached. However, a contact pressure of 600MPa also produced a significant increase in wear rate, indicative of a delay in the severe-to-mild wear transition.

So it can be summarised that a contact pressure of 600MPa is still favorable to produce a stable glaze, but it will take longer to establish at these conditions.

4.7.4.3 Air Pressure/ Partial Pressure of Oxygen

For most metals there is a point, below which, there is insufficient oxygen to produce an oxide film. For Ni alloys this is about 0.1-0.2m bar partial pressure of oxygen (or about 0.5-1.0 mbar total pressure in air). Below this value, oxidation cannot take place and so protective oxide layers cannot form. Any wear will be due to plastic deformation and fracture of metallic surface asperities, resulting in high wear rates and high levels of friction. Above 0.1-0.2 mbar of partial pressure, oxidation can occur and so debris particles are likely to be formed from the oxidised surface. The effect that this has on a system will depend mainly on the temperature[148].

4.7.4.4 Slip Distance

In terms of glaze formation, an increase in slip distance increases the probability of removing debris from the contact zone. Wear debris are essential for glaze formation, and so the severe-to-mild wear transition is either delayed, or in extreme circumstances prevented altogether. Although there has been no research carried out for this particular parameter, we can compare the results from two different authors using similar materials and similar applied loads. The

first author, J.Lang[149], carried out testing using a large slip distance. The second, Iwabuchi[118], carried out testing using a much smaller slip distance.

The results of the tests show that the time taken to reach a coefficient of friction of around 0.2 which is the typical friction value of a glaze was significantly longer for a larger slip distance. Hence, it can be supposed that the severe-to mild wear transition is delayed as you increase the slip distance.

The same rules in terms of glaze formation apply if you decrease the slip distance into the fretting regime (under 100μm). However, it is also well known that fatigue cracks are most likely to initiate under fretting, or more accurately, in the partial slip regime.

4.7.4.5 Slip Speed/ Vibration

Jiang et al[150] reported that the size of wear debris particles increases with increased sliding velocity. As a result, wear particles take longer to break down and become embedded into the wear tracks, and so the formation of protective layers is hindered. An increase in slip speed also increases the probability of removing debris from the contact zone, which is essential for glaze formation. Both factors contribute to the severe-to-mild wear transition being delayed or, if the sliding velocity reaches a critical value, becoming altogether impossible.

4.7.4.6 Surface Condition

It has been theorised that a rougher surface aids debris entrapment, promoting self-lubrication, and in the case of Ni alloys, potential for glaze formation. As such, polishing is reported to be undesirable for fretting fatigue performance[151]. Under normal fatigue situations, polishing improves performance due to the reduction of residual stresses. Under fretting conditions, however, polishing eliminates the surface 'key' that is essential for debris formation and subsequent entrapment.

4.7.4.7 Multi-Directional Movement

Tribology theory states that a multidirectional sliding movement produces a lower friction than a unidirectional one[152]. It is theorised that this effect is due to increased smearing of

wear debris, which accelerates debris breakdown, increases the probability of particle entrapment within existing wear scars, and in the case of Ni alloys, aids glaze formation.

4.8 Shortfall of Fretting Test Rig

As well as the presence of a nickel oxide glaze, another plausible reason for the lack of fretting wear in the high temperature tests is the fretting rig itself and its competence to produce reliable and realistic fretting wear at high temperature.

Since the rig had never been used at high temperature before it was difficult to predict how much slip would occur between the pad and specimen. At room temperature, good wear scars were produced having the characteristics of partial slip fretting, but at high temperatures, thermal stress relaxation in the bolts and clamping plates almost certainly took place. It would have been ideal to encompass pressure sensors between the pad and specimen to provide in-situ pressure force readings to observe the loss in clamping force.

The bolts themselves may have extended as a result of creep at high temperature and this would cause a reduction in force through the fretting pads. The bolts will extend under a steady load at room temperature naturally but in the presence of high temperature, this process is speeded up considerably. Aerospace grade bolts with good tensile strength and creep properties would be an ideal upgrade in order to maintain the clamping force through the fretting pads.

One of the many advantages of bi-axial rigs as used by Oxford University is the ability to maintain a constant force through the fretting pads and set a desired sliding displacement between the fretting pad and specimen. However, with the fretting rig used in this project, it is difficult to determine these parameters. Strain gauges could be adopted into future experiments to measure the sliding distance of the specimen and pad. The measurement of the pad pressure still needs further research but for now there are many reliable finite element analysis packages capable of measuring such contact problems.

The rig was designed as an 'off the shelf' testing apparatus to replicate the fretting wear process. For this reason alone, this rig is suitable to analyse wear scar surfaces and the formation of microcracks that form on the wear scar itself or in the bulk material below it. It

is a relatively cheap test to perform and can produce partial slip fretting comfortably at room temperature. Further research is required to achieve reliable partial slip patterns at high temperature, specifically the use of high temperature materials which would help to relieve the problems of creep and thermal stress relaxation.

5 Conclusion

Contact wear has been a research topic of vast interest for many years but the factors that account for it are poorly understood. Even defining what constitutes specific kinds of wear such as scuffing, galling and fretting has not yet been fully resolved. Fretting specifically, is very difficult to classify due to the number of regimes that fall under its title and the extensive number of variables involved in the process. It has been quoted that there are over 50 variables operating synergistically at one time during the fretting process.

Although much research has been made to better understand this contact wear phenomenon, there still exists a need to formulate guidelines that clearly define various forms of wear damage. It would be valuable to component lifing specialists and failure investigators alike to have a database in place of an array of wear damage and their corresponding fatigue life reduction factors. This would allow for more accurate lifing of engine components which can ultimately extend their service lives, increase the time between inspection intervals or provide a case to end the components working life prematurely if the damage is deemed too high risk. In the long term, research into contact wear such as this can save vast amounts of money in the aerospace industry alone. For example, significantly low service life hours can be assigned to engine discs with slight wear damage due to highly conservative lifing methods, sometimes only reaching a quarter of their service life potential. With increased knowledge on the effect of wear damage on the fatigue lives of components, this can be improved. Furthermore, research into contact wear can provide significant research into the manufacture of surface treatments and lubrications to alleviate the actions of contact wear damage.

In this research, previous wear damage from ex-engine and current engine components has been analysed to extract data such as surface roughness, wear depth and wear scar area as well as characteristic features which help differentiate the various kinds of wear scars. The aim was to gather as much information as possible so that the wear damage could be simulated onto laboratory fatigue specimens to establish fatigue life reduction factors.

The initial wear tests performed at room temperature by Oxford University produced wear scars with a range of damage severity from light fretting marks to heavy galling wear with gross material removal. The worn specimens were then fatigue tested at 600°C to determine

the effect of wear damage on the specimens fatigue life. From the results gained, the following conclusions can be drawn.

- A range of wear scars can be produced by changing the combination of pad sliding distance and the contact pressure. It was possible to determine the wear mechanism by referring to each test's characteristic hysteresis loop at the start, middle and end of the wear process. A large hysteresis loop with a quadratic relationship confirmed that full sliding across the contacts had occurred and a narrower loop illustrated smaller displacement amplitudes as in the case of partial slip. A closed hysteresis loop implied that no sliding had occurred. If the shape of the hysteresis loops changed throughout the test, it was suggested that mixed slip had occurred i.e. the contacts started with full sliding and transitioned to partial slip.
- In essence, If $Q<<\mu P$ there will be no movement of the contacts and this is known as 'stick'. When the tangential force is not large enough to create full sliding of the contact surfaces but is just below the sliding amplitude threshold value, partial slip will occur i.e. $Q<\mu P$. However if the tangential force is equal or larger to the sum of the normal force and coefficient of friction of the material, gross or reciprocating sliding will occur. $Q\geq\mu P$.
- Partial slip fretting patterns were achieved exhibiting the plastically deformed (slip) outer region and the elastically deformed central region (stick) from applying small sliding amplitudes in the range of 0.05mm-0.5mm and contact pressures in the range 100MPa-250MPa. The surface roughness for these specimens varied from the centre to the outside and these proved that partial slip had indeed taken place.
- As the pad sliding distance was increased, the surface roughness and quantity of material removal also increased. This was proven when specimens with the same contact pad pressure but different sliding distances was compared. It was therefore concluded that the rate of material removal is proportional to the sliding amplitude.
- Wear scar morphologies were difficult to control when large pad sliding distances (0.8-2mm) were employed due to the large material removal. This was expected for specimens with anticipated galling wear but it was not expected for specimens with projected scuffing wear. As such, the scuffing and galling wear produced seemed to overlap as the spread of surface roughness and fatigue life reduction factors was very similar. Therefore, it was suggested that to achieve scuffing wear, it is practical to use contact loads smaller than 25MPa.

- The worn specimens were fatigue tested at 600°C and the results showed a positive trend for a larger fatigue life reduction with increased surface roughness. It was suggested that the loss in fatigue life was due to the surface irregularity, multiple stress concentration features and therefore low surface energies that promote perfect platforms for fatigue nucleation.
- The specimens produced an array of fatigue lives with the greatest life reduction measured at 96%. This specimen had large material removal and a large average surface roughness value (Ra) of 5.18μm and a root mean square value (Rq) of 7.27μm.
- It was obvious from the results that fretting wear should be considered on an entirely separate basis to other forms of deleterious wear damage due to the nature of the contact problem and the mechanisms that drive it. Partial slip fretting is considered the most life limiting of its four regimes due to the sharp stress gradients at the stick/slip interface and edge of bedding location. This was proven to be the case when the fatigue life of specimens with projected fretting wear was compared. It was found that the majority of specimens which were subjected to a slip amplitude typical of partial slip (50μm) resulted in the greatest fatigue life reduction. Furthermore, it also suggests that there is an ideal combination of slip amplitude and contact pressure that results in the lowest fretting fatigue life. In this research, a contact pressure of 200MPa and slip distance of 0.05mm (50μm) had a lower life than specimens with same slip distance but a contact pressure of 150MPa and 100MPa respectively, i.e. Fatigue life reduction factor = 200MPa, 50μm > 150MPa, 50μm > 100MPa, 50μm

The next stage of research attempted to focus more specifically on fretting fatigue. To do this, a customised fretting rig was designed and manufactured to include fretting fatigue at high temperatures of 600°C, typical of temperatures experienced by turbine discs at the bore and diaphragm regions. The fretting test uses a pair of clamping plates which hold replaceable fretting pads against the surface of fatigue test specimens. When the specimen is subjected to a cyclic axial stress amplitude, the specimens will extend and cause slip between the pad and specimen.

Initial tests were performed at room temperature using a stainless steel fretting pad. The results are summarised below.

- The number of fatigue cycles deceases as the pad pressure increases from ≈70-250MPa (3Nm to 9Nm tightening torque) but then starts to increase from 220-355MPa (9Nm to 12Nm tightening torque). This can be explained by the Hertzian contact force and relative slip which results from varying the pad pressure. At low contact pressures, the slip between the fretting pad and specimen is relatively large. With a larger sliding displacement, the material removal is larger and any cracks created will be removed more quickly due to the wear process. At larger contact pressures, the relative slip is small and material removal is small, so microcracks are not removed as readily. This is reflected in the surface roughness values of the fretting fatigue specimen with a tightening torque of 12Nm which has the lowest value for all four specimens, suggesting slip in that specimen was less than its counterparts. As in the previous wear tests performed at Oxford University, it is believed that there is combination of pad pressure and slip amplitude that results in the greatest reduction in fatigue life.
- In all cases, failure initiated from the edge of bedding where the stress concentrations are large and where the surface roughness changes drastically. Both these provide the ideal platform for fatigue nucleation.
- A small amount of oxide was present on the outside of the wear scars, where the relative slip is at its maximum. The high friction during sliding creates flash temperatures which increases the oxidation rate.

The next stage of the testing moved to a higher temperature of 600°C using a U720Li fretting pad instead of stainless steel 316. The conclusions from this part of the testing are as follows.

- There was considerably less fretting damage at 600°C compared to room temperature tests and this was thought to be due to the development of a nickel oxide glaze layer which decreases the friction and results in less wear. The nickel oxide glaze can reduce friction to values as low as 0.2. Simple friction tests show that on average, bare Ni alloys have a coefficient of friction of about 0.7. A compacted oxide particle layer formed at room temperature decreases this value to about 0.6. Furthermore, since the contacts are the same material (both U720Li) and the wear rate of U720Li is excellent at high temperatures[135], the rate of wear will be low between these two materials during sliding.
- As in the room temperature fretting tests, the fatigue lives of each specimen with different pad pressures was recorded and plotted in a graphical format. The results showed the

same relationship as the room temperature tests in that the fatigue life decreased with increasing pad pressure to a certain value and then started to increase. The minimum of the curve showed the lowest fatigue life and it was suggested that this was due to an ideal combination of pad pressure and slip distance that produced the most detrimental fatigue life reduction. The pad pressure was measured at approximately 220MPa. At this pad pressure and corresponding slip distance, the stress gradients at the edge of bedding were considered most severe and mircocrack formation was more likely.

- Fatigue life reduction factors were calculated for each specimen and it was observed that two out of the six specimens had a fretting fatigue life greater than the baseline value of 20,000. A 34.5% and 8.3% gain in fatigue life is observed. This was thought to be due to compressive residual stresses created by the large pad pressures. These compressive residual stresses produce a local plastic deformation and aid to suppress the movement of dislocations, effectively slowing down the process of microcracking.
- The failure locations of the specimens in the high temperature tests initiated at different locations from one specimen to the next. Only one specimen was found to have a failure location at the edge of the wear scar. The other specimens initiated cracking at locations away from the wear scar. However, even though this was the case, it is still believed that the contact wear played a role in the failure due to the presence of fissures in both the wear scar and the bulk material in various locations.

6 Future Work

The long term objective is to develop a mechanistic model of fretting fatigue damage initiation and progression which takes into account the known contributory factors that have already been touched upon i.e. surface condition, temperature, sliding distance, contact pressure and bulk stress). It is acknowledged that this is an ambitious goal with large scope and potentially massive economical gains, especially considering the number of engines operating under power-by-the-hour contracts. Hence, the work carried out in this project can be considered as a good introduction to long term objectives.

This work has attempted to capture and disseminate enhanced understanding in the form of a practical guide for R-R personnel to use. The reduction in fatigue life as a consequence of wear damage can be used as a form of risk scoring which illustrates the severity it poses to components. However, to ensure that this can be done in an effective, reliable and accurate way, a much greater datum of information is required to cover the whole spectrum of wear damage witnessed on engine components. This would involve using an extensive combination of sliding distances and pad contact pressures as well as changing additional variables such as mutli-directional sliding and the environment conditions. Comparative analysis between worn specimens and worn engine components would then be performed to determine similarities and differences so that an appropriate safe working life prediction can be calculated for the worn component.

It was also mentioned previously how it would be beneficial to observe the formation and growth of cracks to understand where they initiate and propagate from. Knowing these locations would allow palliatives to be designed, to reduce the stresses in these regions, and introduced back into the design process. Furthermore, it would also allow improved lifing calculations since the rate of crack growth could be observed in real time.

It is well known that lubrications and surface treatments reduce the rate of wear damage by decreasing the friction, and this can increase the working life of a component significantly. Therefore, the addition of lubrications or surface treatments can be tested and compared to the results in this research to determine the differences in wear scar morphology and fatigue

life benefits. Currently, solid dry film lubricants (DFL) such as Metco58 and Everlube 620 which are molybdenum disulfide and graphite based are used. Surface treatments which induce residual stress fields as a way of reducing microcrack formation such as shot peening are used in certain wear prone regions, such as the disc/blade contacts. However, a new method such as low plasticity burnishing (LPB) is also being considered as an alternative method and very little testing has taken place thus far.

The customised fretting fatigue rig in this research was designed as a relatively cheap and quick method of extracting information from straightforward fretting fatigue tests with high temperature capabilities. The rig also allows the fretting pad to be changed to test the effects of material combination and geometry on the fretting fatigue life. Therefore, future research could incorporate new these variables, which increases the scope of data for more efficient and accurate service life predictions.

Restricted by the budget available for this project, it was not possible to include contact pressure sensors to accurately measure the pad pressure before, during and after the fretting tests. The large contact pressures and high temperatures involved also limit the availability of force sensors on the market. Instead, a combination of tightening torque values and finite element analysis was used to measure the force through the pads before the tests began. Nonetheless, it would certainly be advantageous to constantly monitor the pad pressure in order to determine whether there was stress relaxation in the clamping force as a result of creep or thermal effects.

Another point to note is that during the fretting fatigue tests, the slip distance was not recorded. Instead, the wear scars and fatigue life was measured with respect to the contact pressure of the pad which ultimately determines the sliding distance. In future tests, it is possible to use strain gauges which measure the relative slip between the pad and specimen. A strain gauge can measure the deformation (extension) of the specimen as a result of cyclic axial stresses. This is measured in units of distance deformed per unit of distance placed under strain by measuring the change in resistance before and after the strain. Hence, by measuring deformation with a strain gauge and knowing the length of the object placed under strain, the total displacement can be measured and interpreted as the relative slip between the pad and specimen.

Testing may also be performed in a vacuum to determine the difference in wear volume, friction coefficient and wear scar morphology to tests performed in air. The formation of a nickel oxide glaze will be non-existent when in a vacuum and fretting fatigue lives should therefore be higher.

With regards to tracking the progress of crack formation during testing, the tests can either be interrupted at regular intervals to determine the onset of cracking, crack development and its location; or alternatively, a high definition camera could be installed into the test to record the whole crack progression.

7 References

[1] Fatigue Failure of Aircraft Components, Failure Analysis & Accident Investigation Group, Materials Science, Division, National Aerospace Laboratories, Bangalore 560 017, India

[2] Flake C. Campbell :Elements of Metallurgy and Engineering Alloys

[3] Roger C. Reed: The Superalloys: Fundamentals and Applications

[4] Fatigue Failure of Aircraft Components, S.K. Bhaumik' M. Sujata and M.A. Venkataswamy' Failure Analysis & Accident Investigation Group, Materials Science Division, National Aerospace Laboratories, Bangalore 560 017, India

[5] G.E. Maurer, Primary and secondary melt processing – superalloys, in J.K Tien and T, Caulfield, eds, *Superalloys, Supercomposites and Superceramics* (San Diego Academic Press, 1989), pp. 49-97

[6] M.G. Benz, Preparation of clean superalloys, in C.L. Briant, ed., *Impurities in Engineering Materials: Impact, Reliability and Control* (New York: Marcel Dekker Inc., 1999), pp. 31-47.

[7] C.T. Sims, N.S. Stoloff and W.C Hageleds, Superalloys II: *High Temperature Materials for Aerospace and Industrial Power* (New York: John Wiley and Sons, 1987)

[8] Tool Life of TiAlN PVD Coated Carbide Tool in High-speed End Milling of Untreated Inconel 718 under Minimum Quantity Lubrication Condition, Mohd Shahir Kasim Jun 4, 2014

[9] http://www.msm.cam.ac.uk/phase-trans/2003/Superalloys/superalloys.html

[10] M. Durand-Charre, 'The Microstructure of Superalloys' (Amsterdam: Gordon & Breach Science Publishers, 1997).

[11] Hillier, Ph.D. Thesis, University of Cambridge, 1984

[12] D.Furrer and H. Fecht, Ni-based superalloys for turbine discs, *Journal of metals*, 51 (1999), 14-17

[13] http://www.keytometals.com/page.aspx?ID=CheckArticle&site=ktn&LN=EN&NM=236

[14] Roger C. Reed: The Superalloys: Fundamentals and Applications. P 238-259

[15] Nickel alloy for turbine engine components US 5897718 A, published 27/4/1999, Rolls-Royce Plc

[16] **D.U. Furrer, H.J. Fecht, "Ni-based superalloys for turbinedisks", JOM, vol.51, (1999), 14-17.**

[17] **X. Pierron et. Al., "Sub-solidus process for conventional billet conversion"**, *Superalloys 2000*, Ed. T.M. Pollock et. al.,TMS, (2000), 425-433.

[18] A.W. Bachelor, G. W. Stachowiak, G.B. Stachowiak, Control of Fretting Friction and Wear of Roping Wire by Laser Surface Alloying and Physical Vapor Deposition, Wear, Vol.152, 1992, pp.127-150

[19] High-temperature sliding wear of metals, F.H. Stott

[20] http://www.machinerylubrication.com/Read/1375/wear-modes-lubricated

[21] Matlik, J. F., Reynolds, A., (2005) "MMM 5238 – Contact Fatigue Lifing, Part A: Background and Terminology", Rolls Royce Technical Document, Document #: DNS109386, Report #: DHC208940, pp.1-14

[22] Garcia, Grandt

[23] Mindlin, R. D. (1949) "Compliance of Elastic Bodies in Contact", Journal of Applied Mechanics, vol.16, pp.259-268.

[24] Matlik, J. F., Clark, J., Reynolds, A., (2005) "Identification and definition of contact fatigue damage as observed in engine components", Rolls Royce Technical Document, Document #: DNS111588 Report #: DHC212614, pp.1-23

[25] J.Sato, Recent Trend in Studies of Fretting Wear, Transactions JSLE, Vol.30, 1985, pp.853-858

[26] C.Cattaneo, Sul Contatto di Due Corpi Elastici: Distribuzione Locale Degli Sforzi, Rendicont

[27] W.C. Ralph, W.S. Johnson, P. Toivonen, A. Makeev, J.C.NewmanJr., International Journal of Fatigue 28 (2006) 943–950.

[28] Matlik, J. F., Reynolds, A., (2005) "MMM 5238 – Contact Fatigue Lifing, Part A: Background and Terminology", Rolls Royce Technical Document, Document #: DNS109386, Report #: DHC208940, pp.1-14.

[29] R.B Waterhouse, Fretting Corrosion, Permagon Press, Oxford, 1972

[30] J.Sato, A fundamental study of fretting fatigue JSLE, Vol.30, 1985, pp.53-61

[31] K.L Johnson, Surface Interaction between Elastically Loaded Bodies under tangential Forces, Proc. Roy. Soc., London, Series A, Vol.230

[32] http://www.ndt-ed.org/EducationResources/CommunityCollege/Materials/Structure/fatigue.htm

[33] Waterhouse, R. B., (1992), "Fretting Fatigue", International Materials Review, vol 37, n 2,pp.77-96.

[34] W.C. Ralph, W.S. Johnson, P. Toivonen, A. Makeev, J.C.NewmanJr., International Journal of Fatigue 28 (2006) 943–950.

[35] http://www.lambdatechs.com/html/resources/269.pdf

[36] http://www.freepatentsonline.com/EP0678590.html

[37] "Shot Peening," *Tool and Manufacturing Engineers Handbook* (TMEH), Volume 3, Society of Manufacturing Engineers, 1985

[38] A.W. Bachelor, G. W. Stachowiak, G.B. Stachowiak, Control of Fretting Friction and Wear of Roping Wire by Laser Surface Alloying and Physical Vapor Deposition, Wear, Vol.152, 1992, pp.127-150

[39] P.L Hurricks and K.S.Ashford, The Effect of Temperature on the Fretting Wear of Mild Steel, Proc. Inst. Mech. Engrs, London, Vol,. 184, Pt.3L, 1969-70, pp. 165-175

[40] Cook, D., Malkus, D. and Plesha, M. (1989), "Concepts and Applications of Finite Element Analysis", 3rd edition, John Wiley & Sons, Inc., USA.

[41] Dini, D., Nowell, D. (2003) "Prediction of the Slip Zone Friction Coefficient in Flat and Rounded Contact", Wear, vol. 254, pp. 364-369.

[42] Banerjee, N. (2005) "An assessment of the use of boundary element software for modelling crack propagation – SMIGTE milestone S7", Rolls Royce Technical Document, Document #: DNS106019, pp. 1-21.

[43] Johnson, R. P. (1987) "Aids to effective design – FEM or BEM?", CME, vol. 34, no. 9, pp. 27- 31.

[44] Cormier, N.G., Smallwood, B.S., Sinclair, G.B. & Meda, G., "Aggressive submodelling of stress concentrations", International Journal for Numerical Methods in Engineering, vol. 46, 1999, pp.889-909.

[45] Sinclair, G.B., Cormier, N.G., Griffin, J.H., and Meda, G., "Contact stresses in dovetail attachments: finite element modeling", *Journal of Engineering for Gas Turbines and Power*, vol. 124, pp.182-189.

[46] Beisheim, J. R. & Sinclair, G. B., (2003), "On the three-dimensional finite element analysis of dovetail attachments", Journal of Turbomachinery, Vol. 125, pp. 372-379.

[47] Matlik, J. (2004) "High Temperature, High Frequency Fretting Fatigue of a Single Crystal Nickel Alloy", PhD Thesis, School of Aeronautics and Astronautics, Purdue University, West Lafayette, Indiana, USA

[48] Jager, J. (1997) "Half-planes without coupling under contact loading", Journal of Applied Mechanics, vol. 67, pp. 247 – 259.

[49] Nowell, D, David, D. N. (1998), "Analysis of surface tractions in complex fretting fatigue cycles using quadratic programming", Transactions of the ASME, vol. 120, pp. 744-749.

[50] Murthy, H., Harish, G., Farris, T. N. (2004) "Efficient Modeling of Fretting of Blade/Disc Contacts Including Load History Effects", Journal of Tribology, vol. 126, pp. 56-64.

[51] Murthy, H., Rejeev, P., Farris, T. N., Slavik, D. C. (2001) "Fretting fatigue of Ti-6Al-4V subjected to blade/disk contact loading", Developments in Fracture Mechanics for the New Century, 50th Anniversary of Japan Society of Materials Science, eds. K. Kishimoto, S. Kubo, T. Nakamura and T. Sakagami, pp. 41-48.

[52] Spence, D. A. (1973) "An eigenvalue problem for elastic contact with finite friction", Proc. Camb. Phil. Soc., vol. 73, pp. 249-268.

[53] Nowell, D., Hills, D. A., Sackfield, A. (1988) "Contact of dissimilar elastic cylinders under normal and tangential loading", Int. Jnl. Mech. Phys. Solids, vol. 36, no. 1, pp. 59-75.

[54] Rajeev, P.T., Farris, T. N. (2002) "Numerical analysis of fretting contacts of dissimilar isotropic and anisotropic materials", Journal of Strain Analysis, vol. 37, no. 6, pp. 503-517.

[55] Ting, T. (1996) "Anisotropic elasticity: theory and applications", Oxford University Press, New York

[56] Hills, D. A., and Mugadu, A., (2002), "An overview of progress in the study of fretting fatigue", Journal of Strain Analysis for Engineering Design, vol 37, n 6, pp. 591-601.

[57] Hills, D. A., Nowell, D., (1994), "Mechanics of Fretting Fatigue", Kluwer Academic, The Netherlands.

[58] Hills, D. A., Urriolagoitia Sosa, G. (1999) "Origins of partial slip in fretting – a review of known and potential solutions", Journal of Strain Analysis, vol. 34, no. 3, pp. 175-181.

[59] Hills, D. A., Nowell, D., Sackfield, A. (1993), "Mechanics of elastic contacts", Butterworth-Heinmann, Oxford.

[60] Hamilton, G. M., Goodman, L. E. (1966) "The stress field created by a circular sliding contact", Journal of Applied Mechanics, vol. 33, pp. 371-376.

[61] Munisamy, R. L., Hills, D. A., Nowell, D. (1992) "A numerical analysis of an elastically dissimilar three-dimensional sliding contact", Proc. Instn. Mech. Engrs., vol. 206, pp. 203-211.

[62] Munisamy, R. L., Hills, D. A., Nowell, D. (1994) "Static axisymmetric hertzian contacts subject to shearing forces", Journal of Applied Mechanics, vol. 61, pp. 278-283

[63] Giannakopoulos, A., Lindley, T., Suresh, S. & Chenut, C. (2000), 'Similarities of stress concentrations in contact at round punches and fatigue at notches: Implications to fretting fatigue crack initiation', Fatigue & Fracture of Engineering Materials & Structures, Vol. 23, pp. 561-571.

[64] Conner, B. P., Lindley, T. C., Nicholas, T., & Suresh, S., (2004), 'Application of a fracture mechanics based life prediction method for contact fatigue', International Journal of Fatigue, Vol. 26, pp. 511-520.

[65] Dini, D., (2004), 'Fretting Fatigue Test Results for Ti 6/4 (D4.1), Analysis of Results and Validation of Assessment Criteria (D5.2)', UTC Report No. 210, UTC for Solid Mechanics, Oxford University, SMIGTE project, pp.1-55.

[66]Nowell, D., Dini, D., and Hills, D. A. (2004) "Recent Developments in the Understanding of Fretting Fatigue", Proceedings of the ECF15 Conference, Journal of Engineering Fracture Mechanics, in press.

[67] Taylor, D. (2001) "A mechanistic approach to critical-distance methods in notch fatigue", Fatigue and Fracture of Engineering Materials and Structures, vol. 24, no. 4, pp. 215-224

[68] Dini, D., Sackfield, A., and Hills, D.A. (2004) "Comprehensive Bounded Asymptotic Solutions for Incomplete Contacts in Partial Slip", Journal of the Mechanics and Physics of Solids, vol. 53, pp. 437-454.

[69] Farris, T. N., Murthy, H., Matlik, J. F., (2003), "Fretting Fatigue", in R. O. Ritchie & Y. Murakami, eds, 'Comprehensive Structural Integrity: Fracture of Materials from Nano to Macro', Vol. 4, Elsevier Science.

[70] Murthy, H. (2004) "Fretting fatigue in anisotropic contacts at elevated temperatures and in investigation of lifing schemes", PhD Thesis, School of Aeronautics and Astronautics, Purdue University, West Lafayette, IN, USA.

[71] Contact fatigue lifing strategy: modelling and lifing, DNS111715, J F Matlik, N Banerjee

[72] https://engineering.purdue.edu/METL/Fac/FWTM/

[73] Murthy, H., Rajeev, P. T Okane, M Farris, T. N. (2003) " Development of test methods for hig temperature fretting of turbine materials subjected to engine-type loading". In: 'Fretting fatigue: Advances in Basic Understanding and Applications, ASTM STP 1425,' eds. Y Mutoh, S.E Kinyon, West Conshohocken, PA, pp.273-289

[74] Rajeev,P,t., Fariss, T.N (2002) " Numerical analysis of fretting Contacts of Dissimilar Isotropic and Anisotropic Materials" Journal of Strain Analysis, vol 37, n6,pp.503-517

[75] Taylor, D. (2001) "A mechanistic approach to critical-distance methods in notch fatigue", Fatigue and Fracture of Engineering Materials and Structures, vol. 24, no. 4, pp. 215-224

[76] Ruiz, C., Boddington, P.H.B., Chen, K.C. (1984) "An investigation of fatigue and fretting in a dovetail joint", Experimental Mechanics, vol. 126, pp. 56-64.

[77] Szolwinski, M. P., Farris, T. N., (1996), "Mechanics of Fretting Fatigue Crack Formation", Wear, vol 198, pp. 93-107.

[78] Szolwinski, M. P., Farris, T. N. (1998) "Observation, analysis, and prediction of fretting fatigue in 2024-T351 aluminum alloy" Wear, vol. 221, pp. 24-36.

[79] Fatemi, A., Socie, D. F. (1988) "A critical plane approach to multiaxial fatigue damage including out-of-phase loading", Fatigue Fract. Engng. Mater. Struct., vol. 11, no. 3, pp. 149-165.

[80] Smith, R. N., Watson, P., Topper, T. H. (1970) "A stress-strain function for the fatigue of metals", Journal of Materials, JMLSA, vol. 5, no. 4, pp. 767-778

[81] Neu, R. W., Pape, J. A., Swalla, D. R. (2000) Fretting Fatigue: Current Technology and Practices, ASTM STP 1367, edited by D. W. Hoeppner, V. Chandrasekaran, and C. B. Elliott, ASTM, West Conshohocken, PA, pp. 369-388.

[82] Araujo, J. A., Nowell, D. (2002) "The effect of rapidly varying contact stress fields on fretting fatigue", International Journal of Fatigue, vol. 24, no. 7, pp.763-775.

[83] Dang Van, K., Griveau, B., Message, O. (1985) "On a new multiaxial fatigue limit criterion: Theory and application", in Biaxial and Multiaxial Fatigue, ASTM, Philadelphia, 1985, pp.479-496.

[84] Fouvry, S., Kapsa, P., Vincent, L., (2003), in Fretting Fatigue: Advances in the Basic Understanding and Applications, ASTM STP 1425, eds. S.E. Kinyon, D.W. Hoeppner, and Y. Mutoh, ASTM, West Conshohocken, PA, pp. 17-32.

[85] Socie, D. (1987) "Multiaxial fatigue damage models" Journal of Engineering Materials and Technology, vol. 109, pp. 292-298.

[86] Findley, W. N. (1959) "A theory for the effect of mean stress on fatigue of metals under combined torsion and axial load or bending", Journal of Engineering for Industry, pp.301-307.

[87] Chu, C-C., Conle, F. A., & Bonnen, J. J. F., (1993) Critical plane approaches for multiaxial fatigue damage assessment. In Advances in Multiaxial Fatigue – ASTM STP 1191, pp. 7-36, ASTM, Philadelphia.

[88] Doner, M., Bain, K. R., Adams, J. H. (1982) "Evaluation of methods for the treatment of mean stress effects on low-cycle fatigue", Jrnl. Eng. Power, vol. 104, pp. 403-411.

[89] Telesman, J., Ghosn, L. (1989) "The usual near threshold FCG behaviour of a single crystal superalloy and the resolved shear stress as the crack driving force", Engineering Fracture Mechanics vol. 34, no. 5/6, pp. 1183-1196.

[90] Smith, R. N., Watson, P., Topper, T. H. (1970) "A stress-strain function for the fatigue of metals", Journal of Materials, JMLSA, vol. 5, no. 4, pp. 767-778.

[91] Matlik, J. F., Farris, T. N. (2003) "High-frequency, fretting fatigue experiments", Fretting Fatigue: Advances in Basic Understanding and Applications, STP 1425, Y. Mutoh, S. E. Kinyon, and D. H. Hoeppner, Eds., ASTM International, West Conshohocken, PA, pp. 251-272.

[92] Findley, W. N. (1959) "A theory for the effect of mean stress on fatigue of metals under combined torsion and axial load or bending", Journal of Engineering for Industry, pp.301-307.

[93] Giannakopoulos, A. E., Lindley, T. & Suresh, S. (1998),'Aspects of equivalence between contact mechanics and fracture mechanics: Theoretical connections and a life prediction methodology for fretting fatigue', Acta Materialia, Vol. 46, N. 9, pp. 2955-2968.

[94] Dini, D., Hills, D.A. (2003) "Bounded Asymptotic Solutions for Incomplete Contacts in Partial Slip", International Journal of Solids and Structures, vol. 41, pp. 7049-7062.

[95] Dini, D., Sackfield, A., and Hills, D.A. (2004) "Comprehensive Bounded Asymptotic Solutions for Incomplete Contacts in Partial Slip", Journal of the Mechanics and Physics of Solids, vol. 53, pp. 437-454.

[96] Kitagawa, H., Takahashi, S. (1976) "Applicability of fracture mechanics to very small cracks or cracks in the early stage", In Proc. 2nd Int. Conf. on Mech. Behaviour of Matls., ASM, pp. 627 – 631.

[97] El Haddad, M.H., Smith, K.N., Topper, T.H. (1979) "Fatigue crack propagation of short cracks", Journal of Engineering Materials and Technology, vol. 101, pp. 42 – 46

[98] Nishioka K, Hirakawa K. Bull JSME 1972;15:135–44.

[99] Hertz H. J reine und angewandte Mathematik 1982;92:156–71.

[100] Mindlin RD. J App Mech 1949;16:259–68.

[101] Bramhall R. Studies in fretting fatigue. D.Phil. Thesis. University of Oxford, 1973.

[102] Hills DA, Nowell D, O_Connor JJ. Wear 1988;125:129–56.

[103] Szolwinski MP, Farris TN. Wear 1998;221:24–36.

[104] Murthy H, Farris TN. Fretting fatigue of TI-6Al-4V subjected to blade/disc contact loading (Garcia ref1)

[105] Murthy and Farris – Mechanics of fretting fatigue crack formation

[106] https://engineering.purdue.edu/METL/Fac/FWTM/

[107] Initiation and propagation of fretting fatigue cracks – K.Endo and H.Goto

[108] J. Liu, Z.F. Yue, Y.S. Liu, Theoretical and Applied Fracture Mechanics 47 (2007) 35–45.

[109] Krishnakumar Shankar, Ruby Dhamari; Fatigue behaviour of aluminium alloy 7075 bolted joints treated with oily film corrosion compounds

[110] Jose´ Maria Minguez, Jeffrey Vogwell, Effect of torque tightening on the fatigue strength of bolted joints, Engineering Failure Analysis 13 (2006) 1410–1421

[111] Shigley J. Mechanical engineering design. New York: McGraw Hill; 1977.

[112] http://upload.wikimedia.org/wikipedia.8a/Bolted_joint_spring_analogy.png

[113] http://www.boltscience.com/pages/basics5.htm

[114] W.C. Ralph, W.S. Johnson, P. Toivonen, A. Makeev, J.C.NewmanJr., International Journal of Fatigue 28 (2006) 943–950.

[115] W.C. Ralph, W.S. Johnson, P. Toivonen, A. Makeev, J.C.NewmanJr., International Journal of Fatigue 28 (2006) 943–950.

[116] J. Liu, J.X. Kang, W.Z. Yan, F.S. Wang, Z.F. Yue, Prediction of fatigue performance of fastener holes with bolt clamping force based on critical plane approach

[117] **Effect of torque tightening on the fatigue strength of bolted joints, Jose´ Marı´a Mı´nguez, Jeffrey Vogwell,** Engineering Failure Analysis 13 (2006) 1410–1421

[118] Mechanical Fastening Joining Assembly By James A. Speck -- Marcell Dekker 1997 Page 128

[119] Surface Engineering for Corrosion and Wear Resistance By J. R. Davis -- ASM International 2001 Page 76

[120] Notation, 1965 Symposium on Elasto-hydrodynamic Lubrication, Proc. Institute of Mechanical Engineers, Vol. 180, Pt 3B (1965-66) p. 4.

[121] Research Group on Wear of Engineering Materials of the European Organisation for Economic Co-operation and Development, Glossary of Terms and Definitions in the Field of Friction, Wear and Lubrication (Organisation for Economic Co-operation and Development, Paris, 1969) p. 53.

[122] P.M. Ku, ASLE Trans. 19 (1976) 239.

[123] K.C. Ludema, Wear 100 (1984) 315.

[124] R.S. Gates et al., STLE Tribol. Trans. 32 (1989) 423

[125] R.M. Matveevsky, Tribology 2 (1968) 115.

[126] M.D Benedez, FJ Carrioa, I Martinez-Mateo, G Martinez-Nicolas, J.A Rodriguez, EJ Herrera, Wear 248 (2001) 178-186

[127] **W.F. Bowman and G.W. Stachowiak, "A review of scuffing models",** Received 9 February 1996; accepted 29 March 1996, University of Western Austrailia.

[128] Analysis techniques end gear damage, Robert L. Errichello of Geartech | Motion System Design, March 2001

[129] ASTM standard G40 (2006)

[130] Tensile Properties of Ni-Based Superalloy 720Li: Temperature and Strain Rate Effects - k. gopinath, a.k. gogia, s.v. kamat, r. balamuralikrishnan, and u. ramamurty - doi: 10.1007/s11661-008-9585-3

[131] http://www.specialmetals.com/documents/Waspaloy.pdf

[132] www.bossard.com Version T.01.00 – 09.02.2006

[133] Fatigue Testing and Analysis: Theory and Practice By Yung-Li Lee, Jwo Pan, Richard Hathaway, Mark Barkey

[134] Waterhouse, R.B. (2000) "Plastic Deformation in Fretting Processes – A Review", in D. W. Hoeppner, V.Chandrasekaran & C. B. Elliott, eds, "Fretting Fatigue: Current Technology and Practices", ASTM STP 1367, American Society of Testing and Materials, West Conshohocken, PA, pp. 3-18

[135] Waterhouse, R. B. & Taylor, D. E. (1971) "The initiation of fatigue cracks in a 0.7% carbon steel by fretting", Wear, vol. 17, pp. 139-147.

[136] Berthier, Y., Colombie, C., Vincent, L., Godet, M. (1971), "Fretting wear mechanisms and their effects on fretting fatigue", Journal of Tribology, vol. 110, pp. 517-524.

[137] O. Jin, S. Mall, Effects of independent pad displacement on frettingfatigue behaviour of Ti–6Al–4V, Wear 253 (2002) 585–596

[138] www.grantadesign.com

[139] Ko, C.N., Ioannides, E., 1988, "The Associated ResidualStresses and their Effect on the Fatigue Life of RollingBearing: an FEM Analysis",Proc. 15th Leeds-Lyon Symp. ,Leeds, pp.199 207

[140] Chen, Q., Hahn, G.T., Rubin, C.A., Bhargava, V.,1988, The Influence of Residual Stresses on RollingContact Mode II Driving Force in Bearing Raceway", Wear, 26, pp. 17-30

[141] Muro, H., Tsushima, N., Nunome, K., 1973, "Failure Analysis of Rolling Bearings by X-ray Measurements of Residual Stresses", Wear, **25**, pp. 345-356.

[142] Nishioka, K., Hirakawa, K. (1969) "Fundamental Investigations of Fretting Fatigue – Part 2, Fretting Fatigue Testing Machine and Some Test Results" Bulletin of JSME, vol. 12, pp. 180-187.

[143] Matlik, J. (2004) "High Temperature, High Frequency Fretting Fatigue of a Single Crystal Nickel Alloy", PhD Thesis, School of Aeronautics and Astronautics, Purdue University, West Lafayette, Indiana, USA

[144] Fretting Wear Behaviour, and the Effect of Glazes on Nickel Alloys - A Research Summary, Alison Reynolds, 11/11/04

[145] I.M.Hutchings, 'Tribology: Friction and Wear of Engineering Materials', Metallurgy and materials science, 2001

[146] A.Iwabuchi, 'Fretting Wear of Inconel625 at High Temperature and in High Vacuum', 1985.

[147] M.M.Hamdy, 'The Fretting Fatigue Behaviour of a Nickel-Based Alloy (Inconel 718) at Elevated Temperatures', 1979.

[148] A.Iwabuchi, 'Fretting Wear of Inconel625 at High Temperature and in High Vacuum', 1985.

[149] J.Jiang, F.H.Stott, and M. Stack, 'A Mathematical Model for Sliding Wear of Metals at Elevated Temperatures', 1995

[150] J.Jiang, F.H.Stott, and M. Stack, 'A Mathematical Model for Sliding Wear of Metals at Elevated Temperatures', 1995

[151] P.O'Hara, 'Fatigue and Fretting', Problems Addressed by Shot Peening.

[152] Notes from 'The 121h Annual Tribology Course: Tribology - Friction, Wear and Lubrication', 2004.